INVESTIGATING ALTERNATIVE DELIVERY SYSTEMS FOR SELF-AMPLIFYING RNA VACCINES

Author: Giulia Anderluzzi

Supervisor: Barbara C. Baudner, Yvonne Perrie

University of Strathclyde

GSK, Siena, Italy

December 2019

Abstract

The rabies virus is an enveloped, single stranded, negative-sense RNA virus of the Lyssavirus genus, zoonotic pathogens within the family Rhabdoviridae. Although extensive effort has been made in the last decades to develop efficacious vaccines to prevent rabies spread, the virus is still responsible for the mortality of about 24,000 to 90,000 people per year especially in developing countries and it has been classified as one of the major causes of death from infectious diseases in humans. Commercially available rabies vaccines for humans are considered effective, however the production costs are very high and multiple injections are required to achieve protection. Therefore, the development of new vaccines to reduce the toll of rabies disease in the developing world would be highly desirable. Within this project a nucleic acid based vaccine strategy – in particular self-amplifying RNA vaccine (SAM)- has been investigated since this platform was previously reported to elicit protective immune responses, particularly in the case of cell-mediated responses in a safe manner and for a variety of virus disease. To enhance biological stability and cell internalisation, SAM was combined with four cationic delivery systems. Oil-in-water cationic nanoemulsions (CNE), polymeric nanoparticles (NPs), lipid nanoparticles (SLNs) and liposomes were formulated in the absence of or in combination with a specific SAM vaccine. Despite the differences in formulation composition, all samples contained the same concentration of cationic lipid - 1, 2-dioleoyl-3-trimethylammonium-propane (DOTAP), or dimethyldioctadecylammonium (DDA) - known as immunostimulants.

In the preliminary studies, two different manufacturing processes such as Microfluidics and Microfluidisation were applied. As a proof of concept, anionic liposomes and solid lipid nanoparticles were formulated and ovalbumin was encapsulated within the delivery systems as model protein antigen. Resulting carriers were compared in terms of their physico-chemical properties. The purpose was to obtain homogeneous formulations with a diameter in the nanometres range with a given manufacturing method. Furthermore, dialysis, tangential flow filtration (TFF) and size exclusion chromatography (SEC) have been tested as purification methods and compared in terms of the ability to remove both residual organic solvent and unloaded protein from samples without altering physico-chemical attributes.

These process parameters and purification method optimisations were then applied to produce cationic CNE, NPs, SLNs and liposomes in combination with a specific SAM vaccine. In the preliminary studies and during formulations development optimisation, SAM encoding for green fluorescent protein (SAM-GFP) was used as a model SAM with a reporter function, given the ease of detection in *in vitro* cell cultures. However, SAM encoding for rabies glycoprotein (SAM-Rabies) represented the actual antigen of interest, employed in this project

for further *in vivo* analysis. Cationic SLNs, NPs and liposomes were produced using microfluidics, since this method required smaller volumes compared to the Microfluidisation, thus avoiding waste of reagents. However, the Microfluidizer was used to reduce CNE size, due to incompatibility between CNE component and microfluidics chip. Moreover, particles were formulated with SAM encoding the antigen of interest and loaded into or adsorbed onto cationic carriers. All delivery systems were evaluated according to their physico-chemical properties: hydrodynamic radius, sample homogeneity (polydispersity index – PDI) and surface charge. Furthermore, *in vitro* activity was investigated using three different cell lines: bone marrow derived macrophages (BMDM), bone marrow derived dendritic cells (BMDC) and baby hamster kidney cells (BHK). SAM uptake and antigen expression from each formulation in each cell line were used to discriminate and down-select formulations for *in vivo* studies. In the *in vivo* studies, biodistribution of carriers alone or in combination with SAM were performed. Briefly the selected SAM-carriers were administered intramuscularly (i.m.) to BALB/c mice and their movement in the animal body was tracked using a radiolabelling technique thereby allowing measurement of formulations at chosen time-points and in specific organs. The aim of the study was to understand the pharmacokinetic profile of formulations in a mouse model and assess whether biodistribution might correlate with subsequent immunogenicity studies.

The initial attempt of these studies was to (i) find the antigen dose to induce high antibody and cellular responses *in vivo* and (ii) to compare the adjuvant properties of selected cationic candidates (i.e. SAM encapsulating DOTAP NPs, DOTAP liposomes and DDA liposomes) after i.m. injection. Formulations were selected according to the potency of inducing antigen expression *in vitro*. The commercial vaccine Rabipur, which is an inactivated virus rabies vaccine, was used as comparator. The aim was to find a valid and more cost-effective alternative formulation which induced an immune response comparable or superior to the commercial vaccine. Data showed that DOTAP NPs were the most potent in triggering IgG titers among candidates and the antibody levels were equivalent to the ones induced by the commercial vaccine after a single dose. Interestingly, the GMT was well above the protective threshold despite the antigen dose used, thus meaning that elicited antibodies were functional against rabies glycoprotein G. In terms of cellular response all candidates were able to activate both CD4+ and CD8+ T cells in a comparable manner to the vaccine on the market.
Moreover, to evaluate if changing the route of administration might affect carriers' potency, SAM encapsulating candidates were also administered intradermally (i.d.) and intranasally (i.n.), and formulations immunogenicity was evaluated according to IgG titres and cellular response. To do so, DOTAP NPs and DOTAP SLNs were selected; NPs were tested considering the promising outcome from the first *in vivo* study, whereas SLNs were introduced although poor *in vitro* antigen expression. The aim was to understand the power of *in vitro*

models to predict *in vivo* antigen immunogenicity. Results highlighted that SLNs injected i.m. showed increased immunogenicity compared to both NPs and the licenced vaccine after a single dose. Moreover, the potency of SLNs was also seen after intradermal administration, where SLNs were as potent as Rabipur to elicit IgG titer in mice after two vaccinations, inducing comparable innate and adaptive immunity to the vaccine on the market. Herein it was also reported that two doses of SAM SLNs injected i.n. induced a humoral immunity which was higher than the one elicited by Rabipur. Interestingly, intranasal administration of SLNs led to a higher percentage of IL-2 producing antigen specific CD4+ T cells compared to the licenced in both spleens and lungs. Although a significant difference was observed among formulations in the ability to enhance antigen-specific IgG titres, immunogenicity did not directly correlate with biodistribution, where carriers' pharmacokinetics were indeed similar. All together, these findings are encouraging and demonstrate that coformulation of SAM vaccine and solid lipid nanoparticles might be a valid and more advantageous alternative to produce rabies vaccines, with augmented patient' safety and compliance.

Keywords: rabies virus, rabies vaccines, non-viral delivery, self-amplifying RNA, liposomes, solid lipid nanoparticles, emulsions polymeric nanoparticles, antigen expression, pharmacokinetics, immunogenicity.

Contents

List of tables

List of figures

All data were normalised by IPA standard peaks area. Formulations with TFR 10 mL/min and FRR 1:1 has been tested. Results are expressed as the means of three experiments ± S.D. 106

List of abbreviations

^{3}H-Chol	3H-Cholesterol
AE	Adsorption efficiency
APCs	Antigen-presenting cells
ApoE	Apolipoprotein E
BHK	Baby hamster kidney
BMDDCs	Bone marrow derived dendritic cells
BMDM	Bone marrow derived macrophages
CD	Clinical dose
Chol	Cholesterol
CMI	Cell-mediated immunity
CNE	Cationic nanoemulsions
CNS	Central nervous system
cryo-TEM	Cryogenic transmission electron microscopy
CTAB	Cetyltrimethylammonium bromide
CTL	Cytotoxic T-lymphocyte
DC-Chol	3ß-[N-(N',N'-dimethylaminoethane)-carbamoyl]cholesterol hydrochloride
DCP	Dicetylphosphate
DCs	Dendritic cells
DDA	Dimethyldioctadecylammonium (Bromide Salt)
DDCs	Dendritic dermal cells
DilC	1,1'-Dioctadecyl-3,3,3',3'-Tetramethylindocarbocyanine Perchlorate
DLinDMA	1,2-dilinoleyloxy-3-dimethylaminopropane
DLin-MC3-DMA	heptatriaconta-6,9,28,31-tetraen-19-yl 4-(dimethylamino)butanoate
DLS	Dynamic light scattering
DMEM	Dulbecco's Modified Eagle Medium
DMG-PEG2000	1,2-dimyristoyl-rac-glycero-3-methoxypolyethylene glycol-2000
DMSO	Dimethyl sulfoxide
DMTAP	1,2-dimyristoyl-3-trimethylammonium-propane
DOBAQ	N-(4-carboxybenzyl)-N,N-dimethyl-2,3-bis(oleoyloxy)propan-1-aminium

DODAC	Dimethyldioctadecylammonium chloride
DODAP	1,2-dioleoyl-3-dimethylammonium-propane
DOEPC	1,2-dioleoyl-sn-glycero-3-ethylphosphocholine
DOGS	Dioctadecylamidoglycylspermine
DOPE	1,2-dioleoyl-sn-glycero-3-phosphoethanolamine
DOSPA	2,3-dioleoyloxy-N-[2-(spermine-carboxamido) ethyl]-N,N-dimethyl-1-propanaminium
DOTAP	1,2-dioleoyl-3-trimethylammonium-propane
DOTMA	1,2-di-O-octadecenyl-3-trimethylammonium propane
dsAT	Double strand polynucleotides
DSPC	1,2-distearoyl-sn-glycero-3-phosphocholine
EE	Encapsulation efficiency
EQ1	N, N-di-(β-stearoylethyl)-N, N-dimethylammonium chloride
ERIG	Equine rabies immunoglobulin
FACs	Fluorescence-activated cell sorting
FBS	Foetal bovine serum
FCA	Freund's Complete Adjuvant
FDA	Food and Drug Administration
FRR	Flow rate ratio
FSC	Fetal Calf Serum
GM-CSF	Granulocyte-macrophage colony-stimulating factor
GMT	Geometric mean titer
GOI	Gene of interest
HA	Influenza hemagglutinin
HBsAg	Hepatitis B surface antigen
HCV	Hepatitis C virus
HDCV	Human diploid cell vaccine
HI-FCS	Heat inactivated foetal calf serum
HRIG	Human rabies immunoglobulin
HSPC	Hydrogenated soybean phosphatidylcholine
i.d.	Intradermal
i.m.	Intramuscular
i.n.	Intranasal
ICH	International Conference on Harmonisation

IFN	Interferon
IL	Interleukin
ILN	Inguinal lymph node
IPA	2-propanol
IVP	*In vitro* potency
LC	Loading capacity
LCs	Langerhans cells
LE	Loading efficiency
LF	Lipofectamine2000
LNP	Lipid nanoparticles
LUV	Large unilamellar vesicles
Mab	Monoclonal antibody
LNPs	Lipid nanoparticles
M-CSF	Macrophage colony-stimulating factor
MFI	Mean fluorescence intensity
MHC	Major histocompatibility complex
MMG	Monomycoloyl glycerol
MPL	Monophosphoryl lipid A
mRNA	messenger RNA
Mϕ	Macrophages
NPs	Polymeric nanoparticles
nsP	Non structural protein
O/W	Oil in water
ONRAB	Recombinant human adenovirus rabies glycoprotein vaccine
ORF	Open reading frame
OVA	Albumin from chicken egg
p.i	Post injection
PAMPs	Pathogen associated molecular patterns
PBS	Phosphate-buffered saline
PCEC	Purified chick embryo cells
PCL	Polycaprolactone
PDI	Polydispersity index
PDMS	Polydimethylsiloxane
pDNA	plasmid DNA
PE	Egg-phosphatidylethanolamine
PEG-DSPE	Poly(ethylene glycol)–

	distearoylphosphatidylethanolamine
PEI	Polyethyleneimine
PEP	Post exposure profilaxis
PIT	Phase inversion temperature
PKC	Protein kinase C
PLA	Poly (D, l-lactide)
PLGA	Poly (D, L-lactide-co-glycolide)
PLN	Popliteal lymph node
POE	Poly (ortho esters)
PLGA	Poly (D, L-lactide-co-glycolide)
polyA	Poly-deoxy-adenosine
polyT	Poly-deoxy-thymidine
PrEP	Pre-exposure
PRRs	Pattern recognition receptors
PS	Brain Lα-phophatidylserine
PVA	Polyvinyl alcohol
RABV	Rabies virus
RDRP	RNA-dependent RNA polymerase
RPMI	Roswell Park Memorial Institute
S.C	Subcutaneously
SAM	Self-amplifying RNA
SAM-GFP	Self-amplifying RNA encoding for a green fluorescent protein
SAM-Rabies	Self-amplifying RNA encoding for rabies glycoprotein
SCF	Supercritical fluid
SD	Standard deviation
SEC	Size exclusion chromatography
SHM	Staggered herringbone micromixer
SLNs	Solid lipid nanoparticles
SOI	Site of injection
SUV	Small unilamellar liposomes
TDB	Trehalose dibehenate
TFA	Trifluoroacetic acid
TFF	Tangential flow filtration
TFR	Total flow rate
TLRs	Toll-like receptors

TMP	Transmembrane pressure
TNF	Tumor necrosis factor
UTR	Untranslated region
VRPs	Viral replicon particles
WHO	World Health Organization
ZP	Zeta potential

CHAPTER 1

Introduction

1.1 Key concepts in immunology and vaccinology

The aim of vaccination is to generate a strong immune response providing long term protection against infections. Protection against pathogens is a result of multiple interactions between organs, tissues, cells and molecules that build the body's immune system (Moser and Leo, 2010). The immune system is composed by three major defense mechanisms: (a) external barriers including physical (such as skin, ciliated epithelia, mucous membranes) and chemical (such as destructive enzymes in secretions, stomach acids) barriers; (b) innate and (c) adaptive immune responses. Once an infection occurs, the innate immunity acts immediately: the first line of defense in the immune system - antigen presenting cells (APCs) such as dendritic cells (DCs), macrophages and neutrophils – recognise distinct molecules on or in pathogens termed 'pathogen associated molecular patterns (PAMPs)' (Geijtenbeek and Gringhuis, 2016, Goyal et al., 2016) which are different from host markers. APCs express pattern recognition receptors (PRRs) on the surface and in endosomes which bind PAMPs selectively. Among PRRs, Toll-like receptors (TLR) have recently emerged as key components in innate immunity (Lemaitre et al., 1996). After recognition, APCs internalise pathogens through phagocytosis. This mechanism aims to disrupt pathogens by a complex set of digestive enzymes or reactive oxygen species (such as free radicals) produced within the cell (Gulati, 2009). This process referred to as the inflammatory response: after pathogen recognition, phagocytes secrete a series of chemokines (defined as small soluble proteins that function as chemotactic factors by directing cellular migration) that attract phagocytes from the blood circulation to the infection site (Bachmann et al., 2006), and cytokines (defined as proteins released by cells that affect the behavior of other cells) such as tumor necrosis factor (TNF-α) and interleukins that amplify phagocytosis. This cascade process leads to recruitment of cells and plasma proteins to the site of infection, thus inducing signs of inflammation (increased swelling, redness, pain and heat).

However, due to the limited diversity of PRRs, pathogens with a high mutation rate can easily circumvent the innate immune system (Bowie and Unterholzner, 2008). To overcome this issue, vertebrate developed the adaptive immune system which involves antibodies and T cell receptors as recognition systems. Adaptive immunity is mediated by cells such as T and B lymphocytes. The latter cell line produces a set of proteins known as antibodies which can recognise virtually all known pathogens (Brack et al., 1978, Murre, 2007). In the absence of an infection, lymphocytes are accumulated in the bone marrow and each of them expresses multiple copies of a unique antibody as a cell surface receptor (B cell receptor, BCR). Thus, at the beginning, each lymphocyte is mono-specific, i.e. able to recognise a single antigenic molecule. Once they encounter specific antigen, B cells expressing a given antibody are stimulated to divide and differentiate into plasma cells and memory B cells (Burnet, 1976) . Most of these plasma cells return to the bone marrow, where they will produce large amounts

of soluble antibodies with a given specificity that will be released in the blood and other body fluids. Opposite to inflammatory cells, B cells do not need to be present at the site of infection, since they can face the infection "at distance" thanks to soluble antibody generation.

Although antibodies allow the immune system to react with a large variety of antigens, these large molecules cannot cross the cell membrane and cannot bind and destroy intracellular pathogens such as viruses. For this purpose, APCs are involved since they can display peptide fragments derived from intracellular proteins on their cell surface (Alegre et al., 2008, Scarzello et al., 2005). These peptides are bound by transmembrane "presenting molecules" encoded by the major histocompatibility complex (MHC) genes in humans (Rock et al., 2002). These complexes will then display (or "present") these peptides (or "antigens") of intracellular origin to the cell surface (Bjorkman et al., 1987). T lymphocytes are equipped with antigen specific receptors (TCR) that can selectively recognize these complexes. This mechanism is called "antigen presentation". Those T cells which are responsive to these protein fragments express cell surface marker known as the CD8 molecule. These T cells recognise peptide fragments presented by a subset of MHC molecules known as class I MHC molecules (Loureiro and Ploegh, 2006). On the other hand, T cell expressing the marker known as CD4, react to MHC-peptide complexes class II. These peptides originate from limited digestion of extracellular proteins that have been internalized through endocytosis or phagocytosis. In conclusion, CD8-expressing cells detect peptides of cytoplasmic origin presented by MHC class I molecules, while CD4 cells react to proteins of extracellular origin whose processed peptides are loaded on MHC class II molecules. When an antigen enters the body, it binds to cells expressing the corresponding receptors and induces their multiplication and differentiation

It is worth to notice that only a subset of APCs known as dendritic cells (DCs) can activate naïve CD4+ T cells into differentiated T-helper cells (Th cells) (Steinman and Cohn, 1973). The activation process seems to proceed stepwise: (1) antigen processing, (2) migration to lymphoid organs and finally (3) activation of naïve T cells through provision of a combination of antigenic, costimulatory and cytokine signals. These cells are capable to migrate from the infection site to the lymphoid organs where they present antigenic fragments to lymphocytes, thus activating and stimulating T cells. Helper T cells secrete specific cytokines (Mosmann et al., 1986); one of the most abundant is IFN-γ, a cytokine known to increase expression of MHC molecules and to exert potent anti-viral effects. This cytokine is released by Th1 cells and it can promote the differentiation and activity of CD8-expressing cells and phagocytes (Heinzel et al., 1989). Other cytokines such as IL-4, IL-5 and IL-13 are mainly produced by Th2 cells. These cells activate eosinophils and mastocytes often involved in the immune response to large extracellular parasites (Finkelman et al., 2004). However, the over-activation

of these cells induces secretion of high levels of IgE antibodies, responsible for allergic reactions. Moreover, IL-21 is released by follicular helper T cells (fTh), a subset of cells that is often found in close association with B lymphocytes in selected structures (germinal centres) of lymphoid organs has been recently identified. IL-21 is a cytokine known to enhance humoral responses *in vivo* (Breitfeld et al., 2000). Finally, IL-17 and IL-22, cytokines are secreted by Th17 which are involved in regulating the local immune response to gut and lung pathogens (Harrington et al., 2005).
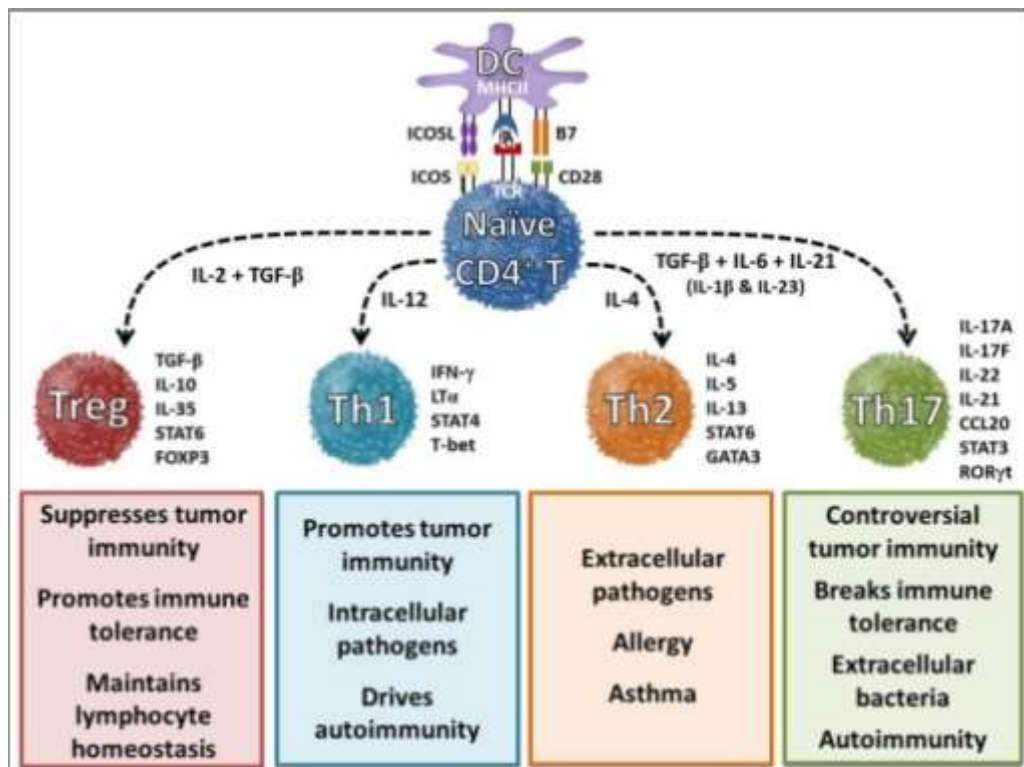
Figure 1.1 The different types of follicular helper T cells subsets. Differentiation of helper T cell subsets is determined by cytokines. In the presence of interleukin-6 (IL-6), IL-21, and transforming growth factor-beta (TGF-β), naïve CD4+ T cells differentiate into a Th17 cell phenotype, which is characterized by the expression of transcription factors retinoic acid receptor-related orphan receptor-γt (RORγt) and signal transducer and activator of transcription 3 (STAT3). IL-1β and IL-23 cytokines can promote and stabilize this phenotype during cell expansion. Once programed, these cells secrete IL-17A, IL-17F, IL-21, and IL-22, which play a key role in enhancing autoimmunity and host defense. Cytokines IL-12, IL-4, and TGF-β and transcription factors T-bet, GATA3, and FoxP3 have been shown to regulate Th1, Th2, and Treg cell development, respectively. These distinct subsets regulate immune response to foreign, self, and tumor antigen.(Bailey et al., 2014)

1.2 Basic principles of modern vaccination and its role in public health

Antigen-presentation and DCs maturation appear as the critical regulatory steps enabling the initiation of an immune response. Vaccination approach takes advantage from the principle of a non-virulent inoculation of a given pathogen, able to elicit a strong and adequate immune response *in vivo* (Zepp, 2010). Attenuated live organisms were the first kind of vaccines

employed since the beginning of the vaccinology era. A protective immune response from live attenuated viral vaccines is a result of combined antigen-specific antibody and T cell responses (Wrammert et al., 2009). Nowadays, several live attenuated vaccines have been licensed, including those against viral (polio, measles, mumps, rubella, influenza, yellow fever, rotavirus, chicken pox) and bacterial diseases (tuberculosis, typhoid fever). However, they might have limitations. For example, the production of these kind of vaccines becomes challenging for those live organisms (e.g., hepatitis C virus (HCV)) which do not grow well *in vitro*. Moreover, attenuated organisms can revert into their virulent state, raising safety concerns for development of live vaccines against highly dangerous pathogens (e.g., Ebola virus).

Thus, modern vaccines more often comprise pathogen-derived subcellular components or recombinant proteins which result to be potentially less risky. However, the limitation of these subunits is strongly related to their potency. Numerous clinical and experimental observations demonstrated the reduced immunogenicity of subcellular or subunit-based vaccines when compared with inactivated/killed whole organisms (Geeraedts et al., 2008). Another possible strategy is the use of vector-based systems, like bacteria and virus, which are currently investigated more in depth due to their capacity of targeting cells and delivering nucleic acid using pathways of cellular entry naturally employed by viruses. Vaccinia (Gilbert, 2013) and adenovirus (Johnson et al., 2013) are the two most common used platforms and they were proved to induce antigen-specific antibody and T cell responses in several clinical trials. However, antivector immunity might interfere with these systems, limiting their application (Saxena et al., 2013). One possible strategy to circumvent this issue is delivering nucleic acid through nonviral systems, such as plasmid DNA, mRNA

1.3 Case study: Rabies - epidemiology, transmission and prevention
1.3.1 Virus epidemiology and transmission

Rabies is an acute, progressive encephalitis caused by a lyssavirus which is bullet-shaped, genetically mono-phyletic, single-stranded, negative-sense RNA virus, taxonomically residing in the Order Mononegavirales, Family Rhabdoviridae (Afonso et al., 2016). The rabies virus (RABV) genome is approximately 12 kb in size and comprises five genes that are encoding nucleoprotein (N), phosphoprotein (P), matrix protein (M), glycoprotein (G) and the RNA-dependent RNA polymerase (L) (Pringle, 1997). Ribonucleoprotein, formed by RNA and N, together with P and L forms the viral replication complex. RABV G and M regulate RNA synthesis and affect RABV pathogenesis by regulating virus replication and by facilitating cell-to-cell spread (Finke et al., 2003, Pulmanausahakul et al., 2008). M bridges the RNP and the cytoplasmic domain of G to form the bullet-shaped virion. A leader sequence at the 3′ end and a trailer sequence at the 5′ end of the RABV genome are conservative. From

the 3′ end, a gradient of transcription occurs that follows the gene order 3′-leader-N-P-M-G-L-trailer-5′. This gradient results in the most abundant viral transcripts of N mRNAs and the least abundant transcripts of L mRNAs in infected cells (Figure 1.2) (Iverson and Rose, 1981, Conzelmann, 1998). More than 17 lyssavirus species have been described since the 1950s.
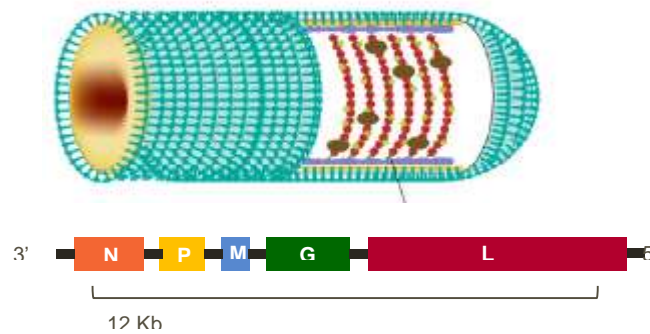
Figure 1.2 Structure of Rabies virus. Rabies genome comprises five genes encoding nucleoprotein (N), phosphoprotein (P), matrix protein (M), glycoprotein (G) and the RNA-dependent RNA polymerase (L). Ribonucleoprotein, formed by RNA and N, together with P and L forms the viral replication complex. RABV G and M regulate the RNA synthesis and affect the RV pathogenesis by regulating virus replication and by facilitating cell-to-cell spread.

These types of viruses can be delivered into a wound from the saliva after an animal bite and they are highly neuropathic. The domestic dog remains the major global reservoir and source of most human infections. Virions undergo retrograde transmission within the neuronal axoplasm, before replication in the central nervous system (CNS) and subsequent passage to the salivary glands (Ugolini and Hemachudha, 2018). The incubation period from the infection to onset of symptoms is generally between 3 and 12 weeks, but it can last longer (several months or even years). The diagnosis can be difficult in the early stages as symptoms may be non-specific and common to many infections. Generally, rabies induces anxiety, headaches and fever. Subsequently, there are spasms of the swallowing muscles making it difficult or impossible for patients to drink (hydrophobia), and respiratory failure sets in.

Rabies virus infects a variety of mammals in many parts of the world, particularly in Asia and Africa (Fisher et al., 2018). It is estimated that between 25,000 and 159,000 people die from rabies each year, almost entirely in developing countries (Hampson et al., 2015). This high number might be due to several reasons, for example, lack of pre-exposure (PrEP) or post-exposure prophylaxis, contact with unvaccinated rabid animals, biodiversity of reservoirs and viruses, diagnostic limitations, inadequate surveillance systems and limited budgets (Octaria et al., 2018).

1.3.2 History of rabies vaccinology and prevention

The development of virus neutralizing antibodies in the host is fundamental to prevent infection (Hooper et al., 1998), and rabies vaccines are efficient at inducing an anti-rabies antibody response. However, a delay in production of neutralizing antibodies during rabies vaccination occurred and it remained unexplained (Hunter et al., 2010). Together with the lack of effective anti-viral treatments for rabies, these factors may be responsible for the high fatality rate associated with the disease (Dacheux et al., 2011).

Since its first application by Pasteur in the late 19th century, vaccines against Rabies have seen great improvements made throughout the 20th century (Rupprecht et al., 2016). These vaccines based on Pasteur's methodology are classified as nerve tissue-based vaccines (NTV) and they consist of attenuated virus in desiccated nerve tissue. Although continuously improved over the years, inactivated NTVs produced in the brains of sheep or goats (Semple) or suckling mice (Fuenzalida) are associated with neurological adverse reactions; therefore, it is strongly recommended that the production and use of NTVs for humans should be discontinued and replaced by modern approaches. Alternatives to Pasteur's methodology included inactivation of infected chick embryos (Koprowski and Cox, 1948) or inactivation of infected suckling mouse brain that has a lower level of myelin compared to the adult brain (Lodmell and Ewalt, 2001). However, due to safety concerns their use as vaccines was never authorized by the World Health Organization (WHO). A further step for rabies vaccines was the development of cell culture for virus propagation. This approach, where rabies virus was grown in a human diploid cell line (Wiktor et al., 1964), led to the development and licensing of a human diploid cell vaccine (HDCV) in the mid-1970s. A more recent alternative to HDCV was a vaccine generated in chick embryo cells (PCE), (Kondo, 1965) which are currently used successfully worldwide. Currently, three human rabies vaccines are WHO prequalified: Rabavert and Rabipur (PCEC vaccines) produced by GSK and Verorab (cell culture vaccine) produced by Sanofi Pasteur. Since the introduction of cell culture vaccines, WHO has advocated the minimum potency of 2.5 IU per single intramuscular dose. However, when larger quantities of antigen are given no additional benefits are seen (Nandi and Kumar, 2010). Furthermore, the use of monoclonal antibodies against rabies was another approach, with "Rabishield" as first licensed human monoclonal antibody (mAb) for human rabies post exposure prophylaxis in India. Table 1.1 gives an overview of currently available human rabies vaccines and their producers.

1.3.3 Routes of vaccine administration and prophylaxis

Rabies vaccines can be given both pre- and post-exposure to virus. Pre-exposure vaccination consists of an intramuscular (i.m) injection of 1 mL vaccine on days 0, 7, 21 and 28. Depending on the vaccine manufacturer, boosting is recommended at 3–5-year intervals (Morris et al., 2007). Post-exposure vaccination is usually accompanied by injection of anti-

rabies immunoglobulin of either human (HRIG) or equine (ERIG) origin and is given typically as an intramuscular injection on days 0, 3, 7, 14 and 30 (Verma et al., 2011).

Nowadays, rabies vaccines are produced as individual doses for intramuscular injection, usually in lyophilised form. After reconstitution with 0.5 or 1 mL of sterile diluent, one intramuscular dose vial assured a potency of ≥ 2.5 IU and can be used for both PrEP and PEP. However, the high production cost of cell culture-based vaccines for intramuscular administration limits their widespread use in many areas where rabies is present. Therefore, moving from intramuscular injection to intradermal (i.d) was promoted by WHO as a safe, immunogenic and cost- and dose-sparing alternative. In this case, less doses are required to complete a full course of PEP by the i.d., route thereby reducing the volume used and the direct cost of vaccine by 60–80% in comparison with standard i.m. injection (Anderson and Shwiff, 2015). Despite these benefits, there is no evidence that vaccines administered intradermally are more potent than those recommended for intramuscular administration (Vigilato et al., 2013).

Table 1. 1 Human rabies vaccines and producers worldwide. HDCV, human diploid cell vaccine; N/A, not available; PCECV, purified chick embryo cell vaccine; PVRV, purified Vero cell vaccine (Rupprecht and Salahuddin, 2019).

Vaccine	Brand	Producer	Country	Cell line	Formulation type
PVRV	N/A	Butantan Institute	Brazil	Vero cells	Liquid
HDCV	Chengdu Kanghua	Chengdu Kanghua	China	Human diploid cells	Lyophilized
PVRV	SPEEDA	Liaoning Chengda Co	China	Vero cells	Lyophilized
PVRV	Verorab	Sanofi Pasteur	France	Vero cells	Lyophilized
HDCV	Imovax	Sanofi Pasteur	France	Human diploid cells	Lyophilized
PCECV	Rabavert	GSK	Germany	Chick embryo cells	Lyophilized
PCECV	Rabipur	GSK	India	Chick embryo cells	Lyophilized
HDCV	Rabivax	Serum Institute of India	France	Human diploid cells	Liquid

1.3.4 Alternative development of rabies vaccines

Despite the efficacy of current commercial vaccines against rabies, there is still extensive work to develop alternatives, ongoing for a number of reasons. For example, the high production cost of cell culture-based vaccines for intramuscular administration limits their widespread use in many areas where rabies is present (Morters et al., 2015). Moreover, most of the vaccines on the market are lyophilized formulations (Table 1.1). Lyophilization is a common

but cost intensive process in the pharmaceutical field (Bhambere et al., 2015). Furthermore, the genetic manipulation approach saw a great development in the last decade, aiming to become a revolutionary technology for future rabies vaccines. Therefore, there is still a need for new and improved vaccines to reduce the toll of rabies disease in the developing world. These vaccines need to be inexpensive, safe, and able to provide sustained protection, preferably after a single administration.

Nowadays, one of the most advanced approach in developing vaccines against rabies is to target virus glycoprotein G. Glycoprotein G is the only surface-exposed protein on the virion particle and many antigenic sites to which neutralizing monoclonal antibodies bind have been identified on this protein (Seif et al., 1985, Prehaud et al., 1988). The aim of this vaccines strategy is to clone the rabies virus glycoprotein into bacterial plasmids and then express the protein in a range of systems or express the glycoprotein in viral vectors(Yarosh et al., 1996, Jallet et al., 1999, Lodmell and Ewalt, 2001). The list of vaccines based on rabies glycoprotein approved for human use include V-RG (Recombinant vaccinia rabies glycoprotein vaccine) and ONRAB (Recombinant human adenovirus rabies glycoprotein vaccine). These vaccines were proven to induce high neutralizing antibodies titers and to efficiently prevent infection in small animal models (Faber et al., 2002, Faul et al., 2008, Zhao et al., 2010). However, due to the high production costs and low acceptance for human use, they have been unable to challenge existing vaccines. Therefore, genetic manipulation of the viral genome seemed to be a valid rational strategy. The first pioneering approach has been done by Conzelmann and Schnell, who recovered the attenuated, fixed strain of rabies virus SAD B19, from a plasmid-encoded genome (De Nardo et al., 2018). This opened a new avenue for research on rabies virus biology and rabies vaccine development through manipulation of the rabies virus genome.

1.4 Nucleic acid based vaccines

Nucleic acid-based vaccines such as viral vectors, plasmid DNA, and mRNA have emerged as an alternative vaccination approach in the last few decades, aiming to address several unmet medical needs (Rappuoli et al., 2011). Nucleic acid–based vaccines have attracted researchers' attention because of their promising ability to elicit immune responses, particularly in the case of cell-mediated responses, in a safe manner. However, so far there is still no licensed nucleic acid–based vaccine for human use (Sardesai and Weiner, 2011). The reason might be due to several factors; for example, recombinant viral vectors are shown to be efficient delivery systems, but due to antivector immunity, production limitations, and safety issues, their use is restricted (Uematsu et al., 2012). Regarding plasmid DNA (pDNA) vaccine, even though they are much safer and broadly effective in small animal models, a large dose of DNA is required to induce a potent immune response in humans (Moon and Wilusz, 2012). These

disadvantages have been partially overcome through optimization of pDNA constructs, coexpression of immune-stimulatory molecules, and improved delivery technologies. Ongoing clinical trials will ultimately determine if these improvements in pDNA vaccines are sufficient to generate practical human vaccines (Margalith and Vilalta, 2006, Nguyen et al., 2009b). One of the most recent alternatives to pDNA is mRNA technology (Geall et al., 2013, Petsch et al., 2012). The advantages are numerous; first, mRNA requires delivery into the cytoplasm of the cells to be translated, while pDNA must be transported across the nuclear membrane which is usually very challenging (Luo and Saltzman, 2000). Second, the integration of pDNA into the host genome post-transfection might affect pDNA safety; on the other hand, RNA technology does not require any intercalation process with a consequent safer profile. Moreover, mRNAs induce transient antigen expression, while DNA vaccines provide a long-lasting expression. Although a transitory gene expression might be desirable as it minimizes potential risks of genetic transformation, this inevitably affects mRNA potency, with a consequent need of vaccine dose increase. A possible strategy to overcome this issue is to use a self-amplifying RNA platform.

1.4.1 Self-Amplifying RNA Vaccines

Nonamplifying mRNAs have several advantages including a simple structure, relatively small size of the RNA compared to a self-amplifying molecule (2-3 kb versus 10 kb), and the lack of additional proteins which might be targets of undesirable immune responses (Schlake et al., 2012). However, the level of antigen expression is low and time-limited due to mRNA short half-life and *in vivo* instability (Kallen et al., 2013). Nonamplifying mRNA contain 5 key elements: cap structure (m^7Gp_3N (N: any nucleotide)), a 5' untranslated region (5' UTR) situated immediately upstream of the translation initiation codon, an open reading frame (ORF) that encodes a gene of interest (GOI), a 3' untranslated region (3' UTR), and the tail of 100–250 adenosine residues (poly(A) tail) of variable length) (Atkins et al., 2008). Thus, mRNA molecules encode only the antigen of interest.

In the case of self-amplifying RNA (SAM) the conventional ORF is larger and encodes four nonstructural proteins (nsP1-4) and a subgenomic promoter. Moreover, the nucleic acid has been built around an α-virus genome, in which the structural genome of the alphavirus that allow the generation of viral particles have been replaced with the genes expressing the antigen of interest (Chatterjee and Pal, 2009). However, significant elements that induce the amplification process of the virus have been left, such as polyproteins which can be cleaved in RNA dependent polymerase that are able to replicate the RNA in multiple copies. This leads to significantly greater immune responses than conventional RNAs. Once SAM reaches the cytosol of a cell, the released mRNA together with the host cell ribosome produce the four functional components of RNA-dependent RNA polymerase (RDRP) or viral genome replication apparatus: nsP1, nsP2, nsP3, and nsp4 (Fros and Pijlman, 2016). These nsPs

transcribe full-length negative-strand copies from the initial native mRNA. This copy will be used as template for two positive-strand RNA molecules: the longer genomic mRNA and the shorter, colinear subgenomic mRNA that corresponds to the 3' third of the genomic RNA. This subgenomic mRNA (also known as the 26S RNA), is transcribed at extremely high levels, allowing the amplification of mRNA encoding the vaccine antigen (Hekele et al., 2013). This auto replicative machinery induces greater and long-lasting antigen expression levels (Figure 1.2). There has been extensive work on delivery of self-amplifying RNA using viral replicon particles (VRPs) where RNA is packaged in a viral particle (e.g., alphavirus) (Shin et al., 2012). As VRPs do not encode the structural proteins needed to spread from cell to cell, they are single-cycle infectious particles. Such VRPs have safely elicited potent immune responses in multiple animal models and in humans (Perri et al., 2003, Rayner et al., 2002).
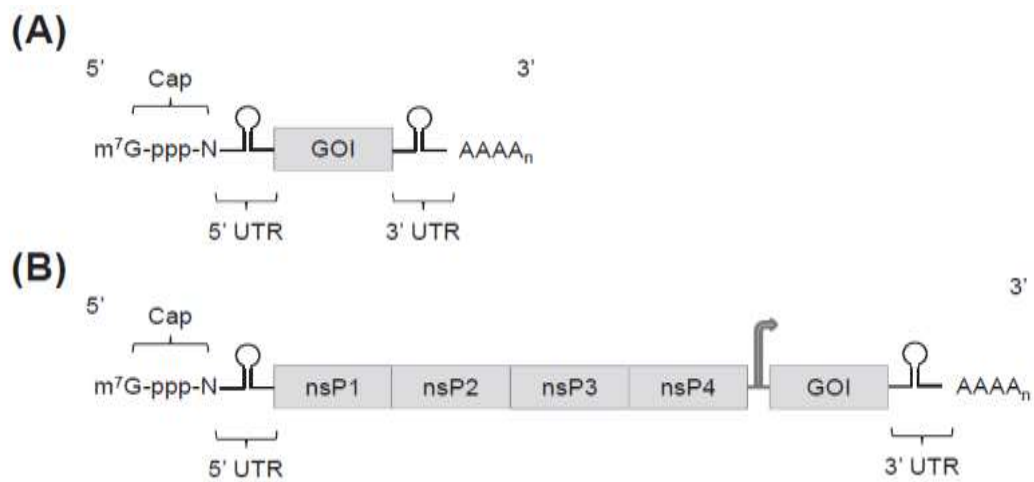
Figure 1. 1 Characterization of nonamplifying mRNA and self-amplifying RNA vectors. (A) Schematic representation of a mature eukaryotic mRNA containing a cap structure (m7Gp3N (n: any nucleotide)), the 5'-untranslated region (5'UTR), an open reading frame encoding a gene of interest (GOI), the 3'-untranslated region (3'UTR), and a tail of 100–250 adenosine residues (poly(A) tail). (B) Schematic representation of a self-amplifying RNA derived from an alphavirus containing a 5'cap, nonstructural genes (nsP1–4), 26S sub genomic promoter (open arrow), the GOI, the 30-untranslated region (3'UTR), and a poly(A) tail (Brito et al., 2014a).
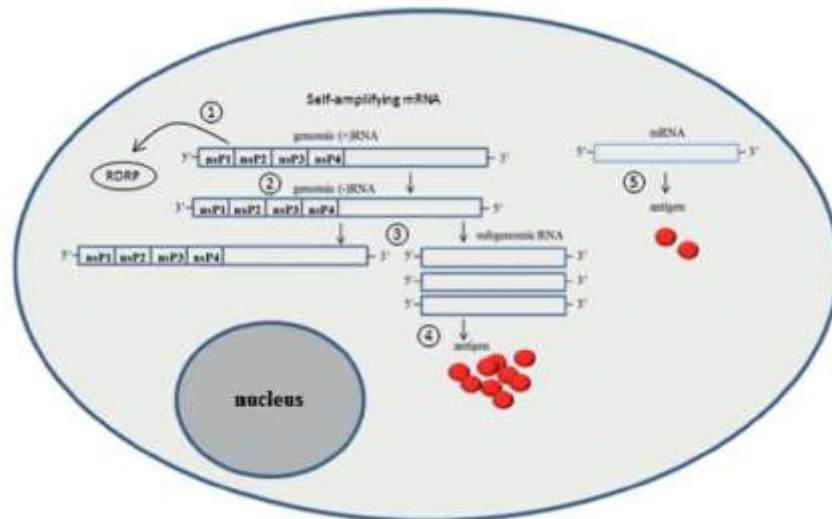
Figure 1. 2 Schematic illustration of difference between self-amplifying RNA and 'conventional' mRNA translation. After the cell delivery, self-amplifying RNA produce the antigen in four phases. 1) The ORF of the genomic (+) RNA encodes for the nonstructural proteins (nsP1, nsP2, nsP3, nsP4) that produce a RNA-dependent RNA-polymerase (RDRP) complex; 2) RDRP generates a genomic (-) strand; 3) RDRP generates from the RNA (-) strand a genomic (+) strand and the sub genomic RNA; 4) the translation of the sub genomic RNA produces the antigen. 5) The conventional mRNA can directly express the antigen (Iavarone et al., 2017).

1.4.2 Delivery of self-amplifying RNA vaccines

One of the main issues which limits the growth of gene therapies based on RNA and DNA is delivery (Whitehead et al., 2009). The reasons behind that are multiple. First, naked nucleic acids are susceptible to degradation processes in biological fluids, so thus their accumulation in target tissues after systemic administration is not completely achieved. RNA-degrading enzymes (ribonucleases or RNases) can be classified in three main categories: endonucleases (which cut RNA internally), 5' exonucleases (which hydrolyze RNA from the 5' end), and 3' exonucleases (which degrade RNA from the 3' end) (Houseley and Tollervey, 2009). These enzymes are known to catalyze transesterification at a specific site (after purines) by promoting attack of the 2' hydroxyl group on the phosphate backbone followed by hydrolysis of the cyclic phosphate diester formed in the first step. Further, RNA and DNA penetration into target cells is challenging due to electrostatic repulsion between nucleic acids and the cell membrane, both negatively charged. In addition, since they are highly hydrophilic, vectors containing nucleic acid are rapidly recognized and eliminated by the immune systems (Bowie and Unterholzner, 2008). Thus, considering these obstacles, it is evident that a nonviral delivery of the nucleic acid to the cell cytoplasm is required to obtain significant antigen biosynthesis.

Over the last 30 years efforts have been made by researchers to develop delivery systems that allow the therapeutic application of genetic drugs. Transportation of RNA or DNA can be achieved via different non-viral delivery like physical delivery technologies such as electroporation or ballistic particle-mediated delivery strategies or chemical particulates made by lipids, polymers, emulsions, or other. These particles have been described in the literature for pDNA, antisense RNA, siRNA, and mRNA transportation, (Deering et al., 2014) aiming to increase nucleic acid cell uptake. The need to enhance cellular internalisation is due to the intrinsic hydrophilicity and strong net negative charge of RNA, which significantly limit the association with the cell membrane. One of the strategies to circumvent this is to electrostatically complex RNA with cationic lipids or polymers (Cu et al., 2013b).

These particles contribute towards enhancing the potency of the vaccine itself and thus they can be classified as vaccines adjuvants. An adjuvant is an ingredient of a vaccine that helps to enhance the immune response (Carter and Reed, 2010). Adjuvants can act as immunostimulants and/or delivery systems. Immunostimulants interact with specific receptors - like membrane-bound PRRs include Toll like receptors (TLRs) and C-type lectin receptors (CLRs) or cytoplasmic PRRs include NOD-like receptors (NLRs) and RIG-I-like receptors (RLRs) - while delivery systems increase the immune response by different mechanisms, depending on their characteristics. Adjuvants are essential for enhancing and directing the adaptive immune response to poorly immunogenic vaccine antigens. This response is mediated by two main types of lymphocytes, B and T cells (Harandi et al., 2009). An adjuvant or immunopotentiator should stimulate high antibody titers, but this process should not induce toxicity or harmful side effects after injection into either animals or human beings. The main function of an adjuvant is to stimulate immune response against a range of antigens, even with small quantities of poorly antigenic substances, preferably in a small number of injections or administrations. These objectives seemed not to be easy to achieve for many reasons like cost and the complex preparation of the injection mixture, and the high reactivity in toxicology tests(Bailey et al., 2014) .

1.5 Non-viral delivery via particulates
1.5.1 Aluminium salts
Aluminum gels or salts have been used as adjuvants since the 1930s (Baylor et al., 2002, Bailey et al., 2014). Aluminum phosphate and Aluminum hydroxide are currently employed, and they can load antigen by direct adsorption. Electrostatic forces (between negatively charged proteins and aluminum hydroxide, and between positively charged proteins and aluminum phosphate) as well as covalent bonds (between antigen phosphates and hydroxyl groups on the adjuvant) are the main interactions occurring in the process (Hem and Hogenesch, 2007). These adjuvants are prepared in house by vaccine companies or purchased

from manufacturers such as Brenntag Biosector, Chemtrade, and SPI Pharma. They are sometimes referred to by their tradenames, such as Alhydrogel, Rehydragel, and Adju-Phos. Another aluminum-containing adjuvant that is commonly used in preclinical experimental studies is ImjectTM Alum (ThermoFisher Scientific). However, this adjuvant is composed of amorphous aluminum hydroxycarbonate and crystalline magnesium hydroxide (Hem et al., 2007).

Despite the extensive use during the last 70 years, the mechanism by which alum enhances the immune response remains disputed. Several mechanisms operate simultaneously to alum adjuvanticity and a full understading might be not trivial. Currently, studies tried to give a satisfactory explanation of the mechanisms that underlie the immune-enhancing effect of aluminum adjuvants. It was reported that adsorption of antigen, although not always, usually enhances the immune response. Adsorption induce precipitain of soluble antigens, which enhances uptake through phagocytosis by dendritic cells(Morefield et al., 2005). Moreover, it favoured antigen presentation, as indicated by increased expression of MHC II-peptide complexes and increased activation of CD4 T cells(Ghimire et al., 2012). Finally, it increases antigen retention at the injection site, enhancing time for recruitment by antigen-presenting cells. However, it was observed that a short-term depot is not necessary for the effect of aluminum adjuvants(Hutchison et al., 2012). Injection of aluminum-adjuvanted vaccines induces a limited amount of necrosis of tissue cells at the site of injection, which may lead to the limited release of some "danger-associated" molecular patterns, including DNA(Marichal et al., 2011), uric acid (Kool et al., 2008), ATP(Riteau et al., 2012), heat shock protein,(Wang et al., 2012b) IL-1α and IL-33 which are molecules that recruit and activate inflammatory cells(Li et al., 2008).

Dendritic cells play a critical role in the immune-enhancing effect of aluminum adjuvants as depletion of these cells impairs the immune response. Aluminum adjuvants increase the transport of antigens via migratory dendritic cells from the injection site to the draining lymph node (Liang et al., 2017) and induce the differentiation of monocytes into dendritic cells. Aluminum adjuvants activate the NLRP3 inflammasome which results in cleavage of pro-IL-1β into IL-1β by caspase-1(Li et al., 2008). However, deletion of MyD88, which is required for signaling through the IL-1 receptor, does not impair the antibody response to aluminum adjuvanted vaccines, suggesting a redundant role of IL-1β in the immune-enhancing effect of aluminum adjuvants (Schnare et al., 2001). Aluminum adjuvants activate phosphoinositide 3-kinase and calcineurinNFAT.122–124 Both pathways may be initiated by the binding of aluminum adjuvants to cell membrane lipids and were dependent on Syk. Activation of NFAT required LPS priming of dendritic cells and led to the secretion of IL-2. Aluminum hydroxide adjuvant also activates the complement cascade(Ramanathan et al., 1979).

However, aluminum adjuvants induce only weak Th1 and Th17 responses, which may not be necessary for the induction of protective immunity against certain infectious diseases, such as malaria and tuberculosis(Hogenesch et al., 2018).

1.5.2 Emulsions

Nanoemulsions are thermodynamically stable isotropic systems in which two immiscible liquids (typically water and oil) are mixed to form a single phase, often with the help of appropriate surfactants/co-surfactants (Souto et al., 2011a). Oil-in-water or water-in-oil emulsions have been used as vaccines adjuvants in the early 1990. One of the first formulations was Freund's Complete Adjuvant (FCA) which combined a killed mycobacteria (Freund et al., 1937) with water-in-oil emulsion (known as Freund's Incomplete Adjuvant; IFA). This formulation was proven to be highly potent in improving immune responses, inducing predominantly Th1 and Th17 biased response with some Th1 cellular response (Bandholtz et al., 2002). However, due to its elevated toxicity and reactogenicity caused partially by the poor quality of the oil, its application in clinical trials was not possible.

A safer alternative to Freund's Incomplete Adjuvant is MF59, which was formulated more than 60 years later. MF59 is a squalene based emulsion and it was approved for use in a human vaccine, Fluad, for seasonal influenza for the elderly in Europe (O'Hagan et al., 2012). Once injected i.m., this emulsion creates an 'immunocompetent environment' within the muscle, that could be exploited by co administration of antigen. Moreover, it leads to recruitment of immune cells into the injection site, thus favouring antigen presentation and DCs maturation and differentiation. (Ott et al., 1995).

Besides Fluad, there are four more adjuvanted influenza vaccines containing squalene emulsions approved for use; for example, Aflunov and Focetria which are MF59 adjuvanted for pandemic influenza or Prepandrix and Pandremix which are AS03 adjuvanted for prepandemic influenza. In addition, squalene-based emulsions have been used in clinical trials for a range of vaccine candidates, including those targeting HSV, HIV, HCV, and CMV (De Gregorio et al., 2008). AS03 is an adjuvant system composed of the immunostimulant α-tocopherol, squalene and polysorbate 80 in an oil-in-water emulsion (Brigelius-Flohe and Traber, 1999). It is widely reported that AS03-adjuvanted vaccines enhance the vaccine antigen-specific adaptive response by activating the innate immune system locally and by increasing antigen uptake and presentation in draining lymph nodes. This phenomenon seems to be related to the presence of *a*-tocopherol in the emulsion. Furthermore, the combination of prepandemic H5N1influenza vaccine and AS03 increased levels of anti-influenza antibody, assuring protection against disease and against virus replication of influenza strains homologous and heterologous to the vaccine strain (Garcon et al., 2012). Nonclinical and clinical data demonstrated the ability of AS03 to induce superior adaptive responses against

the vaccine antigen, mainly in terms of antibody levels and immune memory (O'Hagan et al., 2013).

The reason for using oil-in-water particles carrying antigens is that they have a good safety profile, they are efficiently endocytosed by antigen presenting cells and, because of their small size, they can readily pass from injection sites into lymphatics (Seubert et al., 2008). Squalene-based emulsions have also been applied for pDNA vaccines delivery, where they clearly improved vaccine potency (Ott et al., 2002). More recently, Brito and co-workers developed a positively charged version of MF59 by adding the cationic lipid DOTAP for delivery of self-amplifying RNA (Brito et al., 2014a).This combination prevents RNAse-mediated degradation of nucleic acid and allows the delivery system and RNA to be formulated separately and mixed just before administration. CNE resulted to be efficacious *in vivo* for several diseases, including RSV, CMV, and HIV, inducing high immunogenicity even at low antigen doses (Bogers et al., 2015).

MF59 based emulsions require to be formulated into nanodroplets, as none of the individual components of MF59 are an effective adjuvant. (Calabro et al., 2013); further emulsions act as adjuvant by creating an immunostimulatory environment at the injection site, promoting recruitment and activation of antigen presenting cells in a toll-like receptor independent manner involving ATP (Seubert et al., 2008, Vono et al., 2013).

1.5.3 Nanoparticles

Nanoparticles (NPs) are solid particles ranging in size from 1 to 1000 nm (1 µm). They consist of macromolecular materials and can be used therapeutically or prophylactically, for example, as adjuvants in vaccines or drug carriers, in which the biologically active material is dissolved, entrapped, or encapsulated, or to which the active principle is adsorbed or chemically attached. Polymeric particles are often made of hydrolytically degradable polyesters such as poly (D, l-lactic-coglycolic acid) copolymers (PLGA), poly (D, l-lactide) (PLA), polycaprolactone (PCL) or poly (ortho esters) (POE) (Johansen et al., 2000). Several polymers have been approved by the U.S. Food and Drug Administration (FDA) for medical applications. However, no NP formulation has been approved for vaccination so far. These materials can interact with APCs, presenting antigen to specific CD8+ CTL. It has been reported that antigens delivered by PLGA particles are able to escape endosomal degradation and reach the cytoplasm at a significantly higher level than other antigen forms, and that these antigens are presented on MHC class I more efficiently and for significantly longer durations (Hedley et al., 1998).

It has been seen that PLGA NPs enhanced vaccine accumulation into lymph nodes (LNs) increasing cellular and humoral immunity to a variety of antigens *in vivo* (Reddy et al., 2007). Many studies reported that nanoparticle characteristics such as size, shape or surface

properties can significantly influence their biological activity (Morachis et al., 2012). These attributes might affect targeting to specific cells, antigen uptake and the type of immune response.

NPs can be taken up by cells mainly through two pathways - phagocytosis and pinocytosis (Khalil et al., 2006). Particles with similar size as bacteria are efficiently recognized and taken up by APCs. On the other hand, NPs with a size between 20 and 200 nm are preferentially taken up by DCs through the pinocytosis mechanism, while larger particles (between 0.5 to 5 μm) are mainly engulfed by macrophages through macropinocytosis and phagocytosis (Xiang et al., 2006). Particle size can also affect the uptake efficiency and the immune response induction by APCs. Furthermore, size affected the kind of immune response. Previous studies have shown that PLGA NPs of around 300 nm generate a better DC maturation and more efficient Ag-specific immune responses (IgG2a and CD8+ T lymphocyte) than microparticles counterparts *in vivo* (Wischke et al., 2008). Although optimal size for efficient uptake and immune induction has not yet been established, particles seem to be able to trigger either humoral or cytotoxic immune responses according to their diameter, probably due to the different endocytosis pathway (Joshi et al., 2013). Moreover, particles shapes can influence cellular uptake. Generally, polymeric non-spherical NPs improved membrane attachment, but it reduced uptake by APCs. Thus, this orientation facilitates phagocytosis initiation but leads to slower internalization of these particles (Champion and Mitragotri, 2006). Nevertheless, surface charge has been reported to influence the uptake of NPs. Positively charged particles are easily taken up by APCs, due to charge-to-charge interactions, and they can migrate to LNs; on the contrary, cellular uptake is reduced for negatively-charged polymeric particles, therefore they tend to accumulate to the injection site, prolonging antigen presentation (Yue et al., 2011). Hydrophobicity is another attribute that contributes to NP uptake and immunogenicity. Literature concluded that hydrophobic particles induce greater immune response compared to their hydrophilic counterparts (Liu et al., 2013).

These nanocarriers have been widely employed in many different fields such as drug delivery, imaging, and detection of apoptosis. However, the main area of application is cancer therapy, where they are often used to deliver anticancer drugs (Nagpal et al., 2010). In the last few decades, many papers reported the association of nanoparticles and gene therapy. The combination of DNA/RNA with NPs made from biodegradable polymers was proven to enhance transfection and the efficiency of the process is dependent on complex size, complex stability, toxicity, immunogenicity, protection against DNase degradation and intracellular trafficking, and processing of the DNA/RNA. Furthermore, the degradation of the polymer can be used as a tool to release the plasmid DNA into the cytosol (Borchard, 2001). The nucleic acid can be either encapsulated within or adsorbed onto the surface of the NP. The

former option assures antigen protection which may otherwise degrade rapidly upon injection or induce a short-lived, localized immune response. Moreover, the latter allows presentation of RNA/DNA to the immune systems in a comparable manner to pathogens , thereby generating a similar response (Williamson, 2013). For example, it has been seen that Polyethyleneimine (PEI) based nanoparticles were efficient tools for HPV16 E7 gene transfection in COS-7 cells, but toxicity was observed *in vivo*. In addition, chitosan-linked PEI (CP) nanoparticles were used to deliver plasmid encoded IL-12 *in vivo*. CP/DNA complex was found to be able to efficiently deliver IL-12 *in vivo*, enhancing the antitumor effects on ascites tumour bearing mice (Zhao et al., 2012). Moreover, PLGA/ cetyltrimethylammonium bromide (CTAB) microparticles were recently moved into stage I clinical trials by Novartis for HIV-1 DNA vaccination. PLGA is one of the most widely studied polymers of interest in the vaccine field (Nguyen et al., 2009b). For example, DNA encoding hepatitis B surface antigen (HBsAg)-encapsulated in PLGA nanoparticles could induce enhanced immunity in mice. In addition, PLG encapsulated DNA encoding human papillomavirus antigen has been tested in phase I and II human clinical trials (Espuelas et al., 2005).

A valid alternative to polymeric nanoparticles seemed to be solid lipid particles (SLNs). SLNs are aqueous colloidal dispersions usually in the submicron range (10–1000 nm) and they were first applied as novel carrier for intravenous injection in the early 1990s (Schwarz et al., 1994). SLN consist of a solid matrix where biomolecules can be incorporated. In contrast to other delivery systems, SLNs are less widely studied with a PubMed search identifying only around 200 publications associated with these systems. As delivery systems, solid lipid nanoparticles can offer a range of advantages including high stability in body fluids and tissues, sustained drug release, biodegradability, ease of manufacture and the capacity to scale up to industrial production levels at relatively low cost (van Swaay and deMello, 2013, Joshi and Müller, 2009). In terms of their application, SLNs are most commonly explored as solubilising agents for the delivery of poorly soluble drugs, due to the hydrophobic nature of the particle's matrix. However, they have also been investigated for the delivery of nucleic acids proteins, antigens, or in the food industry (Weiss et al., 2008, Cerqueira et al., 2014) as carriers for bioactive compounds or to protect biomolecules against degradation.

An area of interest is in the development of novel adjuvants. Studies have demonstrated that SLNs have an adjuvant activity and the intensity is related to the size; particles with a diameter of more than 100 nm exhibited a clear adjuvant activity, whereas SLNs with size below 100 nm, in various concentrations, revealed a lower adjuvant activity (Kim et al., 2008). More precisely, SLNs with size >100nm induced the highest antibody titre against mycoplasma bovis antigen in chicken. Furthermore, SLNs in association with interleukin 2 (IL-2) have been shown to increase antibody titre, spleenocyte proliferation, and secretion of IFN-γ and

IL-4 cytokines. The adjuvant effect of SLNs is related to their ability to protect sub-unit antigens from rapid degradation *in vivo*, and to promote delivery and targeting of antigen presenting cells (Almeida and Souto, 2007). Being in the solid state, the lipid matrix of SLN will be slowly degraded with a consequent longer lasting exposure of the loaded antigen to the immune system. Furthermore, the addition of sterically stabilizing surfactants that hinder the anchoring of enzyme complexes can reduce the degradation speed more (Olbrich and Müller, 1999). Literature reported a comparison of SLN with FIA in terms of adjuvanticity in sheep. Two solid lipid particles formulations induced 43 and 73% higher antibody titers compared to FIA used as standard. Given these promising data, SLN are currently being optimized e.g. on surface properties to enhance immune response.

Although SLNs were widely employed for the delivery of poorly soluble drugs, their application for RNA and siRNA delivery has been limited, although recent studies have tested cationic solid lipid nanoparticles (cSLN) as carriers for nucleic acids (Kim et al., 2008). SLNs in combination with nucleic acids are known as "SLNplexes". It has been suggested that the interaction between nucleic acids and SLNs is mainly through adsorption of the nucleic acid to the particle surface thanks to the inclusion of cationic lipids to anionic SLNs. These studies have clearly revealed the importance of endocytosis in nanoparticle internalization and the subsequent need for endosomal escape to release RNA in the cytosol (Minchin and Yang, 2010).

Table 1. 2 Examples of SLN formulations encapsulating water soluble drugs and their method of manufacture. LE (loading efficiency).

Production method	Formulation	Drug	LE%	Ref.
double emulsion method (w/o/w) and solvent evaporation	Lecithin and triglyceride	Catalase	50	(Qi et al., 2011)
	Phosphatidylcholine and tripalmitin	Catalase	78	(qi et al., 2012)
double emulsion and melt dispersion	stearic acid or a mixture of stearic acid and crodamol	Sulforhodamine 101	60	(Becker Peres et al., 2016)
high pressure homogenisation cold dispersion	Witepsol E 85, Softisan 142, propyleneglycol, Superpolystate, cetyl alcohol	Lysozyme	40	(Almeida et al., 1997)
	stearic acid	Cyclosporine	70-90	(Zhang et al., 2006)
high pressure homogenisation hot dispersion	stearic acid	Cyclosporine	80	(Zhang et al., 2000)
Warm microemulsion	Egg lecithin, stearic acid	Thymopentin	<5	(Morel et al., 1996)
	mixture of stearic acid and Epikuron 200,	Cyclosporine	13	(Ugazio et al., 2002)
	stearic acid and lecithin	Insulin	38	(Zhang et al., 2006)
supercritical fluid	Gelucire 50-02 and Dynasan 114	bovine serum albumin	13	(Ribeiro Dos Santos et al., 2002)
	Phosphatidylcholine and tristearin	insulin and recombinant human growth hormone	<3	(Salmaso et al., 2009a)
	tristearin/phosphatidylcholine/dioctyl sulfosuccinate	Insulin	<3	(Salmaso et al., 2009b)
Solvent displacement	Monostearin	Gonadorelin	50	(Hu et al., 2004)
	Lecithin	Insulin	27	(Reithmeier et al., 2001)

It has been demonstrated that cationic SLN produced by modification with N, N-di-(β-stearoylethyl)-N, N-dimethylammonium chloride (EQ1) efficiently transfected the galactosidase expression plasmid pCMVβ in vitro. For instance, SLN-encapsulated antisense oligodeoxyribonucleotide G3139 demonstrated greater immunostimulatory property and antitumor activity compared to its free counterpart (Pan et al., 2009). Further, Tristearin:

DOTAP SLNs loaded with siRNA resulted in prolonged siRNA release after intradermal injection in mice (Lobovkina et al., 2011).Furthermore, it was highlighted that the addition of Protamine to a SLN: pDNA complexes reduced cytotoxic and enhanced transfection efficiency in Na1300 cell line (Vighi et al., 2010). However, given the intrinsic lipid nature of the matrix, less work has been done for the development of SLNs encapsulating water soluble biomolecules, due to poor drug loading. Some of the papers combining solid lipid particles and hydrophilic drugs are listed in Table 1.3. Although challenging, the application of SLNs as entrapment agents for nucleic acids seemed to be promising.

1.5.4 Liposomes and lipid nanoparticles

Liposomes are vesicles made of one or more concentric lipid bilayers alternating with aqueous cores (Joshi and Müller, 2009). The lipid components are usually phospholipids or other amphiphiles such as non-ionic surfactants, often supplemented with cholesterol and other charged lipids. Bilayers can be in a "fluid" or "rigid" state at ambient temperature, depending on the nature of the amphiphile. Since the 1970s the ability of liposomes or nanoparticles to induce immune responses to incorporated or associated antigens has been well known. Referring to publications in the literature, liposomes seem to be the most commonly used nanosystems for delivery of RNA agents. For years, cationic liposomes have been the standard carriers of RNA (Mallick and Choi, 2014). The use of cationic lipids which can electrostatically bind RNA and DNA provided a way forward. Even though these complexes called "lipoplexes" have proven useful for *in vitro* transfection purposes, their utility *in vivo* is limited due to their large size (>1 μm diameter), instability, positive surface charge, and dose-limiting toxic side effects (Lv et al., 2006a). A mixture of cationic and neutral components could be employed because the positive charge helps not only to increase RNA/DNA loading efficiency but also to bind to the cell surface by non-specific electrostatic interactions and to release nucleic acid from the endosome (Hirsch-Lerner and Barenholz, 1999). Lipoplexes are taken up by APC and mediate MHC class I antigen presentation. Liposomes could promote endocytosis of antigen by DC, monocytes and macrophages. Depending on the kind of lipid employed, liposomes could show immunostimulatory properties and they are taken up by DC. Liposomes offer the advantage of preserving RNA against rapid intracellular degradation by APC, therefore prolonging primary activation of T cells *in vivo*. However, development of liposomes technology has been limited by the complexity of the formulation process and lack of large-scale manufacture (Modlin et al., 2004). Table 1.4 lists more commonly used cationic lipids for adjuvant manufacturing.

Table 1. 3 List of commonly used cationic/ionizable lipids for liposomes, emulsion and particles production.

Lipid	Structure	Physico-chemical properties and key attributes	System	Ref.
DOTMA		Monovalent head group (quaternary amine). 2 unsaturated oleyl chains bound by an ether bond to glycerol. Usually combined with DOPE	Lipoplex /Liposome	(Felgner et al., 1987b)
DOTAP		Monovalent head group (quaternary amine). 2 unsaturated oleyl chains bound by an ester bond. R stereoisomer is the active one.	Lipoplex /Liposome (Combined with DOPE or Chol or protamine sulphate), /Solid lipid nanoparticles/Nanoemulsion	(Kim et al., 2015, Souto et al., 2011b)
DC-Chol		Cholesterol moiety attached by an ester bond to a hydrolysable mithetylethlenediamine (tertiary amine). Usually combined with DOPE	Lipoplex /Liposome/ Nanoemulsion/ Solid lipid nanoparticles	(Zhang et al., 2010, Behr et al., 1989)
DOGS		Multivalent head group (Spermine). 2 saturated octadecyl chains bound by an amide group. Known as transfectam. Has shown better transfection than monovalent counterparts. Usually combined with DOPE	Lipoplex /Liposome	(Yamano et al., 2010)
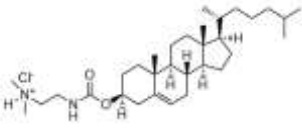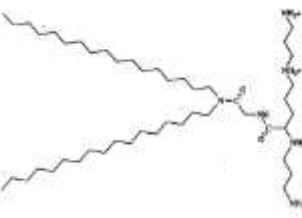
DOSPA		Multivalent cationic head group (spermine). 2 unsaturated oleoyl chains bound. Lipofectamine = DOSPA: DOPE (3:1 ratio). Has shown better transfection than monovalent counterparts.	Lipoplex/Liposome	(Kowalski et al., 2015)
SAINT derivatives		Pyridinium base with a quaternary amine. Two oleyl chains as hydrophobic tail. Usually combined with DOPE	Lipoplex/Liposome	(Adrian et al., 2010)
DOBAQ		Monovalent head group with carboxybenzyl group attached to the amine. 2 oleyl chains bound through ester group	Lipoplex/Liposome	(Vangasseri et al., 2006)
DOEPC		Monovalent head group (ethylphosphocholine) and 2 unsaturated oleyl chains bound through ester bonds. Have shown better activation of co-stimulatory molecules (CD80, CD86) than TAP family (DOTAP)	Lipoplex/Liposome	(Wong et al., 2001)
DODAC		Monovalent head group. 2 acyl chains connected to a quaternary amine. Chloride salt	Liposome	(Wang et al., 2004)
DDA		Monovalent head group. 2 acyl chains connected to a quaternary amine. Bromide salt. May be combined with TDB (CAF01) or DOPE	Liposome	(Henriksen-Lacey et al., 2011b)
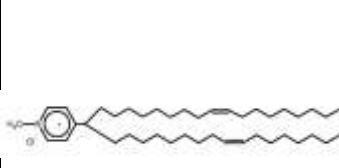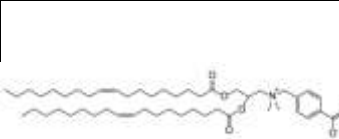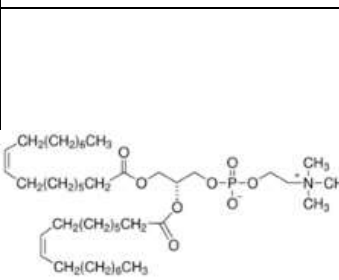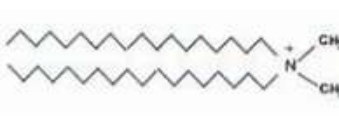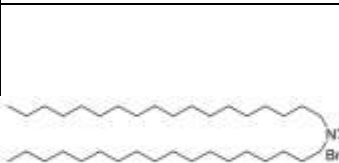
DODAP		Monovalent head group (dimethylammonium propane). 2 oleyl chains bound through ester bonds.	Lipoplex Liposome	(Semple et al., 2001)
DLinDMA derivatives DLin-MC3-DMA DLin-KC2-DMA		Monovalent head group (tertiary amine). 2 linoleic chains bond by different means. May be synthesized or provided by Tekmira Pharmaceuticals. Combination with Chol, neutral lipids and PEGylated lipid.	Stable nucleic acid lipid nanoparticles (SNALP)	(Geall et al., 2012b)
DMRIE		Monovalent head group (quaternary amine). 2 saturated acyl chains connected by ether bonds	Lipoplex /Liposome	(Wang et al., 1996)
Stearylamine		One 18C acyl chain with amine head group	Liposome/Nanoemulsion	(Silva et al., 2016)
DiC14-amidine		Saturated acyl chains. Imine group.	Liposome	(Kim et al., 2004)
DMKE, DMKD		Multivalent head group with. 14C acyl chains bound by ester groups. Strong inducer of CD80 and CD86 in DCs	Lipoplexes/Liposome	(Hirsch-Lerner et al., 2005)
DOPE		Tertiary amine and a phosphate head group linked to two monounsaturated	Liposomes /Solid lipid nanoparticles, / Micelles	(Scarzello et al., 2005)
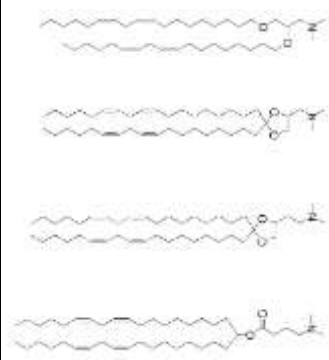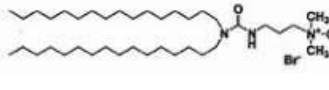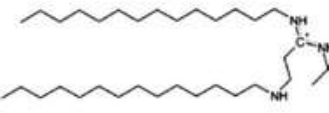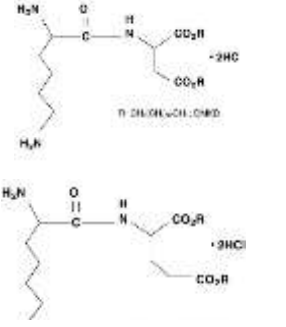
		aliphatic chains through two ester bonds.		
TEPA-PCL		Polyvalent lipid with a phosphate head group linked to a tetraethylene tail through an amide bond.	Liposomes	(Wheeler et al., 1996)
GAP-DLRIE		The basic skeleton of GAP-DLRIE is typical of the 2,3-dioxy-propaniminium class of cationic lipids which also includes DMRIE, DOTAP, DOTMA and DOSPA. This class of cationic lipids has two hydrophobic chains appended to a quaternary ammonium moiety via a polar dioxy-propyl group in a manner affording a central glycerol-like structure.	Liposomes	(Wheeler et al., 1996)

However, it has been seen that, when antigen size and complexity increases (like in virus- or tumour-derived antigens), a higher immune response can be achieved by loading the antigen into the liposome bilayer rather than onto its surface (Barnier-Quer et al., 2013). It has been established that selected cationic lipids containing an ammonium ion head group are immunostimulatory, with dimethyldioctadecylammonium (DDA) salts, 1,2-dioleoyl-3-trimethylammonium-propane (DOTAP) and 3β- [N- (N′, N′-dimethylaminoethane)-carbomyl] cholesterol (DC-Chol) gaining much attention. DOTAP and DC-Chol are commonly cited as transfection agents and vaccine delivery systems for both DNA-encoded (Perrie et al., 2001) and protein (Walker et al., 1992) antigens.

DOTAP is a quaternary ammonium compound coupled with two unsaturated fatty acid chains via ester linkage. DOTAP based liposomes were seen to be highly efficient in transporting plasmid DNA into A549, AGS, Huh7, and COS7 cell lines in a manner independent of

particles size or surface charge. Moreover, DOTAP liposomes effectively delivered siRNA into Human Hematopoietic Stem Cells Differentiating into Dendritic Cells (DC). Results showed that cells were transfected with siRNA for cathepsin S with negligible cytotoxicity and transfection rates above 60%, which was comparable to what was obtained with lentiviral vectors (Martino et al., 2009). Generally, DOTAP-based liposomes have been shown to increase the humoral immune response, with polarization of CD4+ T cells mainly through Th1 phenotype compared with antigen alone (Brgles et al., 2009). Further, these lipids based particles could enhance the immunostimulatory effect of both TLR-2 and TLR-9 ligands triggering MAPK (extracellular signal-regulated kinase and p38) activation in DCs (Yan et al., 2007). This pathway induced DC maturation resulting in an upregulation of CD80, CD83 and CD86 costimulatory molecules with consequent induction of CD4+ Th1 cells and a CD8+ T-cell response. DDA is a quaternary ammonium salt consisting of a nitrogen atom substituted with two methyl groups and two octadecyl groups. DDA is known to induce cell-mediated immunity and delayed-type hypersensitivity. DDA based liposomes have been previously employed as carriers for drugs, as antimicrobial agents and as adjuvants for a range of vaccines for both parenteral and mucosal delivery (Hilgers et al., 1984, Klinguer et al., 2001). In addition, the combination of DDA liposomes and the immunostimulatory glycolipid trehalose dibehenate (TDB), is known as CAF01 and it is currently in phase I clinical trials. This formulation induced strong T-cell response with the T cells producing high levels of IFN-γ and IL-17
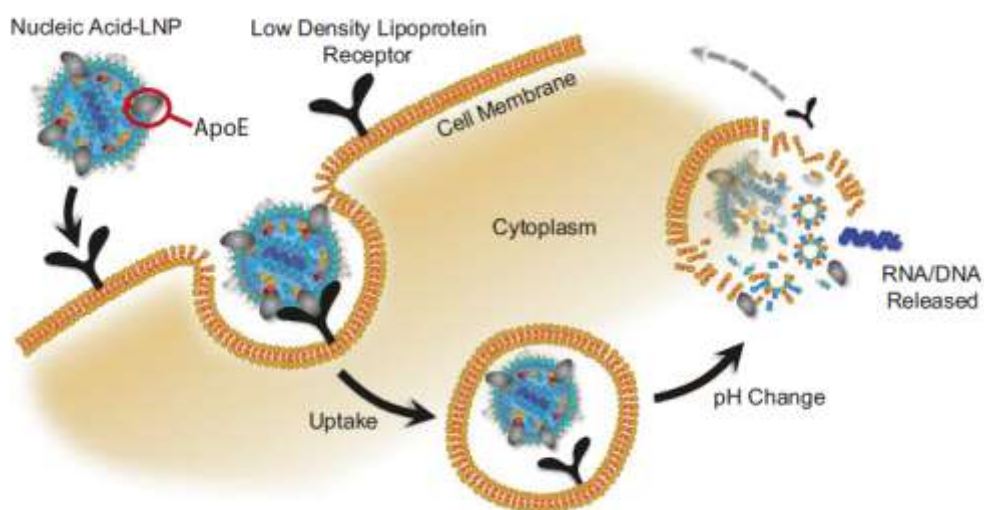
Figure 1.3 Endocytic pathway for Lipid nanoparticles (LNPs) internalization. Lipid nanoparticles resemble low density lipoproteins (LDL) and are taken up by receptor-mediated endocytosis governed by the LDL receptor present on many cell types and Apolipoprotein-E. In the endosome, acidic conditions cause the pH-sensitive ionizable lipids to become cationic where they disrupt the endosome and release their nucleic acid payload A (Thomas et al., 2018).

and low levels of IL-5. When compared with aluminium hydroxide the IgG1 antibody titres were not significantly different, whereas IgG2 antibody titre was significantly higher. It has been seen that CAF01 led to T-cell differentiation into TNF-α+IL-2+ and IFN-γ+TNF-α+IL-2+ multifunctional CD4+ T cells (Lindenstrøm et al., 2009). The adjuvant effect of DDA based formulations is due to their ability to prolong the deposition of the antigen at the injection site and thus lengthening antigen presentation, perhaps through active actin-dependent endocytosis. (Kaur et al., 2012b)

Recently the ionizable cationic lipid 1, 2-dilinoleyloxy- 3-dimethylaminopropane (DLinDMA) has been widely investigated for delivering siRNA *in vivo* (Heyes et al., 2005). DlinDMA and similar cationic lipids are weak bases with a dissociation constant pKa of 6.7. So then, the degree of protonation depends on the pH of the aqueous environment. Thus, while formulating, they can act like bases and become protonated by using acidic buffers, therefore enhancing RNA loading. However, once released *in vivo*, the physiological pH of the body imparts a net neutral surface charge to the lipid with a consequently less toxicity concerns. Furthermore, once into the cell, DlinDMA particulates enter the endosomes where they become protonated, thus facilitating endosomal escape due to destabilising interactions of the endosomal membrane (Figure 1.3). This promotes release of the nucleic acid into the cytosol (Hafez et al., 2001b).

These ionizable cationic lipids are often combined with neutral or helper lipids like DSPC or cholesterol and hydrophilic polymers like PEG to form so called lipid nanoparticles (LNPs). Previous experiments demonstrated that LNPs have an interior lipid core containing the nucleic acid complexed with ionizable cationic lipids organised in inverted micelles (Tam et al., 2013). As reported in literature, delivery of RNA vaccines with LNPs elicits antigen-specific humoral and cellular immune response. In a mouse model, LNP delivery of self-amplifying RNA enhanced Th1 responses, with slightly elevated titres of antigen-specific IgG2a relative to IgG1. Furthermore, antigen-specific interferon-γ producing CD4+ and CD8+ T cell proliferation was enhanced (Cu et al., 2013a).

1.6 Manufacturing challenges in nanoparticle, liposomes and emulsions production

In general, manufacturing of drug delivery systems represents a real challenge and it can be a great obstacle to overcome, given the cost and relative complexity of their production. Multiple characteristics and attributes need to be considered while formulating the final product, including the drug substance, the lipids/polymer and non-lipid/polymer components of the system (Rantanen and Khinast, 2015). Given that pharmacological, toxicological and pharmacokinetic properties of the delivered bioactive molecule can be dictated by components of the delivery system, quantification of the amount

of therapeutic molecule incorporated and retained within the system must be defined. Furthermore, since pharmacokinetic profiles are dictated by the carrier physicochemical properties (e.g. size, morphology, surface characteristics, particles structure and integrity, net charge etc.), these should be characterised and defined (Rantanen and Khinast, 2015). Indeed, these are key critical quality attributes of a product and they are often dependent on the method of manufacture. Given the recent issues seen in the manufacture of liposome and particles and to facilitate the transition of more products from bench to clinic, it is important that new, low-cost and scalable manufacturing methods are developed.

In terms of manufacturing processes for solid lipid particles, high-pressure homogenization and microemulsion-based techniques are the most used methods. These processes have been summarized in Table 1.4. However, these methods have limitations such as poor drug loading capacity, drug expulsion after polymeric transition during storage and relatively high-water content of the dispersions. Furthermore, the drug loading capacity of conventional SLNs is limited by the solubility of drug in the lipid melt, the structure of the lipid matrix and the polymeric state of the lipid matrix. If the lipid matrix consists of similar molecules (i.e. tristearin or tripalmitin), a perfect crystal with few imperfections is formed. Since incorporated drugs are located between fatty acid chains, between the lipid layers and in crystals imperfections, a highly ordered structure cannot hold large amounts of drugs.

Regarding liposomes, there are two main ways of forming them: either to produce large vesicles and then employ size reduction methods (e.g. homogenisation, microfluidisation, high-sheer mixing and sonication), or alternatively bottom up methods, which promote the formation of small vesicles from individual lipid monomers. Commonly, liposomes are produced by the lipid film hydration method. This method gives rise to multilamellar vesicles (MLVs) of several hundred nanometres in size with a broad size distribution. Because it is based on the macroscopic mixing of organic and aqueous phases, it also offers poor batch-to-batch reproducibility. Consequently, additional size reduction techniques (e.g. extrusion or probe sonication) are often required. Although homogeneous liposome dispersions with relatively narrow size distribution can be obtained, scaling-up these methods can be challenging (Bangham et al., 1965). Furthermore, to achieve a homogeneous liposome suspension, generally particle size reduction to below 100 nm is required, and it is difficult to form homogenous populations of larger liposome systems using these methods. Ethanol injection is another popular technique for producing large unilamellar liposomes that consists of rapidly injecting an ethanol solution containing lipids into an aqueous phase (Pons et al., 1993). However, this method is not easy to translate to large scale and is more commonly used to produce SUV. Recently, microfluidic emerged as a valid alterative technique; it enables not only reliable laminar flow dynamics and thus robust liposome formulation, but also ease

of scale-up (Jahn et al., 2004). Moreover, microfluidics promotes effective incorporation of both hydrophilic and hydrophobic drugs simultaneously with higher encapsulation efficiencies compared to conventional techniques.

Table 1. 4 List of the most common methods to manufacture solid lipid nanoparticles (Mukherjee et al., 2009).

High energy approaches	
High pressure homogenization	a) Homogenization of hot pre-emulsion
	b) Homogenization of cold pre-suspension
High shear homogenization	
Ultrasonication	a) Probe ultrasonication
	b) Bath ultrasonication
Electro-spray technique	
Low-energy approaches	
Microemulsion method	
Membrane contactor	
Phase inversion temperature (PIT) method	
Coacervation method	
Double emulsion method	
Approaches with organic solvents	
Emulsification-solvent evaporation	
Emulsification solvent diffusion	
Solvent injection	
Supercritical fluid (SCF) technique	

Generally, whilst the production of large vesicles followed by size reduction is the commonly adopted method at the laboratory scale, such methods of liposome manufacture lack industrial scalability and encapsulation efficiencies are usually low. In contrast, methods that exploit fluidic control to build liposomes from the bottom-up tend to offer more industrial applicability.

Concerning nanoemulsions, they can be generated in different ways. Usually, the preparation method can be distinguished as low-energy (self-emulsification, phase transition, and phase inversion temperature methods) and high-energy methods (high-pressure homogenization and ultrasonic emulsification). For example, the phase inversion temperature method uses the specific properties of polyethoxylated surfactants to modify their partitioning coefficient as a function of the temperature. Continuous systems formed at a temperature close to the phase inversion temperature are broken up by dilution and temperature drop to generate oil-in-water nano-emulsions (Anton et al., 2008). Most of the new methods of emulsifications are based on mechanical processes and are related to the high-energy emulsification techniques.

Alternatively, extrusion process can be used. Here, the dispersed phase is filtered through a microfiltration device and size-tuneable droplets can be prepared. Furthermore, spontaneous emulsification process is another important emulsification technique which occurs when the two bulk phases are brought into contact without stirring during the very rapid diffusion of the organic phase prepared with water miscible solvent i.e. acetone or ethanol in the aqueous phase (Vitale and Katz, 2003).

Regarding polymeric nanoparticles, the most commonly used manufacturing methods involve two main steps: first the preparation of an emulsified system followed by nanoparticle formation either by the precipitation or the gelation of a polymer or by polymerization of monomers. Nanoemulsions can be generated by the methods described above. After emulsion generation, nanoparticle formation can be obtained, for instance, by applying polymer precipitation by solvent removal. Solvent can be extracted from the organic phase by different strategies such as solvent evaporation, fast diffusion after dilution or salting out (Bilati et al., 2005).

The first technique involves the formation of a polymeric nanoemulsion in volatile solvents. After evaporation of the solvent under vacuum, polymer diffuses through the continuous phase of the emulsion. Regarding obtaining nanoparticles by emulsification–solvent diffusion, the polymer solvent used to prepare the emulsion needs to be partly soluble in water (Quintanar-Guerrero et al., 2005). Then, the emulsion is prepared with water saturated with the polymer solvent composing the oil phase and with an oil phase saturated with water as continuous phase. Once the oil-in-water emulsion is obtained, it is diluted with an excess of pure water. Thus, diffusion of additional organic solvent from the organic phase contained in the dispersed droplets can be achieved, leading to the precipitation of the polymer (Quintanar-Guerrero et al., 1997). Furthermore, the emulsification–reverse salting out method is very similar to the method described above. The main difference consists in the composition of the emulsion, which is a mixture of polymer solved in solvent totally miscible with water, i.e. acetone (Ibrahim et al., 1992). To emulsify the polymer solution in the aqueous phase, a high concentration of salt or sucrose (several mol/L), chosen for their strong salting out, are added (e.g. magnesium chloride, calcium chloride, and magnesium acetate). These molecules retain water for their own solubilisation, resulting in modification of the miscibility properties of water with other solvents such as acetone. The precipitation of the polymer dissolved in the droplets of the emulsion can easily be obtained by dilution of the emulsion with a high quantity of water, hence inducing a reverse salting out effect. This dilution reduces salts or sucrose concentration inducing the polymer solvent to migrate out of the emulsion droplets (Allémann et al., 1992).

Other methods to produce nanoparticles from emulsion are to gelify the polymer dissolved in the emulsion droplets. This method requires the use of polymers displaying gelling properties (i.e. agarose). With a polymer like agarose, gels can be formed by cooling down the temperature of the solution which is prepared at a high temperature. Other polymers like alginate and pectin, requires the addition of a second component or alteration of the pH of the polymer solution to induce gelation (Tokumitsu et al., 1999).

Finally, nanoparticles can be obtained by in situ polymerization of a monomer. Herein, the monomer is added in the emulsion instead of a polymer solution and the polymer forms by polymerization. nanocapsules are then obtained by performing interfacial polymerization or polycondensation reactions in emulsions or in microemulsions (Bouchemal et al., 2006).

1.7 New platforms available

In the present study two different methods – microfluidics and microfluidizer - were investigated for nanocarrier production. The aim was to find newer and cost-effective scale up manufacturing methods that answer pharmaceutical companies' requests. Regarding microfluidics, one of the key approaches exploited was miniaturizing the assay systems so it was possible to operate on micron dimension samples, using lab on-a-chip technology. The application of microfluidic tools for carriers manufacturing is based on the theory of a nanoprecipitation reaction resulting from rapid mixing at the nanolitre scale. In contrast to the top-down methods, this nanoprecipitation can produce liposomes and nanoparticles in a one-step process (Bally et al., 2012) with no further disruption of the resulting product. The advantages of microfluidic-based technologies include enhanced control over processing conditions, offering reproducible and robust manufacturing of uniform liposome size distributions and, by working at reduced volumes during development processes, costs can be reduced, whereas throughput is also increased (Jensen, 2001).

Generally, two or more inlet streams (an organic solvent and an aqueous phase) are rapidly mixed together and flow profile in the chamber itself are of low Reynolds numbers and categorized as laminar (Karnik et al., 2008b). Using microfluidic systems, a tight control of the mixing rates and ratio between aqueous and solvent streams is achieved, with low liquid volume required, which facilitates process development by reducing time and production costs. The systems are designed with the option of high-throughput manufacturing and are generally considered as less harsh compared to conventional methods of nanoparticles manufacturing, based on mechanical nanoprecipitation. In microfluidics, a chaotic advection micromixer, a Staggered Herringbone Micromixer (SHM), is used. The fluid streams pass through the series of herringbone structures that allow for the introduction of a chaotic flow profile, which enhances advection and diffusion. A chaotic advection micromixer, as well as flow focusing methods, were shown to allow for scalability, associated with defined particle

size (Belliveau et al., 2012). Sample mixing is essentially achieved by enhancing the diffusion effect between the different species flows. A passive mixing occurs in the chip, where the contact area and contact time of the species samples are increased through specially-designed microchannel configurations. The diminutive scale of the flow channels in microfluidic systems increases the surface to volume ratio and is therefore advantageous for many applications. However, Reynolds number (Re = 1 $\rho v/\eta$) of liquid flows in such microchannels is very small (Lee et al., 2011a). For example, typical water-based microfluidic systems with a channel width of 100 μm and a liquid flow rate of 1 mm/s have a Re around 0,1: in these conditions, turbulent mixing does not occur, and hence diffusive species mixing plays an important role but is an inherently slow process. Consequently, the aim of microfluidic mixing is to enhance the mixing efficiency such that a thorough mixing performance can be achieved within shorter mixing channels, which can reduce the characteristic size of microfluidic devices.

A

B
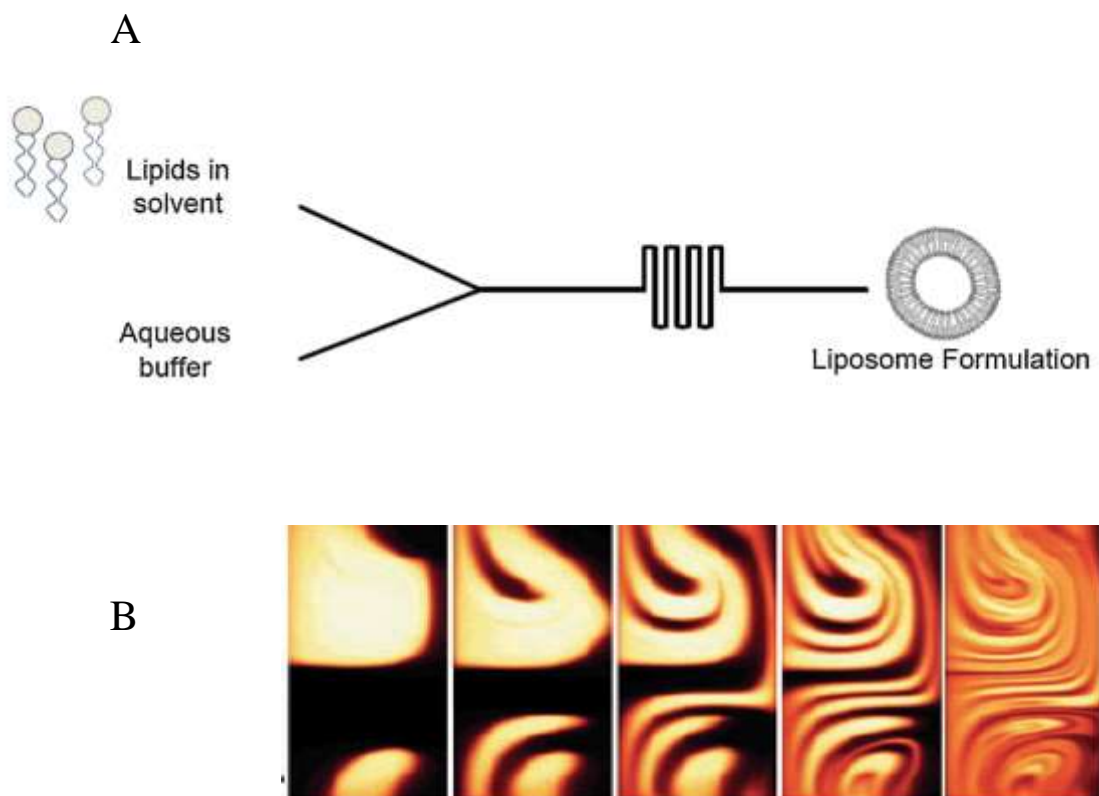
Figure 1. 4 Vesicles and particles formation using microfluidics. a) Schematic description of the liposome and particles formation process based on the SHM design, b) Staggered herringbone micromixer flow investigated by Stroock and co-workers (Stroock and McGraw, 2004).

Due to the inherently laminar characteristics of micro-scaled flows, mixing in passive micromixers relies predominantly on chaotic advection effects realized by manipulating the

laminar flow within the microchannel or by enhancing molecular diffusion by increasing the contact area and contact time between the different mixing species. Also, the geometry of microfluidic mixer is a key feature to control instrument performances. Mixing efficiency of the serpentine microchannel was observed to be twice that obtained in a conventional straight microchannel (Vijayendran et al., 2003).
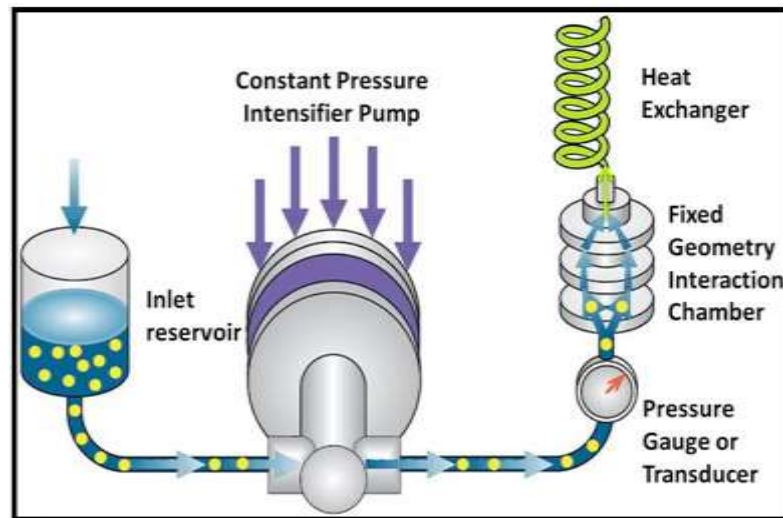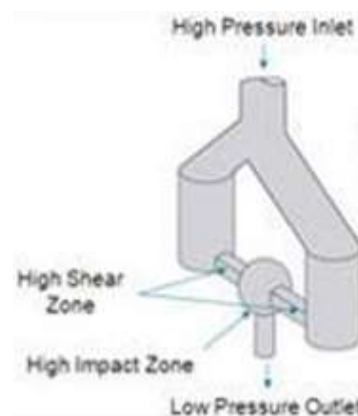
Figure 1. 5 M-110P Microfluidizer for Continuous High Shear Fluid Processing a) Schematic depiction of the liposome and particles formation process using M-110P Microfluidizer b) Y-Type Interaction Chamber: Channel velocities over 400 m/s, channel minimum dimensions typically 50-300 microns, shear rates up to $10^{7}s^{-1}$.

The other method that has been tested in our laboratory was the microfluidisation processing. This technology combines high pressure values to deliver product into the interaction chamber with fixed geometry patented interaction chamber itself (Helgason et al., 2015). Molecules dissolved in fluids with different polarity are loaded in the inlet reservoir. The intensifier pump generates extremely high pressure to accelerate the product into the interaction chamber. In this chamber the pressure energy is converted in kinetic energy. The Y shape of the chamber allows separation of the stream in two microchannel (Chung et al., 2014). The product stream collides upon itself, producing incredible forces of impact and shear which help to reduce sample size and polydispersity (Chung et al., 2014). By changing Microfluidizer parameters like pressure values at which the pump works or number of sample cycles into the machine it has been possible to control particles physico-chemical properties.

1.8 Aim and objectives

Nucleic acid–based vaccines have attracted researchers' attention because of their promising ability to elicit immune responses, particularly in the case of cell-mediated responses, in a safe manner. Additionally, self-amplifying RNA (SAM) technology due to its intrinsic auto-amplification capacity, leads to the generation of multiple copies of the RNA, therefore inducing significantly greater immune responses than conventional RNAs. However, SAM activity might be restricted by enzymatic degradation and limited entry into cells cytoplasm. Hence, nonviral delivery of nucleic acids has been explored.

To achieve this aim, the overall objectives of the work were:

- Formulate different cationic delivery systems - solid lipid (SLNs) and polymeric nanoparticles (NPs), nanoemulsions (CNE) and liposomes, both containing either the cationic lipid 1,2-dioleoyl-3-trimethylammonium-propane (DOTAP) or dimethyldioctadecylammonium (DDA) – using innovative manufacturing technologies (microfluidics and microfluidisation).
- Produce stable and homogeneous cationic particles in combination with a specific self-amplifying RNA (SAM) encoding for the model antigen rabies glycoprotein (SAM-Rabies), which can efficiently encapsulate or adsorbed the antigen thereby protecting it from nucleases degradation.
- Evaluate the potency of delivery systems to successfully transfect different cell lines, therefore enhancing antigen expression *in vitro*.
- Screen a range of cationic formulations to investigate the pharmacokinetics and adjuvant properties of these particles by different routes of administrations in an *in vivo* model.

CHAPTER 2

Scalable manufacturing processes for solid lipid nanoparticles
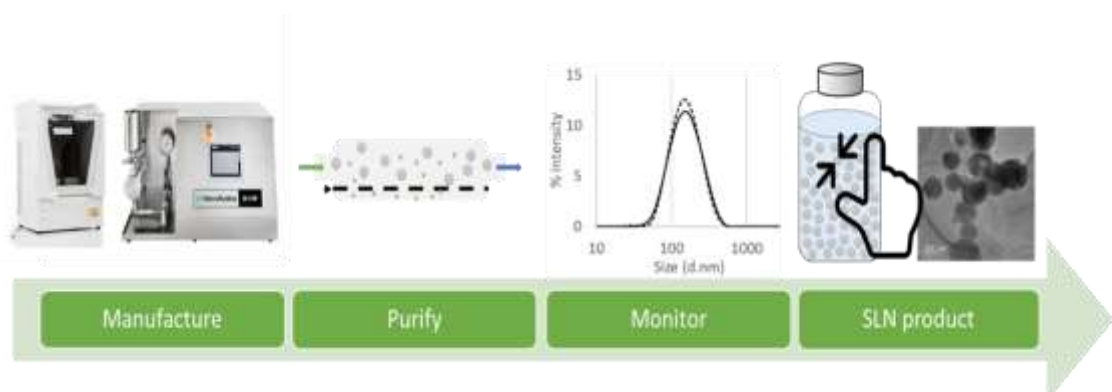
The work presented in this chapter has been previously published in:

1. Drug Delivery Letters (Anderluzzi and Perrie, 2019)
2. Pharmaceutical Nanotechnology (Anderluzzi et al., 2019)

2.1 Introduction

In the development of nanomedicines, there is a wide range of delivery systems available including polymer based systems, protein based systems and lipid based systems. Within the lipid area, liposomes, emulsions and solid lipid nanoparticles can all be formulated to deliver drugs in a controlled and/or targeting mechanism, with each system offering advantages depending on the drug to be delivered, the rate of delivery, the route of administration and the target site. The use of solid lipids to develop solid lipid nanoparticles (SLNs) offers the potential for longer controlled release compared to emulsions and liposomes, because the drug mobility in these systems is reduced. Solid lipid nanoparticles consist of solid hydrophobic core with a monolayer coating of phospholipid. The solid core contains drug dissolved or dispersed in the solid high melting lipid matrix with the hydrophobic chains of phospholipids also embedded in this matrix (zur Mühlen et al., 1998). Due to their lipid nature, solid lipid nanoparticles are biocompatible and they can be manufactured without the use of organic solvents, which is also advantageous (Muller and Stefan, 1999). However, solid lipid nanoparticles have limitations including lack of scale-up manufacturing processes and poor drug loading capacity (Müller et al., 2002). Indeed, currently there are no clinically approved solid lipid nanoparticle-based medical products.

In terms of their characteristics, generally, the solid lipid nanoparticle lipid matrix determines the pharmaceutical properties of the particles. Currently, stabilisers such as surfactants, co-surfactants and coating materials are widely employed in solid lipid nanoparticle formulations. Antioxidants, electrolytes, preservatives, viscosity enhancing agents, adhesives, absorption enhancers and other excipients can also be added to improve formulations attributes. For example, a combination of Tristearin and pegylated lipids can be used to formulate solid lipid nanoparticles; Tristearin or glyceryl tristearate is a triglyceride derived from three units of stearic acid, widely used in the pharmaceutical field due to its high biocompatibility and biodegradability and the fact it is approved for oral and parental administration (Abdelaziz et al., 2019). Poly(ethylene glycol)–distearoylphosphatidylethanolamine (PEG-DSPE) is a linear PEG phospholipid with saturated C18 stearoyl fatty acid (Abou-Saleh et al., 2014). Once incorporated in the particle, the PEG shell remains on the surface of the matrix and it can generate a hydrophilic coating which potentially reduces the *in vivo* clearance of carriers and their opsonisation by plasma proteins (Panyam et al., 2002). The presence of PEG-DSPE could prolong the body circulation time of the carrier and release drugs at a sustained rate in an optimal range of drug concentrations.

As mentioned, despite the advantages of solid lipid nanoparticles and the variety of formulations that can be explored, there remains a lack of cost-effective and scalable production methods and this has hampered the development of solid lipid nanoparticles. Current manufacturing and formulations approaches can be classified into three main groups

– high energy approaches, low-energy approaches and methods employing organic solvents (Battaglia et al., 2015). This includes emulsification, extrusion/homogenisation, solvent evaporation methods and the adoption of supercritical fluids. Depending on the method of manufacture and the drug loaded, drug loading varies widely, and production must be optimised for the given formulation. However, with many of these methods, dispersion quality is often compromised by the presence of micro particles. To overcome these technical issues, two methods were investigated to produce SLNs 1) the application of microfluidisation and 2) microfluidics.

2.1.1. Production of SLNs using microfluidisation

One of the key features of microfluidisation process is the combination of high pressure delivery (which converts into kinetic energy) of the feed-stock into the interaction Y-shaped chamber (Mayhew et al., 1984, Washington and Davis, 1988, Saheki et al., 2012). The Y shape of the chamber separates the stream in two micro-channels. The product stream collides upon itself, producing impaction and shear which reduces the particle size and polydispersity, and by controlling the process parameters (pressure and number of cycles) particle size can be controlled (Mahdi Jafari et al., 2006, Sorgi and Huang, 1996). An additional advantage of this system is the direct scalability of the process from bench to manufacture. Indeed, many papers reported the application of microfluidisation for drug carriers manufacturing, especially emulsions, polymer particles, crystalloid solids and liposomes (Bodmeier and Huagang, 1990, Siqueira et al., 2010, Takahashi et al., 2009, Thompson and Singh, 2006). For example, soy lecithin based liposomes were demonstrated to have a diameter below 50 nm and low polydispersity after the homogenization process (Laye et al., 2008, Gibis et al., 2014, Lajunen et al., 2014). Furthermore, the Microfluidics M110P was used for particles size reduction of three different liposome formulations composed of 1) hydrogenated soy phosphatidylcholine, 1,2-dioleoyl-3-trimethylammonium-propane and cholesterol, 2) 1,2-dimyristoyl-sn-glycero-3-phosphocholine, 1,2-dimyristoyl-3-trimethylammonium-propane (DMTAP) and cholesterol, or 3) egg phosphatidylcholine, DMTAP and cholesterol. All three of these liposome formulations were shown to be monodisperse and highly stable, with diameter reduced to sub-micron sizes after 3 passages through the Microfluidizer (Lajunen et al., 2014). Similarly, this technology has been employed for silica nanoparticle manufacturing and for particles agglomerating study, with encouraging results for both applications (Gavi et al., 2018).

2.1.2 Production of SLNs using microfluidics

Microfluidics technology is based on controlled manipulation and mixing of fluids in the microliter to picolitre range. Since its first application in the 1980s (Whitesides, 2006), microfluidics has emerged as a lab-on-a-chip based technology for process development

(Bjork and Joensson, 2019), to automate laboratory procedures in the fields of pharmaceutical industry and biotechnology (M. Squires and R. Quake, 2005) and to produce nanomedicines (Kastner et al., 2014, Kastner et al., 2015, Forbes et al., 2019, Dimov et al., 2017, Joshi et al., 2016). In general, microfluidics involves the controlled mixing of fluids, with fluid mixing being dictated by the design of the microfluidic cartridge (with numerous formats and mixing-steps having been investigated) and the process parameters adopted (including the flow rate through the cartridge and the mixing ratios employed during the process). In terms of a mixing process, microfluidics offers a range of advantages including scalable working volumes from very low volumes to high-throughput, short reaction times, reduced cost, controlled mixing and enhanced parameter control combined with process automation (Yu et al., 2009, Pihl et al., 2005, David J. Beebe et al., 2002, Jahn et al., 2010). Therefore, microfluidics has been used to produce a range of nanoparticle systems including lipid nanoparticles, liposomes, polymeric nanoparticles and solid lipid nanoparticles. By using microfluidics to rapidly mix liquids of different polarities, the nanoprecipitation of dissolved molecules can be promoted and uniform nanoparticle suspensions produced (Park, 2017).

2.1.3 Aim and objectives

Given the positive results with other particulate systems for both high-shear mixing and microfluidics, the aim of the work within this chapter was to investigate both manufacturing platforms for their potential as a scalable manufacturing process for solid lipid nanoparticles. To achieve this, the objectives were:

- Evaluation of critical process parameters to produce protein loaded SLNs.
- Application of tangential flow filtration for protein and solvent removal.
- Protein loading and *in vitro* release quantification.

2.2 Materials and Methods
2.2.1 Materials

Tristearin (Grade II-S, ≥90%) and trifluoroacetic acid (TFA) were obtained from Sigma-Aldrich Company ltd, Poole, UK. 1,2-Distearoyl-phosphatidylethanolamine-methyl-polyethyleneglycol conjugate-2000 (DSPE-mPEG-2000) was obtained from Lipoid GmbH (Ludwigshafen Germany). Ethanol and methanol were obtained from Fisher 141 Scientific UK, Loughborough, UK. TRIS Ultra-Pure was obtained from ICN 142 Biomedicals, Inc., Aurora, Ohio. Phosphate-buffered saline (PBS) and Albumin from chicken egg (OVA), were obtained from Sigma-Aldrich Company ltd, Poole, UK. Sephadex G-75 size exclusion columns were obtained from GE Healthcare Life Science -Little Chalfont-Buckinghamshire, UK.

2.2.2 Preparation of solid lipid nanoparticles

2.2.2.1 Microfluidics

Solid lipid nanoparticles formulations using the micromixer were performed on a benchtop NanoAssemblr instrument (NanoAssemblr, Precision Nano- Systems Inc.). The two inlet streams comprised lipids dissolved in ethanol and aqueous buffer (Tris, 10 mM, pH 7.4), syringe pumps allowed for controlling the flow rates and the flow ratios between the two inlet streams. Solid lipid nanoparticles were prepared with the Nanoassemblr; 1.3 mg of Tristearin and either 1% w/w or 16% w/w of mPEG-DSPE were dissolved in 1 mL of ethanol (70°C) and OVA (when added) was dissolved in 1 mL TRIS buffer pH 7.4 10 mM. Both solutions mixed via microfluidics and particles were collected in a 15-mL falcon tube. The total flow rate (TFR) was varied between 5 and 20 mL/and the aqueous/solvent ratio (FRR) was varied between 1:1, 3:1 and 5:1.

2.2.2.2 Microfluidisation

Solid lipid nanoparticles were prepared using the M-110P Microfluidizer (Microfluidics Inc, Westwood, Massachusetts, US). mPEG-DSPE-2000 (1 or 16% w/w) was dissolved in 10 mM TRIS buffer at pH 7.4 and heated up at 75°C. Tristearin 1.3 mg/mL was melted at 75°C and the liquid mass was emulsified with the aqueous phase under vigorous stirring. Buffer solution (75°C) was added to the O/W emulsion to a final volume of 75 mL. The emulsion was loaded in the inlet reservoir of an M-110P Microfluidizer processor and the effect of the number of process cycles (1 to 5) and of process pressure change (20,000, 25,000 and 30,000 psi) were investigated. The size, PDI and Z-potential were measured with Zetasizer Nano ZS and Zetasizer AT (Malvern Instruments Ltd). OVA loaded Tristearin: mPEG-DSPE (5:1 w/w) solid lipid nanoparticles were similarly prepared: mPEG-DSPE-2000 16% w/w was dissolved in 10 mM TRIS buffer at pH 7.4 and heated up at 75°C. To formulate loaded particles, Ovalbumin (0.1, 0.5 and 1 mg/mL; OVA) was added to the aqueous phase. Tristearin 1.3 mg/mL was melted at 75°C and the liquid mass was emulsified with the aqueous phase under vigorous stirring. Buffer solution (75°C) was added to the O/W emulsion to a final volume of 75 mL. The emulsion was loaded in the inlet reservoir of an M-110P Microfluidizer processor to reduce particles size.

2.2.3 Purification methods

2.2.3.1 Solvent elimination via dialysis after microfluidics

To remove residual organic solvents from formulations, dialysis was applied as purification method. Briefly, after being produced with Nanoassemblr, 1mL sample SLNs was put into a 14 kDa dialysis membrane; the organic solvent was then let diffuse through membrane porous against 200 mL TRIS buffer 10 mM pH 7.4 under stirring for one hour.

2.2.3.2 Size exclusion chromatography (SEC) for solvent and free protein removal after microfluidics

To achieve removal of organic solvent, 1 mL sample made with Nanoassemblr was loaded on top of a G-25 spin column (GE Healthcare) and eluted with 3 mL TRIS buffer 10mM, pH 7.4 as recommended from manufacturer instructions. Purified samples were collected into a 15-mL falcon tube. Moreover, to eliminate both organic solvent and unloaded protein from samples prepared in presence of OVA, G-75 spin column (GE Healthcare) was used. Samples of 1 mL were added on top of the column and, after equilibration, they were eluted with 3 ml TRIS buffer pH 7.4 10 mM following manufacturer instructions.

2.2.3.3 Protein and solvent removal using tangential flow filtration method after microfluidics and microfluidisation

Tangential flow filtration (TFF – KR2i TFF System) was investigated as a method for both organic solvent and free protein removal from formulations made by Nanoassemblr. As part of the validation process, the sufficient number of washes required to eliminate organic solvent was evaluated. On this purpose, samples prepared in presence of OVA were used. TFF filtration speed was set up at 27 mL/min. Residual methanol after 4, 8,12,16 and 20 times TFF washes with TRIS buffer was detected using gas chromatography (GC-MS, Agilent Technologies) adding 1% 2-propanol (IPA) as internal standard; flow: 1.561 mL/min, pressure: 18.678 psi, column: Agilent 122-1334, 0-260 $^{\circ}$C, 30 m $\times$ 250 μm $\times$ 1.4 μm); peaks area was normalised by IPA peak area and related to solvent concentration through a calibration curve with a linearity of $R^2 = 0.9502$. All measurements were within the level of detection and level of quantification.

The minimum volume of buffer needed to eliminate free OVA was investigated using different OVA stocks at concentrations between 1 mg/mL and 0.1 mg/mL. TFF filtration velocity was set up at 36 mL/min and stocks were washed with 20 mL of buffer. Filtrate was collected in aliquots of 1 mL each. For both stocks and aliquots, the absorbance at 230 nm has been measured using the Nanodrop 2000c (Thermo Scientific). OVA quantification was achieved by referring to a calibration curve (R^2=0.999). The same method was applied to samples prepared with M-110P Microfluidizer.

Once the minimum washing volume was established, the concentration process after M-110P Microfluidizer was performed with a 75-ml feed volume of solid lipid nanoparticles dispersion (0.5 mg/mL) and the TMP maintained at 10 psi. The retentate was circulated back to the feed bottle at filtration speed of 36 mL/min. As more filtrate was generated, the concentration of retentate increased. Once the retentate volume reached 1 mL, purification was stopped. The purified sample was assessed for particle size distribution and zeta potential. Between purification of batches, the TFF system was cleaned by 1-h continuous circulation of 0.1 M NaOH followed by flushing with a large volume of water ($\geq$1 L).

Table 2. 1 Working parameters for Gas Chromatography method.

Rate (°C/min)	Value (°C)	Hold time (min)	Run time (min)
Initial at O	60	1	1
Ramp at 10	120	0	7
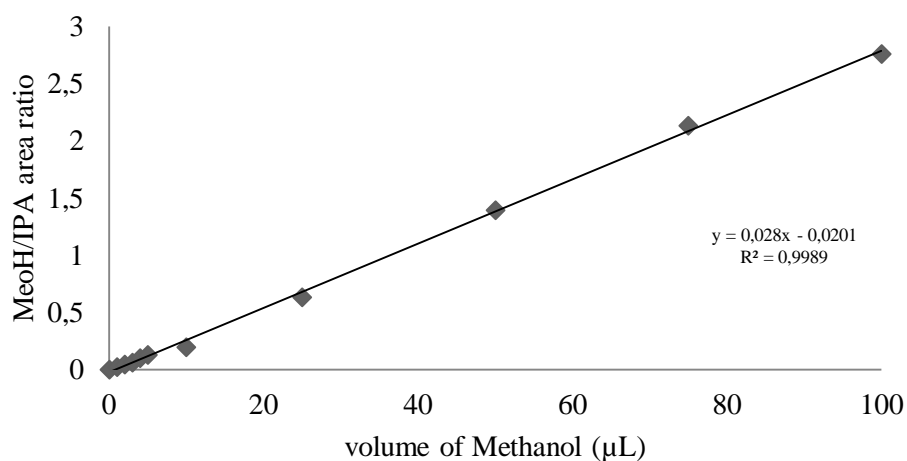
Figure 2. 1 Calibration curve for solvent quantification. Calibration curve for the determination of residual methanol in samples. $R^2 = 0.9989$

Table 2. 2 Calibration curves parameters.

Characteristic	Calibration curve A	Reference
LOD (µg/mL)	1.3	Calculated according to ICH guideline Q2 (R1): "Validation of Analytical procedures: Text and Methodology (2005)"
LOQ (µg/mL)	3.8	

The graph shows a calibration curve with the equation y = 5,203x - 0,0614 and R² = 0,9998, plotting Absorbance (230 nm) on the y-axis against [OVA] mg/mL on the x-axis.
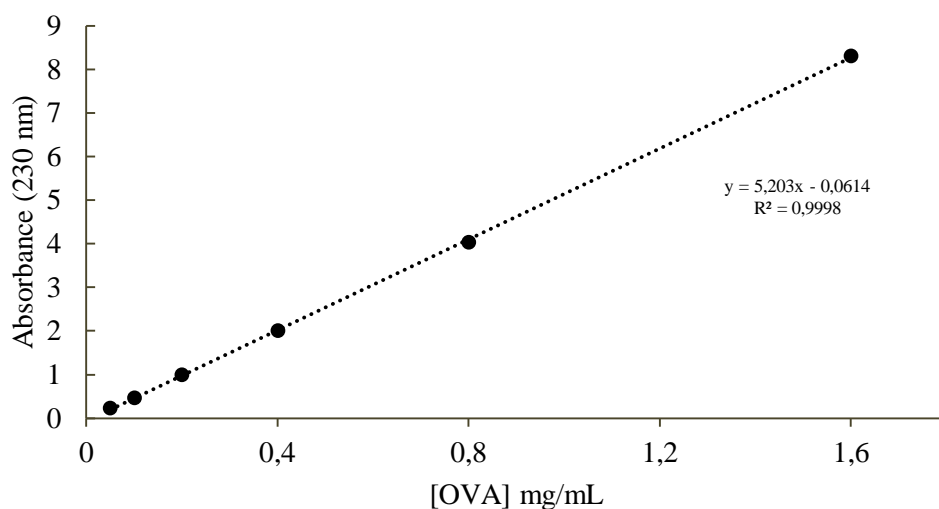
Figure 2. 2 Calibration curves for protein quantification. Calibration curve for the determination of OVA concentration in samples. R^2= 0.9998.

2.2.4 Characterization of solid lipid nanoparticles

2.2.4.1 Characterization of particle size, zeta potential and morphology

The dynamic light scattering (DLS) technique was used to report the intensity mean diameter (z-average) and the polydispersity of all solid lipid nanoparticles formulations (Malvern Zetasizer Nano-ZS (Malvern Instruments, Worcs., UK)). The measurements of particles size and polydispersity were carried out at 25 °C in Tris buffer (1:10 dilution, 10 mM, pH 7.4). Zeta potential was measured in Tris buffer (1:10 dilution, 10 mM, pH 7.4) using the Malvern Zetasizer Nano-ZS (Malvern Instruments, Worcs., UK). All measurements were undertaken in triplicates. Furthermore, The Zetasizer AT (Malvern Instruments, Worcs., UK) was used as an on-line measurement of particle size. 2.5 mL of samples were diluted 1:10 in Tris buffer (1:10 dilution, 10 mM, pH 7.4) at 25 °C and the volume was let circulate between the mixing tank and the homogenizer, until the measurement was completed. Data obtained with the two instruments were compared.

To visualize particles and assess the integrity and morphology, cryogenic electron microscopy (cryo-EM) was used. Briefly, samples (3 µL) were deposited on a pre-cleaned lacey carbon-coated grid and flashed frozen by plunging into liquid ethane cooled by liquid nitrogen. Samples were then observed in a cryo-holder in electron microscope Tecnai 12 G2 (FEI, Eindhoven) at liquid nitrogen temperature and 80 KV with magnifications ranging from 40,000X to 135,000X.

2.2.4.2 Lipid recovery

Lipid recovery after dialysis, TFF and spin column was performed by adding 1,1'-Dioctadecyl-3,3,3',3'-Tetramethylindocarbocyanine Perchlorate (DilC) 0.2% mol total lipid concentration

solved in ethanol to lipid stocks before being loaded in the Nanoassemblr. DilC fluorescence was measured before and after TFF, dialysis and spin column (PolarStar, BMG LABTECH GmbH). Lipid quantification was achieved by referring to a calibration curve with a linearity of R^2=0.995. All measurements were within the level of detection and level of quantification.
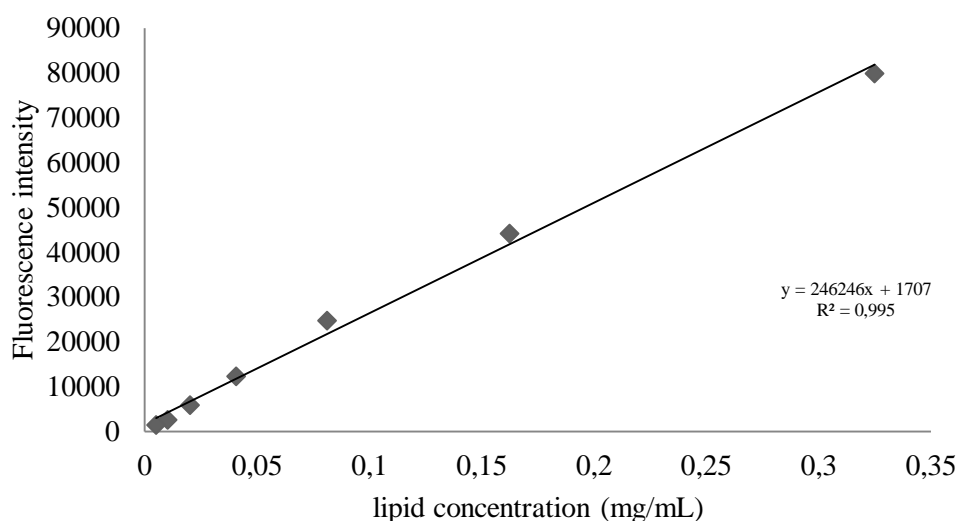
Figure 2. 3 Calibration curve for lipid quantification. Calibration curve for the determination of residual lipid concentration after TFF in SLN samples. R² = 0.995.

Table 2. 3 Calibration curves parameters.

Characteristic	Calibration curve A	Reference
LOD (µg/mL)	0.014	Calculated according to ICH guideline Q2 (R1): "Validation of Analytical Procedures: Text and Methodology (2005)"
LOQ (µg/mL)	0.045	

Recovery of lipids was also performed after samples preparation with M-110P Microfluidizer and concentration with TFF. DilC 0.2% mol total lipid concentration was solved in the melt lipid before being loaded in the Microfluidizer. DilC sample fluorescence was measured before and after TFF (PolarStar, BMG LABTECH GmbH). Lipid quantification was achieved by referring to a calibration curve with a linearity of R2=0.995. All measurements were within the level of detection and level of quantification (refer to chapter 3.2.3 for details).

2.2.4.3 Protein loading quantification

The loading efficiency was measured using reverse phase HPLC (Agilent 1100 Series) with a mobile phase of TFA 0.1 % and methanol with 0.08% TFA with a flow rate of 2.0 mL/min, λmax of 215 nm. At these conditions the OVA retention time is 9.6 min. The particles were

destroyed using a solution of IPA: TRIS 50:50 vol/vol. The solution was left at room temperature for 1 hour to achieve complete particle dissolution. All measurements were within the level of detection and level of quantification.

$y = 5596,8x + 28,233$
$R^2 = 0,9994$
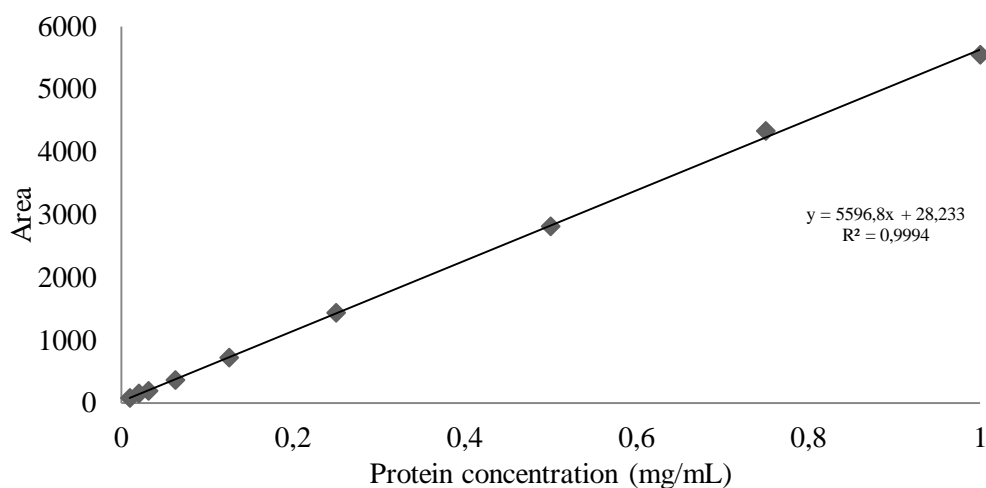
Figure 2. 4 Calibration curve for protein quantification. Calibration curve for the determination of encapsulated OVA concentration in SLN samples. $R^2 = 0.999$.

Table 2. 4 Calibration curve parameters.

Characteristic	Calibration curve	Reference
LOD (µg/mL)	3	Calculated according to ICH guideline Q2 (R1): "Validation of Analytical Procedures: Text and Methodology (2005)"
LOQ (µg/mL)	10	

2.2.4 *In vitro* release of protein from solid lipid nanoparticles

For the release study of 0.5 mg/mL initial ovalbumin from solid lipid nanoparticles, nanoparticles were prepared using either Nanoassemblr (TFR 10 mL/min FRR 3:1) or M110p Microfluidizer (number of passes 5, pressure 25000 psi). All formulations were dialysed against 80 mL PBS pH 7.4 at 37 °C (membrane cut off 300 kDa). The absorbance of aliquots from the outer buffer was analysed at different time points (up to 48 h) using NanoDrop 2000c UV-Vis spectrophotometer (Thermo Fisher Scientific Inc). Released OVA was detected by measuring the protein absorbance at 230 nm (NanoDrop 2000c, UV-Vis Spectrophotometer) and these values were related to the concentration using a calibration curve (linearity $R^2 = 0.998$).

2.2.5 Statistical analysis

Unless stated otherwise, the results were calculated as mean ± standard deviation (SD). One-way ANOVA followed by Tukey post hoc analysis was performed for comparison and significance was acknowledged for p values less than 0.05. All the calculations were made using GraphPad Prism 8.

2.3 Results

2.3.1 High-throughput manufacturing of solid lipid nanoparticles via microfluidisation

Solid lipid nanoparticles consisting of Tristearin and mPEG-DSPE-2000 were formulated using the microfluidisation method. The aim was to optimise parameters to control particle size by varying the operating pressure from 20,000 to 30,000 psi as well as the number of circulation cycles from 1 to 5. Figure 2.5A demonstrates that all particles produced by Microfluidizer processor had a diameter of 250 nm or below with a polydispersity index between 0.2 and 0.3. The results also show that changes in pressure values between 20,000 and 30,000 psi did not significantly influence particles size. However, at pressures of 20,000 psi the variability within the particle size was the lowest (Figure 2.5A) therefore demonstrating that this pressure can be adopted to produce solid lipid nanoparticles. Furthermore, increasing the number of cycles did not significantly reduce the particle size and at 20,000 psi particles of around 200 nm and polydispersity around 0.25 were formed irrespective of the number of passes demonstrating the particles are easily formed via this method.

When considering the zeta potential of the formulations, all solid lipid nanoparticles were anionic in nature, as would be expected given their composition (approximately -20 to -30 mV; Figure 2.5B) and these values were not significantly affected by either number of cycles or applied pressure.
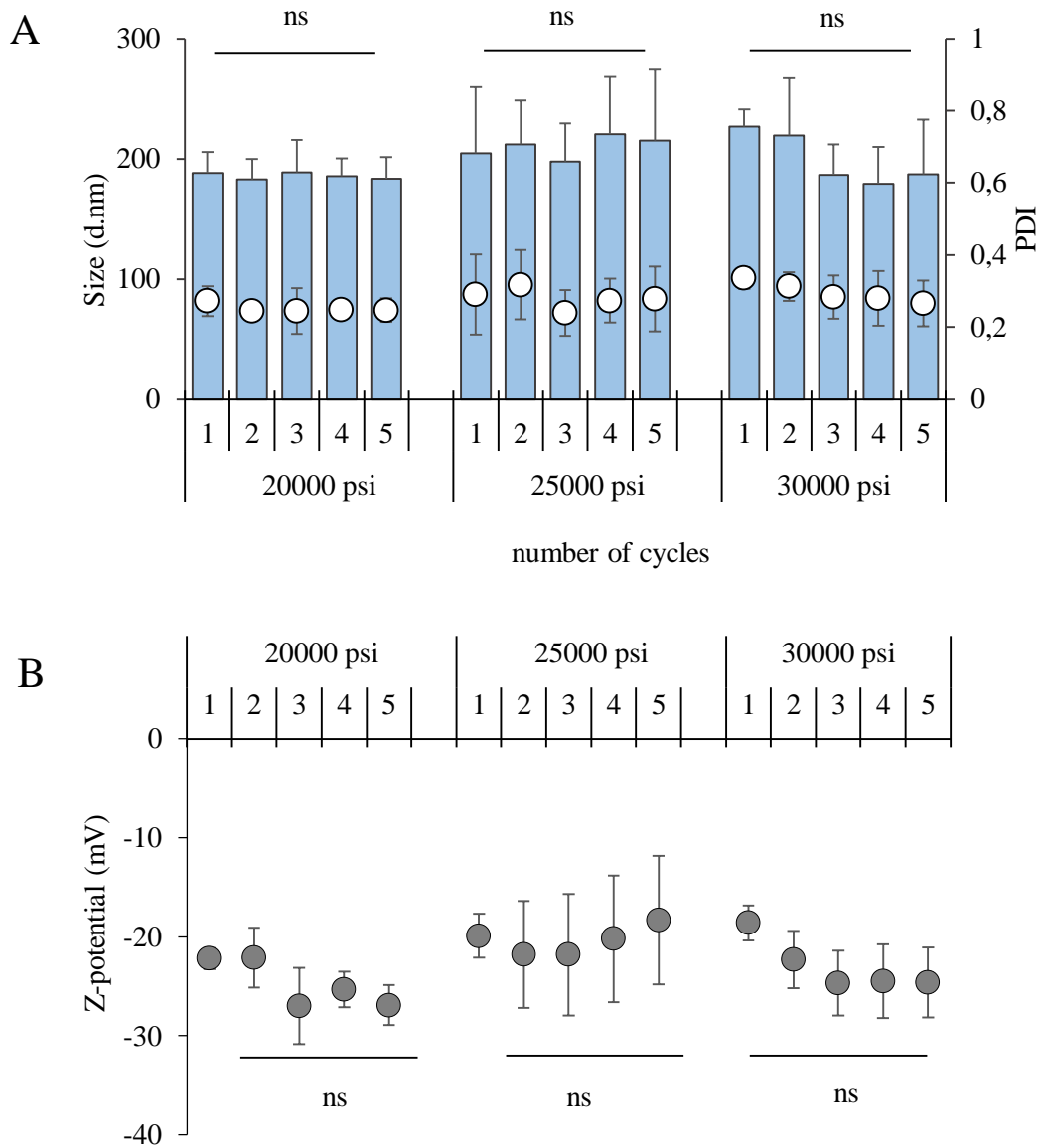
Figure 2. 5 The effect of processing pressure and passes on SLN attributes. A) Size (columns), polydispersity (dots) and B) Z-potential of Tristearin: mPEG-DSPE SLNs obtained with Microfluidizer processor. Samples with pressure from 20000 to 30000 psi as well as cycle numbers from 1 to 5 had been tested. Results are expressed as the means of three independent experiments ± S.D, n=3.
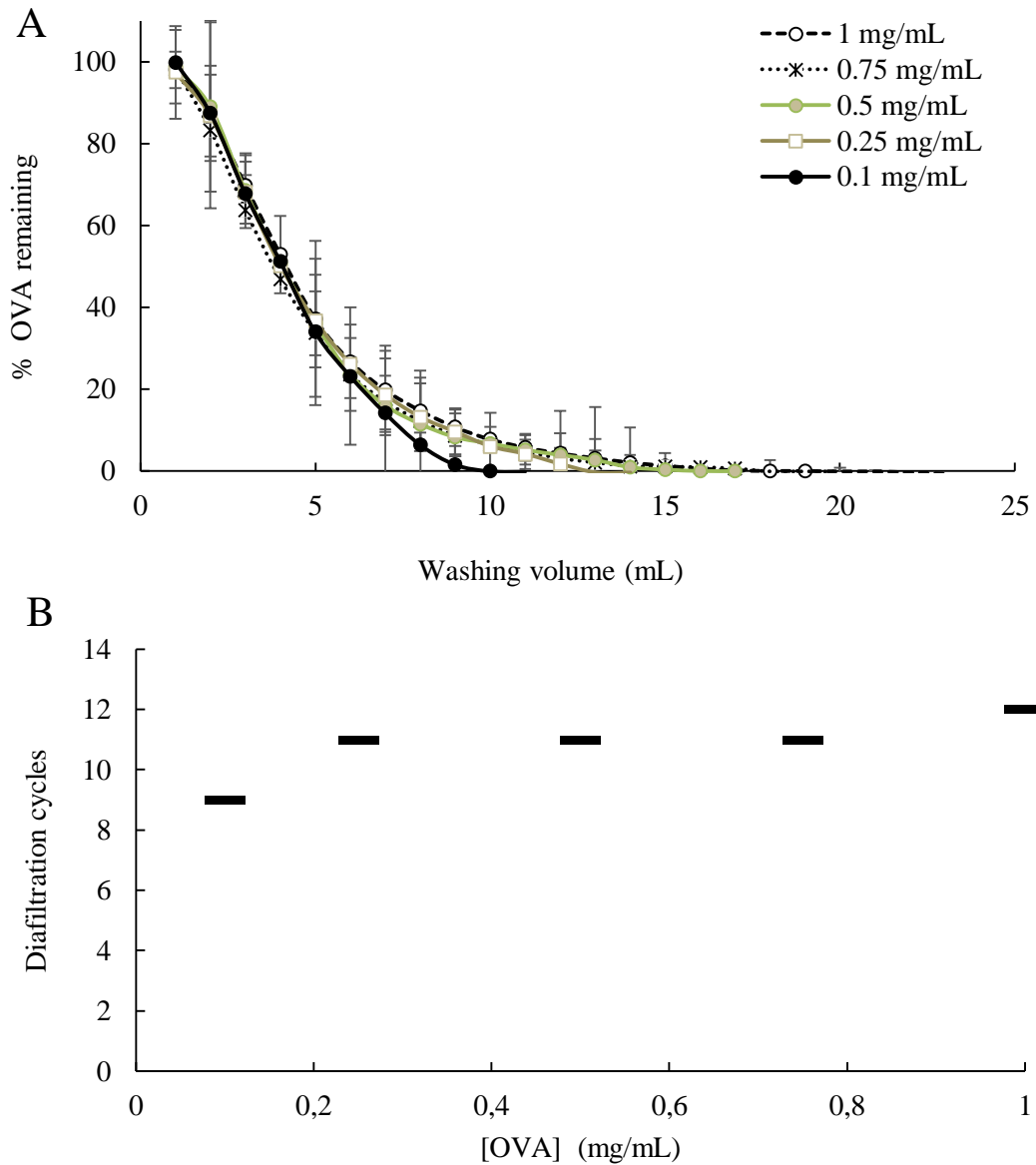
Figure 2. 6 Purification and removal of non-incorporated protein via TFF. A) Percentage of residual OVA (mg/mL) after 20 washes at initial protein concentrations from 0.1 to 1 mg/mL. B) Minimum number of diafiltration cycles required to have a protein remained concentration below 5% (w/w). Results are expressed as the means of three independent experiments ± S.D, n=3.

Table 2. 5 Solid lipid nanoparticles attributes after purification via TFF. Results represent mean ± SD, n = 3.

Solid lipid nanoparticles attributes	
Size	142 ± 3 nm
PDI	0.23 ± 0.01
Protein loading capacity	100 ± 24 µg/mL
Particle recovery	96 %

2.3.2 Development of a high-throughput purification of solid lipid nanoparticles and in-line particle size monitoring

To support the rapid purification and concentration of solid lipid nanoparticles, tangential flow filtration (TFF) was applied. Initially, the TFF process was optimized to ensure effective removal of non-incorporated protein with protein concentrations of 0.1 to 1 mg/mL being mixed with pre-formed solid lipid nanoparticles and the removal of Ovalbumin measured. The results in Figure 2.6A demonstrate that across this range the purification process was similar with 12 diafiltration cycles effectively removing non-loaded protein (Figure 2.6B). This process was then used to purify solid lipid nanoparticles prepared with OVA loaded. The lipid recovery and the SLN attributes (size, PD, Zeta potential and protein loading) was measured for Tristearin: PEG SLNs (5:1 w/w) after purification via this TFF protocol (Table 2.5) with the SLNs being approximately 140 nm in size with a PDI of 0.2 with high protein loading (100 µg/mL) and particle recovery was 96% (Table 2.5). The SLNs were also subjected to a 10 times concentration step via TFF, and there was no significant change in particle size and PDI (Figure 2.7B) or morphology (Figure 2.7C).

An important parameter in the development of effective manufacturing processes is the ability to rapidly monitor critical quality attributes of a product and in the case of nanoparticles, particle size is a key attribute. Therefore, the potential to monitor the particle size of SLNs using the Zetasizer AT was investigated. This method offers on-line measurement of particle size using Dynamic Light Scattering to enable real time monitoring of the particle production. To achieve this, an at-line system was set up, such that samples could be tested during production as a process monitoring control or alternatively at the end of the production as a quality control.

The standard off-line particle sizing (Malvern Zetasizer) and in-line data was compared. Figure 2.8 outlines the set-up and demonstrates that continuous monitoring of the particles size and polydispersity after TFF purification and concentration was achieved with no significant difference in particle size when measured off-line and in-line.

A

B

C
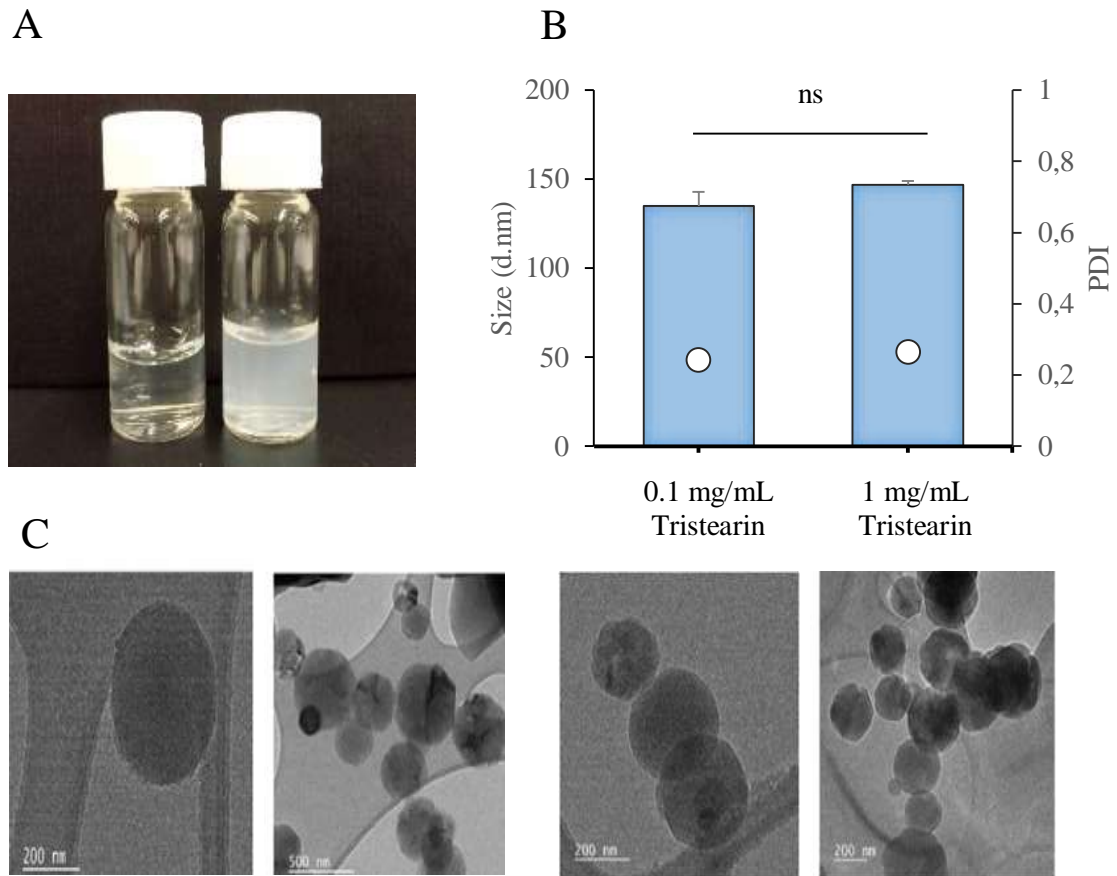
Figure 2. 7 Production and in-line monitoring of SLNs after production via Microfluidizer processor after concentration via TFF A) visual appearance, B) Size (columns) and PDI (dots) of Tristearin: PEG SLNs before and after 10 times TFF concentration and C) cryo-EM images of Tristearin: PEG SLNs made by Microfluidizer processor before (two images on the left) and after (two images on the right) 10 times TFF concentration. Where appropriate, results are expressed as the means of three experiments ± S.D, n=3. Mann-whitney non- parametric t-test was used for statistical analysis.
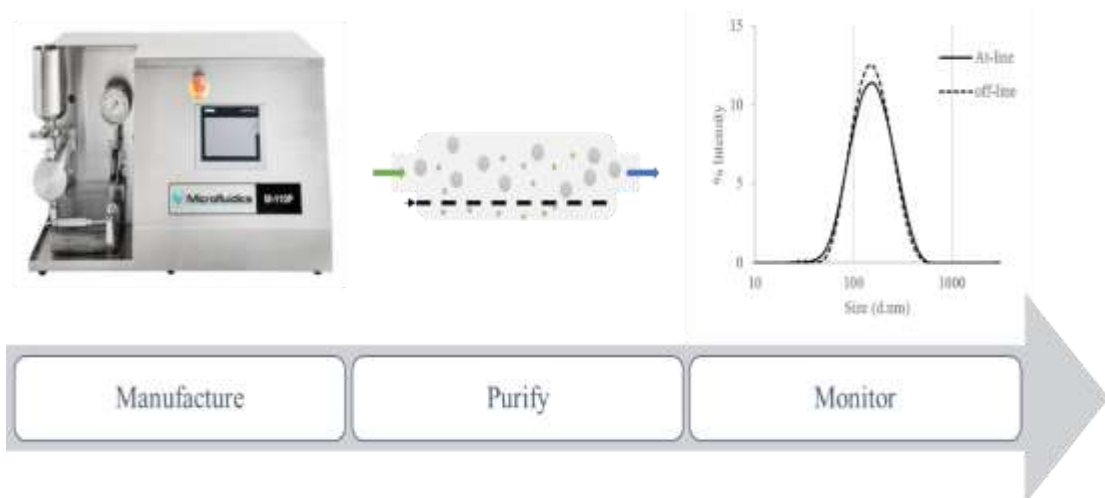
Figure 2. 8 Production and in-line monitoring of SLNs after production via Microfluidizer processor. SLNs were produced, purified via TFF and the particle size measured by circulation between the mixing tank and the homogenizer, until complete detection. Data obtained with at-line and off-line dynamic light scattering were compared.
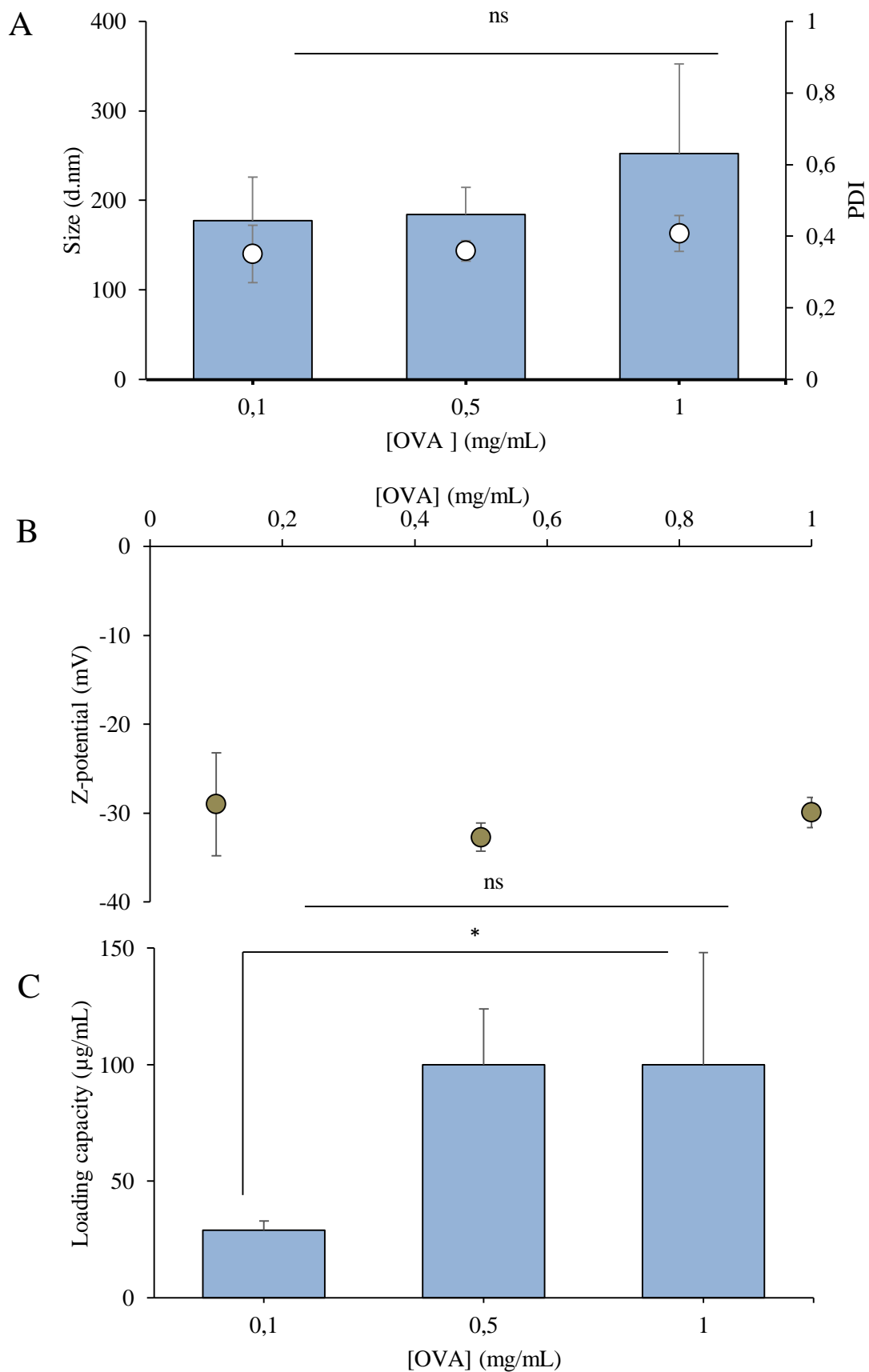
Figure 2. 9 OVA-loaded solid lipid nanoparticles made by Microfluidizer processor A) Size (columns), PDI (dots) and B) Zeta potential and C) Loading efficiency of Tristearin: mPEG-DSPE SLNs expressed as percentage of the initial protein amount (µg/mL). Results are expressed as the means of three independent experiments ± S.D, n=3.
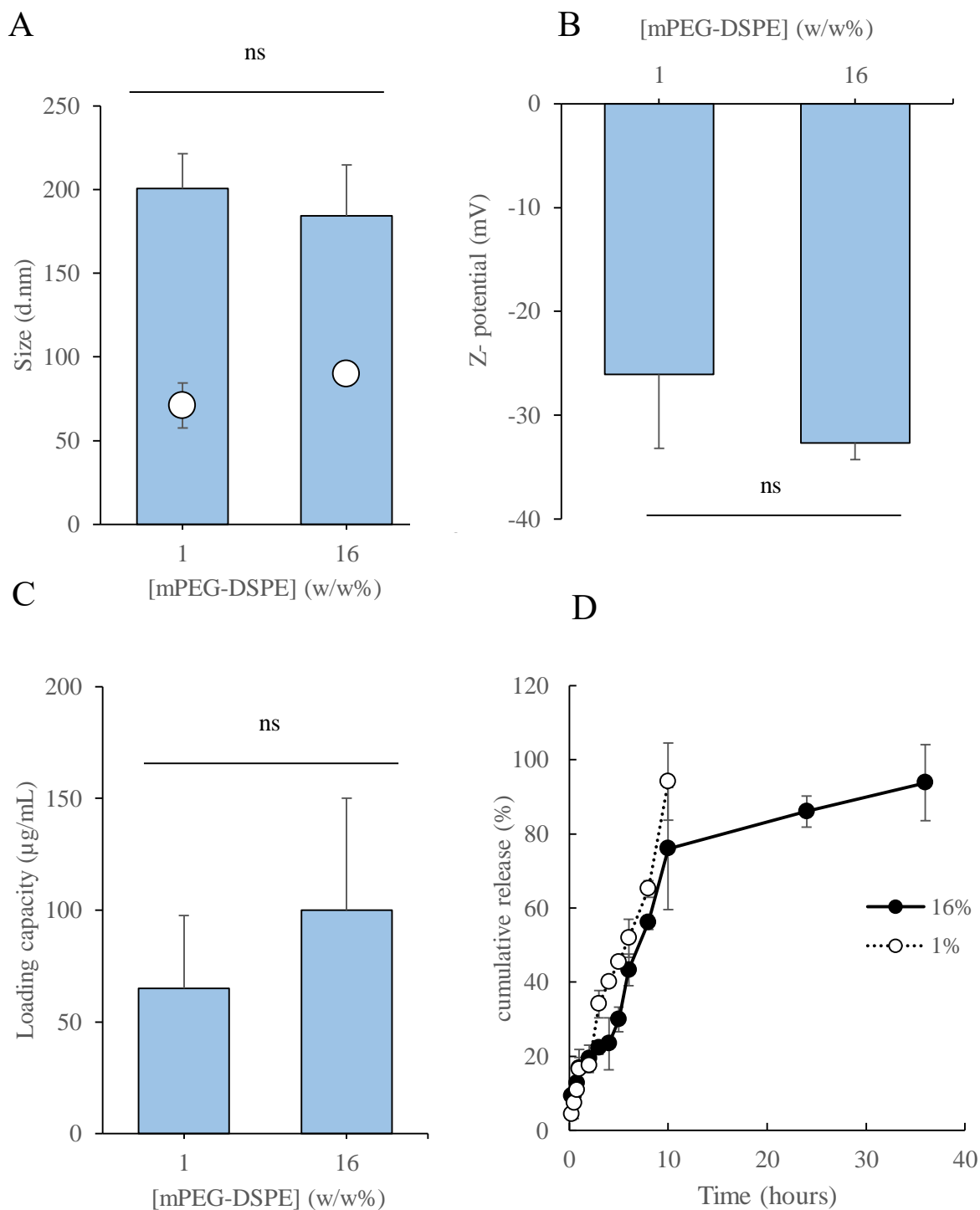
Figure 2. 10 The effect of PEG. The effect of PEG on SLN attributes A) size and PDI, B) Zeta Potential, C) Loading and D) release profile. Results are expressed as the means of three experiments ± S.D, n=3. Mann-whitney non- parametric t-test was used for statistical analysis.

Table 2. 6 R^2 values of cumulative release profile of OVA (%) replotted according to zero-order (µg) and first-order models (Ln).

	R^2 (%)	R^2 (µg)	R^2 (Ln)
PEG 16%	0,809	0,809	0,643
PEG 1%	0,981	0,981	0,829

2.3.3 Manufacture of protein-loaded solid lipid nanoparticles

To assess the ability of the M110-P Microfluidizer processor as a potential high throughput manufacturing method for protein loaded lipid particles production, Tristearin:PEG SLNs were formulated in presence of different protein (Ovalbumin -OVA) concentrations. As it shown in figure 2.9A, increasing the protein concentration had no impact on particles attributes. However, initial OVA concentrations of 1 mg/mL induced high size variability and less homogeneous particles (PDI of 0.4 ± 0.05). The initial protein concentration did not impact on zeta potential with all particles being around - 30 to - 35 mV (Figure 2.9B) and OVA loaded within the SLNs could be increased up to a maximum of 100 µg/mL for the given lipid concentration (Figure 2.9C). Finally, the impact of increasing the amount of mPEG within the SLNs was tested, given that low levels of PEG may be useful in the formulation of vaccine delivery systems whilst high levels of PEG can be useful for avoiding rapid clearance from the circulation. As shown in Figure 2.10, increasing the amount of PEG had no significant effect on particle size, zeta potential and protein loading, suggesting that these systems can be prepared with low and high degrees of pegylation without impacting on the particle size, PDI and loading. However, increasing PEG concentration from 1 to 16% w/w affected the protein release kinetics. As shown from the R^2 values listed in table 2.6, OVA released from SLNs containing 1% PEG followed a zero-order profile - R^2 (µg) = 0,981 - while increasing PEG till 16% changed the kinetics to pseudo-first order - R^2 (µg) = 0,809. Despite that, the amount of released protein over time was not significantly different between the two SLNs formulations.

2.3.4 SLNs manufacturing by microfluidics: particles size can be process controlled

Solid lipid nanoparticles consisting of Tristearin and PEG-DSPE were prepared using the microfluidics method and the aim of this study was to evaluate how the microfluidic process parameters impact on particles size and polydispersity. More precisely the percentage of organic phase was reduced from 50% to 17% and differences in particles attributes were evaluated. Figure 2.11A showed the effect of modifying flow rate ratio (FRRs; ratio between organic and aqueous phase) on SLNs size distribution; by enhancing the FRR from 1:1 to 3:1, the diameter was significantly ($p<0.05$) reduced from 180 ± 65 nm to 65 ± 23 nm. However, further increasing the FRR to 5:1 did not significantly impact on the particle size (59 ± 17 nm; Figure 2.11A). Across the FRR tested the PDI remained low (between 0.2 and 0.3; figure 2.11A) and the size intensity plots are shown in figure 2.11B. Regarding the zeta potential, values were independent from the FRR (Figure 2.11C); among all aqueous/solvent ratio tested, the zeta potential remained slightly negative (between -17 and -20 mV) as expected, with no significant difference.
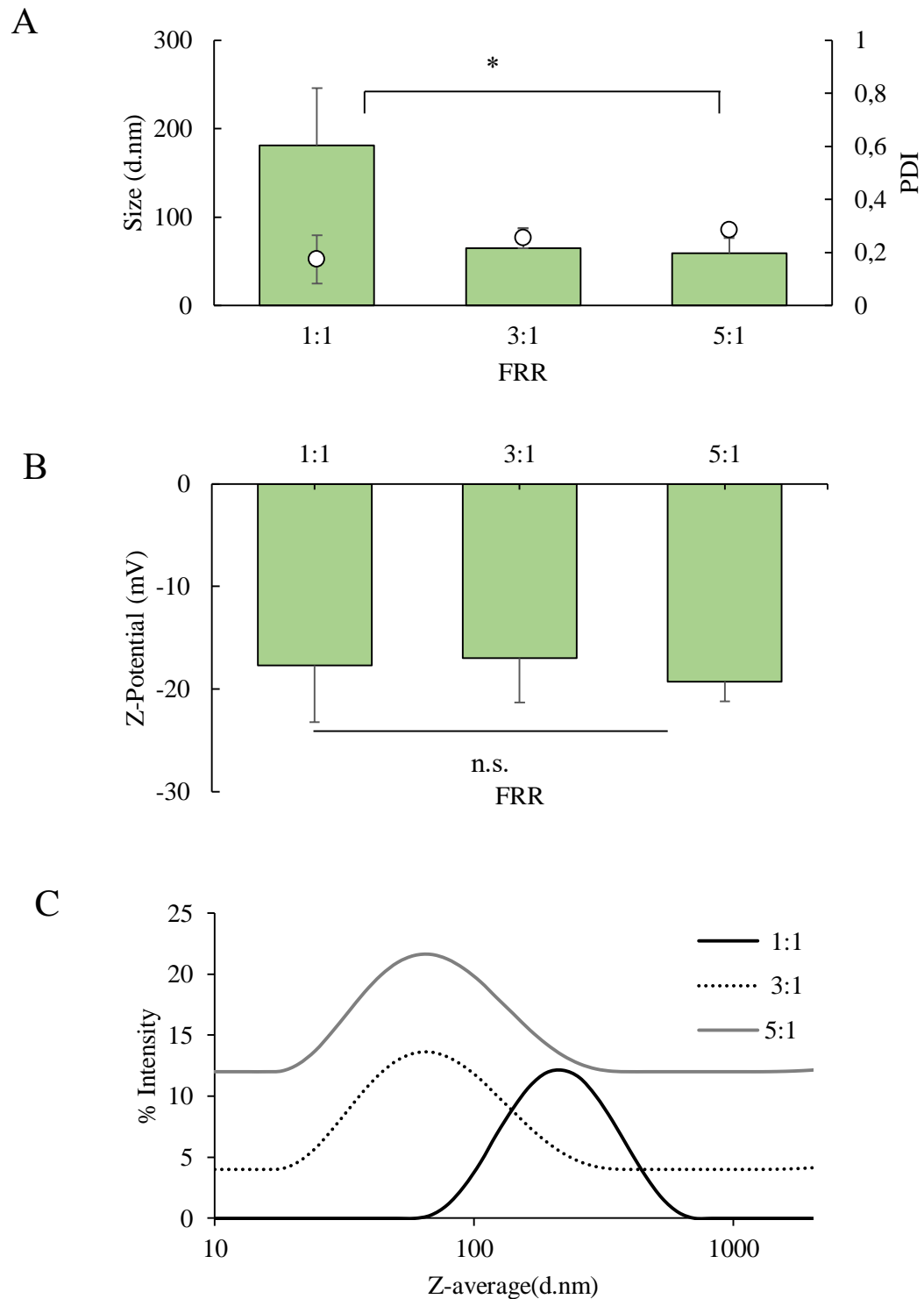
Figure 2. 11 SLNs attributes A) Size (columns) and PDI (dots) and B) Zeta-potential of Tristearin: mPEG-DSPE SLNs using Nanoassemblr after dialysis. Formulations with TFR 10 mL/min and FRR from 1:1 to 5:1 had been tested. C) Intensity plot of SLNs made by Nanoassemblr and sized after dialysis purification method. Formulations with TFR 10 mL/min and FRR 3:1 had been tested. Results are expressed as the means of three experiments ± S.D, n=3.

2.3.5 Purification process for SLNs produced by microfluidics

Given that after microfluidic manufacturing samples contain organic solvent, several purification methods were investigated. SLNs were prepared using microfluidics at a FRR 1:1; in these conditions the concentration of ethanol in the final sample is 50 %, thus aiming to challenge each of purification systems tested. Figures 2.12A and B show that at least 12 washing cycles are required to reach a residual organic solvent concentration below 0,5% in the sample which corresponds to 5000 ppm, as recommended into the International Conference on Harmonisation of technical requirements for registration of pharmaceuticals for human use (ICH).

Then dialysis, TFF and spin column were compared according to their feasibility as purification methods. Parameters like particles physico-chemical attributes, lipid recovery and residual solvent levels were evaluated. As it shown in figure 2.13A, by using either spin column or dialysis it was possible to collect almost 100% particle yield.
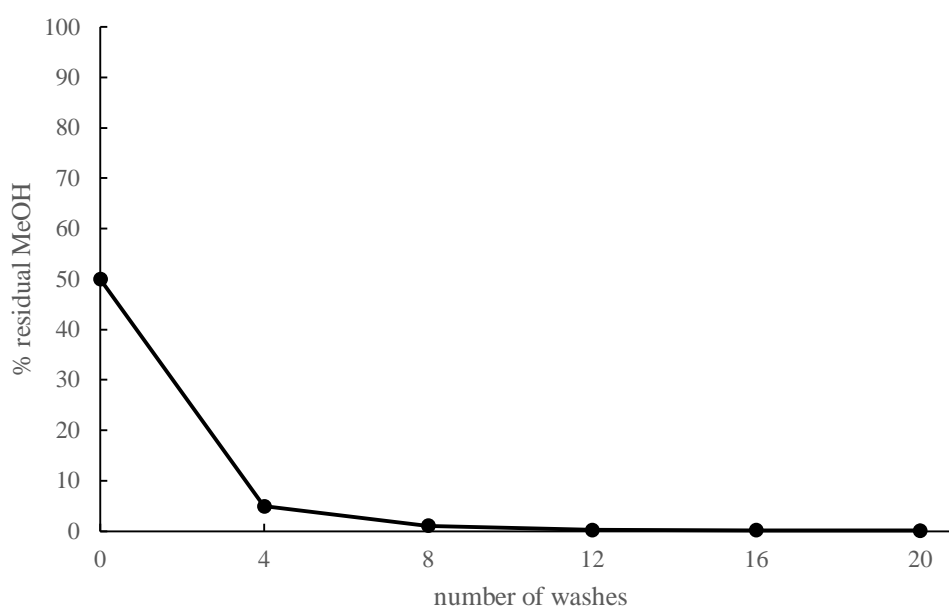
Figure 2. 12 Solvent removal using TFF. Residual solvent content after 0, 4, 8, 12, 16 and 20 washing cycles with TFF expressed as percentage of residual methanol. All data were normalised by IPA standard peaks area. Results are expressed as the means of three experiments.

In contrast, recovery of SLNs after TFF purification was lower (72%; Figure 2.13C). Figure 2.13D also shows that all three methods tested could efficiently remove the organic solvent from the sample to below 1%, and both TFF and dialysis achieved residual ethanol levels below 0.5 %, in line with ICH guidelines for residual ethanol levels.
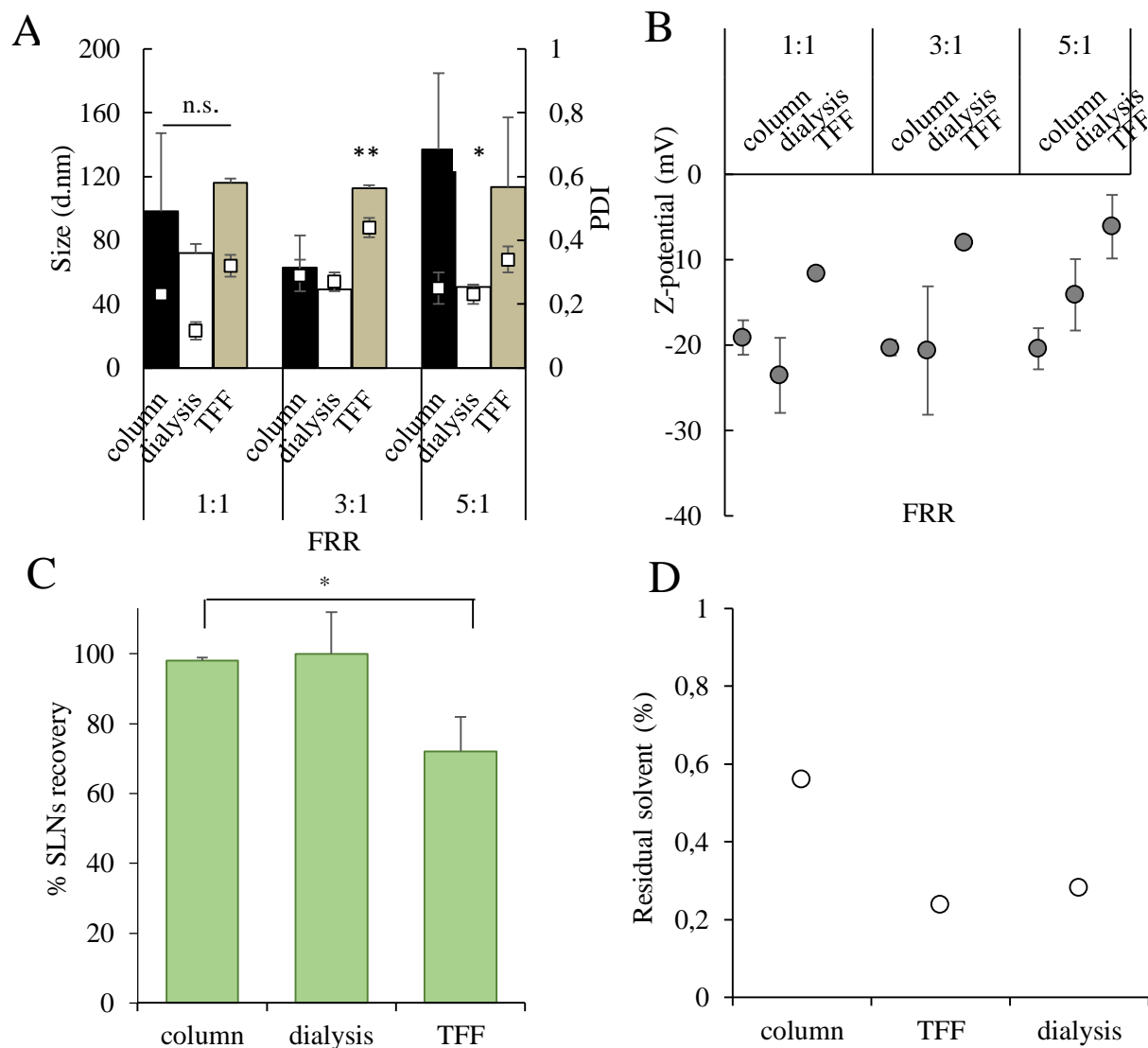
Figure 2. 13 Comparison of different purification methods for SLNs samples. A) Size (columns), PDI (dots) and B) Zeta potential values of Tristearin:mPEG-DSPE SLNs after spin column (black), dialysis (white) and TFF (grey) purification. Formulations with TFR 10 mL/min and FRR from 1:1 to 5:1 were tested. C) Lipid recovery of Tristearin: mPEG-DSPE SLNs after spin column, dialysis and TFF purification and C) Residual solvent after spin column, dialysis and TFF expressed as percentage of remained ethanol (mL%). All data were normalised by IPA standard peaks area. Results are expressed as the means of three independent experiments ± S.D.

2.3.6 Protein-loaded solid lipid particles production using Nanoassemblr: loading efficiency as a function of manufacture process

Using these optimised parameters, the next stage was to evaluate the suitability of microfluidics for producing SLNs containing proteins. To consider this, three different protein

(OVA) concentrations were used and loading compared. To achieve this, initially the extraction process was optimised and drug loading was measured at different time points (3 min, 6 hours and 24 hours post digestion). Spin column purification was applied for both solvent and free protein removal. Figure 2.14A shows that subjecting the OVA-loaded SLNs to prolonged exposure to IPA: TRIS 50:50 vol/vol resulted in reduced protein loading, which may be a result of protein degradation in the IPA. Therefore, for all further studies, all formulations were subjected to no more than 30 min digestion. Figure 2.14A also shows the effect of initial OVA concentration on loading capacity. As expected, with increasing initial OVA concentrations, SLNs can incorporate higher concentrations up to approximately 140 µg/mL when initial concentrations of 1 mg/mL OVA are used. When expressed as % loading efficiency, the maximum that can be achieved is 36% when an initial concentration of 0.1 mg/mL OVA is used (Figure 2.14B), and in terms of loading capacity (protein/lipid w/w) the trend again shows increasing loading (up to 11%) with increasing initial OVA concentrations (Figure 2.14C). Therefore, high protein loading can be achieved when high initial protein concentrations are used, but this is at the expense of loading efficacy as would be expected (Figure 2.14).

2.3.7 Influence of flow rate on particle characteristics and drug loading

To consider the impact of production speed, the TFR was varied and the SLN particle size and protein loading was investigated. The total flow rate values were varied from 5 mL/min to 20 mL/min, while the ratio between aqueous and solvent stream was maintained constant at 3:1. Figure 2.15A shows the effect of flow rate changes on particles size and polydispersity. Increasing the production speed from 5 to 10 mL/min made no significant difference in particles size (between 70 and 90 nm); however, enhancing TFR values to 15 mL per min or above reduced the particle sizes to a minimum of 40 ± 4 nm without affecting samples homogeneity (PDI approx. 0.25). The same trend was seen when particle zeta potential was measured (Figure 2.15B) with the zeta potential at TFR 5 mL/min being more variable at low (5 mL/min) TFRs, and at 10 mL/min or above the zeta potential was less variable (around -30 mV; Figure 2.15B). With respect to the loading efficiency, using an initial 0.5 mg/mL protein concentration, the capability was not significantly influenced by the total flow rate; however, less variability in protein loading was seen at flow rates of 10 mg/mL or more with loading of 80 - 90 µg/mL (Figure 2.15C).
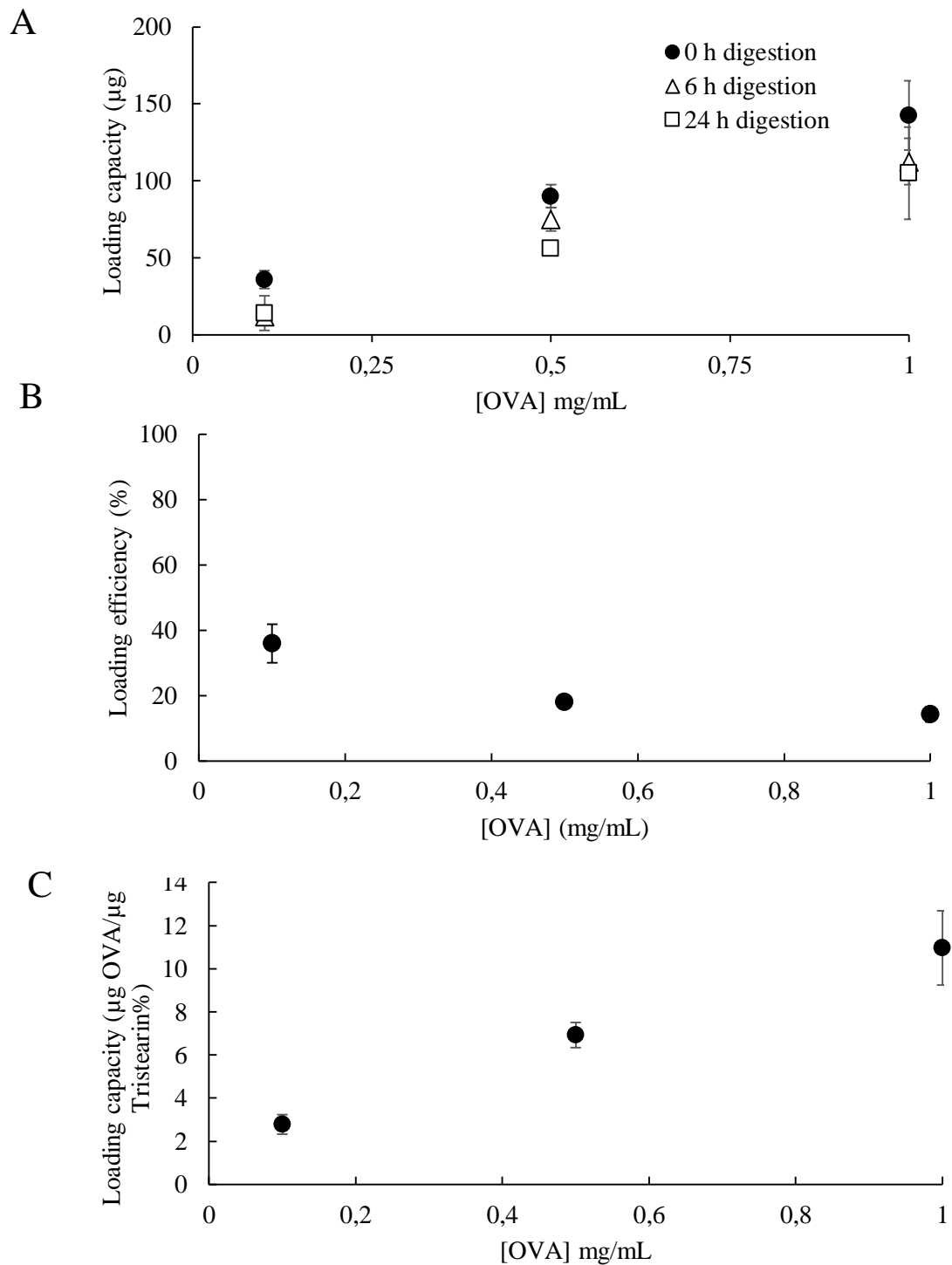
Figure 2. 14 The effect of digestion method on entrapment. Solid lipid nanoparticles encapsulating 0.1, 0.5 and 1 mg/mL initial OVA content were formulated using the Nanoassemblr platform. A) Protein encapsulation efficiency was determined after 0 hours, 6 hours and 24 hours post IPA digestion. Protein incorporation also expressed as B) Protein loading efficiency (%) and C) Loading capacity (w OVA/w Tristearin). Results are expressed as the means of at least four experiments ± SD.
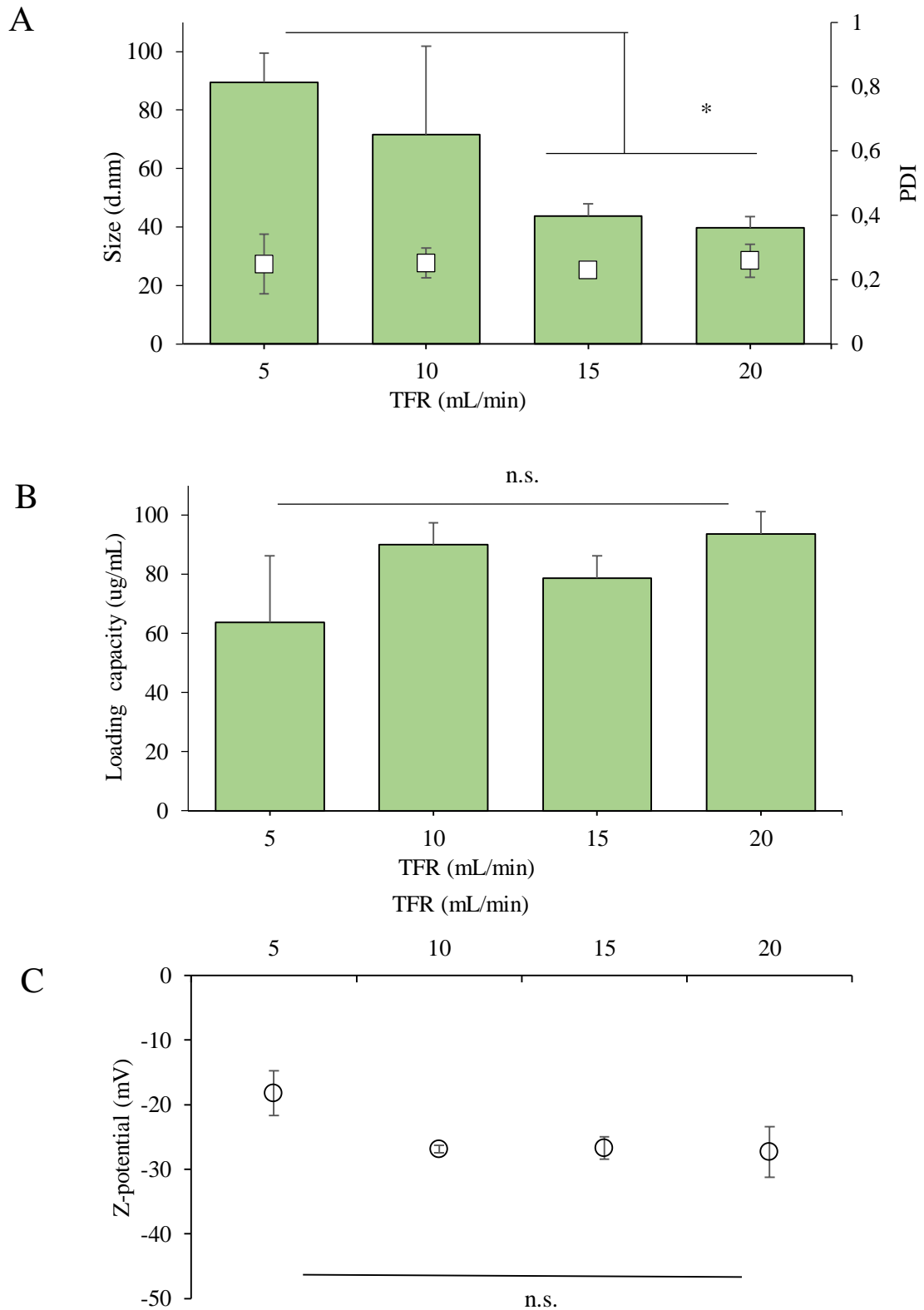
Figure 2. 15 OVA Loaded SLNs attributes. A) Size (columns), PDI (dots), B) Loading capacity (μg/mL) and C) Zeta potential of OVA loaded SLNs. Protein initial concentration was 0.5 mg/mL. FRR was set up at 3:1 while TFR were increased between 5 and 20 mL/min. OVA Protein initial concentration was 0.5 mg/mL. Results are expressed as the means of at least four experiments ± SD.
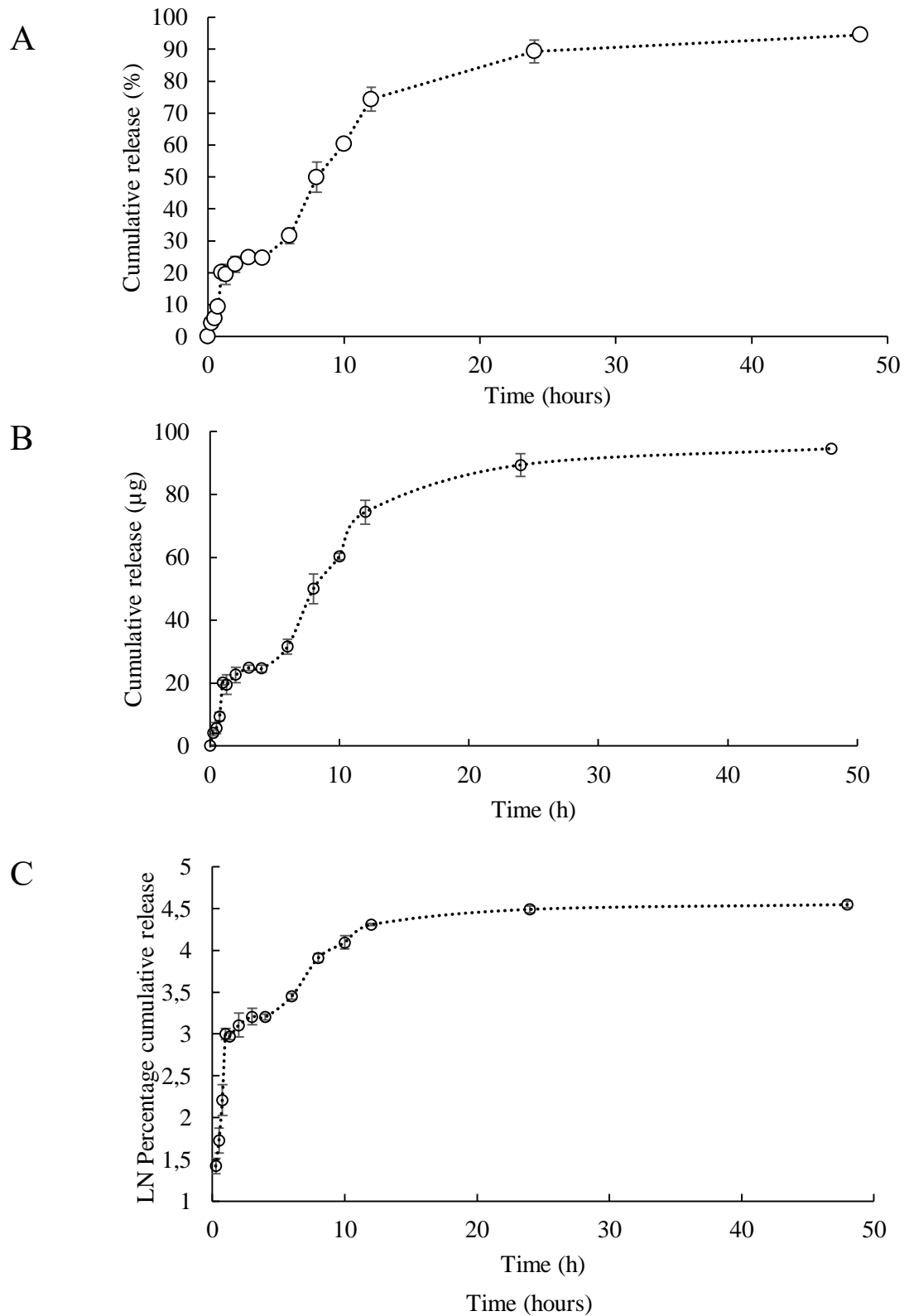
Figure 2. 16 Release study. A) The cumulative release profile of OVA under physiological conditions from SLNs (PBS buffer, pH = 7.4, at 37°C). Data was also replotted according to B) zero-order and C) first-order models. Results represent percentage cumulative release of initially incorporated OVA and are expressed as the means of three experiments ±SD.

The release profiles of OVA from SLNs produced was also investigated. As shown by results previously described in figure 2.10D of this chapter, changing PEG content in the formulation seemed not to alter the amount of protein released over time. Therefore, only particles containing 16% w/w PEG were used to perform OVA release study from SLNs.

To do so, particles were prepared from a FRR 3:1, TFR 10 mL/min and OVA initial concentration of 0.5mg/mL. The results in figure 2.16 show that the SLNs give a rapid release of up to 90% within the first 24 h and the release does not follow a zero-order profile. The release was also plotted as Ln cumulative percentage of drug released vs time (Figure 2.16B) and the data suggests the release does not follow a first-order model. These findings suggested that none of the models accurately described the kinetics of protein released from SLNs.

2.3.8 Comparison of methods

Table 2.7 outlines a summary of the key attributes of the SLNs prepared by microfluidisation and microfluidics. From these results both methods were suitable for production of homogeneous solid lipid nanoparticles (PDI<0,3) between 100-200 nm in size and slightly negative surface charge (Zeta potential of around -20 mVolt). Moreover, both microfluidisation and microfluidics allowed the encapsulation of high protein content (LC between 70 and 100 μg/mL) without altering SLNs physicochemical attributes. In addition, release of OVA from SLNs matrix seemed to be independent from the manufacturing method used, with a pseudo-first order release kinetics for both SLNs containing higher PEG content produced by either microfluidisation and microfluidics

Table 2. 7 Comparison of microfluidisation and microfluidics methods in terms of SLNs production suitability. Parameters like size, PDI, ZP (Z-potential), LC (loading capacity) and release kinetics were evaluated

	Microfluidisation					Microfluidics				
Formulation composition	*Size (nm)*	*PDI*	*ZP (mV)*	*LC% (μg/mL)*	*Release kinetics*	*Size*	*PDI*	*ZP*	*EE%*	*Release kinetics*
Tristearin, mPEG-DSPE 16% w/w	≈200	≈0,3	≈ -25	≈100	Pseudo first order	≈100	≈0,2	≈ -20	≈90	Pseudo first order
Tristearin, mPEG-DSPE 1% w/w	≈200	≈0,3	≈-25	≈70	Zero order	-	-	-	-	-

2.4 Discussion

Solid lipid nanoparticles offer a range of advantages for drug delivery due to their biocompatibility, biodegradability and physical stability. Despite these advantages, their application has been limited by the lack of cost-effective and scalable methods for their preparation. Furthermore, the loading of hydrophilic, biologically active compounds is challenging, due to the intrinsic lipophilic nature of solid lipid nanoparticles. Microfluidisation is commonly applied as a method for particles size reduction with decreasing particles size occurring after a few recirculation cycles (Salminen et al., 2017, Asumadu-Mensah et al., 2013). For example, liposomes made by 1,2-dipalmitoyl-sn-glycero-3-phosphocholine, 1,2-dipalmitoyl-sn-glycero-3-phosphoglycerol and cholesterol reached size values of around 80 nm and PDI 0.11 after 12 cycles at 10,000 psi (Fox et al., 2014). Similarly, liposomes prepared by this method and formulated from hydrogenated soybean phosphatidylcholine and N-(Carbonyl-methoxypolyethyleneglycol2000)-1,2-distearoyl-sn-glycero-3-phosphoethanolamine (mPEG2000-DSPE) were highly homogeneous with average diameter of 90-110 nm (Cui et al., 2007). Generally, solid lipid nanoparticles tend to be larger in size and previous studies using three recirculating cycles in microfluidizer platform at 10,000 psi produced Tristearin based SLNs at around 200 nm with low polydispersity (Salminen et al., 2017). Within these studies (Figure 2.5) it was demonstrated that this method can be employed to produce SLNs in a high through-put and efficient production of SLNs at flow rates of up to 155 mL/min depending on the process pressure.

In addition to their productions, solid lipid nanoparticles (and other nanoparticles) generally require purification to remove non-entrapped drug and tangential flow filtration offers a scalable process. Therefore, TFF manufacturing process has been exploited to effectively remove un-entrapped protein with SLNs being purified and retaining their physico-chemical attributes (Figure 2.7) with good particle recovery (Table 2.5). TFF has recently emerged as an innovative purification method, and several studies describe the effective purification and concentration of nanoparticles using tangential flow filtration(He et al., 2018, Dalwadi and Sunderland, 2007). For instance, nanoparticles composed of poly (D, L-lactide-co-glycolide) (PLGA) and polyvinyl alcohol (PVA) were purified by tangential flow filtration with a 300K MWCO membrane and the purified particle dispersions were stable and free of aggregation (Dalwadi et al., 2005). Moreover, it was demonstrated that phosphatidylcholine and cholesterol based liposomes were successfully purified by TFF application, with no change in particles size (approximately 115 nm) and PDI (0.15) and a total lipid recovery after diafiltration (Dimov et al., 2017) . TFF was also applied to remove unbounded protein; Ovalbumin was used as model biomolecule (Conrad et al., 2009, Sharma et al., 1996). As a water soluble compound, its encapsulation in lipid based systems is challenging (Kastner et al., 2014) (McLaren et al., 2011). Therefore, the choice of OVA has a sound rational to

challenge the production method. Herein, it was proved that protein loading solid lipid nanoparticles could be manufactured, purified and concentrated using scalable and cost-effective methods, without any alterations in particles physicochemical properties (Figure 2.10). Within these studies, it was also demonstrated that high protein concentrations destabilise the inner colloidal structure of particles, increasing sizes and inducing aggregation (Figure 2.9) (van de Weert et al., 2000, Hong et al., 2015, Colletier et al., 2002). Many factors can physically destabilise solid lipid nanoparticles leading to significant increase in particles size and consequent aggregation. The use of the PEG in particle formulation is a well-known technique to improve physical stability of particles. PEG generates a hydrophilic polymeric coating and PEG chains help to keep particles separated (Kenny et al., 2010, de Lima et al., 2018, Luangtana-Anan et al., 2010). The presence of PEG shield favours particles repulsion thus reducing particle growth and collapse.

In vitro release study from SLNs revealed that protein release increased over time; after 10 hours all protein content (>80% of the initial concentration) was released irrespective of the PEG content (figure 2.10D). Drug release from almost all the SLNs follows Weibull and Higuchi equations better than first-order equation (Chen et al., 2001, Venkateswarlu and Manjunath, 2004). The pseudo-first order release kinetics maintains the drug concentration in the blood or target tissue at a desired concentration for longer. Furthermore, the presence of high amount of PEG on particle surface reduced kinetics of the process: several coherent explanations could be given for this phenomenon. According to the Stocks-Einstein equation (Brillo et al., 2011), the diffusion coefficient is inversely proportional to solution viscosity: diffusion could be slowed down by increasing solution viscosity. The presence of polyethylene glycol molecules on the particle surface enhanced the bulk viscosity of water reducing the speed at which OVA could cross the lipid barrier. Secondly, PEG chains are very flexible, and they give larger hydrodynamic radius in aqueous media. According to Fick's first law of diffusion (Fick, 1995), the rate of diffusion is related to membrane thickness, in a reverse proportional manner.

One possible limitation which inevitably affects the applicability of the specific Microfluidizer used within this project at bench scale is the requirement of large volumes for sample production (up to 75 mL). Therefore, even though additional techniques like TFF can efficiently circumvent this issue by concentrating samples, this machine might not be suitable for development of new formulations at early stage or for samples containing expensive excipients. Thus, microfluidics was employed as alternative technology for SLNs production, since it requires smaller operating volumes (between 1 and 10mL). Although there has been extensive work on delivery of hydrophobic molecules using SLNs (due to their lipid-based matrix facilitating drug incorporation) their applicability as water soluble nanosystems has received less attention. Therefore, to consider this, these systems were investigated for the

delivery of water soluble proteins (ovalbumin). Within this chapter it was demonstrated that protein-loaded SLNs can be manufactured with their particle size being process controlled (Figure 2.11A). Most of the studies based on microfluidic technologies have attempted to understand how process parameters might impact on particle attributes and flow rate ratio, total flow rate and lipid concentration are commonly investigated. Previous studies on microfluidics confirmed the effect of flow rate ratio on particles dimensions, in agreement with what has been reported in this present work (Maeki et al., 2015, Patra et al., 2006, Jahn et al., 2010). For example, cationic 1,2-dioleoyl-3-trimethylammonium-propane (DOTAP) based liposomes formed at 1:5 solvent/aqueous formulation were smaller in size (50–75 nm) compared to the 1:1 solvent/aqueous formulation (175–200 nm) (Kastner et al., 2014). Furthermore, 1,2-distearoyl-sn-glycero-3-phosphocholine (DSPC) and cholesterol liposomes formed at low flow rate ratio (1:1) resulted to be larger in size (200 nm) with respect to their counterparts formulated at higher FRRs (around 90–120 nm) (Joshi et al., 2016). However, it was also seen that increasing the FRR increased polydispersity (Kastner et al., 2015); a possible explanation for this phenomenon would be related to the reduced particles fusion (Ostwald ripening) that occurred at higher FRR, due to the lower amount of residual solvent. Thus, the formation of smaller monodisperse particles is achieved (Zhigaltsev et al., 2012, Zook and Vreeland, 2010). On the other hand, at higher FRRs, a dilution of the organic phase occurred, reducing the tendency of lipids to diffuse, with an effect on sample polydispersity; these observations were confirmed by previous studies where a staggered herringbone mixer was used (Kastner et al., 2015). The higher the FRR, the lower the lipid concentration, and consequently the lower the rate of diffusion. This phenomenon led to partly incomplete nucleation and a lower rate of particles formation (Balbino et al., 2013). However, it should be noted that at these high flow rate ratios, the concentration of SLNs will be reduced. This can be mitigated by concentration of the batch during the TFF step. Alternatively, higher initial lipid concentrations can be considered (Joshi et al., 2016).

When looking at the surface charge of the SLN particles, zeta potential values remained unchanged across the FRRs tested (around -20mV; Figure 2.11B). Tristearin or glyceryl tristearate is a triglyceride derived from three units of stearic acid, without any charged group at neutral pH (Mehnert and Mäder, 2001, Xue and Wong, 2011, Wissing et al., 2004). However, PEG-DSPE is a linear phospholipid, a block copolymer of a hydrophobic part (DSPE) and a hydrophilic part (PEG) (Wang et al., 2012a). The phosphoethanolamine group is completely ionised at pH 7.4, giving the PEG a net negative charge. By adding PEG-DSPE to SLNs formulation the distearoyl tail is incorporated to the tristearin solid layer and the hydrophilic PEG-phosphoethanolamine part remained on lipid surface, making particles negatively charged (Lobovkina et al., 2011, Uner and Yener, 2007, Kashanian et al., 2014). It is also known that the addition of PEG may help the manufacture of more homogeneous

particles (Bahl et al., 2017). Direct incorporation of PEG onto the surface of the particle in a single step process has advantages over addition via conjugation post production in terms of reduced process steps and PEGylation of nanoparticles is used in a range of approved products e.g. Doxil which is a PEGylated liposome product.

In the development of manufacturing processes, production speed is important. Here it was demonstrated that total flow rates of 20 mL/min can easily be adopted with no effect on the particle size or protein loading (Figure 2.15). This is in line with previous work on liposomes, where increasing the flow rate from 10 to 20 mL/min had no effect on liposome size, PDI or protein loading (Forbes et al., 2019). Within the microfluidic cartridge, even although the surface to volume ratio is relatively high (due to the reduced dimensions of the channels), the Reynolds number (Re=1 $\rho v/\eta$) of liquid is quite low (around 1) (Lam et al., 2009, Huang et al., 2006). In these conditions, the flow tends to be laminar and driven by diffusive forces, with a direct consequence on mixing process speed. To overcome these issues, either the contact area or the contact time between solutions need to be enhanced. To address this, the inner geometry of the cartridge plays an important role with the serpentine shape of the microchannel doubling the mixing efficiency of conventional straight microchannel (Forbes et al., 2019). Thus, microchannel shape and materials used for developing microfluidic devices are critical aspects that should be considered in the production process. For instance, it has been seen that the combination of micromixer geometry and hydrodynamic flow focusing regime affected particles size.(Jahn et al., 2010). Additionally, polydimethylsiloxane (PDMS) is currently the most commonly used materials for cartridge fabrication (Chaudhury and Whitesides, 1991, Morra et al., 1990).

As part of the production process, the residual ethanol concentration in the final product is one of the characteristics that must be considered. Ethanol is a Class 3 solvent, which is considered less toxic and a lower risk solvent compared to Class 1 and 2 solvents and levels of 50 mg per day or less (corresponding to 5000 ppm or 0.5%) being acceptable without justification (Klok and Windhorst, 2006, Qin et al., 2004). For laboratory production of SLNs, three methods were considered and both TFF, spin column and dialysis can remove solvents to below the required ICH levels (Figure 2.13D). Moreover, TFF was shown to give slightly lower recovery compared to the other methods (Figure 2.13C) and particles physico-chemical attributes were altered after filtration (Figure 2.13A-B). These results are opposite to previous reports, where TFF has been demonstrated for the purification of other nanomedicines. For example, poly-vinyl alcohol (PVA) and sodium cholate were shown to be removed from monomethoxy poly (ethylene glycol) – poly (D, L-lactide-co-glycolide) (mPEG-PLGA) co-polymer nanoparticles using TFF, without changing particles properties (Dalwadi and Sunderland, 2007). Furthermore, tangential flow filtration was applied to purify Poly (d, l-lactic acid)

nanoparticles from poloxamer 188. Within this study, the authors reported that purification of the nanoparticles from the excess surfactant using tangential flow filtration enabled better drying results when the different sugars were studied (Hirsjärvi et al., 2009). It should be considered, however, that in these studies the chemical composition of TFF column was slightly different compared to the one used in this chapter; these changes might minimize non-specific binding between the inner column area and the particles surface. Furthermore, in the works mentioned above, the use of high quantities of surfactants might help to increase particles stability during TFF purification, avoiding particles breakage and reassembly into less homogeneous structures. However, the application of spin column as alternative SLNs purification method to old-established dialysis resulted to be successful, with no alterations in particles attributes and lipid recovery (Figure 2.6). Spin column, known as size exclusion chromatography (SEC), is the simplest and mildest of all the chromatography techniques which allows separation of molecules based on differences in size, enabling group separation of biomolecules that are above the exclusion limit of the medium (Davis and Gregoriadis, 1987, Lesieur et al., 1991). When an aqueous solution is used to transport the sample through the column, samples are processed using an isocratic elution and larger molecules are eluted in or just after the void volume, as they pass through the column at the same speed as the flow of buffer; instead small molecules such as salts that have full access to the pores move down the column, and they are eluted later. These findings were in line with what has been previously reported in literature. For instance, the use of a G-25 Sephadex column for purification of egg-phosphatidylethanolamine (PE) and brain Lα-phophatidylserine (PS) anionic liposomes allowed the recovery of almost 100% of the lipid materials (Ruysschaert et al., 2005). Moreover, docetaxel-loaded liposomes (DSPC: Chol: DSPE-PEG2000) physicochemical properties were maintained after SEC purification. Therefore, the combination of both fast manufacturing and purification can accelerate SLNs product generation.

Considering protein loading within solid lipid nanoparticles, drug loading via microfluidics is a passive mechanism, where a simultaneous dispersion of drug and lipids in the aqueous phase occurs and microfluidics can promote higher encapsulation efficiency compared to conventional techniques. Herein, high protein (OVA) loading was achieved even at lower OVA concentrations (around 40% LE at 0.1 mg/mL initial OVA; Figure 2.14 and 2.15). This is higher than commonly reported for SLNs manufactured by other methods. For example, it has been seen that egg lecithin and stearic acid based SLNs made through warm microemulsion were able to encapsulate below 5% of the water soluble immunostimulant thymopentin (Morel et al., 1996). The same technique was applied for cyclosporine loading into SLNs made of a mixture of stearic acid and Epikuron 200. However, the loading efficiency was not promising (just 13%) (Ugazio et al., 2002). Further, supercritical fluids

(e.g. CO_2) were applied to SLN manufacturing. However, many papers reported that the entrapment efficiency of small peptides – e.g. Insulin – within Tristearin based SLNs was very low (<3%) (Salmaso et al., 2009a, Salmaso et al., 2009b). This improved loading via microfluidics has also been shown with other nanoparticle systems, for example, 1,2-distearoyl-sn-glycero-3-phosphocholine (and cholesterol liposomes made by microfluidics gave approximately 30 % protein loading (0.18 mg/mL initial OVA concentration). This is in comparison to below 5 % with lipid hydration and extrusion or sonication (Forbes et al., 2019). Furthermore, the concentration of sulforhodamine B in liposomes prepared with microfluidics was found to be unexpectedly high due to a spatial concentration enhancement induced by viscosity anisotropy in the microchannel (Jahn et al., 2007). Therefore, the combination of the fast production step and higher entrapment efficiency of protein demonstrates the suitability of microfluidics as effective alternative method for protein loaded solid lipid nanoparticles. This can translate directly into cost savings and improvement in product method performance.

In terms of release from the SLNs (Figure 2.16), most of the protein was released within 24 h. The initial fast release of OVA maybe resulting from OVA associated at the surface layer of the solid lipid nanoparticles (Xu et al., 2015) and the PEG coating on SLNs surface could accelerate the release of proteins or drugs from lipid matrix. It has been seen (Liu et al., 2007) that PEGylated particles showed a faster protein release with an initial burst, probably due to protein diffusion through polymer pores and impaired protein interaction with lipophilic molecules (Zhang et al., 2014).

2.5 Conclusions

The work reported here demonstrates that it is possible to effectively formulate, manufacture, purify and monitor the particle size of SLNs produced by two different methods – microfluidisation and microfluidizer. Within this study, SLNs at approx. 200 nm or below containing low and high PEGylation and incorporating OVA were formulated with both techniques. The modification of the PEGylation will allow evaluation of these delivery systems as potential adjuvants (low PEGylation) and for therapeutic drug delivery (high PEGylation). However, despite promising results obtained with microfluidisation - rapid manufacture (2 cycles) and at a low pressure (20,000 psi) and removal of non-entrapped protein achieved after 12 diafiltration cycles - the need of large volumes for sample production might limit its applicability for development of new formulations at early stage or for samples containing expensive excipients. Therefore, herein microfluidics was demonstrated to be a valid alternative method for high-throughput manufacturing of both empty and protein loaded solid lipid nanoparticles which require low operating volumes (between 1 and 5 mL). Both the total flow rate and the flow rate ratio were identified as critical process parameters and

particles physicochemical attributes were confirmed to be suitable for pre-clinical and clinical applications. Furthermore, using the microfluidics method it was possible to combine particles manufacturing and drug encapsulation in a single process step, with evident benefits for time of production. Additionally, these promising results emphasise the suitability of this method to be adopted for further development of adjuvants for a self-amplifying RNA vaccine.

CHAPTER 3

Manufacturing of different delivery systems for a self-amplifying RNA (SAM) vaccine
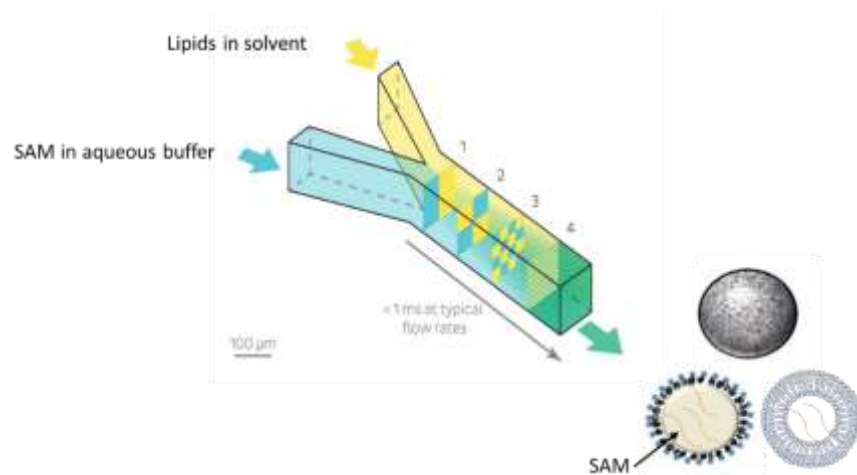
3.1 Introduction

Nucleic acid-based vaccines such as viral vectors, plasmid DNA, and mRNA have emerged as an alternative vaccination approach in the last few decades, aiming to address several unmet medical needs. These new generation vaccines are very promising due to their ability to elicit both humoral and cellular immunity in a safe manner (Smerdou and Liljestrom, 1999). However, so far there is still no licensed nucleic acid–based vaccine for human use. The reason might be due to several factors; for example, recombinant viral vectors are shown to be efficient delivery systems, but, due to antivectorial immunity, production limitations, and safety issues, their use is restricted (Smerdou and Liljestrom, 1999). Regarding plasmid DNA (pDNA), even though they are much safer and broadly effective in small animal models, a large dose of DNA is required to induce a potent immune response in humans (Kutzler and Weiner, 2008). These disadvantages have been partially overcome through optimization of pDNA constructs, coexpression of immune-stimulatory molecules, and improved delivery technologies. Ongoing clinical trials will ultimately determine if these improvements in pDNA vaccines are sufficient to generate practical human vaccines (Sardesai and Weiner, 2011). A promising alternative to pDNA is mRNA technology (Wolff et al., 1990). The advantages of mRNA vaccines are numerous; first, mRNA need only be delivered to the cytoplasm of the cells to be translated, while pDNA must also be transported from the cytoplasm across the nuclear membrane (Weissman, 2015, Petsch et al., 2012). Second, the integration of pDNA into the host genome following transfection is an additional safety concern; on the other hand, RNA technology does not suffer from this issue. Several means of mRNA delivery have been explored, including injecting naked mRNA, device-mediated delivery such as the gene gun or electroporation, (Hoekstra, 2001, Behr et al., 1989) or formulating with synthetic delivery vehicles, such as liposomes, lipoplexes, and cationic polymers. mRNA potency can be further increased by using a Self-amplifying RNA (SAM) strategy (Heidenreich et al., 2015) (Geall et al., 2012a). Here, the vaccine is based on an α-virus genome, in which the structural genes of the alphavirus that form viral particles have been replaced with the mRNA encoding an antigen of interest (Kramps and Elbers, 2017). However, significant elements that induce the amplification process of the virus have been left, such as polypeptides which, when cleaved which makes a RNA dependent polymerase that amplifies the mRNA by generating multiple copies of the RNA (Choi and Chang, 2013). This leads to significantly greater immune responses than conventional RNAs. However, the most challenging step in realizing the full potential of self-amplifying RNA vaccines is the efficient nonviral delivery of the nucleic acid to the cell cytoplasm, where it can amplify and express the encoded antigen (A L Audouy et al., 2002, Pollard et al., 2013, Kallen and Theß, 2013). When administered into the body, SAM might undergo biological degradation via RNases present at the injection site (Choi et al., 2004). Moreover, SAM must translocate through the cellular membrane to enter the cytoplasm

and initiate translation of the non-structural proteins. However, due to its hydrophilicity and net negative charge, cellular uptake is limited (Hoerr et al., 2000). Therefore, to overcome these issues, delivery systems are required. Lipid nanoparticles (LNP) systems are currently the lead non-viral delivery systems for enabling the clinical potential of genetic drugs. They are composed of an ionizable amino lipid, an helper lipid (usually a phosphatidylcholine i.e. 1,2-distearoyl-sn-glycero-3-phosphocholine - DSPC), cholesterol and a coat lipid (polyethylene glycol based lipid) (Jayaraman et al., 2012). heptatriaconta-6,9,28,31-tetraen-19-yl 4-(dimethylamino)butanoate (DLin-MC3-DMA) is currently the most active ionizable lipid being used in clinical trials. It is also currently the gold standard cationic lipid for silencing liver targets (Jayaraman et al., 2012). However, the application of DLin-MC3-DMA-based LNPs might be limited due to its high cost and sophisticated synthetic pathway (Heyes et al., 2005). Hence, development of a less expensive alternative carrier with comparable ability of SAM protection and antigen expression might be beneficial. For this purpose, two cationic lipids – DOTAP and DDA- were used. There has been extensive work in identifying both lipids as efficient transfection agents and immunostimulant. DDA is known to induce cell-mediated immunity and delayed-type hypersensitivity (Klinguer-Hamour et al., 2002). DDA based liposomes have previously been evaluated as carriers for drugs, (Carmona-Ribeiro et al., 1997) as antimicrobial agents (Lincopan et al., 2003) and as adjuvants for a range of vaccines for both parenteral and mucosal delivery (Hilgers et al., 1984, Klinguer et al., 2001, Snippe et al., 1977, Lima et al., 2001, Tsuruta et al., 1997). Recently they have been used as part of more complex adjuvant systems for experimental subunit vaccines (Brandt et al., 2000b, Lindblad et al., 1997, Holten-Andersen et al., 2004, Rosenkrands et al., 2005). In addition, the association of DDA with the immunostimulatory glycolipid trehalose dibehenate (Davidsen et al., 2005) is currently in phase I clinical trials. Moreover, DOTAP is commonly cited as transfection agent, usually in combination with the helper lipid DOPE. This helper lipid can form the inverted hexagonal structure in liposome and cause freeing DNA/RNA from lipoplex and releasing into cytoplasm (Dass and Choong, 2006, Caracciolo et al., 2007) due to its ethanolamine head group. It has been seen that by encapsulating antigen-encoding plasmid DNA (pDNA) into cationic liposomes composed of PC, DOPE and DOTAP, improved antibody responses and antigen specific cytotoxic T-lymphocyte (CTL) responses were obtained after intramuscular administration in mice, as compared to naked pDNA (Gregoriadis et al., 1997, Bacon et al., 2002). Besides, this formulation improved the immune response after administration of antigen-encoding pDNA via the subcutaneous or oral route (Perrie et al., 2002, Perrie et al., 2003). The increased potency of liposome-encapsulated pDNA as a vaccine was ascribed to the protective effect of DOTAP liposomes against enzymatic degradation of pDNA, and improved interaction with negatively charged cellular

membranes. This leads to improved transfection and consequently higher antigen levels (Perrie et al., 2001).

3.1.1 Aim and objectives

Within this chapter, as validation step, cationic liposomes composed of 1,2-dioleoyl-phosphoethanolamine (DOPE) and 1,2-dioleoyl-3-trimethylammonium-propane (DOTAP) were produced using microfluidics. Further, the impact of changes in process parameters like flow rate ratio (FRR), total flow rate (TFR) and lipid concentration on vesicles attributes were analysed. The aim was to:

- Better understand the suitability of microfluidics to prepare cationic liposomes.
- Use this methodology for further applications as delivery systems and antigen adjuvants production.

Moreover, these findings were then adopted to produce different carriers - liposomes, solid lipid nanoparticles (SLNs), polymeric nanoparticles (NPs) and cationic nanoemulsions (CNE) - for a self-amplifying RNA (SAM) vaccine. Formulations differed in physico-chemical attributes, but they all contained one cationic lipid - 1,2-dioleoyl-3-trimethylammonium-propane (DOTAP) or dimethyldioctadecylammonium (DDA). The aim of the project was to:

- Compare empty and SAM loaded carriers according to their physico-chemical properties (hydrodynamic radius, polydispersity index – PDI - and surface charge).
- Evaluate the ability of cationic formulations to efficiently encapsulate or adsorb SAM, thereby protecting the antigen from enzymatic degradation.

3.2 Materials and methods

3.2.1 Materials

Poly (D, L-lactide-co-glycolide) lactide: glycolide (50:50), mol wt 30,000-60,000, Dimethyl Sulfoxide, Tristearin (Grade II-S, ≥90%) Cholesterol and squalene were obtained from Sigma-Aldrich Company ltd. Dipalmitoylphosphatidylcholine (DSPC), 1,2-dimyristoyl-rac-glycero-3-methoxypolyethylene glycol-2000 (DMG-PEG2000), Dimethyldioctadecylammonium (DDA) and 1,2-dioleoyl-3-trimethylammonium-propane (DOTAP) were obtained from Avanti Polar Lipids, Alabama. Ethanol, methanol, 2-propanol, 1,1'-Dioctadecyl-3,3,3',3'-Tetramethylindocarbocyanine Perchlorate (DilC), Tween 20 and Span 80 were obtained from Fisher Scientific UK, TRIS Ultra-Pure was obtained from ICN Biomedicals. Tertiary cationic lipid "X" was provided by Discovery, Drug Product Development department Rockville, USA.1,2-Distearoyl-phosphatidylethanolamine-methyl-polyethyleneglycol conjugate-2000 (DSPE-MPEG-2000) was obtained from Lipoid GmbH (Germany). Sephadex G-25 size exclusion columns were obtained from GE Healthcare Life Science (UK). MicroKros hollow

fibre filter (750K MPES 0.5MM MLL X FLL 1/PK) was obtained from Spectrum Laboratories, Inc (UK).

3.2.2 Preparation of liposomes

Liposomes formulations were prepared using benchtop NanoAssemblr instrument (NanoAssemblr, Precision Nano- Systems Inc.). Briefly, lipid mixture composed of DOTAP and DOPE (1:1 w/w, 4 mg/mL initial concentration) was dissolved in methanol. TRIS buffer pH 7.4 10 mM was used as aqueous phase. Both solutions were mixed via microfluidics and vesicles were collected in a 15-mL falcon tube. The total flow rate (TFR) was varied between 5 and 20 mL/min and the aqueous/solvent ratio (FRR) was varied between 1:1, 3:1 and 5:1. To evaluate the effect of lipid concentration on liposomes size, initial lipid mixture content was varied from 0.25 to 10 mg/mL. Liposomes were manufactured using the Nanoassemblr as previously described. Process parameters – FRR and TFR – were set up at 1:1 and 15 mL/min respectively.

3.2.3 Solvent purification methods

To consider solvent purification methods, liposomes attributes (size, PDI and zeta potential) as well as residual solvent levels were quantified after tangential Flow Filtration (TFF – KR2i TFF System – Filtration speed 27 mL/min, washing volume 20 mL), dialysis (1-hour, membrane cut off 14 000 KDa) and spin column (3 mL elution buffer volume). Residual solvent was detected using gas chromatography (GC-MS, Agilent Technologies) adding 1% 2-propanol (IPA) as internal standard; peaks area was normalised by IPA peak area and related to solvent concentration through a calibration curve with a linearity of $R^2 = 0.9502$. All measurements were within the level of detection and level of quantification (refer to chapter 2.2.3 for details).

3.2.4 Lipid recovery quantification after purification

Lipid recovery after dialysis, TFF and spin column was performed by adding 1,1'-Dioctadecyl-3,3,3',3'-Tetramethylindocarbocyanine Perchlorate (DilC) 0.2% mol total lipid concentration solved in ethanol to lipid stocks before being loaded in the Nanoassemblr. DilC fluorescence was measured before and after TFF, dialysis and spin column (PolarStar, BMG LABTECH GmbH). Lipid quantification was achieved by referring to a calibration curve with a linearity of $R^2=0.995$. All measurements were within the level of detection and level of quantification (refer to chapter 2 for details).

3.2.5 SAM synthesis

DNA plasmids encoding the self-amplifying RNAs were constructed using standard molecular techniques. Plasmids were amplified in Escherichia coli and purified using Qiagen Plasmid Maxi kits (Qiagen). DNA was linearized immediately following the 3′ end of the self-amplifying RNA sequence by restriction digest. Linearized DNA templates were transcribed

into RNA using the MEGAscript T7 kit (Life Technologies) and purified by LiCl precipitation. RNA was then capped using the Vaccinia Capping system (New England BioLabs) and purified by LiCl precipitation before formulation. Both self-amplifying RNA encoding for a green fluorescent protein (SAM-GFP) and self-amplifying RNA encoding for rabies glycoprotein (SAM-Rabies) were used in the study.

3.2.6 SAM-formulations preparation

<u>Formulation of liposomes</u>: SAM-liposomes were prepared in the Nanoassemblr Platform. Briefly, lipid mixtures, composed of DOPE and a cationic lipid (DOTAP or DDA) were prepared in methanol at 1:1 mole ratio. Then, the lipids and an aqueous phase (10 mM TRIS buffer pH 7.4) were injected simultaneously in the micromixer. Empty liposomes were prepared at 4 mg/mL initial lipid concentration, 1:1 aqueous: organic flow rate ratio (FRR) and 15 mL/min total flow rate (TFR).

<u>SAM-Lipid Nanoparticles (LNPs) manufacturing</u>: SAM-LNPs were prepared in the Nanoassembr by mixing tertiary cationic lipid "X": Chol: DSPC: 14:0-PEG2000 (10:48:40:2 mol%) in methanol at 4 mg/mL initial lipid concentration. Citrate buffer 20mM pH 6 was used as aqueous phase. TFR and FRR were set up at 10 mL/min and 3:1.

<u>Solid-lipid nanoparticles (SLNs) and polymeric nanoparticles (NPs) preparation</u>: cationic SLNs were prepared with the Nanoassemblr ;1.3 mg of Tristearin, 2mg of DOTAP and 2% w/w of 14:0 PEG 2000 were solved in 1mL hot ethanol (70°C); TRIS buffer pH 7.4 10 mM was used as aqueous phase. Both solutions were injected inside the chip and particles were collected in a 15-mL falcon tube. The same technique was applied for polymeric nanoparticles (NPs) preparation. Poly (D, L-lactide-co-glycolide) lactide: glycolide (50:50), mol wt 30,000-60,000 (PLGA) 2 mg/mL and DOTAP 2 mg/mL were solved in DMSO. Furthermore, DDA based SLNs and NPs were obtained by substituting the cationic lipid DOTAP with DDA, following the method described above.

<u>Emulsion preparation</u>: to make oil in water (O/W) cationic nanoemulsions (CNE), DOTAP or DDA in chloroform was placed in a beaker and the volume allowed to evaporate to 200 ml, Tween (0.5%, w/w), Squalene (5.0%, w/w) and Span (0.5%, w/w) were added and vortexed for 1 min to provide a homogeneous feedstock. This primary emulsion was passed 5 times through M110-p Microfluidizer at 25,000 psi to reduce droplets size. Chloroform was let evaporate leaving the sample overnight under vigorous stirring. In order to prepare anionic nanoemulsions (MF59-like) the protocol described above was followed without adding any cationic lipid during the sample preparation. To encapsulate either SAM-GFP or SAM-Rabies inside formulations, liposomes, SLNs and NPs were formulated with the addition of RNA 8:1 mol/mol N:P (Nitrogen –N- in the cationic lipid and Phosphate- P- in SAM) in the aqueous phase of Nanoassemblr, following the protocol explained above. To load RNA on the surface, the nucleic acid (8:1 mol/mol N: P) was mixed with formulated liposomes, SLNs, NPs and

CNE under mild stirring. Dialysis was applied to liposomes, LNPs, SLNs and NPs as purification method (1h against 200mL aqueous buffer, membrane cut off 14000 Da).

3.2.7 Quantification of SAM loading and adsorption efficiency

After organic solvent removal, SAM encapsulation efficiency (EE%) was measured using Quant-iT RiboGreen RNA Assay Kit. Briefly, 100 µL of the diluted fluorescent dye was added to each formulation and incubated in the absence of light for 5 min. This allowed the dye to quantitatively bind free nucleic acid. The concentration of non-loaded SAM was determined by measuring fluorescence (λ_{em}=480 nm, λ_{ex}=520nm) using either Polarstar Omega (BMG Labtech) or Synergy H1 Hybrid Multi-Mode Reader (BioTek Instruments, Inc) and referring to a calibration curve (Figure 3.1). The actual loading was obtained by subtracting the unloaded SAM to the initial nucleic acid concentration. Furthermore, to quantify SAM adsorption rate, SAM adsorbing samples were ultracentrifuged for 20 min at 10000 rpm (Beckman Coulter Airfuge Air-Driven Ultracentrifuge) to separate free SAM from adsorbed ones. Then the subnatant containing non- adsorbed nucleic acid was used for SAM quantification. The adsorption efficiency (LE%) was calculated using the method above.

3.2.8 Physiochemical characterization of formulations

All formulations were characterized in terms of hydrodynamic size (Z-average), polydispersity index (PDI) and surface charge (zeta-potential) by dynamic light scattering (DLS) in a Zetasizer Nano ZS (Malvern, UK) at 0.1 – 0.2 mg/mL at 25 ˚C.
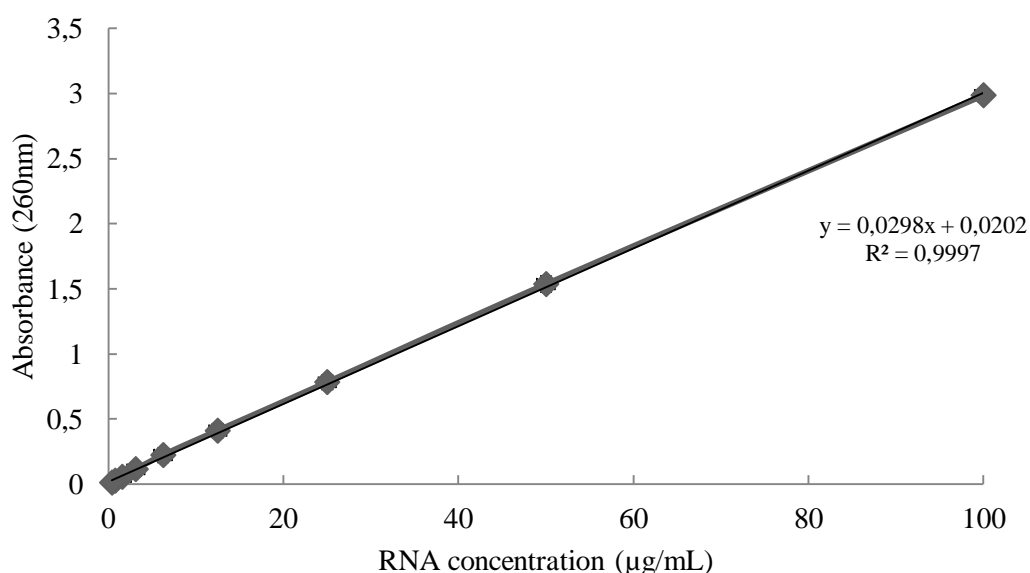
Figure 3. 1 Calibration curve for RNA quantification. Calibration curve for the determination of RNA R^2 = 0.999. Data were obtained using PolarStar, BMG LABTECH GmbH Spectrophotometer.

3.2.9 RNA gel electrophoresis and RNase protection assay

To assess the ability of DOTAP or DDA based formulations to protect RNA from RNase degradation, each RNA/formulation complex was exposed to 0.5 µAU of RNase A (Ambion, Austin, TX) per microgram of RNA for 30 minutes at room temperature. RNase was inactivated by proteinase K (Novagen, Darmstadt, Germany) and incubating the sample at 55 °C for 10 minutes. To extract the remaining RNA from lipid formulations, ethanol or 2-propanol 1:20 v/v was added to the solution, mixed, and centrifuged at 12K RPM for 15 minutes. The aqueous phase containing RNA was removed and used to analyse RNA integrity by denaturing gel electrophoresis. A 1% denaturing precast agarose gel was used (Bio-Rad, Hercules, CA). 1 µg of RNA was loaded per lane. Millennium markers (Ambion) were used to approximate the molecular weight of the RNA. The gel was run at 100 V and then stained using 0.1% SYBR gold according to the manufacturer's guidelines (Invitrogen, Carlsbad, CA) in water by rocking at room temperature for 1 hour. Gel images were taken on a Bio-Rad Chemidoc XRS imaging system.

3.3 Results

3.3.1 Effect of operational parameters – total flow rate and flow rate ratio

To initially optimise the production method for cationic systems, the well-reported DOPE:DOTAP liposomes formulation was selected. Herein, microfluidics was used as manufacturing method for homogeneous liposomes production and process parameters like the total flow rate (TFR) and the solvent/aqueous ratio (FRR) were investigated. As shown in Figure 3.2A, increasing the flow rate ratio (FRR) from 1:1 to 5:1 increased the vesicle size; for example, for formulations with TFR 10 mL/min the size went from around 41 ± 3 nm at FRR 1:1 to around 148 ± 40 nm for the FRR 5:1.
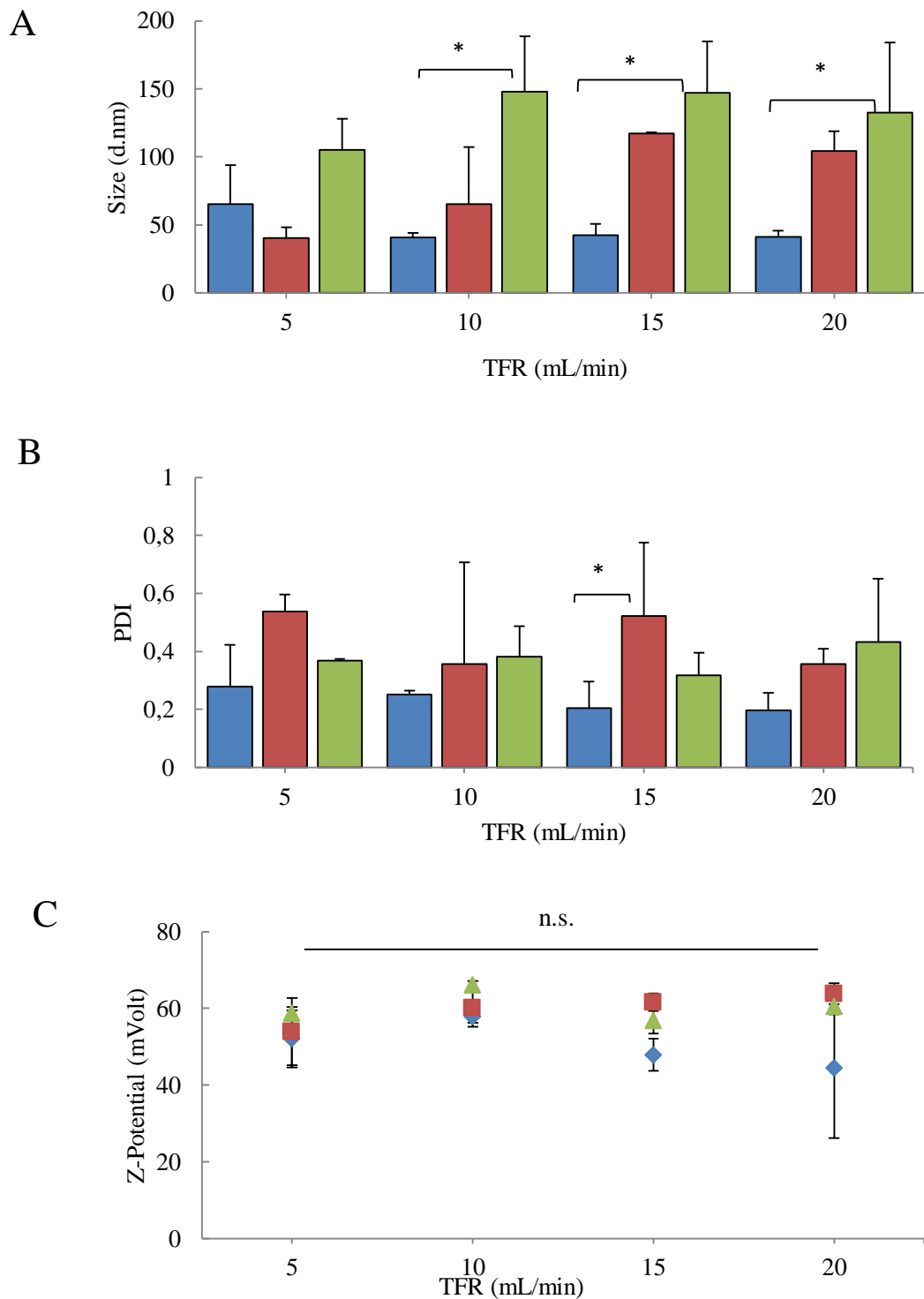
Figure 3. 2 DOTAP:DOPE liposomes made by Nanoassemblr. DOTAP:DOPE liposomes made by Nanoassemblr changing TFR and FRR a) size b) PDI and c) Z-potential increasing TFR from 5 to 20 mL/min. Blue, red and green columns/lines represent formulations with FRR 1:1, 3:1 and 5:1 respectively; Results are expressed as the means of three independent experiments ± S.D.

However, particles attributes seemed to be independent from the TFR applied. Polydispersity index tended to follow a similar trend, with more homogeneous particles obtained at lower FRRs, despite the TFR choice (Figure 3.2B). For instance, at TFR 20 mL/min, enhancing solvent/aqueous ratio from 1:1 to 5:1 resulted in PDI increase of more than two-fold. Furthermore, liposomes surface charge was maintained highly cationic, regardless of alterations in flow rates and ratios with the liposomes having a positive zeta potential of 50-60 mV (Figure 3.2C).

3.3.2 Effect of lipid concentration

As known, the increase in FRR will induce dilution of liposomes and lower liposome concentrations in the final formulation. A subsequent concentration process based on filtration, chromatography or centrifugation adds additional processing time and may alter the final product. Therefore, to circumvent this additional process step, the dilution of the lipids at higher FRR was counteracted by increasing initial lipid concentrations introduced to the micromixer at the desired FRR. Through this method the lipid amount was varied from 0.25 to 10 mg/mL. As is shown in figure 3.3A, increasing the lipid concentration resulted in smaller liposome size; more precisely, at lipid content of 0.25 mg/mL size was 153 ± 43 nm, while increasing DOTAP: DOPE concentration of 40 times, vesicles became smaller (40 ± 2 nm). A similar trend was followed by PDI values; at initial lipid amount below 1 mg/mL liposomes tended to be very heterogeneous with PDI>0.4. However, increasing lipid stock above 4 mg/mL led to more homogeneous and monodisperse samples production with PDI<0.2 (Figure 3.3A). Zeta potential values seemed to be independent from lipid concentration and they remained highly positive (around +40 mVolt) among the different concentrations tested (Figure 3.3B).

3.3.3 Comparison of different purification processes for cationic liposomes produced by microfluidics

Samples produced by microfluidics contain up to 50% of organic solvent, thus a purification step is required after manufacturing. Therefore, DOTAP: DOPE liposomes were prepared using microfluidics at TFR 15 mL/min and FRR from 1:1 to 5:1. Tangential flow filtration (TFF), size exclusion chromatography (SEC) and dialysis were compared in terms of solvent removal suitability. As shown in Figure 3.4A, comparing formulations made at the same FRR, dialysis and SEC seemed to give comparable size and PDI values. For example, at FRR 1:1 liposomes were around 40 nm in size with a polydispersity index of 0.25 after both purification steps. Moreover, increasing aqueous/solvent ratio resulted in bigger and less homogeneous vesicles as seen in the previous chapter. More precisely, moving from FRR 1:1 to 5:1 vesicle size was 3-fold and 4-fold higher after SEC and dialysis respectively. However, liposomes obtained after TFF washes   seemed to be larger in size and higher in polydispersity compared

to the other purification methods tested, (Figure 3.4A). For instance, at FRR 1:1 size and PDI after TFF were 2-fold higher compared with what was obtained with dialysis and spin column. Nevertheless, solvent removal technique seemed to dictate the final vesicles surface charge. More in details, as shown in Figure 3.4B, only dialysis method could maintain a positive Z-potential (between +50 and +60 mV) as expected from liposomes made of cationic lipids, while both TFF and spin column reduced charge close to neutrality.
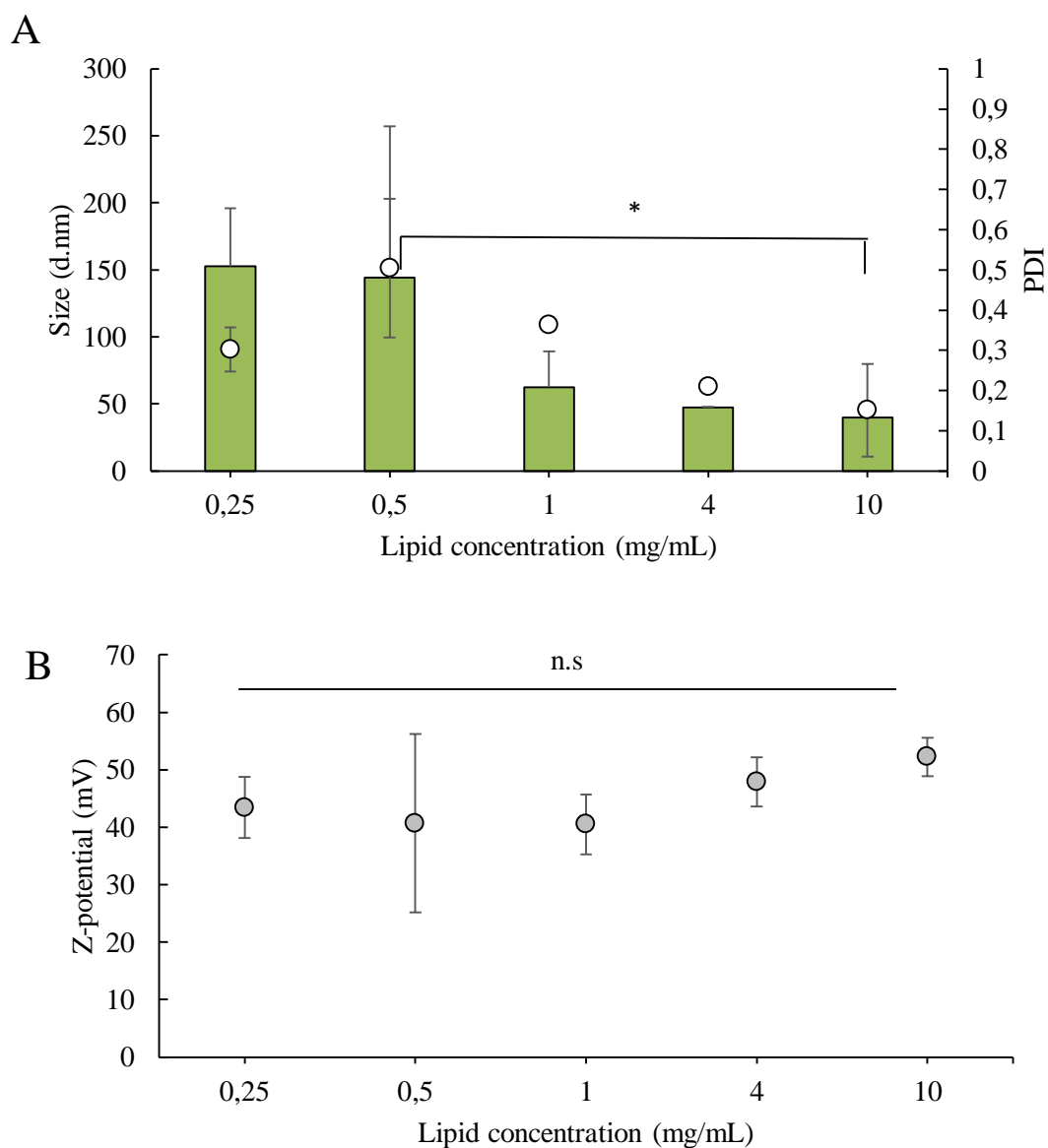
Figure 3. 3 Effect of changing lipid concentration on liposomes attributes A) size (columns), PDI (dots) and B) Z-potential of DOPE: DOTAP liposomes increasing lipid concentration from 0.25 to 10 mg/mL. TFR and FRR were set up at 15 mL/min and 1:1 respectively. Results are expressed as the means of three experiments ± S.D.
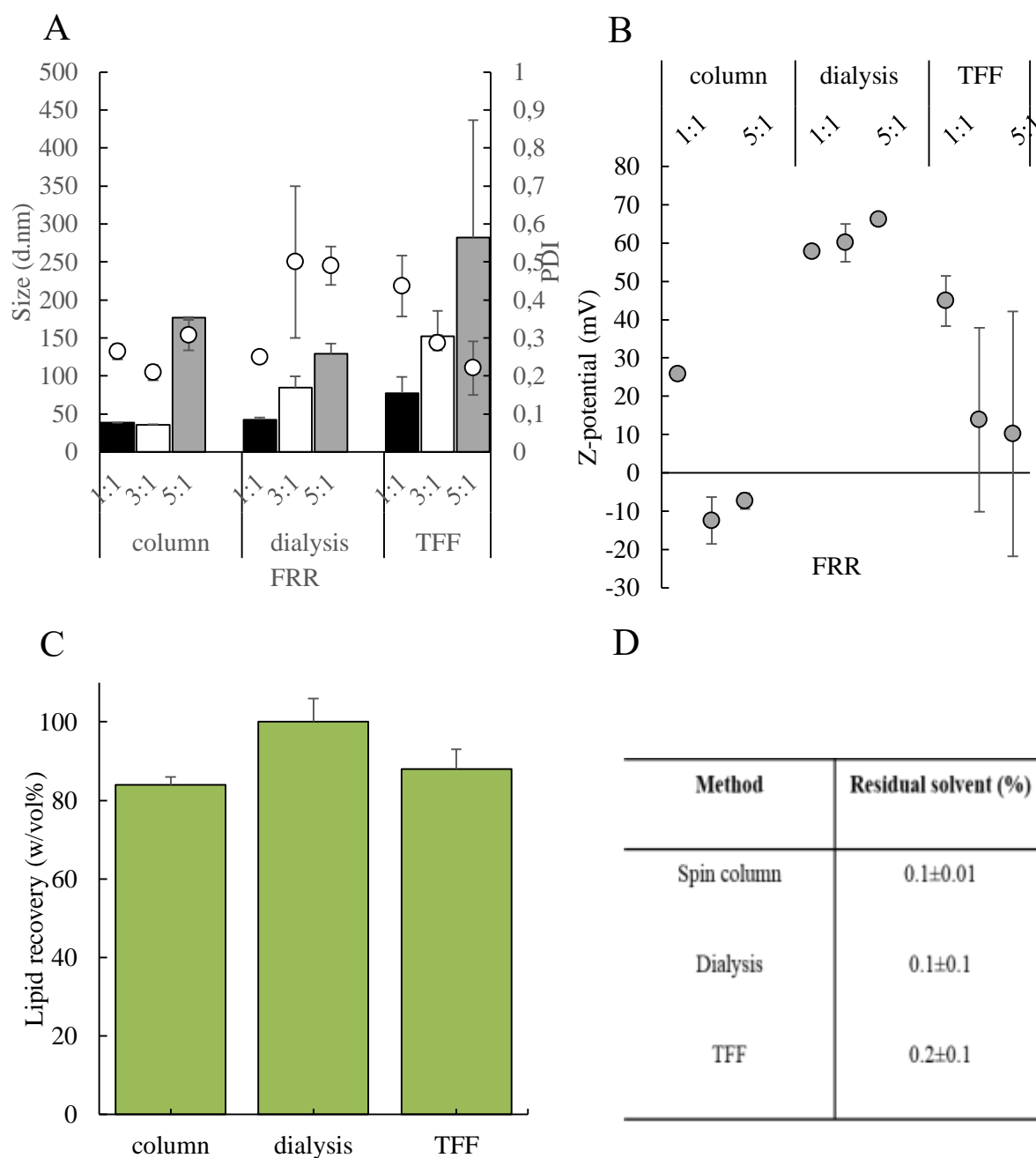
Figure 3. 4 Comparison of different purification methods for DOPE: DOTAP liposomes
A) Size (columns) and PDI (dots) of DOPE: DOTAP liposomes after spin column, dialysis and TFF. Formulations with TFR 10 mL/min and FRR 1:1 (black), 3:1 (white) and 5:1 (grey) were tested. B) Zeta potential of DOPE: DOTAP liposomes after spin column, dialysis and TFF purification. Formulations with TFR 10 mL/min and FRR from 1:1 to 5:1 were represented. C) Lipid recovery of DOPE: DOTAP liposomes after spin column, dialysis and TFF (grey). Formulations with TFR 10 mL/min and FRR 1:1 were tested. D) Residual solvent after spin column, dialysis and TFF expressed as percentage of remained methanol (mL%). All data were normalised by IPA standard peaks area. Formulations with TFR 10 mL/min and FRR 1:1 has been tested. Results are expressed as the means of three experiments ± S.D.

Despite differences in vesicles physico- chemical attributes, lipid recovery seemed to be independent from the purification method applied (Figure 3.4C); TFF, dialysis and spin column were equally able to recover above 85% of initial lipids. Moreover, the efficiency to remove organic solvents from samples was comparable among all three methods tested (Figure 3.4D). Figure 3.4D showed that the percentage of residual methanol after TFF, dialysis and spin column was <0,1 % (which corresponds to 1000 ppm) in accordance to ICH guidelines for residual solvent levels.

3.3.4 Evaluating SAM-GFP polymeric particles, cationic emulsions and lipoplex formulations

Microfluidics optimised parameters were then adopted to produce cationic carriers for self-amplifying RNA vaccines platform. Proof of concept for non-viral delivery of SAM vaccines was obtained using a set of cationic formulations – liposomes, NPs, SLNs and CNE- either adsorbing or encapsulating SAM encoding for a green fluorescent protein (GFP). Samples were analyzed according to their physico-chemical properties and compared to the gold standard formulation lipid nanoparticles (LNPs). Carriers exhibited different composition, but they all contained the same cationic lipid (DOTAP or DDA). With respect to DOTAP based formulations, the hydrodynamic size of empty liposomes, SLNs and NPs was around 50 nm, while CNE one was slightly above 150 nm (Table 3.1); size data were similar to what has been obtained for LNPs (size and PDI). As it is shown in Table 3.1, by adding SAM inside or onto formulation surface, it induced an increase in NPs, SLNs and liposomes particles size (up to 200nm, 180 nm and 100 nm respectively) while emulsions droplets diameter remained equivalent to what had been measured in the absence of antigen (around 180 nm). All formulations showed unimodal size distributions with PDI below 0.3. Empty formulations were highly cationic (zeta-potential > 30 mV); however, the addition of SAM slightly reduced this parameter, with values <25 mV for most of the formulations. As expected, LNPs surface charge was neutral. Moreover, the capability to incorporate or adsorb the nucleic acid was evaluated using a fluorescence based assay; data in Table 3.1 revealed that liposomes, SLNs and NPs could encapsulate almost 100% of the initial RNA added. When RNA is added on the surface, the adsorption efficiency of liposomes, SLNs, and emulsions was above 90%; on the other hand, the presence of nucleic acid on the surface seemed to induce PLGA NPs aggregation, which denied the possibility to quantify the adsorption efficiency. These results were in line with what has been obtained for the positive control LNPs. With respect to DDA based formulations, their physicochemical attributes are listed in Table 3.2. As shown, only SAM encapsulating DDA-liposomes have been produced (size around 190 nm, PDI of 0.2, ZP around 50 mV); on the other hand, due to the sample instability induced by the addition of SAM inside formulations, it was impossible to characterize SAM loaded particles. By adding SAM on the surface, liposomes, SLNs and NPs size and polydispersity were increased, with

a reduction in the zeta potential values (Table 3.2). This behavior is less evident on CNE, where the presence of SAM on the surface reduced droplets diameter with a minor effect on zeta potential. Despite that, moving from DOTAP to DDA did not affect the ability of particles to adsorb or encapsulate SAM, with both adsorption (AE) and encapsulation efficiency (EE) above 90% for all formulations (Table 3.2).

Table 3. 1 Physico-chemical properties of DOTAP based formulations. All formulations were prepared at 1 mg/mL final cationic lipid concentration. SAM encoding for a green fluorescent protein was used as model antigen. Results are represented as mean ± SD of three measurements within the same sample. CNE (cationic nanoemulsions), NPs (polymeric nanoparticles), SLNs (solid lipid nanoparticles), LNPs (lipid nanoparticles) EE (encapsulation efficiency), AE (adsorption efficiency).

Delivery system	SAM	Size (d.nm)	PDI	ZP (mV)	SAM EE (%)	SAM AE (%)
CNE	No	151.4 ± 8.5	0.05 ± 0.01	40 ± 1.5	-	-
	Encapsulated	-	-	-	-	-
	Adsorbed	182 ± 33	0.2 ± 0.02	25 ± 2	-	94
SLNs	No	64 ± 0.3	0.1 ± 0.01	30 ± 4	-	-
	Encapsulated	187 ± 21	0.1 ± 0.07	23 ± 0.7	98	-
	Adsorbed	119 ± 0.6	0.2 ± 0.02	15 ± 0.2	-	97
NPs	No	39 ± 11	0.1 ± 0.09	50 ± 7	-	-
	Encapsulated	198 ± 6	0.2 ± 0.04	24 ± 7	98	
	Adsorbed	-	-	-	-	-
Liposomes	No	41 ± 3	0.25 ± 0.006	57.8 ± 1.5	-	-
	Encapsulated	85 ± 4	0.16 ± 0.02	26.5 ± 2.5	96	-
	Adsorbed	118 ± 20	0.3 ± 0.16	38.7 ± 5	97	-
LNPs	No	96 ± 5	0.22 ± 0.003	4 ± 0,3	-	-
	Encapsulated	136 ± 19	0.14 ± 0.02	0 ± 1	99	-
	Adsorbed	-	-	-	-	-

Table 3. 2 Physico-chemical properties of DDA based formulations. All formulations were prepared at 1 mg/mL final cationic lipid concentration. SAM encoding for a green fluorescent protein was used as model antigen Results are represented as mean ± SD of three measurements within the same sample. CNE (cationic nanoemulsions), NPs (polymeric nanoparticles), SLNs (solid lipid nanoparticles) E.E. (encapsulation efficiency), AE (adsorption efficiency).

Delivery system	SAM-GFP	Size (d.nm)	PDI	ZP (mV)	SAM EE (%)	SAM AE (%)
CNE	No	196 ± 22	0.20 ± 0.08	38 ± 2	-	-
	Adsorbed	208 ± 17	0.16 ± 0.03	35 ± 2	-	91
	Encapsulated	-	-	-	-	-
SLNs	No	71 ± 4	0.26 ± 0.02	46 ± 3	-	-
	Adsorbed	201 ± 74	0.30 ± 0.04	26 ± 2	-	99
	Encapsulated	-	-	-	-	-
NPs	No	58 ± 1	0.06 ± 0.01	38 ± 5	-	-
	Adsorbed	268 ± 40	0.30 ± 0.05	26 ± 2	-	99
	Encapsulated	-	-	-	-	-
Liposomes	No	40 ± 5	0.2 ± 0.03	44 ± 5	-	-
	Adsorbed	186 ± 17	0.16 ± 0.02	27 ± 1	-	99
	Encapsulated	195 ± 12	0.20 ± 0.04	42 ± 3	99	-

3.3.2 The choice of antigen did not alter particles physicochemical properties

In this chapter, model SAM encoding for a green fluorescent protein (SAM-GFP) antigen was substituted with the antigen of interest SAM-encoding for rabies glycoprotein (SAM-Rabies). Formulations were prepared with Nanoassemblr or Microfluidizer platform and their physicochemical properties were compared to the standard gold LNPs. All SAM formulations had an average diameter between 100 and 200 nm, PDI <0.3 and slightly positive zeta-potential. With respect to DOTAP based formulations (Figure. 3.5A), the hydrodynamic size of SAM-Rabies liposomes was around 75 and 114 nm when SAM was encapsulated or adsorbed respectively. Polydispersity index was around 0.3 for both formulations. Similar results have been obtained with SAM-GFP. Regarding solid lipid nanoparticles, SAM-Rabies encapsulating and adsorbing SLNs had a diameter of 176 and 100 nm respectively, with PDI around 0.3 and the change from SAM-Rabies to SAM-GFP did not alter particle parameters (Figure 3.5A). Furthermore, both SAM-Rabies and SAM-GFP NPs or CNE size was around

200 nm with PDI<0.2. Formulations resulted to be similar in size compared to the gold standard LNPs which had an average diameter of around 100 nm and PDI around 0,1 despite the choice of antigen (Figure 3.5A). Graph in figure 3.5B reported the surface charge of SAM formulations. As shown, all formulations were slightly positive regardless the loaded antigen: compared to LNPs which had a neutral surface charge at pH 7.4, formulations zeta potential was between +20 and +50mVolt in presence of either SAM-GFP or SAM-Rabies (Figure 3.5B).

A

B
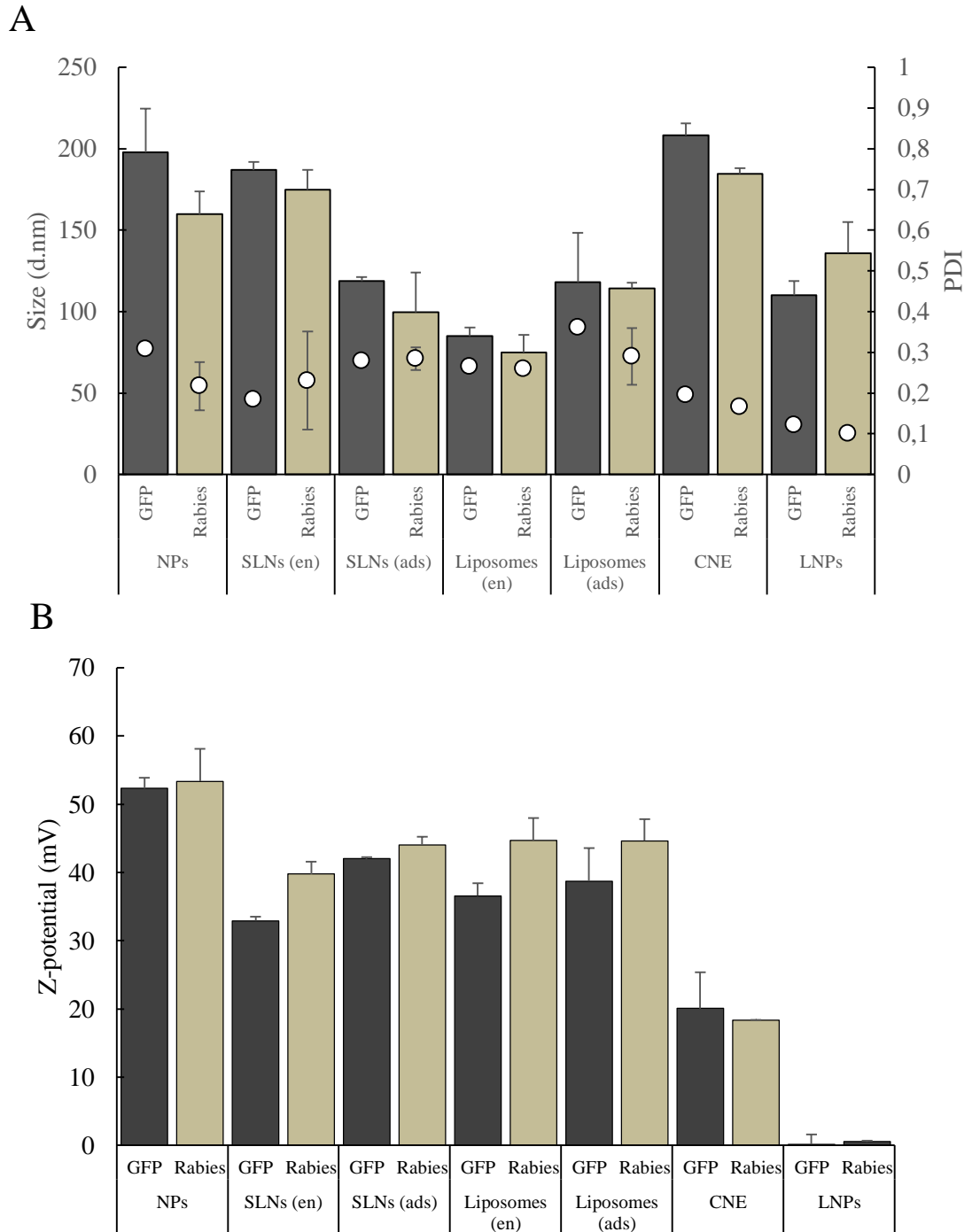
Figure 3. 5 Formulation attributes A) Size (columns), PDI (dots) and B) Zeta potential of empty, SAM-GFP (black) or SAM-Rabies (grey) based DOPE:DOTAP liposomes, Tristearin:DOTAP SLNs, PLGA:DOTAP NPs and DOTAP:CNE. Both antigen adsorbing and antigen encapsulation particles attributes were represented. Formulations were compared with the gold standard LNPs. Results are expressed as the means of three experiments ± S.D. Mann-Whitney non- parametric t-test was used for statistical analysis.
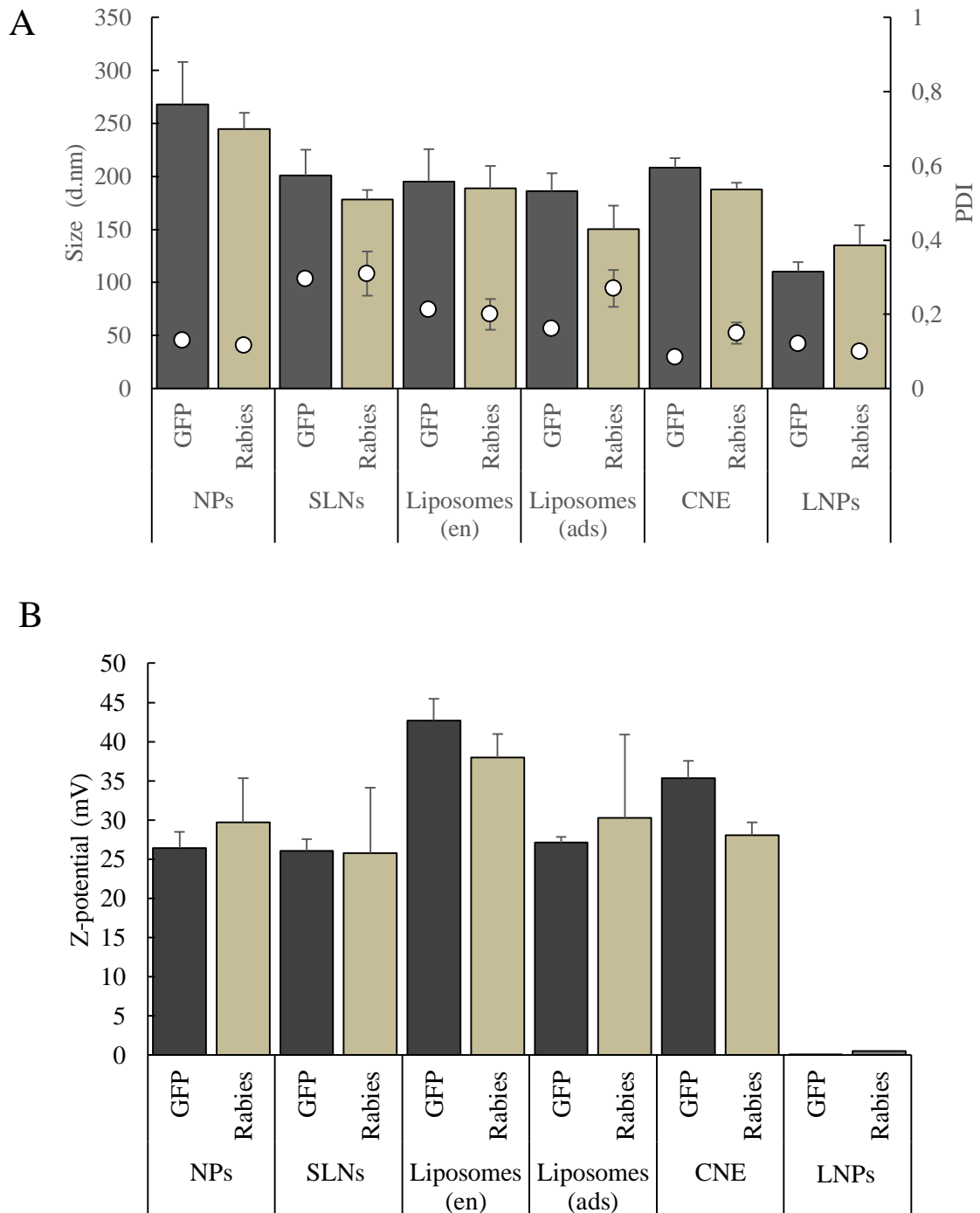
Figure 3. 6 Formulation attributes A) Size (columns), PDI (dots) and B) Zeta potential of empty, SAM-GFP (black) or SAM-Rabies (grey) based DOPE:DDA liposomes, Tristearin:DDA SLNs, PLGA:DDA NPs and DDA:CNE. Both antigen adsorbing and antigen encapsulation particles attributes were represented. Formulations were compared with the gold standard LNPs. Results are expressed as the means of three experiments ± S.D. Mann-Whitney non- parametric t-test was used for statistical analysis and resulted in non significant difference between GFP and Rabies groups.

Table 3. 3 Encapsulation efficiency (EE) and adsorption efficiency (AE) of SAM-GFP and SAM-Rabies in DOTAP based liposomes, SLNs, NPs and CNE. Results are expressed as the means of three experiments ± S.D.

	EE% (GFP)	AE% (GFP)	EE% (Rabies)	AE% (Rabies)
Liposomes	96	97	98	99
SLNs	98	97	99	99
NPs	98	-	88	
CNE	-	94	-	90
LNPs	95		98	

Table 3. 4 Encapsulation efficiency (EE) and adsorption efficiency (AE) of SAM-GFP and SAM-Rabies in DDA based liposomes, SLNs, NPs and CNE. Results are expressed as the means of three experiments ± S.D.

	EE% (GFP)	AE% (GFP)	EE% (Rabies)	AE% (Rabies)
Liposomes	99	99	99	99
SLNs	-	99	-	98
NPs	-	99	-	99
CNE	-	91	-	90

With respect to DDA based formulations, their physicochemical attributes are listed in Figure 3.6A. Changing from DOTAP to DDA generally induced an increase in particles size and polydispersity, while still maintaining comparable surface charge values (Figure 3.6 A and B). For example, DDA SLNs adsorbing SAM Rabies or GFP had a diameter of around 100nm with PDI of 0.3. These values were significantly higher compared with DOTAP ones ($p<0.01$), which were around 100 nm. Tables 3.3 and 3.4 reported the encapsulation efficiency (EE) and adsorption efficiency (AE) values of all DOTAP and DDA particles. Clearly, both EE% and AE% were above 90%, proving that the initial added at the beginning was either fully encapsulated or adsorbed, despite the choice of antigen and cationic lipid. These data were comparable with what was obtained with LNPs.

3.3.3 DOTAP and DDA based formulations could efficiently protect RNA from degradation

RNase-mediated degradation of an RNA vaccine in tissues after administration may be a limiting factor in delivering an intact transcript to the cell cytoplasm. To evaluate the protective effect of DOTAP or DDA based formulations on RNA stability, self-amplifying RNA encoding for rabies glycoprotein was incubated with RNase A in the presence or absence of formulations. Agarose gel electrophoresis showed that RNA integrity was maintained during formulation (Figure 3.7A-D, Figure 3.8 A-B, lane 4). Furthermore, it was demonstrated that unformulated SAM RNA treated with RNase was fully degraded (Figure 3.7-3.8 lane 3), and the band was deleted. On the contrary, DOTAP or DDA particles protected the nucleic acid when it was adsorbed to the surface or inside particles. However, the efficiency of protection varied among formulations with DOTAP liposomes being poorly protective against RNAse degradation (Figure 3.7 A)
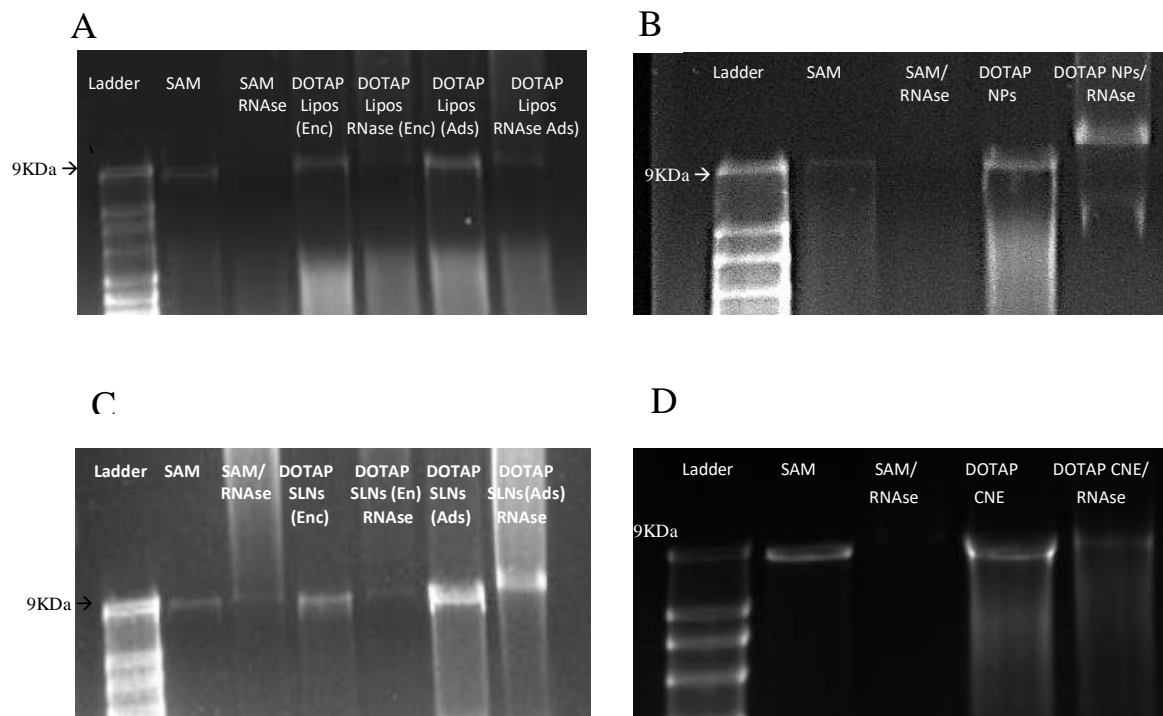
Figure 3. 7 Denaturing RNA agarose gel electrophoresis showing protection of SAM RNA from RNAse A) molecular weight ladder (lane 1), SAM RNA (lane 2), SAM RNA after incubation with RNase (lane 3), encapsulated (lane 4) and adsorbed (lane 6) SAM RNA after extraction from DOTAP Liposomes (Lipos), DOTAP Liposomes with SAM RNA encapsulated (lane 5) and adsorbed (lane 7) after RNase exposure, inactivation of RNase, and RNA extraction from DOTAP Liposomes. B) molecular weight ladder (lane 1), SAM RNA (lane 2), SAM RNA after incubation with RNase (lane 3), SAM RNA after extraction from DOTAP NPs (lane 4), DOTAP NPs with SAM RNA after RNase exposure, inactivation of RNase, and RNA extraction from DOTAP NPs (lane 5). C) molecular weight ladder (lane 1), SAM RNA (lane 2), SAM RNA after incubation with RNase (lane 3), encapsulated (lane 4) and adsorbed (lane 6) SAM RNA after extraction from DOTAP SLNs, DOTAP SLNs with SAM RNA encapsulated (lane 5) and adsorbed (lane 7) after RNase exposure, inactivation of RNase, and RNA extraction from DOTAP SLNs. D) . molecular weight ladder (lane 1), SAM

RNA (lane 2), SAM RNA after incubation with RNase (lane 3), SAM RNA after extraction from DOTAP CNE (lane 4), DOTAP CNE with SAM RNA after RNase exposure, inactivation of RNase, and RNA extraction from DOTAP CNE (lane 5).

A

B

C
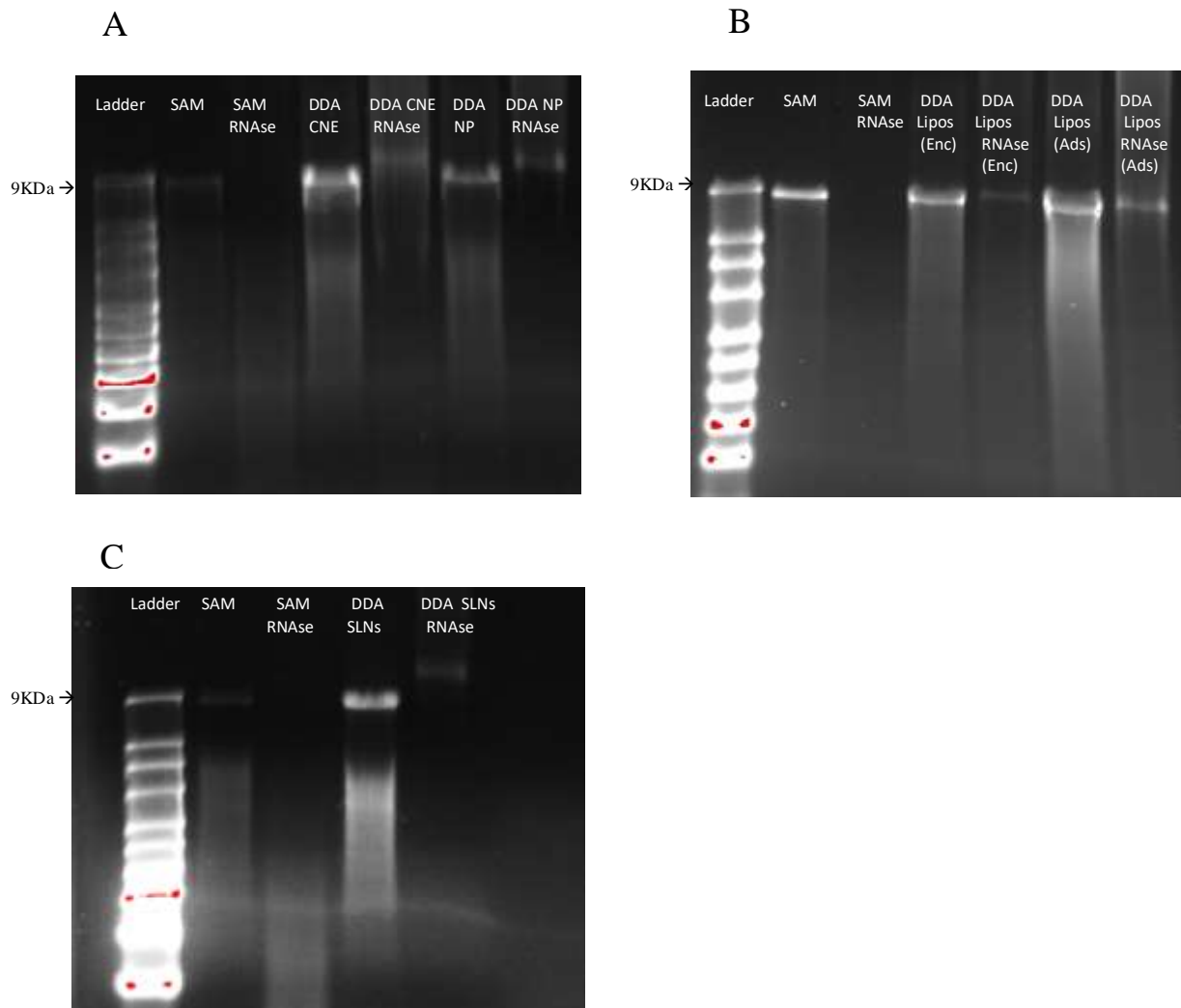
Figure 3. 8 Denaturing RNA agarose gel electrophoresis showing protection of SAM RNA from RNAse A) molecular weight ladder (lane 1), SAM RNA (lane 2), SAM RNA after incubation with RNase (lane 3), SAM RNA after extraction from DDA CNE (lane 4), DDA CNE with SAM RNA after RNase exposure, inactivation of RNase, and RNA extraction from DDA CNE (lane 5), SAM RNA after extraction from DDA NPs (lane 6), DDA NPs with SAM RNA after RNase exposure, inactivation of RNase, and RNA extraction from DDA NPs.(lane 7). B) molecular weight ladder (lane 1), SAM RNA (lane 2), SAM RNA after incubation with RNase (lane 3), encapsulated (lane 4) and adsorbed (lane 6) SAM RNA after extraction from DDA Liposomes (Lipos), DDA Liposomes with SAM RNA encapsulated (lane 5) and adsorbed (lane 7) after RNase exposure, inactivation of RNase, and RNA extraction from DDA Liposomes. C) molecular weight ladder (lane 1), SAM RNA (lane 2), SAM RNA after incubation with RNase (lane 3), SAM RNA after extraction from DDA SLNs (lane 4), DDA SLNs with SAM RNA after RNase exposure, inactivation of RNase, and RNA extraction from DDA SLNs (lane 5).

3.4 Discussion

In this chapter a novel manufacturing approach to produce size-tunable cationic delivery systems was investigated. It has been seen that microfluidics provides a unique tool to formulate liposomes with consistent size and size distribution compared to conventional methods such as extrusion or probe sonication. Moreover, liposome size can be controlled via adjustments of microfluidic operating parameters such as flow rate ratio (FRR), total flow rate (TFR) and lipid concentration, depending on lipid composition and micromixer design (Ali et al., 2010). In the present work it has been demonstrated how microfluidics could be a suitable technique to make homogeneous cationic DOTAP:DOPE vesicles, just by varying process parameters. The main factor which seemed to affect vesicles physicochemical attributes was the aqueous/solvent ratio; despite no significant changes in surface charge values, liposomes formulated at higher FRRs (1:1) were smaller in size and more homogeneous compared to those obtained at lower aqueous/solvent ratios (Figure 3.2). The formation of liposomes within a staggered herringbone micromixer (SHM) was hypothesized to be a consequence of alcohol and aqueous buffer mixing in the microchip, which increased the polarity of the lipids' solvent. This fact progressively reduced lipids solubility and increase the likelihood to precipitate and self-assemble into planar lipid bilayers (Hayward et al., 2006, Thorsen et al., 2001, Shestopalov et al., 2004). As these planar bilayer discs grow, they begin to bend to reduce the surface area of hydrophobic chains exposed to polar solvent around the perimeter of the disc. The increase in polarity throughout the chamber leads to the formation of small unilamellar liposomes (SUV) within milliseconds of mixing (Stan et al., 2013). For their formation, it was widely reported that the ratio of aqueous to solvent stream is a crucial factor. However, the effect of this parameter on particles attributes remained controversial. Many papers observed an increase in particles size at higher FRRs, in line with what has been shown in this chapter. A reasonable explanation given for this phenomenon was related to the reduced stabilizing effect of organic solvent at high FRRs. Since mixing occurs very quickly at high FRRs, the alcohol concentration decreases rapidly, leaving the lipid discs to grow with less stabilization from alcohol around the exposed hydrophobic edges. As demonstrated here, at TFR<5 mL/min, the effect of FRR on size was not significant, while it became evident at higher injection velocities. Given that at higher TFRs the fluid residence time in the microchip decreases, it might be probable that the combination of high injection speeds at low aqueous/solvent ratios resulted in uncontrolled lipid self-assembling, with consequently less sample homogeneity (Leng et al., 2003). On the contrary, it was also observed that, increasing aqueous/solvent ratio decreases particles size because of the reduction of final solvent concentration at high FRR (Belliveau et al., 2012). Consequently, the polarity between the two phases is increased and induction of nanoprecipitation of more homogeneous liposomes

is driven. Moreover, particle fusion is reduced and lipid exchange (Ostwald ripening) after complete mixing is achieved (Kastner et al., 2014, Kastner et al., 2015, Zhigaltsev et al., 2012). However, data shown here seemed to disagree with these findings, with larger particles size obtained at higher aqueous:solvent ratios. These results together suggested that the final effect of FRR is not unique and it might be a consequence of several factors (lipids composition, FRR range and TFR/FRR choice). It is worth underlining that studies conducted previously with microfluidics also referred to lower sample homogeneity at higher FRRs, in accordance with data shown here. For example, with liposomes prepared with Egg phosphatidylcholine (PC) and cholesterol, increasing aqueous/solvent ratio from 1:1 to 5:1 increased PDI almost 2-fold (Kastner et al., 2015). A direct proportionality between higher flow rate ratios and lower homogeneity may be a result of increased dilution at higher FRR reducing the rate of diffusional mixing within the microchip. Given that low lipid concentrations reduced the tendency of molecules to diffuse from the organic phase to the aqueous counterpart, increasing FRR inevitably induced lipid content dilution, with consequent less diffusivity and efficiency in liposomes nucleation (Balbino et al., 2013). Furthermore, these results correlated with what has been seen in Chapter 2 of this thesis, which reported the production for a different delivery system (i.e. solid lipid nanoparticles) using the same microfluidics platform. Overall, these findings demonstrate that a FRR of 1:1 results in liposomes of the smallest size and polydispersity. Furthermore, the SHM method enhances the diffusional mixing due to the herringbone structures on the microchip, (Stroock et al., 2002) which results in a more efficient mixing compared to other techniques (Jahn et al., 2004, Jahn et al., 2007, Jahn et al., 2010).

The zeta potential of liposomes was maintained despite alterations in flow rates and ratios with the liposomes having a positive zeta potential of 50-60 mV (Figure 3.2). These data were in agreement with data previously reported for DOPE: DOTAP liposomes prepared by the lipid hydration method following sonication or by Microfluidics (Weibel and Whitesides, 2006, Karnik et al., 2008a). The net positive charge of liposomes is due to the presence of DOTAP, which is a phospholipid with an ammonium head group that is completely protonated at neutral pH. On the other hand, DOPE instead is a zwitterionic phospholipid with a phosphate group and a tertiary amine both ionized at pH 7.4, making lipid total charge close to neutrality (Zuidam et al., 1999). Interestingly, the velocity at which both aqueous and solvent streams were injected in the micromixer seemed not to alter vesicles size, size distribution and surface charge (Figure 3.2). Previous reports indicated that the TFR had a slight impact on particle formation (Jahn et al., 2007, Jahn et al., 2004, Lo et al., 2010). Even though the TFR is inversely proportional to the fluid residence time in the microchip, these findings suggested that the fluid residence time in the microchannel was sufficient for liposome formation in the explored range, even at higher TFRs. The low influence of TFR on

vesicle size might indicate that the microfluidic system can operate at higher total volumetric flow rates, which could be potentially beneficial for productivity and scalability.

The initial lipid amount in the solvent stream is also an important consideration in the production of liposomes using microfluidics. As known, the increase in FRR would inevitably induce dilution of liposomes, therefore lower particles content in the final sample. Thus, a subsequent concentration process based on filtration, chromatography or centrifugation would add additional processing time and might alter final product attributes (Wagner et al., 2002, Pattnaik, 2009). Hence, to avoid additional process steps, the dilution of lipids at higher FRR was mitigated by increasing initial lipid concentrations in the lipid stock. Within this chapter it was demonstrated that lower levels of lipids tended to promote larger and less homogeneous vesicles (Figure 3.3A). Results correlate with what has been reported in literature. For example, increasing the initial concentration of PC and cholesterol from 0.25 to 2 mg/mL resulted in larger liposomes with no effect on final surface charge (Joshi et al., 2016). A possible explanation for this phenomenon might be given considering that decreasing lipid content may affect the rate of diffusion between aqueous and organic phases within the micromixer. As known, the lower is the lipid content in the solvent stream the lower will be the tendency of lipids to diffuse; this fact might lead to inefficient lipid monomers self-assemble and more inhomogeneous vesicles formation (Joshi et al., 2016). Moreover, at low concentrations, liposome size can be increased due to solvent incorporation into the bilayer (Joshi et al., 2016). Furthermore, it has been reported that diluted lipid mixtures required longer mixing channels and time to achieve complete water–solvent mixing (Jahn et al., 2010); thus, at lower lipid concentrations an increase of injection speed (TFR) might be required to improve liposomes attributes.

The use of microfluidics for scalable delivery systems production allows for the cost-effective and rapid production of liposomes and lipid particles. The need to use a continuous process is not only related to the manufacturing, but also to the purification step. The purpose of this work was to identify a more suitable method to remove residual organic solvent in the sample after Nanoassemblr. Therefore, tangential flow filtration, dialysis and spin column were compared. As shown in figure 3.4 A and B, across all the purifications methods tested, dialysis seemed to maintain cationic lipid vesicles attributes, while spin column and TFF failed. The most dramatic effect was observed on Z-potential values, with liposomes charge being almost neutral after spin column and TFF (Figure 3.4 B). This fact could probably be caused by the chemical composition of the purification column: Sephadex G75 and modified polysulfone are slightly negative at pH 7.4 and they could induce the absorption of positively charged liposomes (Busatto et al., 2018) .Moreover, high shear forces occurred at high TFF filtration speed or high-pressure values applied on top of spin column could induce breakage of such

fragile particles and their reassembly in bigger and less homogeneous structures (Lesieur et al., 1993). These findings suggested a step of gel pre-saturation with lipids to avoid loss of efficiency during spin column or TFF (Reynolds et al., 1983). Generally, pre-treatment is preferentially carried out with sonicated liposomes as their small sizes ensure efficient penetration of the lipids within the gel pores (Grabielle-Madelmont et al., 2003). Despite this fact, all three methods were successfully able to remove organic solvent, with a liposome recovery above 85%. Therefore, within this study, it was demonstrated that purification remains a significant hurdle step in the optimization of liposomal products and the identification of optimal operating conditions should be considered while developing new vaccine adjuvants.

These findings were then adopted to produce four different delivery systems – liposomes, lipid and polymeric nanoparticles and emulsions. Table 3.1 and 3.2 showed that this technique could produce either empty or SAM-encapsulating/adsorbing carriers. Interestingly, while all formulations were monodispersed and < 200 nm in size, all newly formulated particles were highly cationic (Z-potential>30mV) compared to gold standard LNPs which are neutral. This discrepancy between surface charge values was due to differences in the physico-chemical structure of cationic lipid components. Chemical structures revealed that both DOTAP and DDA contained an ammonium head group (pKa~ 9) that is completely protonated at neutral pH , giving a net positive charge at the particle surface (Henriksen-Lacey et al., 2011a). On the other hand, tertiary cationic lipid X is a ionizable amino-lipid containing a tertiary amine with a pKa of 6.4, resulting in a neutral charge at physiological pH. It was widely reported that the choice of cationic lipid dictates the structure of the delivery system and the subsequent classification in either liposomes or lipid nanoparticles. Molecular modeling and cryogenic transmission electron microscopy (cryo-TEM) images revealed that, while liposomes (in particular large unilamellar vesicles – LUVs) contain lipids organized in a single bilayer separating the interior aqueous medium from the exterior (Cullis and de Kruijff, 1979). LNPs possess a largely hydrophobic core consisting of inverted micelles of lipid encapsulating oligonucleotides surrounded by a coating of PEG-lipids (Leung et al., 2015). It has been seen that the activity of these LNP systems was highly sensitive to the species of cationic lipid employed (Semple et al., 2010). More precisely, the dominant factors determining the cationic lipid potency were the unsaturation of the acyl chains, introduction of ether linkages, and most notably, the pKa of the amino function of the cationic lipid (Jayaraman et al., 2012). Specifically, LNP siRNA systems containing cationic lipids with amino functions exhibiting a pKa between 6.2 and 6.4 are by far the most effective for hepatocyte gene silencing (Jayaraman et al., 2012).

Generally, observing data reported here, the encapsulation of SAM inside or adsorption onto formulation surface resulted in larger particles, with a less positive Z-potential. These findings

agreed with what has been previously shown. The application of cationic liposomes as vaccine delivery systems and adjuvants has been investigated extensively over the last few decades (Oberle et al., 2000, Tabatt et al., 2004a). For example, cationic DOTAP:DOPE liposomes made by microfluidics were around 50 nm in size with a low polydispersity index (<0.2) (Kastner et al., 2014) and net positive charge (>40 mV). However, the addition of either single strand homopolynucleotides with purine or pyrimidine ring (poly-deoxy-adenosine (polyA), and poly-deoxy-thymidine (polyT), respectively) or double strand polynucleotides (dsAT) increased liposomes size up to 200–250 nm (Ciani, 2004). Furthermore, cationic nanoparticles based on the block-copolymer PLGA were monodisperse and around 200 nm in size (Patil and Panyam, 2009) after the complexation with an siRNA. Regarding SLNs, it has been seen that for example a PEGylated cationic solid-lipid nanoparticle formulation encapsulating TNF-α-siRNA, had an average diameter of approximately 120 nm (Aldayel et al., 2018). With respect to nanoemulsions, they have been used extensively throughout the pharmaceutical industry for delivery of poorly water-soluble drugs, and the vaccine industry has optimized them for use as vaccine adjuvants (Teixeira et al., 2001, Hippalgaonkar et al., 2010). CNE have been described previously for delivery of pDNA (Choi et al., 2004, Ott Gael et al., 2002). It has been seen that the addition of mRNA on DOTAP-CNE did not dramatically alter formulations attributes, but induced a slight increase in droplets size of around 30 nm compared to the antigen-free counterpart (Brito et al., 2014a). Moreover, LNPs composed of 1,2-dilinoleyloxy-3-dimethylaminopropane (DLinDMA) and encapsulating a self-amplifying RNA vaccine encoding RSV-F resulted in particles Z-average diameters from 130 to 164 nm with a polydispersity index from 0.09 to 0.14 using ethanol injection method. The size distributions were characterized by a single peak with a low polydispersity index, indicating a relatively monodisperse size distribution. These data correlated with what has been obtained herein this work with Nanoassemblr platform, indicating that Microfluidics might be a comparable and consistent alternative technique to the ethanol dilution process (B Jeffs et al., 2005). Furthermore, changing from DOTAP to DDA usually induced an increase in diameter and PDI, while still maintaining comparable surface charge values (Table 5.2). For example, DOTAP liposomes were around 85 nm in size, while their DDA counterparts was 2-fold larger. (Table 3.1 and 3.2). The higher size increase of DDA-based carriers might be due to the intrinsic rigidity of particles formulated with this cationic lipid. The cationic synthetic amphiphile lipid dimethyldioctadecylammonium (DDA), known to induce cell-mediated immunity and delayed-type hypersensitivity, (Korsholm et al., 2007) is an unsaturated fatty acid with a phase transition temperature around 50°C. On the other hand, the melting point of N-[1-(2,3-dioleoyloxy) propyl]-N, N, N-trimethylammonium (DOTAP) is close to 0°C due to the higher degree of unsaturation compared to DDA (Campbell et al., 2001). This difference in phase transition temperature was proven to influence the final rigidity of particles lipid layer

(Tabatt et al., 2004b). The bilayer fluidity, which is related to the lipid gel-liquid crystal transition temperature and its effects on immune responses, is of important interest when designing efficacious vaccines (De Serrano and Burkhart, 2017). Since DDA is solid at room temperature, the lipid layer of DDA based liposomes, NPs and SLNs will be solid and less fluid compared to the DOTAP counterpart. This lack of fluidity might translate into a greater increase of particles size when the antigen was incorporated. It has been widely reported that the use of high transition temperature lipids for particle formulations affected their associated immune response, with greater antibody induction for lipids with phase transition temperature >20°C (Yasuda et al., 1977, van Houte et al., 1981). Thus, these findings provide a sound rationale to further investigate the use of either DOTAP or DDA for SAM delivery. Despite that, encapsulation efficiency (EE) and adsorption efficiency (AE) values seemed to be independent from differences in lipid structure between the two cationic lipids, with values above 90% for all formulations tested (Table 3.1-3.2). The strategy of using positively charged lipids for nucleic acid delivery was widely established. It was reported in the literature that the implementation of delivery systems with cationic lipids was fundamental to associate nucleic acid polymers with lipid-based particles, enhancing antigen loading due to charge-to-charge interactions (Felgner et al., 1987a, Behr et al., 1989, 1998). Positively charged carriers could also promotes binding with the negatively charged cell membrane, thus enhancing cell uptake and consequently the likelihood to express the antigen and induce a greater immunity (Mislick and Baldeschwieler, 1996, Kopatz et al., 2004). Furthermore, the combination of cationic and anionic lipids facilitated the formation of nonbilayer structures that increase intracellular trafficking (Hafez et al., 2000). It might be worth underlining that, while direct mixing between non-ionizable lipids and nuclei acid can be achieved and spontaneous association occur even at physiological pH, efficient encapsulation of negatively charged biomolecules with ionizable cationic lipids (pKa <7) can be obtained at pH<pKa, where the ionizable lipids are positively charged. Subsequently, the pH can be raised to physiological values, leading to LNPs with a relatively neutral surface.

Changing from model SAM encoding for a green fluorescence protein to its rabies glycoprotein counterpart did not lead to significant alterations in liposomes, SLNs, NPs or CNE physico-chemical attributes. All formulations were < 200 nm in size, monodisperse (PDI<0.3) and with Z-potential between 0 and +50mV (Figure 3.5 and 3.6). Gold standard LNPs were in line with these findings. Further, both DOTAP and DDA based formulations were efficiently able to either encapsulate or adsorbed the two employed SAM platforms with AE and EE % above 90 (Table 3.3 and 3.4). These observations emphasise the versatility of newly formulated cationic delivery systems, with remarkable advantages and benefits for further applications as carriers for nucleic acid based vaccines.

To maximize its therapeutic application, it is essential that RNA based vaccines remain active under physiological conditions during their systemic application. However, in the blood RNAs are exposed to serum RNases known to degrade single-stranded RNAs within seconds (Braasch et al., 2003). Therefore, all mRNA-based therapies would benefit from the utilization of stabilized mRNA that have enhanced resistance towards ribonucleases contained in physiologic fluids, cell culture media and on the surface of the skin. Based on these observations, one of the criteria which might be worth evaluating during development of new delivery systems is the ability of carriers to prevent SAM degradation. Within the study, it has been observed that, despite differences in physico-chemical attributes, all formulations were able to protect SAM-GFP antigen from enzymatic degradation (Figure 3.7 and 3.8). However, the efficiency of protection changed among formulations, with DOTAP liposomes less able to maintain SAM integrity after RNAse incubation. These findings agreed with what has been shown in the literature. For example, (Brito et al., 2014a) it was demonstrated the ability of DOTAP CNE in protecting a 9 kb self-amplifying RNA after RNase addition. Moreover, it was shown how DLinDMA LNPs efficiently protected the RNA from degradation by RNase A (Ott et al., 2002). Regarding DOTAP liposomes, opposite findings were obtained by Blakney and co-workers, who repoterd full protection of SAM from enzymatic degradation when formulated with DOTAP based LNPs(Blakney et al., 2019). However, it might be worth noticing that , whithin the aforementioned paper, LNPs were produced by a different microfluidics approach than what has been used herein this thesis (SHM vs µEncapsulator) . Moreover, the ratio of complexing lipid to RNA was higher than what has been reported in the present chapter (N/P ratio of 8:1 vs 12:1) (Blakney et al., 2019). These changes might presumably impact on the association between the RNA and the cationic particles, with consequently different protection efficiency.

Preliminary work, shown within this chapter, suggests that it will be fruitful to pursue a more extensive evaluation of those cationic formulations as a nonviral delivery strategy for self-amplifying RNA. Next, the suitability of particles to express the antigen *in vitro* will be evaluated, aiming to select the best candidate to move forward in an *in vivo* immunogenicity test.

3.5 Conclusions

In this chapter two formulation approaches for cationic liposomes, polymeric and solid lipid nanoparticles and nanoemulsions preparation were investigated. Results suggested that both Microfluidics and Microfluidizer were equally able to produce small and monodisperse particles with a highly positive electronic dense core. Moreover, the addition of nucleic acid inside or outside particles notably increased formulations average diameter; however, formulations' stability was not detrimentally compromised. Indeed, particles physicochemical

attributes were confirmed to be suitable for pre-clinical and clinical applications. Moreover, cationic carriers were able to protect SAM from biological degradation. However, the efficiency of protection varied among formulations, with DOTAP liposomes less able to maintain SAM integrity after RNAse incubation. Encapsulation or adsorption efficiencies were >90%, regardless of particles composition. Thus, these formulations will be further investigated in an *in vitro* model to better understand their efficiency in transfecting cells and induce antigen transcription.

CHAPTER 4

In vitro self-amplifying RNA (SAM) vaccine delivery properties of cationic formulations
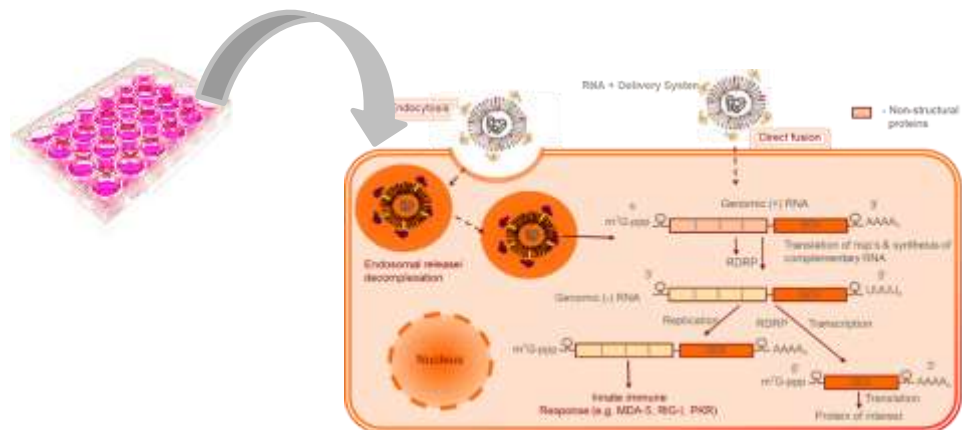
4.1 Introduction

The aim of vaccination is to generate a strong immune response providing long term protection against infections. Unlike attenuated live vaccines, killed whole organism or subunit vaccines generally require the addition of an adjuvant to be effective. It has been proven that adjuvants are able to affect the type of immune response and to markedly enhance a cytotoxic T-cell response against the particle-associated antigen (Grabielle-Madelmont et al., 2003, Indrova et al., 2001). This is due to the unique capability of some professional antigen-presenting cells (APCs– dendritic cells (DCs) and macrophages (Mφ) - to efficiently internalise foreign particulate material such as microparticles and bacteria. This process called phagocytosis becomes activated by the recognition of the antigenic material to process and present both self and foreign antigens to other cells of the immune system (Hirayama et al., 2017). Presentation on major histocompatibility complex class I and II on APCs elicits cellular as well as humoral immune responses (Drake, 2019). This opens the opportunity to use antigen-loaded delivery systems for vaccination purposes. It was seen that only antigen-presenting dendritic cells could prime naive T-lymphocytes, inducing a strong T-cell response *in vitro* and *in vivo*. Additionally, DCs efficiently present antigens derived from phagocytosed apoptotic cells and are capable to stimulate MHC class I-restricted CD8+ cytotoxic T-lymphocytes(Drake, 2019) . The priming of naive T cells and the stimulation of CD8+ T-cells are crucial to fight viral infections and tumour cells and make DCs a logical target for vaccines.

It has been demonstrated that both Mφ and DCs are able to capture antigens, whole microbes, apoptotic bodies, and particles(McCarthy et al., 2014). Therefore, the potentiality of DOTAP or DDA based liposomes, nanoparticles and emulsions to target APCs and deliver the antigen was evaluated. Many papers reported the suitability of these delivery systems as *in vitro* antigen transfection agents. De Beuckelaer and co-workers have reported that delivery of conventional mRNA with DOTAP: DOPE liposomes in macrophages cell lines (De Beuckelaer et al., 2016). Moreover, it has been reported that solid lipid nanoparticles were able to efficiently transport pDNA into a neuronal cell line (Na1300) and induce antigen (GFP) expression in vitro (Vighi et al., 2010). Within this chapter, γ-irradiation was used to sterilise the formulations. Herein, the toxicity induced by four different cationic formulations – liposomes, solid lipid nanoparticles (SLNs), polymeric nanoparticles (NPs) and nanoemulsions (CNE) - to bone marrow-derived DCs and MΦs using Alamar blue was studied. Subsequently, internalisation of the formulations in both cell types using flow cytometry (FACs) was confirmed. Alamar blue (AB) colorimetric assay was used as water-soluble dye for in vitro cells viability quantification (Ansar Ahmed et al., 1994). Furthermore, cellular uptake quantification was performed using fluorescence-activated cell sorting (FACs), which is a specialised type of flow cytometry for sorting a heterogeneous mixture of biological cells into two or more containers, one cell at a time, based upon the specific light scattering

and fluorescent characteristics of each cell (Ducat et al., 2011). Despite promising results, antigen efficient transfection of MΦs *in vitro* failed, therefore baby hamster kidney – BHK – cells were used as alternative cell line; these cell lines have been used extensively for a variety of studies, including transfection and expression of cloned genes. BHK cells have been characterised as fibroblastoid with some epithelial phenotypic traits (Stoker and Macpherson, 1964).

4.1.1 Aim and objectives

The aim of this work was to:

- Test the suitability of γ-irradiation to efficiently sterilise cationic particles prior in vitro assays performance.

- Find the critical concentration of cationic lipid at which formulations cause cytotoxicity.

- Evaluate the ability of different delivery systems to efficiently induce particle uptake and consequent antigen expression *in vitro*.

- Screen among formulations to select the most promising candidates for an *in vivo* immunogenicity test.

4.2 Materials and Methods

4.2.1 Materials

Poly (D, L-lactide-co-glycolide) lactide: glycolide (50:50), mol wt 30,000-60,000, Dimethyl Sulfoxide, Tristearin (Grade II-S, ≥90%) Cholesterol and squalene were obtained from Sigma-Aldrich Company ltd. Dipalmitoylphosphatidylcholine (DSPC), 1,2-dimyristoyl-rac-glycero-3-methoxypolyethylene glycol-2000 (DMG-PEG2000), Dimethyldioctadecylammonium bromide (DDA) and 1,2-dioleoyl-3-trimethylammonium-propane (DOTAP) were obtained from Avanti Polar Lipids. Alamar blue was obtained from Bio-Rad Laboratories, Inc. Ethanol, methanol, 1,1'-Dioctadecyl-3,3,3',3'-Tetramethylindocarbocyanine Perchlorate (DilC), LIVE/DEAD™ Fixable Aqua Dead Cell Stain, Lipofectamin2000), Gibco phosphate buffer saline (PBS), Roswell Park Memorial Institute (RPMI1640 Medium, Tween 20 and Span 80 were obtained from Fisher Scientific UK, Dulbecco's Modified Eagle Medium (DMEM) and foetal bovine serum (FBS) were obtained from Gibco. APC-labelled anti-CD11c, FITC-labelled anti-F4/80 antibodies and anti-Fc antibody (Fc block) were obtained from BD Biosciences UK. Penicillin-streptomycin, L-glutamine,and pontamine blue were purchased from Sigma. TRIS Ultra-Pure was obtained from ICN Biomedicals. Cytofix-cytoperm solution was obtained from BD Biosciences. Tertiary cationic lipid X was provided by Discovery, Drug Product Development department Rockville, USA

4.2.2 Sterilisation of formulations

All formulations were produced either via a Microfluidics or the Microfluidizer platform (refer to chapter 3.2.3 for preparation details). Subsequently 1 mL of either liposomes, NPs, SLNs or CNE was sterilised by γ-irradiation before addition into cells. Samples were irradiated for 10 min at 10 Gy in an X-RAD 225 Biological Irradiator (Precision X-Ray).

4.2.2.1 Formulation characterisation

Formulations were characterised before and after irradiation, in terms of hydrodynamic size (Z-average), polydispersity index (PDI) and surface charge (zeta-potential) by dynamic light scattering (DLS) in a Zetasizer Nano ZS (Malvern, UK) at lipid concentrations of $0.1 - 0.2$ mg/mL in 10 mM TRIS pH 7.4 at 25 °C. SAM integrity after sterilisation was assessed by performing an RNA agarose gel electrophoresis as described in chapter 3.2.9. Sterility after irradiation was checked by incubating samples (10 μL) in a precast agar plate at 37°C. Plate was monitored daily and picture of the plate collected 5 days post incubation.

4.2.3 Isolation and culture of bone-marrow derived macrophages and dendritic cells

All protocols have been subject to ethical review and were carried out in a designated establishment. Female BALB/c mice 6-8 weeks were terminated by cervical dislocation and tibias and femurs were collected. Bone marrow cells were then flushed from bones with RPMI 1640 Medium (Moore et al., 1967).

4.2.3.1 Bone marrow derived macrophages

Bone marrow derived macrophages were grown in petri dishes (10 mL) in DMEM supplemented with 30% (vol/vol) L-cell-conditioned media, 20% heat inactivated foetal calf serum (HI-FCS) and 2% L-glutamine penicillin and streptomycin (macrophage medium). Cells were cultured for 10 days at 37 °C and 5% CO_2. Briefly, fresh macrophage media (10 mL) was added at day 3. At day 7, 15 mL of the medium were replaced by fresh macrophage medium. L-cell-conditioned medium was obtained by harvesting the metabolized medium from cultured cells of the murine fibroblastic cell line L-929. This conditioned medium provides a source of macrophage colony-stimulating factor (M-CSF) and Granulocyte-macrophage colony-stimulating factor (GM-CSF), necessary for the growth and differentiation of bone marrow stem cells into mature macrophages.

4.2.3.2 Bone marrow derived dendritic cells

Bone marrow derived dendritic cells (BMDDCs) were grown in petri dishes (10 mL) in completed RPMI-1640 (RPMI supplemented with 10% HI-FCS and 1% penicillin and streptomycin) and 10% GM-CSF (DC medium). Cells were grown for 7 days at 37 °C and 5% CO_2. Briefly, fresh DC media (10 mL) was added at day 2. At day 5, 10 mL of the medium were replaced with fresh DC medium.

4.2.4 Cell proliferation assay of bone-marrow derived macrophages and dendritic cells

Macrophages and dendritic cells were harvested from petri dishes and plated in 96-well plates at a cell density of 100,000 and 50,000 cells/well in complete RPMI-1640 and left overnight at 37 °C in 5% CO_2 to allow the cells to adhere. On the next day cells were incubated with serial dilutions of cationic liposomes, NPs, SLNs and CNE (refer to paragraph 3.2.2 for preparation details). Cationic formulations were standardised according to the final cationic lipid (i.e. DOTAP) concentration. Then, after 24 hours 200 μL of AlamarBlue was added to each well. Non- treated cells were used as negative control. After 6 hours incubation the absorbance was measured at 600 nm and 570 nm, then the percentage of reduction from resazurin to resorufin in the treated cells was calculated by using the following formula:

$$\text{eq (1)} \quad \text{Percentage of reduction} = \frac{(\varepsilon_{ox}\,600)(\text{Abs }570) - (\varepsilon_{ox}\,570)(\text{Abs }600)}{(\varepsilon_{red}\,570)(\text{Control Abs }600) - (\varepsilon_{red}\,600)(\text{Control Abs }570)} \times 100$$

4.2.5 Cellular uptake in bone-marrow derived macrophages and dendritic cells

Macrophages and dendritic cells were harvested from the petri dishes at day 10 and 7 respectively with RPMI 1640 medium and centrifuged at 1400 rpm for 5 min. Pellets were resuspended in complete RPMI-1640 and plated in 24-well plates at a cell density of 50,000 cells/well and incubated overnight at 37°C in 5% CO_2 to allow cells to adhere. Empty or SAM-GFP loading liposomes, NPs, SLNs and CNE were co-formulated with the lipophilic fluorescent dye DilC (0.2% mole %) to track the cellular uptake (Refer to chapter 3 for preparation details). The lipophilic dye DilC can be only incorporated within the lipid layer and thus its concentration is constant for monodisperse formulations regardless of their size. Formulations were then added at 5 μg/mL of cationic lipid (either DOTAP or DDA) to the cells at different time points (0.5, 1, 4 and 24 h) at 37 °C and 4 °C. Subsequently, cells were harvested from the well-plates, washed and resuspended in PBS supplemented with 5% FCS and specific antibodies: APC-labelled anti-CD11c Ab and FITC-labelled anti-F4/80 antibodies for detection of dendritic cells and macrophages respectively. Cells were incubated for 30 min at 4°C in the absence of light. Then, they were washed twice with PBS supplemented with 5% FCS. As controls, unstained cells and stained cells without formulations were used. All flow cytometry data were collected on BD FACSCanto™ (BD Biosciences) and analysed using FlowJo software 7.6.

4.2.6 Cell proliferation assay in baby hamster kidney cells

Baby hamster kidney cells (BHK) cells were grown in flasks (20 mL) in complete DMEM (DMEM supplemented with 10% HI-FCS and 1% penicillin and streptomycin). Cells were grown for 2-3 days at 37 °C and 5% CO_2. BHK cells were seeded at a density of 5×10^5 cells

in 500 µL cDMEM (DMEM+ 5% heat inactivated FBS, 1% penstrep and 1% L-glutamine) in each well of a 24-well plate and incubated for at least 6 hours to allow cell adhesion. Then, cells were incubated with serial dilutions of SAM Rabies-Liposomes, NPs, SLNs and CNE (refer to chapter 6.2.3 for preparation details) starting from a cationic lipid concentration of 100 µg/mL to 400 ng/mL through a 3-fold serial dilution. As positive control, BHK were also transfected with LNPs following the same experimental conditions described above. Then, cells were trypsinised, transferred in 96-well plates and stained with 100 µL of diluted LIVE/DEAD™ Fixable Aqua Dead Cell Stain for 20 min at room temperature in the darkness. After two washes with PBS, cells were resuspended in PBS and the percentage of LIVE/DEAD+ cells with respect to untreated control was measured by FACs analysis. All flow cytometry data was collected on FACSCANTO II flow cytometer and analysed using FlowJo software 7.6.

4.2.7 Cellular uptake in baby hamster kidney cells

BHK cells were seeded at a density of 5×10^5 cells in 500 µL cDMEM (DMEM+ 5% heat inactivated FBS, 1% penstrep and 1% L-glutamine) in each well of a 24-well plate and incubated for at least 6 hours to allow cell adhesion. SAM-Rabies formulations, prepared in presence of 0.2% mol of the DilC fluorescent dye, were then added at 11 µg/mL of cationic lipid to the cells at different time points 16 hours before analysis at 37 °C. As positive control, BHK were also transfected with LNPs following the same experimental conditions described above. Moreover, Lipofectamine2000 was used as additional positive control following manufacturer instructions. Subsequently, cells were harvested from the well-plates, washed and resuspended in PBS supplemented with 5% FCS and the percentage of DilC+ cells with respect to untreated control was measured by FACs analysis. All flow cytometry data was collected on FACSCANTO II flow cytometer and analysed using FlowJo software 7.6.

4.2.8 *In vitro* potency of SAM-GFP formulations

A total of 50,000 BHK cells were plated per well in 24-well plates in cDMEM and allowed to adhere for at least 6 hours at 37 ^{0}C and 5% CO_2. Then liposomes, NPs, SLNs and CNE co-formulated with SAM-GFP were added at SAM concentrations ranging from 500 to 65 ng/mL as a 2-fold 8-point curve. Lipofectamine2000 (LF) and LNPs were used as positive controls. After 16 hours, cells were trypsinised, washed twice with PBS + 5% FBS and collected in FACS tubes. Subsequently, the *in vitro* potency (IVP) of SAM-formulations was determined by flow cytometry as percentage of GFP+ cells with respect to untreated control cells in a FACSCANTO II flow cytometer.

4.2.9 *In vitro* potency of SAM-Rabies formulations

BHK cells (50,000 cells/well) were plated as previously described. After 6-8 hours, cells were incubated for 16 hours with SAM-Rabies-liposomes, NPs, SLNs and CNE at antigen concentration of 400, 200 and 100 ng/mL. Lipofectamine 2000 and LNPs were used as a

positive control for cells transfection as described above. Then, cells were trypsinised and transferred in 96-well plates, washed twice with PBS, fixed and permeabilised with Cytofix-cytoperm solution containing 4% paraformaldehyde (PFA). After incubation cells were washed twice with PBS and stained with primary antibody dilution (Anti-Rabies Antibody, Glycoprotein, clone 1:1000 dilution) for 1 hour at room temperature. Then, after washing, cells were incubating with secondary antibody dilution (Anti Mouse IgG2a, 1:1000 dilution) for 1 hour at room temperature in the darkness. Finally, cells were washed and resuspended in PBS for FACs analysis (FACSCANTO II flow cytometer). The percentage of Rabies+ formulations was calculated with respect to untreated control cells.

4.2.10 Statistical analysis
Unless stated otherwise, the results were calculated as mean ± standard deviation (SD). One-way ANOVA followed by Tukey post hoc analysis was performed for comparison and significance was acknowledged for p values less than 0.05. All the calculations were made using GraphPad Prism 8.

4.3 Results
4.3.1 The effect of sterilisation process on formulation size
Since formulations require to be incubated with cells to perform in vitro assays sterility of the formulations is a key consideration. Hence, contamination driven by non-sterile samples should be avoided. Previous studies (Pattnaik, 2009) have already shown that cationic formulations could not be filter sterilised due to electrostatic interactions and loss of product. Therefore, γ-irradiation was investigated as sterilisation method for the different formulations since it has previously been shown to be effective for cationic liposomes (Mohammed et al., 2006). Antigen-free DOTAP cationic formulations (SLNs, liposomes, NPs and CNE) were manufactured with Nanoassemblr or Microfuidizer. The size of all formulations was determined by dynamic light scattering before and after sterilisation. As shown in figure 4.1A and B, size and PDI did not change after γ-irradiation. For example, cationic SLNs diameter was around 100 nm before and after irradiation (Figure 4.1). The same trend seemed to be followed by zeta potential values; as it is shown in Figure 4.1C, despite the type of formulation tested, after 10 minutes irradiation, zeta potential of SLNs, NPs, liposomes and CNE remained like the non-sterile counterpart, thus providing a simple and effective method for sample sterilisation. Moreover, agarose gel electrophoresis in Figure 4.2A showed that SAM integrity was maintained during sterilisation and all DOTAP based formulations protected the RNA from γ -irradiation. Moreover, the agar plate picture in Figure 4.2B confirmed that sterility by γ -irradiation was achieved and maintained up to 5 days.

4.3.2 Evaluating the cytotoxic range for cationic formulations in bone-marrow derived macrophages and dendritic cells

Prior to any *in vitro* assay performance, complete differentiation of bone-marrow stem cells was investigated. The percentage of BMDM was determined as percentage of F4/80+ cells (Figure 4.3A). F4/80 is a membrane glycoprotein that has been widely used as a specific cell marker for murine macrophages. The percentage of F4/80+ cells was >80% as determined by flow cytometry. Moreover, CD11c+ cells, which represent bone marrow-derived dendritic cells (BMDDCs), were > 50% (Figure 4.3B). Histograms showed a net peak shift compared to the negative control after differentiation, clearly representative of a positive cell population expressing one of the two membrane surface markers tested.

The cytotoxicity of all formulations was determined in macrophages and dendritic cells after 24 hours by the colorimetric cell proliferation-based assay Alamar Blue. Cationic formulations were prepared at a cationic lipid content (i.e. DOTAP) of 2 mg/mL in absence of antigen. As shown in Figure 4.4A, which represents the cell viability of Mϕ incubated with cationic formulations at different concentrations, liposomes seemed to be more toxic compared to the other cationic formulations, especially at higher cationic lipid content. For example, at 125 µg/mL [DOTAP], the percentage of live macrophages incubated with liposomes was 37%, while the percentage was above 70% for the other formulations.
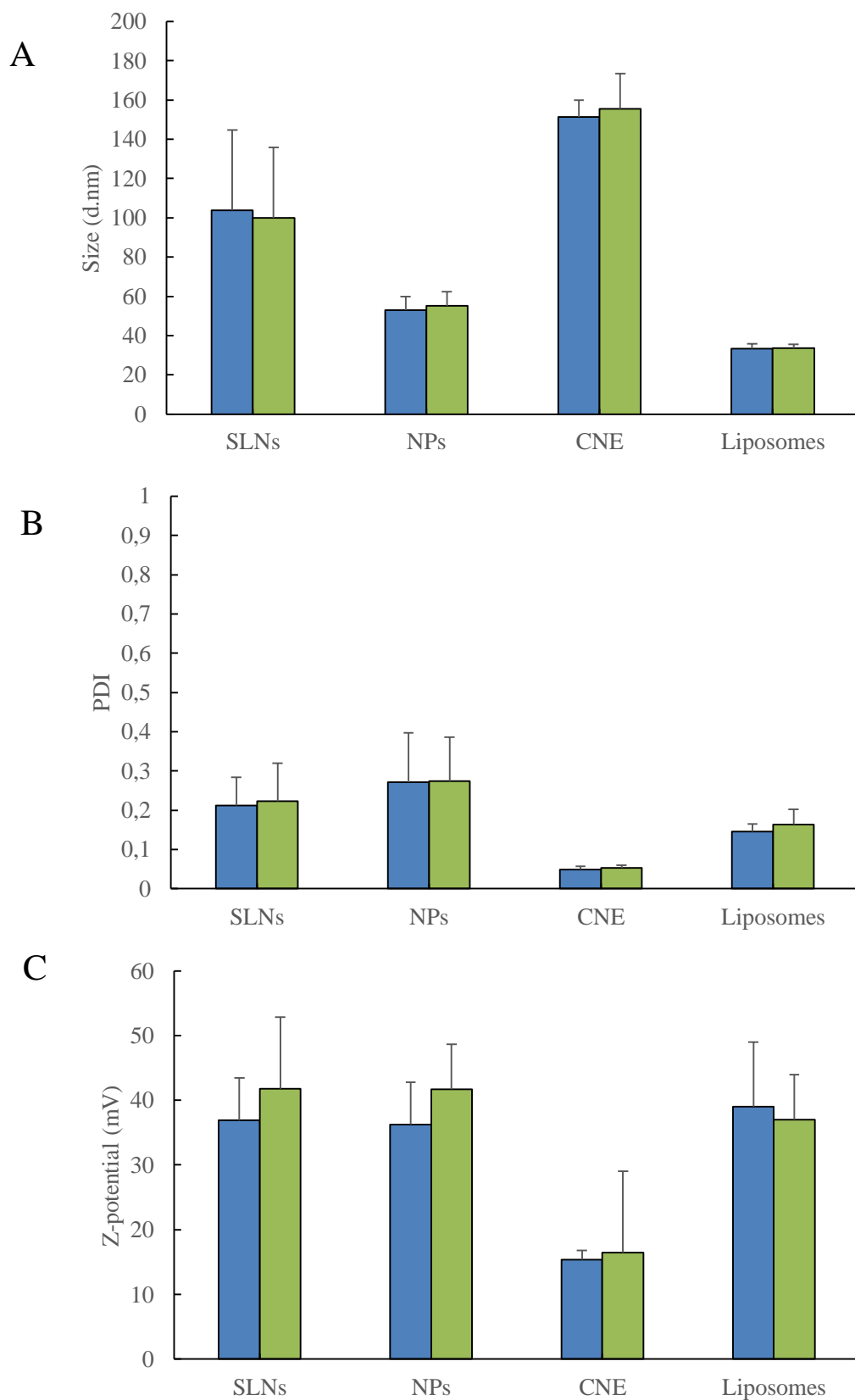
Figure 4. 1 The effect of γ-irradiation on formulations attributes. A) Size, B) polydispersity (PDI) and C) Z-potential of solid lipid nanoparticles (SLNs), polymeric nanoparticles (NPs), cationic nanoemulsions (CNE) and liposomes before (blue) and after (green) γ -irradiation. Results are expressed as the means of three experiments ± SD. Statistical analysis was performed using Mann-Whitney non- parametric t-test.
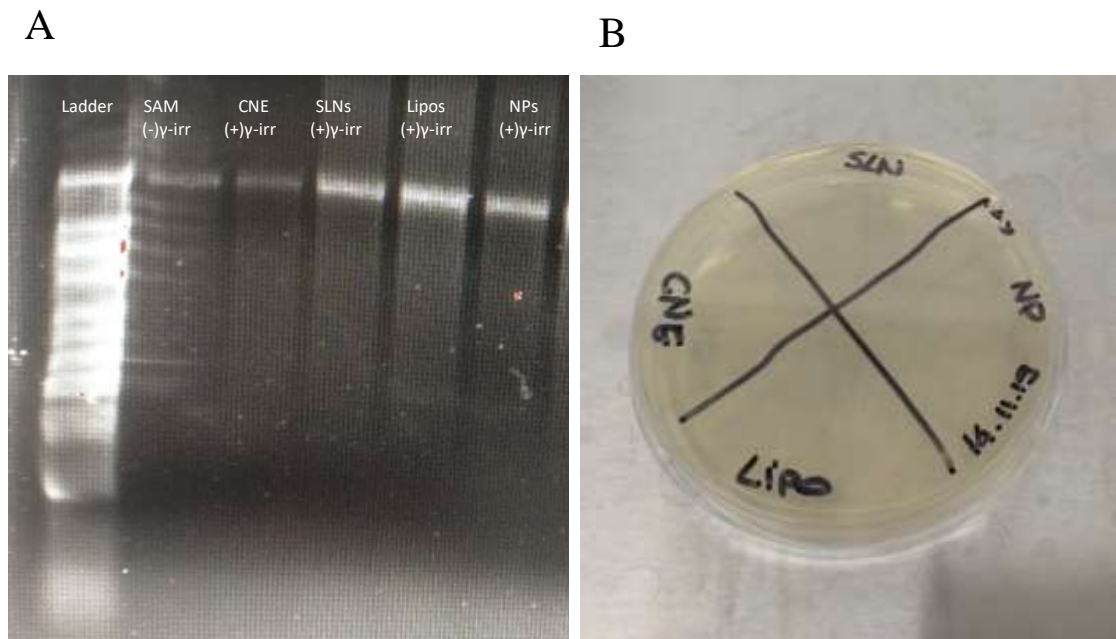
Figure 4. 2 The effect of γ-irradiation on formulations attributes. A) RNA agarose gel electrophoresis: RNA ladder (lane 1), self-amplifying RNA (lane 2), self-amplifying RNA after exposure to γ-irradiation formulated with DOTAP based cationic nanoemulsions (CNE - lane 3), solid lipid nanoparticles (SLNs - lane 4), liposomes (lane 5), polymeric nanoparticles (NPs – lane 6). B) Agar plate picture collected after 5 days incubation with self-amplifying RNA formulated with DOTAP based solid lipid nanoparticles (SLNs), polymeric nanoparticles (NPs), cationic nanoemulsions (CNE) and liposomes sterilised by γ -irradiation.
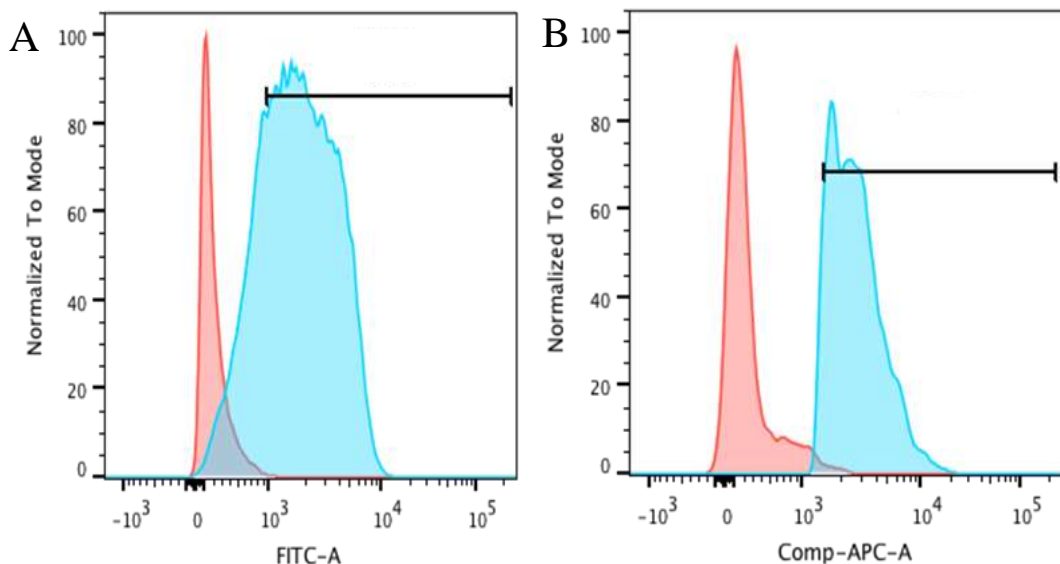
Figure 4. 3 Differentiation of stem cells into macrophages and dendritic cells. Representative flow cytometry plots of A) F4/80+ and B) CD11c+ cells (blue) with respect to control cells (red). F4/80+ and CD11c+ cells identified stem cells differentiation into macrophages and dendritic cells respectively.

Furthermore, NPs and CNE seemed to be nontoxic even at the highest DOTAP concentration tested (125 µg/mL). However, due to non-specific cell over reduction activity induced by CNE, it was not possible to quantify the percentage of live cells at [DOTAP] concentration >10 µg/mL for CNE formulations. Therefore, only values below this concentration were reported. Furthermore, by comparing the two different cell types, it seemed that dendritic cells (Figure 4.4B) were more sensitive to the formulations tested than macrophages, especially to NPs and SLNs. This trend was more evident at the highest [DOTAP] of 100 µg/mL which corresponds to 200 µg/mL of particles. More precisely, above 32 µg/mL of DOTAP, the percentage of live cells incubated with NPs was 99 and 56% for macrophages and dendritic cells respectively.

Further, after 24 hours incubation of Mφ with 125 µg/mL DOTAP:SLNs, the cell viability was 70%, instead when DCs were tested in the same conditions the percentage was reduced to 54%. However, liposomes seemed to be less toxic in DCs, with a IC_{50} of 250 µg/mL and 125 µg/mL in DC and Mφ respectively. CNE did not show any cytotoxic effect among all concentrations tested.

A
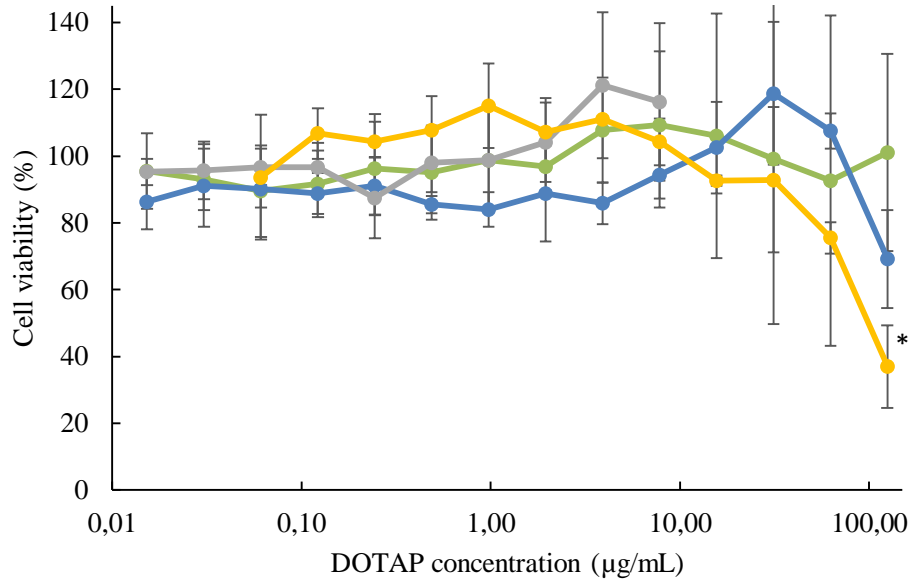
B
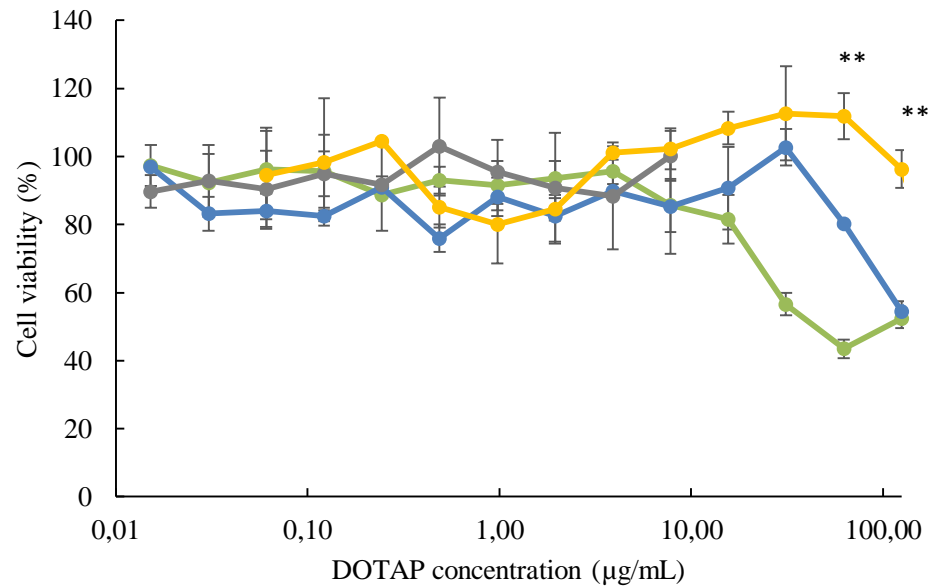
Figure 4. 4 Cell viability test. Cytotoxicity in A) bone marrow derived macrophages and B) in bone marrow derived dendritic cell of cationic formulations - NPs (green), SLNs (blue), emulsions (grey) and liposomes (yellow). Results are represented as mean ± SD of 3 independent experiments.

4.3.3 Uptake of empty and SAM-GFP loaded liposomes, SLNs, NPs and CNE by bone marrow derived macrophages (BMDM)

In order to assess the cell uptake of DOTAP based liposomes, NPs, SLNs and CNE, an optimal sub-toxic concentration of 11 µg/mL of cationic lipid was established. At this concentration, the viability of macrophages and dendritic cells was above 90%, as previously described (Figure 4.4). Formulations were prepared and sterilised before incubation using gamma irradiation (section 4.2.2). Cell uptake was first determined in macrophages at times points of 4 and 24 h at 37 °C (Figure 4.5). Figure 4.5A shows the uptake profile of empty DOTAP based formulations. The uptake process tended to be time dependent only for liposomes with 15% and 76% of liposomes+ macrophages after 4 and 24 hours incubation respectively. SLNs, NPs and CNE seemed to be engulfed to a similar extent irrespective of incubation time, with around 50% of uptake efficiency. Thus, data reported here highlighted that macrophages required more time to engulf DOTAP liposomes, but the actual number of particles taken up after 24 hours was higher compared to other formulations (Figure 4.5). With respect to SAM loaded formulations, the uptake kinetics are shown in Figure 4.4B. In line with previous observations, uptake was time independent with no significant difference after 4 or 24 hours post incubation. However, by comparing different formulations' uptake efficiency, SAM encapsulating NPs and SLNs and SAM adsorbing emulsions were engulfed more, with above 70% uptake efficiency, while SAM adsorbing SLNs and SAM encapsulating liposomes resulted to be taken up slightly less (around 60%). Regarding SAM adsorbing liposomes, just 47% of macrophages were liposomes+. After 24 hours, this trend was maintained, with average uptake efficiency between 70 and 80%. According to the graph in Figure 4.5 B, macrophages seemed to be less able to engulf SAM adsorbing liposomes, with just 58% of liposomes positive cells after 24 hours.

Regarding DDA based formulation, the uptake kinetic profile in macrophages is represented in Figure 4.6A. As previously reported for DOTAP formulations, 24 hours incubation resulted in higher particles uptake. However, the difference between percentage of uptake measured at 4 and 24 hours was not statistically significant. For example, after 4 hours, 50% and 40% of DilC+ cells incubated with CNE and SLNs respectively were detected, as seen with DOTAP based formulations. In contrast, cells seemed to be less able to engulf both NPs and liposomes, with less than 30% uptake efficiency. Furthermore, after 24 hours, this trend seemed to be maintained, with CNE having the highest uptake efficiency (around 80%). SLNs, liposomes and NPs uptake percentages were 64, 51 and 42% respectively. Compared to DOTAP formulations, the kinetics resulted to be inverted. More precisely, cells were less sensitive to DDA liposomes and polymeric nanoparticles. With respect to SAM loaded formulations, the uptake values in Mφ is shown in Figure 4.6B. Herein the difference between formulations was more evident. More precisely, after 4 hours incubation, SAM encapsulating liposomes and

SAM adsorbing emulsions were the ones which have been taken up the most by macrophages (around 60%). Regarding SAM adsorbing SLNs and liposomes, the uptake efficiency was comparable (around 35%), while NPs showed the lowest value (around 20%). After 24 hours, both SAM encapsulating liposomes and SAM adsorbing emulsions had the highest uptake (around 80%), while SAM adsorbing SLNs and liposomes uptake efficiency was between 50 and 60%. (Figure 4.6B).
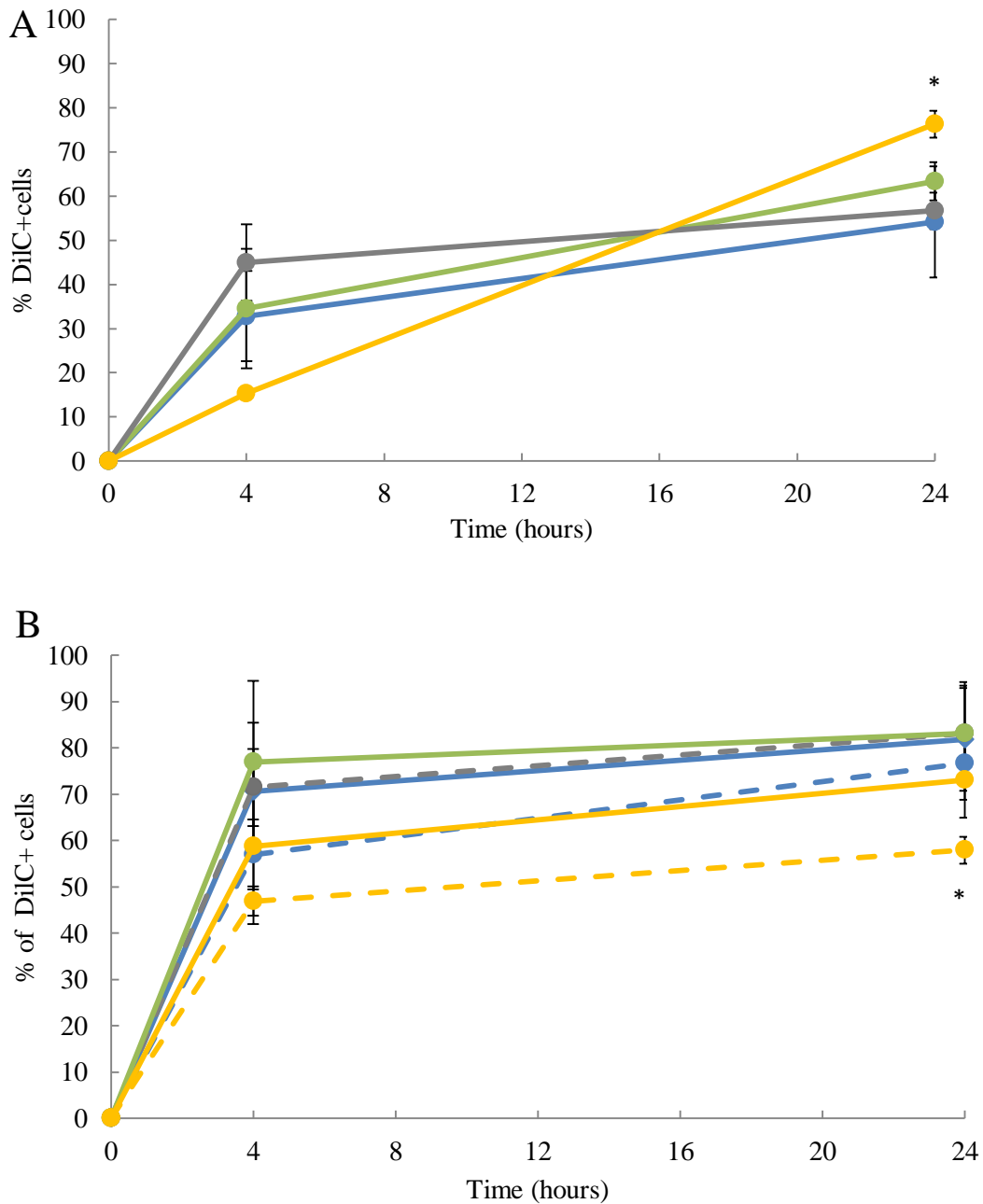
Figure 4. 5 Cell uptake of DOTAP based formulations. Cell uptake of A) empty and B) SAM-GFP loaded DOTAP based liposomes (yellow), solid lipid nanoparticles - SLNs (blue), polymeric nanoparticles - NPs (green) and cationic nanoemulsions- CNE (grey) in bone marrow derived macrophages. Solid and dash lines represent SAM-GFP encapsulating and SAM-GFP adsorbing formulations respectively. Results are expressed as the means of three independent experiments ± S.D.
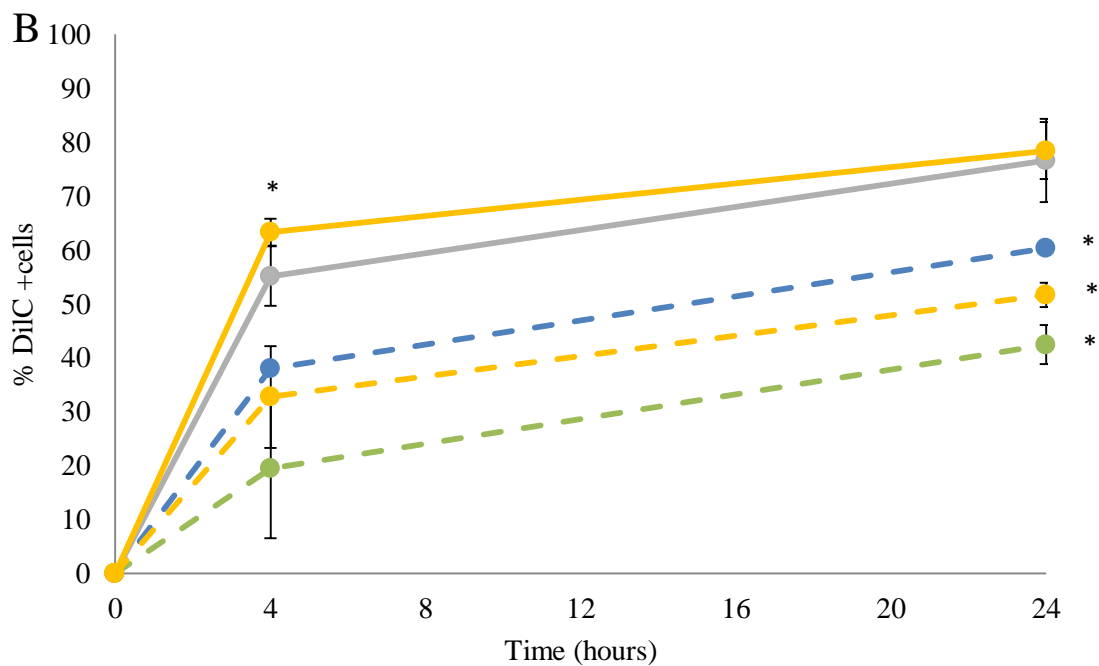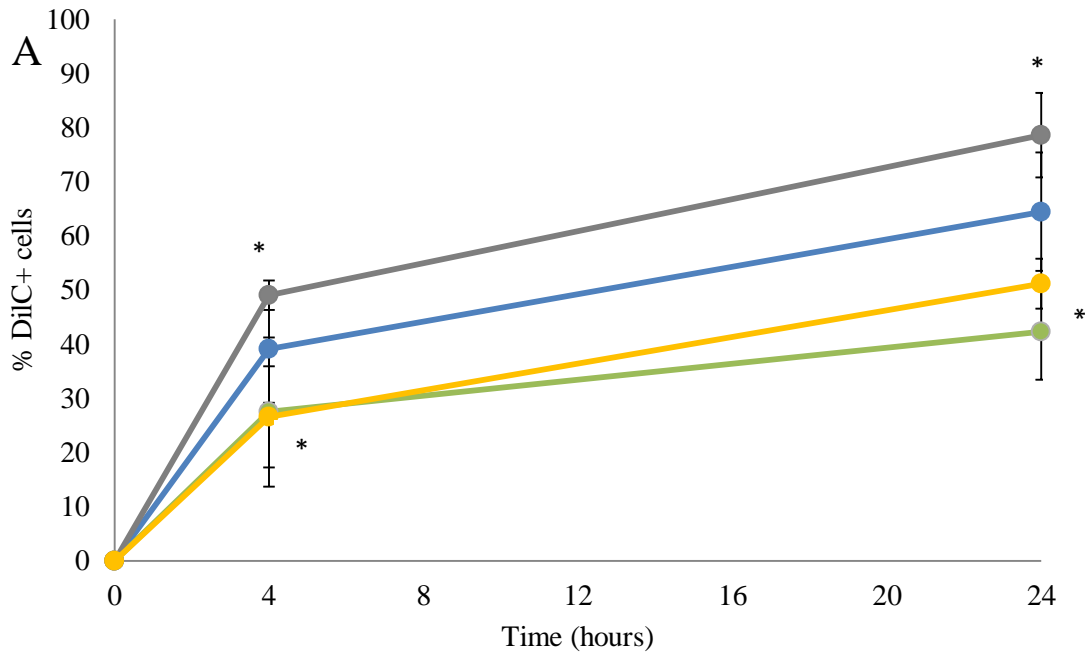
Figure 4. 6 Cell uptake of DDA based formulations. Cell uptake of A) empty and B) SAM-GFP loaded DDA based liposomes (yellow), solid lipid nanoparticles - SLNs (blue), polymeric nanoparticles - NPs (green) and cationic nanoemulsions- CNE (grey) in bone marrow derived macrophages. Solid and dash lines represent SAM-GFP encapsulating and SAM-GFP adsorbing formulations respectively. Results are expressed as the means of three independent experiments ± S.D.

Furthermore, Mφ capability to engulf SAM adsorbing DDA NPs was still low compared to the other DDA based formulations even after 24 hours (around 40%). Thus, while SAM loading DOTAP based formulations uptake efficiency was comparable across all samples

tested, DDA based particles showed differences between the formulations, with SAM encapsulating liposomes and SAM adsorbing emulsions having much higher uptake (Figure 4.6B).

Moreover, the ability of cationic formulations to induce antigen expression in macrophages was performed. However, antigen transfection was very poor (<15%), even with the positive control Lipofectamine 2000.

4.3.4 Evaluating the cytotoxic range for cationic formulations in BHK cell line

Due to unsuccessful transfection in macrophages, primary cells were substituted with baby hamster kidney – BHK – cell line; these cell lines have been used extensively for a variety of studies, including transfection and expression of cloned genes. BHK cells have been characterised as fibroblastoid with some epithelial phenotypic traits. The cytotoxicity of all formulations was determined in BHK cells after 16 hours by an amine reactive dye such as LIVE/DEAD. In cells with compromised membranes, the dye reacts with free amines both in the cell interior and on the cell surface, yielding intense fluorescent staining. In viable cells, the dye's reactivity is restricted to the cell-surface amines, resulting in less intense fluorescence. The difference in intensity is typically greater than 50-fold between live and dead cells, allowing for easy discrimination.(Robertson et al., 2019) The aim of the study was to understand the sub-toxic concentration to work at in further in vitro experiments like *in vitro* potency (IVP) or cell uptake. As it shown in Figure 4.7, as a general overview, DDA based formulations are generally more toxic compared to DOTAP formulations at the same concentrations.
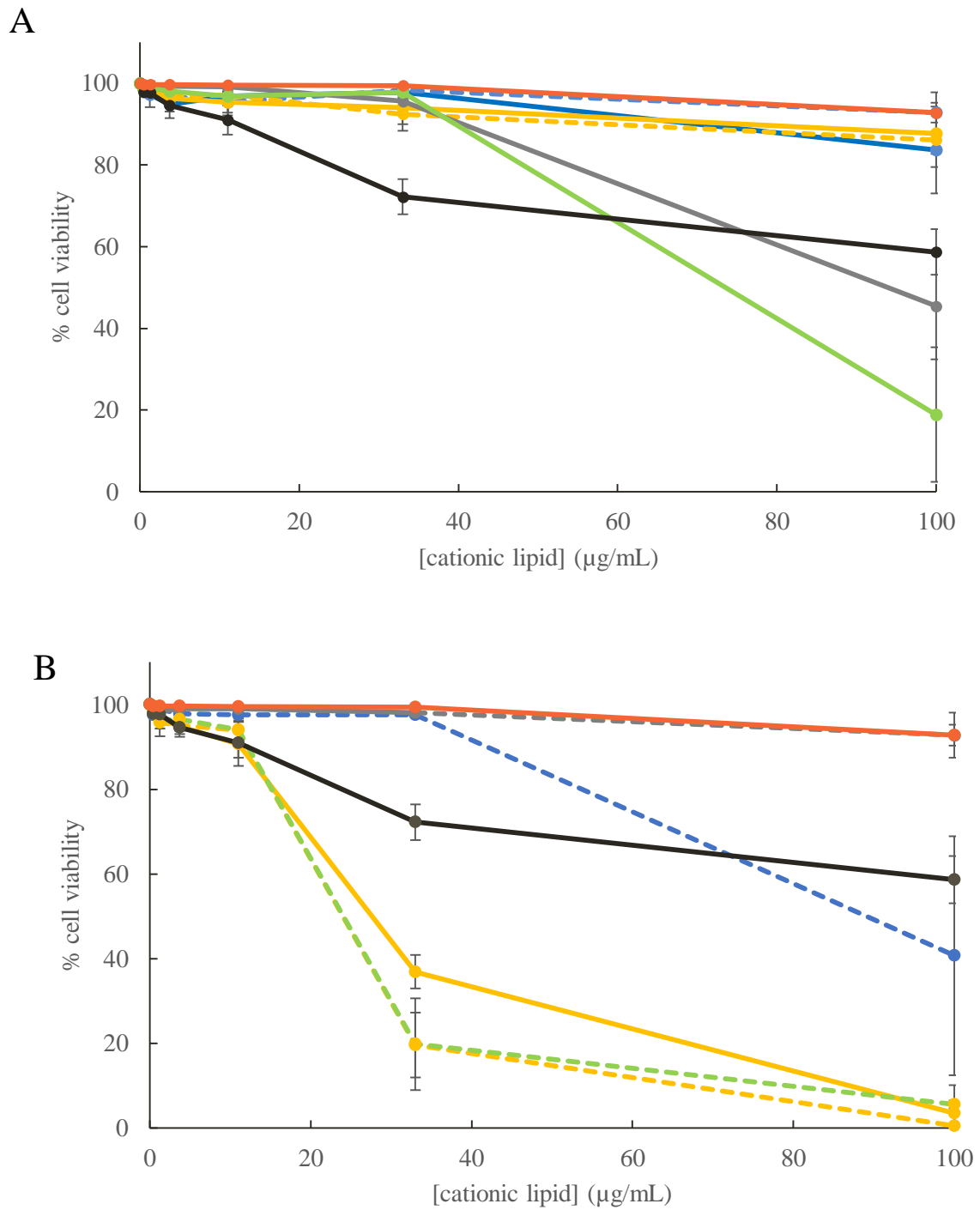
Figure 4. 7 Cell viability test in BHK cell line. Cytotoxicity in BHK of A) DOTAP based and B) DDA based NPs (green) SLNs (blue), CNE (grey) and liposomes (yellow). SAM-Rabies encapsulating and adsorbing formulations are represented as solid and dash lines respectively. LNPs (red) and Lipofectamine (black) 2000 were used as controls. Results are represented as mean ± SD of 3 independent experiments.

For example, at 33 μg/mL of cationic lipid, the percentage of alive cells after incubation with DOTAP NPs and DDA NPs was 97 and 20 respectively (Figure 4.7). Furthermore, liposomes seemed to follow the same trend: at 33 μg/mL of cationic lipid, below 40% of BHK were alive when incubated with DDA liposomes, while more than 90% of cells were found to be non-apoptotic when the same amount of DOTAP liposomes was added in the well. Regarding DOTAP CNE and DDA SLNs, they did not induce a toxic effect among all the concentrations tested but the highest (100μg/mL): at this DDA dose the cell viability was around 40%, which is comparable with what has been measured for Lipofectamine 2000, while DOTAP SLNs (with both SAM encapsulated or adsorbed) were nontoxic (cell viability above 80%). On the other hand, the rest of the formulations seemed to be nontoxic among the concentration range tested with more than 80% of alive cells (Figure 4.7). Generally, for most of the particles, toxicity was dependent on the lipid content, where higher concentrations were more toxic than low concentrations. Looking at Figure 4.7 it was evident that the half maximal inhibitory concentration (IC_{50}) of DDA NPs and DDA Liposomes was between 20 and 40 μg/mL of cationic lipid, with IC_{50} DDA NPs> IC_{50} DDA liposomes. Regarding DOTAP NPs the IC_{50} was between 70 and 90 μg/mL of DOTAP concentration, while for the rest of the formulations these values were above the highest cationic lipid concentration tested, despite the presence of antigen inside the particles or on their surface.

4.3.5 Cell uptake of SAM-Rabies loaded liposomes, SLNs, NPs and CNE in BHK cell line

In order to assess the cell uptake, DilC was used as *in vitro* tracker for lipid based particles. All formulations were added to the cells at an optimal sub-toxic concentration of 11 μg/mL of cationic lipid (i.e. either DOTAP or DDA). At this concentration, the cell viability of BHK was above 90% (Figure 4.7). To test the effect the type of cationic lipid has on the cellular uptake, a direct comparison between DOTAP (Figure 4.8A) and DDA (Figure 4.8B) based formulations was performed. Particles were incubated for 16 hours in cells containing either complete media containing 5% FCS or in FSC-free media, due to possible inhibitory effect of serum on particle uptake. Looking at Figure 4.8, where DOTAP based formulations were compared, the percentage of DilC+ cells was not significantly different among samples; thus, despite differences in physico-chemical properties, formulations were taken up by fibroblasts to the same extent, with an average percentage of DilC positive cells of around 95%. Moreover, depletion of serum did not affect the ability of particles to be engulfed by BHK; indeed, all formulations induced comparable values of DilC+ cells, which were not significantly different from what has been obtained in complete media. A similar trend was followed by DDA based formulations. Again, more than 95% of BHK resulted to be DilC+, therefore meaning that most particles were successfully taken up by fibroblasts (Figure 4.8B). In this case, neither the particle composition nor the cell growth media altered cellular

internalisation, with >95% DilC+ cells under the different conditions tested. Interestingly, gold standard LNPs were used as a positive control, showed a different internalisation pathway when incubated in presence or absence of FCS with almost 100% of BHK becoming DilC+ when incubated with SAM-Rabies encapsulating LNPs in complete media versus only 36% of DilC positive fibroblasts in FBS free media.
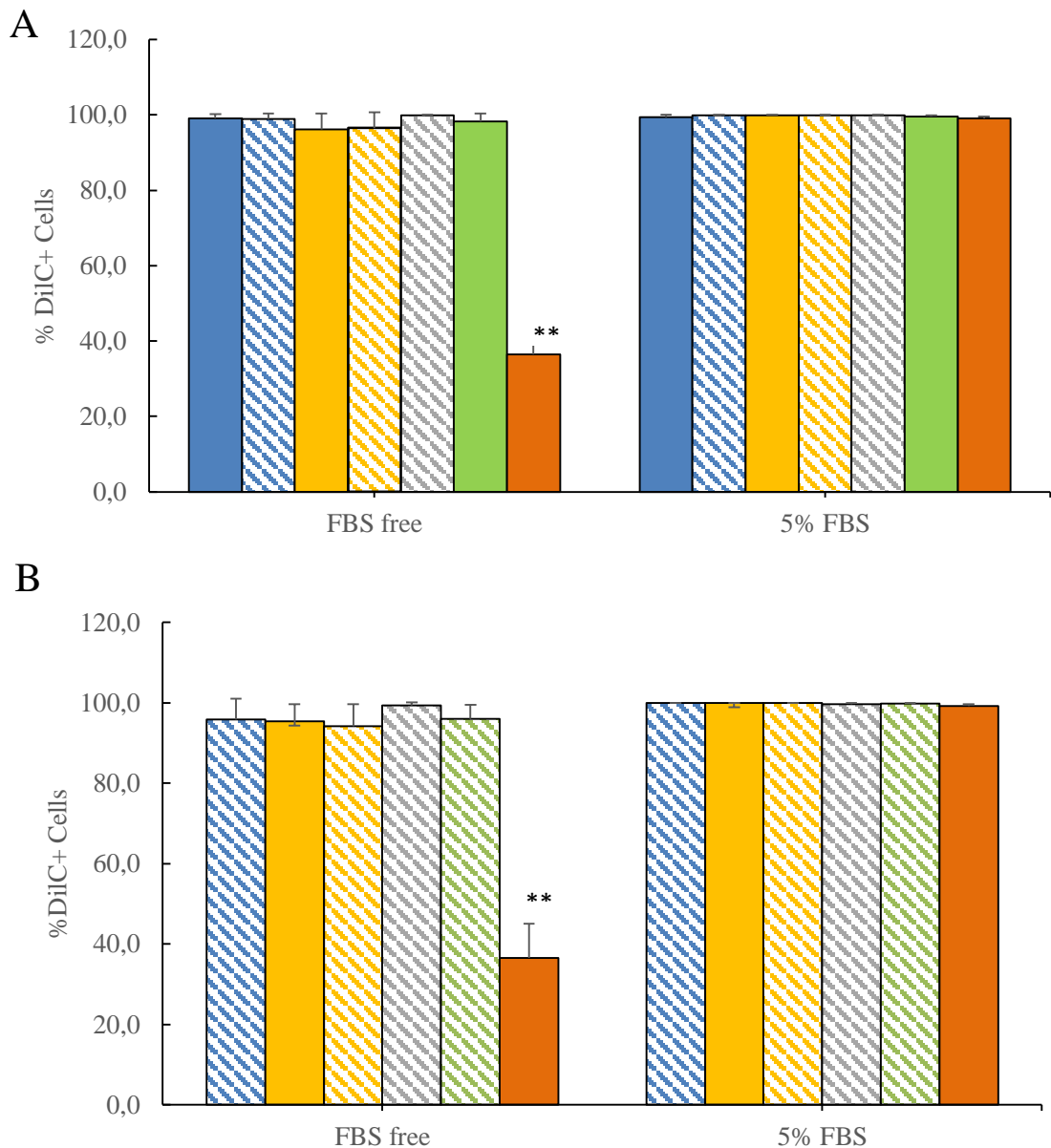
Figure 4. 8 Cellular uptake of formulations in BHK cell line expressed as DilC positive cells. Percentage of DilC positive BHK cells after 16 hours incubation with A) DOTAP based and B) DDA based NPs (green) SLNs (blue), CNE (grey) and liposomes (yellow) in both complete and FBS-free media. SAM-Rabies encapsulating and adsorbing formulations are represented as solid and dash columns respectively. LNPs (red) was used as control. Results are represented as mean ± SD of 3 independent experiments.
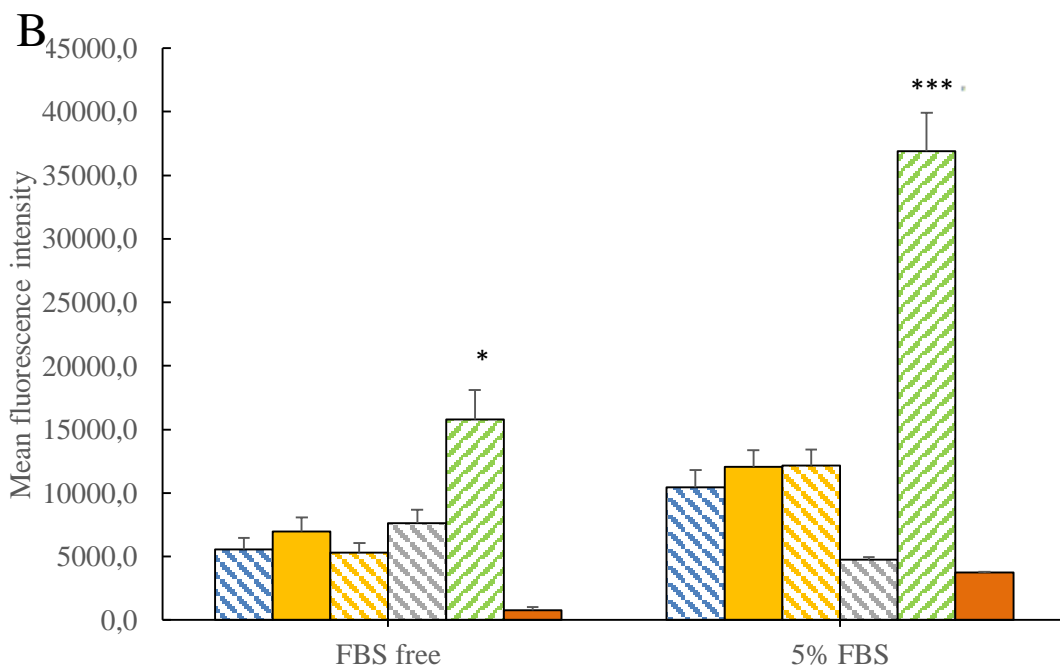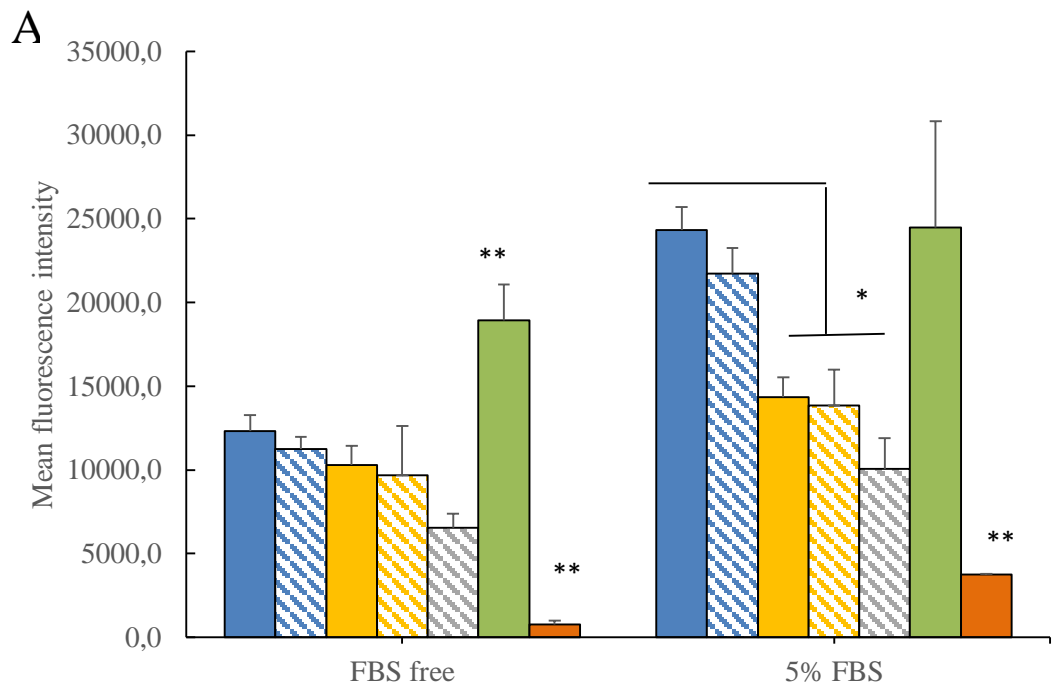
Figure 4. 9 Cellular uptake of formulations in BHK cell line expressed as mean fluorescence intensity (MFI). Mean fluorescence intensity of DilC positive BHK cells after 16 hours incubation with A) DOTAP based and B) DDA based NPs (green) SLNs (blue), CNE (grey) and liposomes (yellow) in both complete and FBS-free media. SAM-Rabies encapsulating and adsorbing formulations are represented as solid and dash columns respectively. LNPs (red) was used as control. Results are represented as mean ± SD of 3 independent experiments.
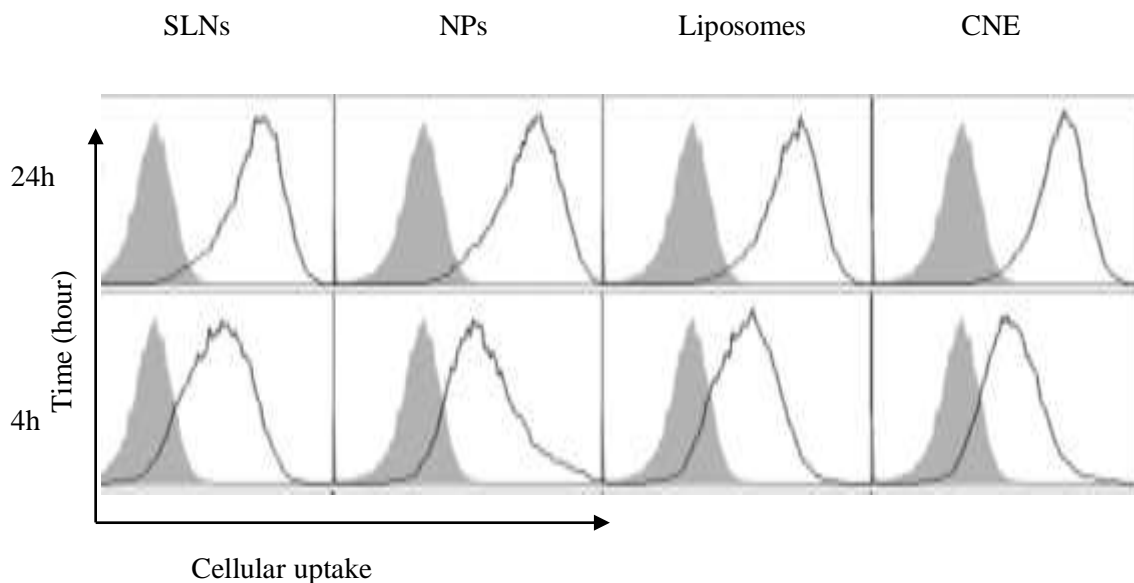
Figure 4. 10 Representative flow cytometry plots of particles uptake. DOTAP based particles uptake at 4 and 24 hours (black) with respect to control cells at time zero (shaded grey) in complete media (5% FBS). Results are represented as mean ± SD of three independent experiments.

However, although no significant difference in particles uptake has been shown by expressing data as percentage of DilC+ cells, discrepancies among formulations in uptake efficiency were indeed evident by analysing mean fluorescence intensity values (MFI) (Figure 4.9). The mean fluorescence intensity measured by flow cytometry is equivalent to the amount of fluorescent dye taken up by BHK, which is directly proportional to the product of the number of particles by liposome fluorescence; hence MFI is proportional to the amount of DilC+ cells. Looking at figure 4.9A and focusing on formulations incubated in complete media, it seemed that induced MFI of DOTAP SLNs and NPs was significantly higher compared to the other formulations; more in details SLNs and NPs MFI was >24300, while MFI of all the other DOTAP based carrier was <14300. However, despite absolute values being lower compared to 5%FCS condition, in FCS-free media, NPs resulted in the highest MFI (around 20000), which directly translated into more polymeric particles uptake by BHK. A similar trend was followed by DDA based formulations (Figure 4.9B), with again DDA NPs showing the greatest mean fluorescence intensity (~ 37000 and~ 16000 in 5% FBS and FBS-free media respectively), despite cell growth conditions. The extent of NPs uptake per cell correlated with increased toxicity reported in figure 4.7; it is known that induction of cytotoxicity by particles is determined by the entry pathway and intracellular localization; thus higher intracellular trafficking might lead to reduced cell viability (Foroozandeh and Aziz, 2018). It might be worth, however, to underline that moving from DOTAP to DDA reduced the overall MFI of

144

formulations. If, for example, MFI of SAM-Rabies adsorbing DOTAP SLNs was > 11000, DDA counterpart value was significantly inferior (around 5500). Interestingly, fibroblasts incubated with positive control LNPs showed the lowest mean fluorescence intensity (between 1000 and 3000), regardless the incubation conditions (Figure 4.9B)**.**

4.3.*5 In vitro* **potency assay with SAM-GFP formulations**

To understand the suitability of cationic delivery systems to efficiently transfect cells and induce antigen expression, an *in vitro* potency assay (IVP) was performed. To do so, formulations at 11 µg/mL of either DOTAP or DDA were used. LNPs were used as positive control. GFP was used as model antigen, since its detection and quantification *in vitro* did not require any additional staining, due to the intrinsic fluorescence of the protein. Figure 4.11 showed the percentage of GFP+ cells when SAM was transfected with either DOTAP (Figure 4.11A) or DDA (Figure 4.11B) based NPs, CNE, liposomes and SLNs. Figure 4.11 shows that polymeric nanoparticles resulted in higher protein expression at SAM concentrations of 500 ng/mL, irrespective of the cationic lipid used ($p < 0.05$); when 500 ng/mL of SAM was delivered through DOTAP and DDA NPs the percentage of GFP + cells was around 60% and 40% respectively. However, in general, LNPs and liposomes were more potent at SAM concentrations of 65 ng SAM/mL compared to other formulations ($p < 0.05$) (Figure 4.11).

Regarding SLNs, it seemed that the presence of DOTAP enhanced the ability of particles to deliver SAM compared to DDA, with consequently higher percentage of cells expressing GFP at SAM concentration of 250 ng/mL. As it shown in figure 4.11B, when the
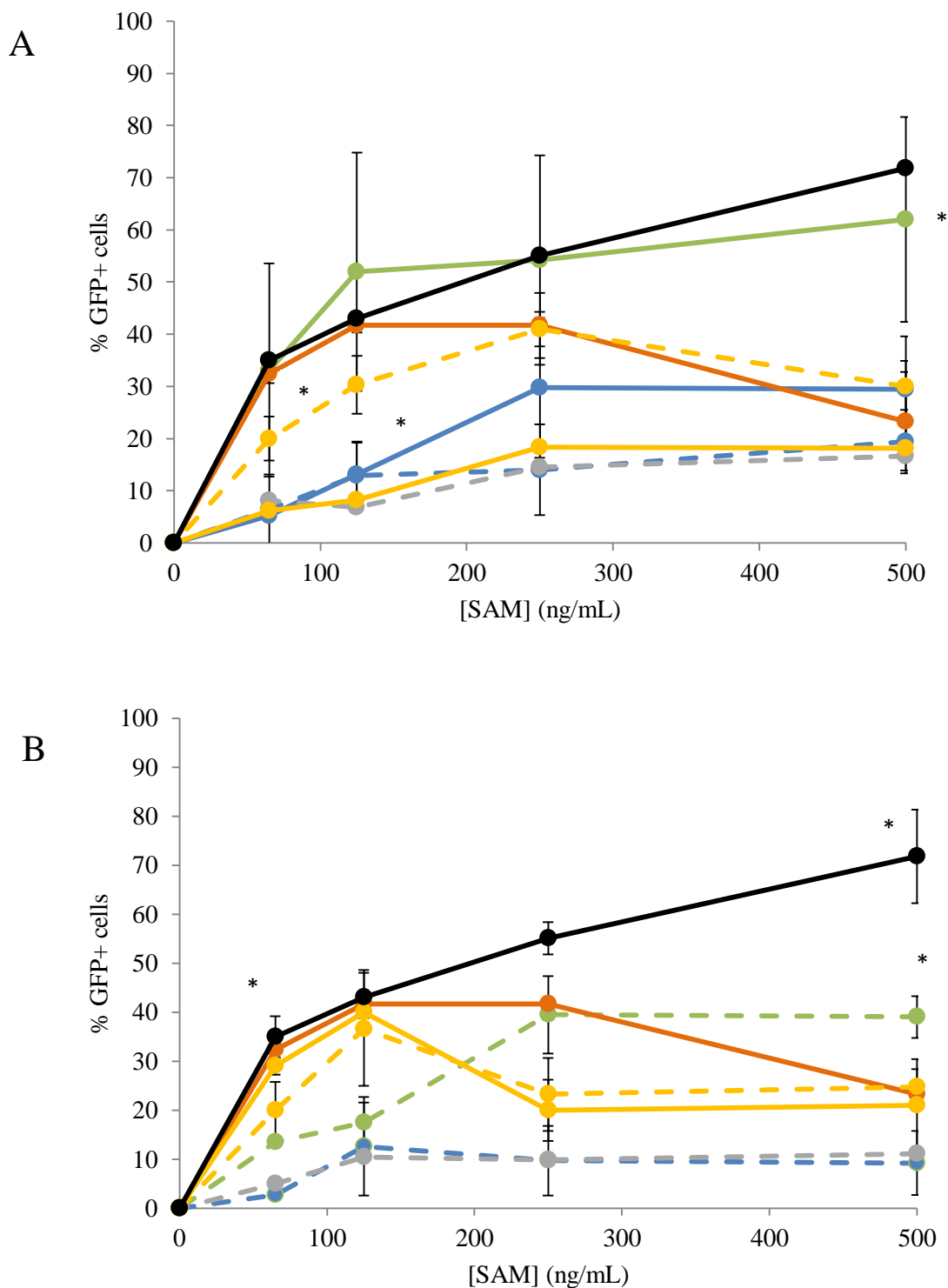
Figure 4. 11 *In vitro* potency of SAM GFP-NPs, SLNs, CNE and Liposomes in BHK fibroblasts. A) Percentage of GFP positive cells with A) DOTAP based and B) DDA based formulations incubated with different cationic delivery systems - NP (green), Liposomes (yellow), CNE (grey) and SLNs (blue). SAM adsorbing and SAM encapsulating formulations are represented by dashed lines and solid line respectively. LNPs (red) and Lipofectamine2000 (black) were used as positive controls. Results are represented as mean ± SD of three independent experiments.

same nucleic acid concentration was adsorbed onto DDA based SLNs, the percentage of GFP+ cells was lower compared to DOTAP SLNs (<15% vs 30%; $p<0,05$)). However, the change in cationic lipid did not alter the potency of CNE to induce antigen transfection (<14%; Figure 4.11).
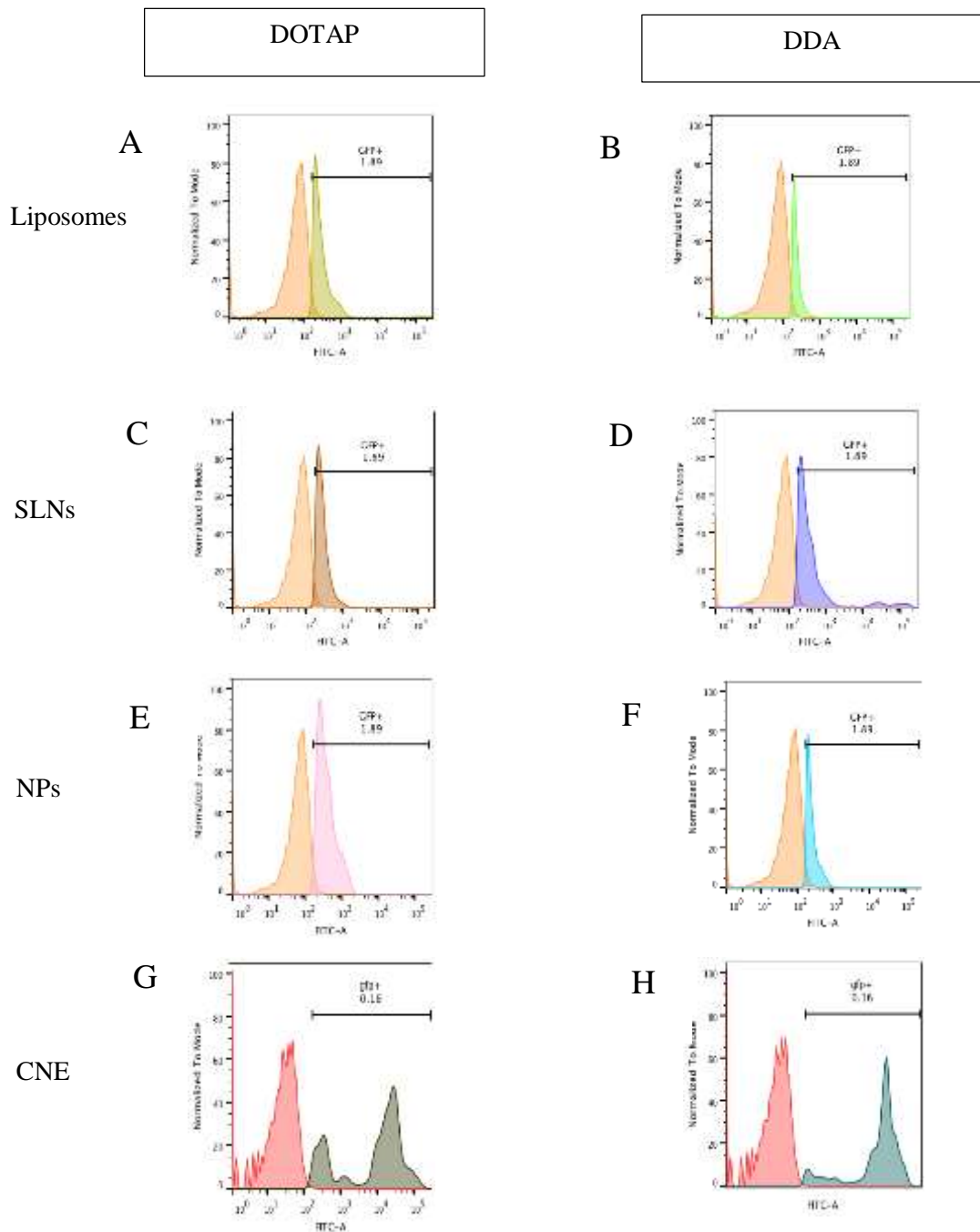
Figure 4. 12 Histograms of *in vitro* potency of SAM GFP-NPs, SLNs, CNE and Liposomes in BHK fibroblast. Representative flow cytometry plots of DOTAP A) Liposomes, C) SLNs, E) NPs, G) CNE, and DDA B) Liposomes, D) SLNs, F) NPs, H) CNE. All formulations were prepared with 500 ng/mL of SAM. Histograms represent GFP+ cells induced by formulations (colored) with respect to control cells (orange).
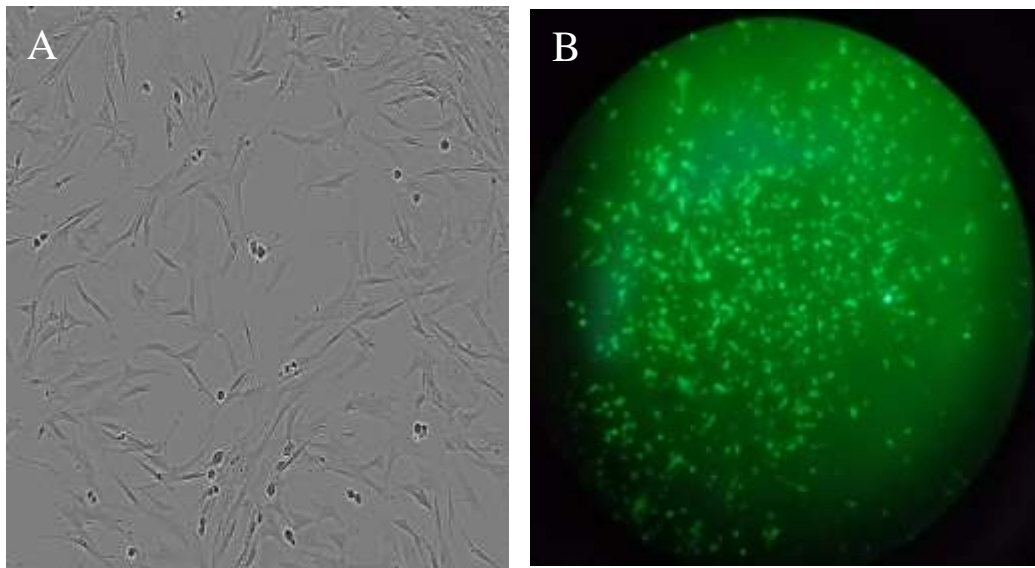
Figure 4. 13 GFP expression in BHK cell line. Images of BHK at A) 0 and B) 16 hours incubation with DOTAP polymeric nanoparticles encapsulating 500 ng/mL SAM-GFP. The cells were observed under a fluorescent microscope (Zeiss Axio Scope A1 Microscope) B) with or A) without a green filter.

With respect to DOTAP liposomes it seemed that SAM adsorbing vesicles were more efficient in delivering the nucleic acid in fibroblasts compared to the SAM encapsulating ones. For example, when 250 ng/mL of SAM were adsorbed on or encapsulated in liposomes, the percentage of GFP+ cells was 40 and 18 respectively (p<0.05). However, when DDA was used in the liposomes formulation, the ability of both SAM encapsulating and adsorbing vesicles to induce antigen expression was similar and it was comparable to gold standard LNPs at 125 ng of SAM/mL (Figure 4.11B).

To confirm the suitability of the method, Lipofectamine 2000 (LF) was used as an additional positive control. When LF was employed to deliver SAM inside BHK, expression was above 70% (Figure 4.10 and 4.11). Further, when looking at the flow cytometry plots (Figure 4.12), while a peak shift is only observed for DOTAP and DDA NPs, DOTAP SLNs, DOTAP and DDA liposomes (Figure 4.12A, B, C, E, F), transfection of BHK cells with DDA SLNs and DDA and DOTAP CNE also resulted in cells overexpressing GFP with a clearly differentiated population of GFP positive cells (Figure 4.12D, G and H). Microscope observations correlated with FACs data. More precisely, images in Figure 4.13 showed production of green fluorescence when BKH were incubated for 16 hours with DOTAP polymeric nanoparticles encapsulating 500 ng/mL SAM-GFP (Figure 4.13 B) compared with the non-treated counterpart (Figure 4.13 A).

4.3.6 *In vitro* potency assay with SAM-Rabies formulations

Once the consistency of the method was established, model antigen SAM-GFP was substituted with the antigen of interest SAM-Rabies. Formulations were prepared at the highest [SAM-Rabies] of 400 µg/mL. Figure 4.13 represents the percentage of Rabies-positive cells after 16 hours incubation of SAM-loaded DOTAP (Figure 4.14A) or DDA (Figure 4.14B) particles at different antigen concentrations in complete media. After 16 hours incubation with BHK cells, it can be seen that all particles were able to transfect fibroblasts, however polymeric nanoparticles and liposomes showed the greater ability to induce antigen transcription *in vitro* compared to CNE and SLNs ($p < 0.05$). Moreover, the transfection efficiency seemed to be SAM dose independent; indeed, increasing SAM content, the percentage of Rabies+ cells increased significantly. However, the potency of the transfection varied among particles. For example, focusing on DOTAP based formulations, at the lowest antigen dose tested, NPs and liposomes (with SAM adsorbed or encapsulated) could transfect between 40 and 60% of BHK, while for the rest of the formulations, antigen+ cells were comparable to or below the positive control (LNPs) values. This discrepancy became even more evident at the highest SAM content tested, with NP and liposomes showing a transfection efficiency comparable with LF, while SLNs were significantly lower compared to LF ($p < 0.05$). Regarding SLNs and CNE, the percentage of antigen positive cells was below 50 as measured for LNPs, despite the change of cationic lipid or the increase of antigen content.

Due to possible inhibitory effect by the serum contained in the media on gene delivery, IVP testing was also performed in the absence of serum to better understand if the binding of serum proteins to the SAM-particles complex might modulate the activity of formulations in culture. These additional tests might also help to better discriminate among formulations according to their antigen expression efficiency, thus aiming to identify which formulation/s will be moved further for *in vivo* immune study. As shown in Figure 4.15A and B, particles mediated antigen expression in serum free media followed the trend seen in the presence of serum; however, the percentage of transfected cells increased in absence of FBS for most of the formulations. For instance, at the highest SAM dose, the percentage of Rabies+ cells for DOTAP NPs, DDA and DOTAP liposomes was between 80 and 100%, values which were comparable with ones of LF. Furthermore, the ability of CNE to transport particles inside cells and consequently induced antigen transcription seemed to be higher in FBS free media ($p < 0.05$). For example, at 400 ng/mL SAM, Rabies + cells were 13% for DOTAP CNE and 45% for DDA CNE in presence of serum; however, once the FBS was depleted, these values became much higher (60 and 70% respectively- $p < 0.05$).

A
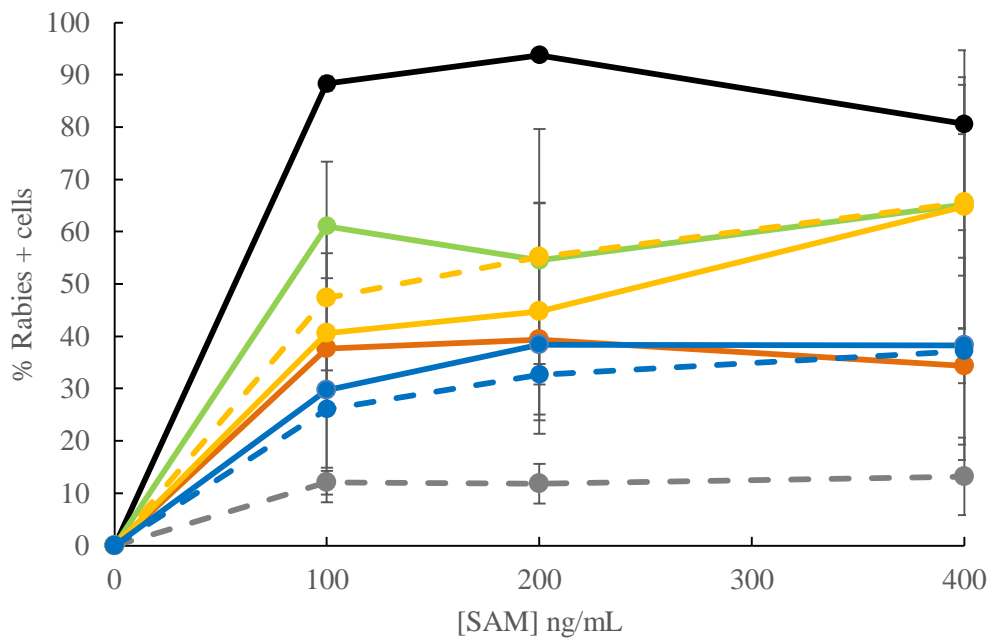
B
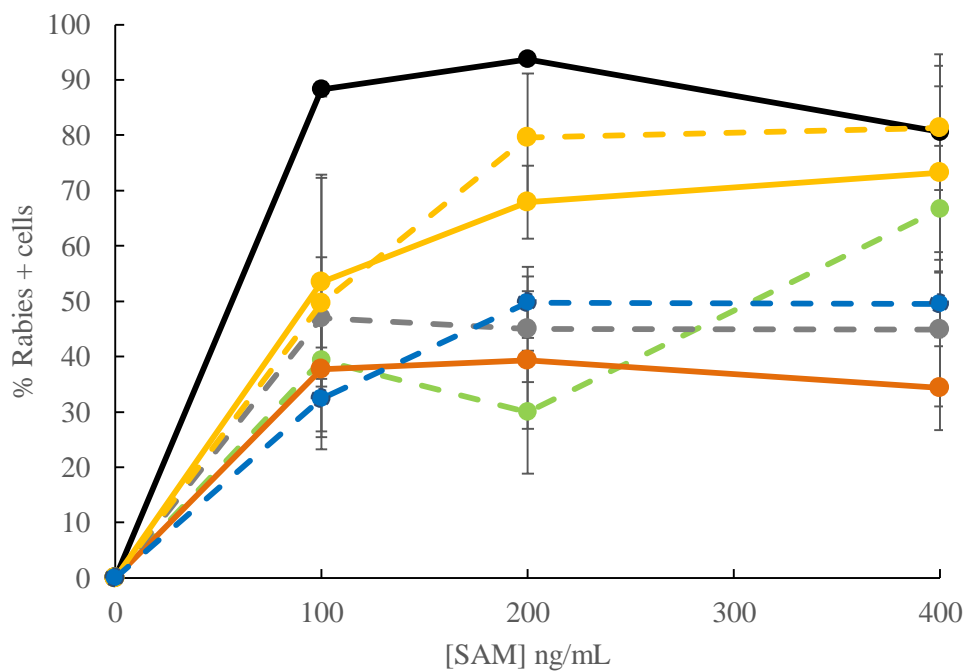
Figure 4. 14 ***In vitro*** **potency (IVP) in BHK cell line in complete medium.** IVP in BHK in cDMEM supplemented with 5% FCS of A) DOTAP based and B) DDA based formulations prepared with SAM-Rabies at different concentrations - NPs (green) SLNs (blue), CNE (grey) and liposomes (yellow). SAM-Rabies encapsulating and adsorbing formulations are represented as solid and dash lines respectively. LNPs (red) and Lipofectamine2000 (black) were used as controls. Results are represented as mean ± SD of 3 independent experiments.
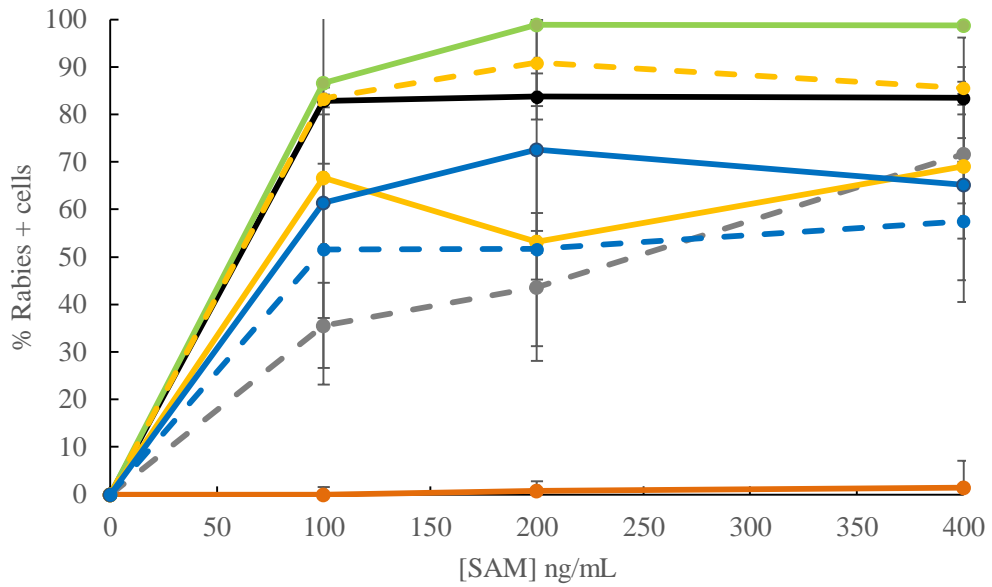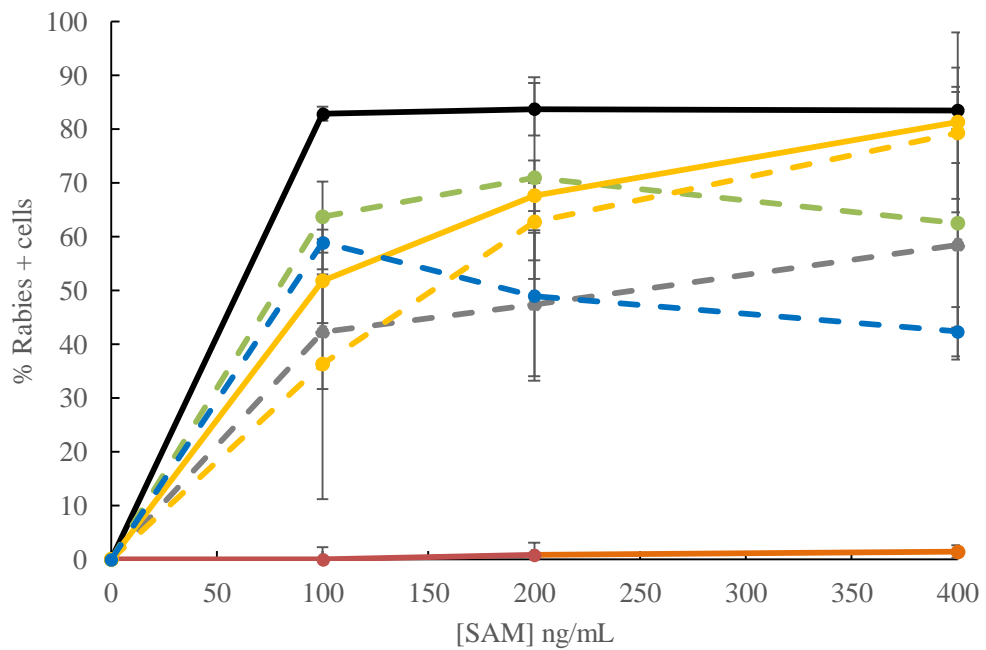
Figure 4. 15 *In vitro* potency (IVP) in BHK cell line in absence of serum. IVP in BHK in FCS-free medium of A) DOTAP based and B) DDA based formulations prepared with SAM-Rabies at different concentrations - NPs (green) SLNs (blue), CNE (grey) and liposomes (yellow). SAM-Rabies encapsulating and adsorbing formulations are represented as solid and dash lines respectively. LNPs (red) and Lipofectamine2000 (black) were used as controls. Results are represented as mean ± SD of 3 independent experiments.
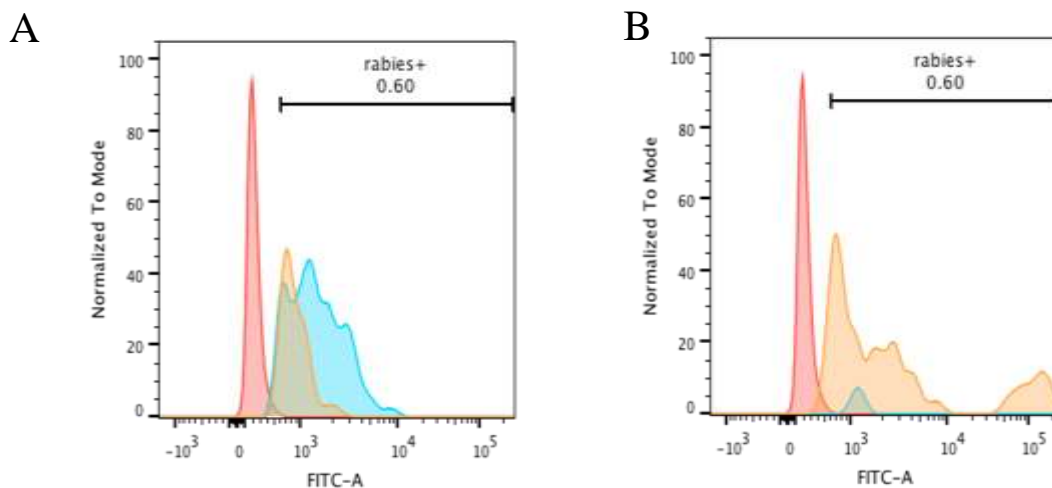
Figure 4. 16 The effect of serum on antigen transcription. Representative flow cytometry plots of A) SAM-Rabies DOTAP NPs and B) LNPs (on the right). Red, blue and yellow histograms represent the peaks of control cells, cells incubated without serum and cells incubated with serum respectively. All formulations were prepared with 400 ng/mL of SAM.

On the contrary, SAM transfection with gold standard LNPs was more efficient in complete medium (p<0.05). By comparing Figure 4.14A and 4.15A, looking for example at 200 ng SAM/mL, the percentage of Rabies+ cells were around 40 and 2 in presence or absence of serum respectively. The flow cytometry plots in Figure 4.16 confirmed these observations, even though cells expressing antigen were clearly represented by a separate and left shifted peak compared to the control (red), the intensity and degree of separation varied among experimental conditions. For instance, while just a small peak of Rabies+ cells were observed with LNPs (Figure 4.16B) in absence of serum (blue), a more intense histogram represented antigen expressing cells when SAM was transfected with LNPs in complete media (orange). An opposite trend was observed for DOTAP NPs (Figure 4.16 A), with a wider and more right shifted Rabies+ cells population peak (blue) in FSC free media compared to the one in 5% FCS (orange). Despite these differences, all particles could deliver both SAM-GFP and SAM-Rabies to BHK cells and induced antigen transfection. However, according to this data, SAM-Rabies encapsulating DOTAP NPs, SAM-Rabies encapsulating DOTAP and DDA liposomes resulted in greater and more consistent antigen expression compared to SLNs and CNE.

4.4 Discussion

Within this chapter the suitability of four different cationic nanoparticulates – liposomes, solid lipid nanoparticles, polymeric nanoparticles and cationic nanoemulsions - to efficiently induce transfection and consequently antigen expression *in vitro* was investigated. Self-amplifying

RNA encoding for a green fluorescence protein (SAM-GFP) and for a rabies glycoprotein (SAM-Rabies) were formulated with carriers either on the surface or inside the formulation. The optimal SAM delivery system should be non-toxic, protect SAM from RNase degradation, facilitate intracellular uptake followed by escape from endosome vesicles into the cytosol and finally encourage effective antigen expression (Oh and Park, 2009).

4.4.1 The effect of sterilisation method on formulations attributes

Prior to *in vitro* assays assessments, SAM adsorbing or SAM encapsulating cationic formulations were sterilised via γ-irradiation. The importance of developing contaminants-free formulations is relevant not only for *in vitro* purposes, but it might be also extended to further *in vivo* applications and larger scale production steps. Although filtration is a well-established and relatively cheap method of formulations sterilisation at small scale, (Meure et al., 2008) its applicability suffers from size restriction and particles surface composition limitations. Therefore, particles larger than 200 nm are retained by the pores of the filter; moreover, highly cationic formulations can potentially establish chemical interactions with filters made of polycarbonate or depth filters made from cellulose acetate, (Goldbach et al., 1995) with consequently loss of materials and poor lipid recovery. Alternatively, a sterilization method able to maintain formulations attributes would be therefore highly advantageous. Compared to other sterilisation techniques, γ-irradiation is known to have the highest reliability in killing, requiring moderate operating temperature (35–40°); herein, it has been shown that application of γ-irradiation for samples sterilisation did not alter particles attributes and SAM integrity (Figure 4.1-4.2). These findings are in line with previous reports. For example sterilization of drug-loaded PLGA nanoparticles was performed by γ irradiation at the dose of 25 kGy, and it was shown to have no adverse effect on particle size, drug release behaviour, or ex vivo arterial uptake of the nanoparticles (Song et al., 1997). In another study, cationic liposomes based on DDA–TDB incorporating mycobacterial fusion protein Ag85B-ESAT-6 were compared in terms of size and surface charge before or after sterilisation (Mohammed et al., 2006).

It was concluded that the values obtained prior to sterilisation were not significantly different to those after γ irradiation, with no alteration in liposomes properties and antigen structure including *in vivo* efficacy (Mohammed et al., 2006). Therefore, these encouraging results emphasised the suitability of γ irradiation as an efficient method for cationic formulations sterilisation.

4.4.2 Targeting bone marrow derived macrophages and dendritic cells

Moving into *in vitro* assays, it was first attempted to target bone marrow derived macrophages (BMDM) and dendritic cells (BMDDCs). The cytotoxicity data revealed that, despite differences in formulation composition, the toxic effect of most of the cationic formulations

was cationic lipid dose dependent in both cell types. (Figure 4.2). The toxic effect is mainly determined by the cationic nature of the vector (Gao and Hui, 2001). Generally, the cytotoxic effects of cationic lipids are mainly due to the structure of its hydrophilic group. Quaternary ammonium amphiphiles are more toxic than their tertiary amine counterparts (Hyvönen et al., 2000). One rational solution would be spreading the positive charge of the cationic head by delocalizing it into a heterocyclic ring. Heterocyclic cationic lipids containing imidazolium or pyridinium polar heads (Meekel et al., 2000, Roosjen et al., 2002) have been reported to display higher transfection efficiency and reduced cytotoxicity when compared with classical transfection systems (Ilies et al., 2003). Further, the interaction between cationic lipids and critical enzymes such as protein kinase C (PKC) might increase lipids toxicity (Bottega and Epand, 1992). To circumvent that, it has been shown that many derivatives of cholesterol which contain tertiary or quaternary nitrogen head-groups can inhibit PKC activity, with consequently reduced toxicity (van der Woude et al., 1997). Moreover, the type of linker bonds might play a role in lipids cytotoxicity. Although compounds with ether linker render better transfection efficiency, they are too stable to be biodegraded and thus cause toxicity. Cationic lipids with ester bonds such as DOTAP in the linker zone are more biodegradable and associated with less cytotoxicity in cultured cells (Leventis and Silvius, 1990, Farhood et al., 1992, Qiao et al., 2012); however, these linkers are liable to decompose in the circulation system. One alternative approach might be substituting esters with carbamate-linked lipids which would be stable (Ren et al., 2001) at physiological pH while they decompose at lower endosomal pH (Qiao et al., 2012). Furthermore, an increase in the length of the linker segment led to decreased toxicity in cell culture (Hafez et al., 2001b). The cytotoxicity of charged formulations on a wide range of cell lines has been well established; it is known that the presence of a positive charge density on formulation surface induces toxicity. Mayhew (Mayhew et al., 1987) and Campbell (Campbell, 1983) reported that inclusion of the cationic lipid stearylamine into anionic formulations increased the cytotoxicity and it was also dependent on the amount of this lipid added per well. Moreover, it has been seen that cationic lipids and cationic polymers for gene delivery may cause toxic effects *in vitro* and *in vivo* (Floch et al., 2000).

Moreover, it seemed that BMDM were more sensitive to DOTAP:DOPE liposomes (cell availability <35%), while BMDDCs were more affected by high concentrations of DOTAP based SLNs and NPs with <55% cell survival. The fact that cationic liposomes are highly toxic toward macrophages could be explained by the enhanced relative phagocytic activity of macrophages, confirmed by uptake efficiency data collected within this work. It was observed that lipoplexes caused several changes to cells, which included cell shrinking, reduced number of mitoses and vacuolization of the cytoplasm (Mosmann, 1983). The fact that the liposomes were the most toxic compared with all formulations tested in macrophages might be due to

the presence of DOPE. This is a pH-sensitive phospholipid that can destabilize the endosomal membrane at acidic pH and assist liposomes in delivering their contents into the cytoplasm (Hui et al., 1996). The association of DOPE with cationic lipids may therefore be responsible for the toxicity observed toward macrophages. Indeed, Phillips and co-workers (Filion and Phillips, 1997) found that the progressive replacement of DOPE by DPPC significantly reduced toxicity towards macrophages. The replacement of DOPE by DPPC did not completely abolish the toxicity, but the toxicity never exceeds 15% at the concentrations used. However, the reason why SLNs and NPs were more toxic in dendritic cells was not well understood, therefore it might be worth performing additional cell uptake experiments to see if there is any correlation between cytotoxicity and increased phagocytic activity.

Moreover, uptake of empty and SAM-GFP loaded formulations in BMDM revealed that the association with the model antigen altered particles internalization pathway of cationic particles. Considering DOTAP based formulations, the addition of SAM generally increased particles uptake during the timeframe tested (Figure 4.4). This improvement might be due to increased particles size after SAM encapsulation or adsorption as reported previously in Chapter 3. These results are in agreement with previous works, where cellular uptake was reported to increase with increase in liposome size. For instance, it has been seen that the uptake of ciprofloxacin-hydrogenated soybean phosphatidylcholine (HSPC), cholesterol (Chol) and dicetylphosphate (DCP) liposomes by peritoneal macrophages was particle size-dependent over the range 100–1000nm with larger particles taken up in a greater extent compared to the smaller counterpart (Chono et al., 2006). Moreover, this sensitivity of macrophages to vesicle size was also reported by Schwendener and co-workers who saw that the delivery of aqueous drugs to macrophages can be further improved using large unilamellar vesicles made of egg phosphatidylcholine and cholesterol because of their greater internal volume (Schwendener et al., 1984). Although the uptake mechanism of SAM loaded particles by BMDM cells was not investigated in the present study, previous works showed that cationic lipid-based delivery systems containing plasmid (Lin et al., 2013) and oligonucleotide (Yotsumoto et al., 2008, Maeki et al., 2018) accumulate in cells by endocytosis (for particles <100 nm in size) or phagocytosis (for particles between 200 and 2000 nm in size) (Harashima et al., 1999). However, another work using LNP-siRNA delivery systems containing "lipidoid" cationic lipids has suggested entry by macropinocytosis (Love et al., 2010). A more recent paper on LNP-siRNA hypothesised a more complex internalization pathway, with uptake predominantly driven by clathrin-mediated endocytosis and macropinocytosis (Lin et al., 2013). A substantial body of literature concluded that RNA-lipid particles enter cells via endocytosis pathways, (Schroeder et al., 2010, Ziello et al., 2010) more specifically by the clathrin-mediated pathway. The success is generally attributed to the interactions of charged lipids with the anionic components of endosomal membrane, and the effects of helper lipid on

the cellular membranes structure, leading to the material escaping from endosomal vesicles (Hui et al., 1996). It has also been proposed that the caveolae-mediated pathway may play a role in a successful gene delivery, due to avoiding the delivery systems' 'entrapment' in endosomes and lysosomes (Kiss and Botos, 2009). However, clathrin-mediated pathway remained predominant.

Regarding DDA based formulations, the size-dependent uptake path seemed to be less evident, with no significant difference in terms of DilC+ cells between empty and SAM-loaded particles after 24 hours. (Figure 4.5). These data suggest that other factors, such as surface charge and lipid rigidity, might contribute to particles internalization *in vitro*. As already discussed in Chapter 3, the addition of the antigen either inside or onto particles surface induced a significant reduction in positive Z-potential values. This loss might therefore compromise particles uptake by BMDM *in vitro*. In agreement with what has been hypnotised, literature reported that receptor-targeted cationic head-group induced the greatest increase in cellular uptake, followed by cationic amine head-groups, both being superior to neutral (zwitterion) lipids or to negatively-charged head-groups (Akinc et al., 2010). Moreover, in non-phagocytic cells, negative charge on the particle has been shown to reduce cellular uptake due to electrostatic repulsion between the negatively-charged particle and the negatively-charged cell membrane (Lu et al., 2016). Thus, the more positive formulations are the higher is the likelihood of them to be internalized by cells. Moreover, it is known that lipid particles uptake and consequent transfection potency is strongly related to cationic lipid pKa (Semple et al., 2010). More specifically, higher pKa will result in a higher surface charge for formulations containing DOTAP or DDA, which would be expected to encourage association with the negatively charged membrane of the macrophage cell line *in vitro* and thus enhance uptake (Zimmermann et al., 2006). On the other part, membrane flexibility of cationic particles is an important factor for appropriate wrapping of plasmid (Zuhorn et al., 2005) and bilayer fluidity of lipoplexes or polyplexes influences the interaction of vector with cell membrane (Ferrari et al., 2002). It is generally accepted that hard and faceted particles are preferable for cellular uptake compared to soft and round particles (Anselmo et al., 2015). However, it was proven that lipoplexes containing unsaturated lipids were more fluid and less regular in structure, thus resulting in weaker binding of pDNA within the lipoplex (Ferrari et al., 2001). Conversely, the presence of the long, saturated side chains may serve to anchor the lipids in the membrane. As a result, the lipoplex structure may be less flexible, with a more regular placement of the positively charged head groups on the lipid surface, allowing tighter and more uniform coverage of the pDNA (Ferrari et al., 2001). This more uniform positive surface charge could facilitate binding by serum proteins with consequently less internalization and reduced transfection efficiency (Ferrari et al., 2001). Hence, this might mitigate size increase effect after SAM addition in DDA based formulations.

However, despite promising results on cellular internalization, antigen expression in BMDM was unsuccessful. It is known that primary phagocytes are poorly transfection permissive due to their inherent resistance to transfection with DNA constructs (Lemmon et al., 2011). Transfection resistance of the primary phagocytes is thought to be due to the innate ability of these cells to degrade foreign nucleic acids within the endo-lysosomal system (Burke et al., 2002). Methods that circumvent DNA degradation within these compartments, such as electroporation, also result in lower transfection efficiencies in phagocytes, indicating that there are additional factors contributing to this resistance (Matthews et al., 1995). Although non-viral transfection of *ex vivo* and *in vivo* macrophages and dendritic cells has generated interest for the potential to use these cells as targets or vehicles in gene therapy, transfection efficiencies using this methodology were modest (Lemmon et al., 2011).

4.4.3 Targeting baby hamster kidney cells

Therefore, another cell line - baby hamster kidney cells (BHK) – was used as target for antigen expression, as they are a well-established model for SAM transfection. Moreover, BHK are more permissive to nucleic acids internalization since they are type I IFN deficient cell line (Spuul et al., 2011). The presence of viral dsRNA in an animal cell is an indication of the pathogen invasion and it is recognized by the innate immune system as a non-self entity, as vertebrate genomes do not encode RNA-dependent RNA polymerase (RdRp) activity. Recognition of viral dsRNA by specific pathogen recognition receptors (PRRs) leads to the induction of type I interferons (IFN; e.g. IFN-a and IFN-b), (Takeuchi and Akira, 2009) which promote an antiviral IFN response state of the cell (Samuel, 2001). Thus, type I IFN acts as an inhibitory molecule that reduces virus replication, as a sort of non-self viral replication knockdown (Kurane et al., 1993). Therefore, lack in this regulatory molecule triggers to more permissive cells generation and consequent more efficient RNA transfection. Cytotoxicity data in BHK cells showed that, as a general overview, DDA based formulations were more toxic compared to DOTAP ones at comparable concentrations (Figure 4.6). These findings are in agreement with studies performed on mammalian cell lines (Lappalainen et al., 1994b). The greater toxic effect of DDA was confirmed by other studies reported in literature. For example, it has been seen that DDA:DOPE liposomes were more toxic than DOTAP counterparts. More precisely, CaSki human cervical cancer cells treated with 40 µg DOTAP were found to be alive, while toxic effect was reported at the same concentration of DDA liposomes (Lappalainen et al., 1994a). Moreover, within that study, morphological data highlighted that DOTAP caused minor cellular changes - cell shrinking, reduced number of mitosis and vacuolization of the cytoplasm – compared to DDA counterparts at the same cationic lipid content (Lappalainen et al., 1994a). The lower toxicity of DOTAP formulations might be attributed to higher degradability *in vitro* of DOTAP compared to DDA; the ester linker on DOTAP structure is known to be susceptible to hydrolysis in an aqueous environment, which

promotes DOTAP metabolism therefore avoiding accumulation in cells compartments (Lv et al., 2006).

Data shown within this chapter highlighted that, *in vitro*, cationic particles were readily taken up by BHK, with approximately 100% particles+ cells after 16 hours despite the growth media composition (Figure 4.8). It might be worth noticing that the gold standard LNPs behaved differently in either presence or absence of FCS, with significantly lower DilC+ cells in FSC-free conditions (<37% vs >99%). This may be due to depletion of Apolipoprotein E (ApoE) in FSC-free media. It has been widely reported that the internalization of LNPs siRNA for hepatocyte gene silencing has been attributed to association with apolipoprotein E, which leads to uptake through the scavenging receptor (Akinc et al., 2010). However, herein, differential uptake of cationic formulations by BHK was more evident when analysed in terms of mean fluorescence intensity (MFI – Figure 4.9). Generally, particles internalisation was higher in presence of FCS in the growth media, with DOTAP SLNs, DOTAP NPs and DDA NPs having the greater MFI values. These findings were partially in agreement with what has been seen previously. Serum has been reported to exert its inhibitory effect by binding serum proteins to the complex of cationic lipids and nucleic acid (lipoplexes), which leads to structural reorganization, aggregation, and dissociation of the complexes (Marchini et al., 2009). However, the cholesterol-based cationic lipid CHOL-E has shown high transfection efficiency even in the presence of serum as compared to Lipofectamine (Marchini et al., 2011). Furthermore, DC-Chol, a well-known cholesterol derived cationic lipid, has shown to have better transfection efficiency in the presence of serum (Caracciolo et al., 2010). These data suggested that DDA and DOTAP based SLNs, NPs, CNE and Liposomes may enter cells by caveolae mediated endocytosis and macropinocytosis in addition to the clathrin-mediated endocytosis in the presence of serum. Several studies have reported that the nanoparticle associated "protein corona" from plasma or other bodily fluids is important in the cell−nanoparticle interaction (Caracciolo et al., 2011). Most of proteins surrounding nanoparticles were apolipoproteins, immune response-related proteins, immunoglobulins, acute-phase proteins, coagulation-related proteins, and cell adhesion proteins (Walczyk et al., 2010, Capriotti et al., 2011). Serum proteins such as albumin and heparin are also known to bind to lipid membranes, causing aggregation of lipoplexes and an increase of the size (Zelphati et al., 1998, Almofti et al., 2003). The change in endocytosis pathway may be a consequence of these changes of particles. Lipoplexes approximately of 300 nm or less were preferentially enter cells via the clathrin-mediated endocytosis, and lipoplexes larger than 500 nm were reported to be internalized via caveolae mediated endocytosis (Rejman et al., 2004). The addition of serum might presumably have increased SLNs, CNE, NPs and liposomes particles size, therefore, these particles may use more than one pathway in the presence of serum, taking advantage of alternative trafficking processes. Further, as discussed previously

for the uptake in BMDM, DOTAP formulations were taken up in a greater extent compared to DDA counterparts. Again, this might be attributed to the differences in Z-potential values and in the overall final rigidity of different cationic particles, parameters which is known to affect non-viral gene transfection *in vitro.*

In vitro potency (IVP) assays with both SAM-GFP and SAM-Rabies based formulations showed that DOTAP polymeric nanoparticles and both DDA and DOTAP liposomes had the greater ability to induce antigen expression in BHK cells, regardless of the choice of the encoded antigen (Figure 4.9 and 4.13). Moreover, increase in SAM concentration did not result in higher antigen expression. This lack of dose response with SAM loaded formulations *in vitro* could result from saturation of either the uptake pathway, which is likely different from that of lipofectamine, or translation capacity of the cells. The internalisation of lipid particles for gene delivery is a complex machinery which involves several endocytic pathways (Kaksonen and Roux, 2018, Lim and Gleeson, 2011) and it is affected by numerous cellular phenomena. It is strongly believed that obstacles to transfection in vitro is the presence of serum which exerts its inhibitory effect (Zelphati et al., 1998, Yang and Huang, 1997). Thus, within this study, the IVP experiment in absence of serum was performed, showing greater expression potency in FCS-free conditions despite the kind of delivery system employed. These additional data partially supported what was previously discussed, as there was no strong correlation between particle internalisation and antigen expression in complete media. It is well documented in literature that cationic lipoplexes and polyplexes accumulated in cells by endocytosis (Yotsumoto et al., 2008). However, it has been observed that micropinocytosis might be an alternative mechanism for LNP-siRNA uptake (Love et al., 2010). Despite the endocytic pathway, it has been observed that serum might interfere with these processes by the binding of serum proteins to the complex of cationic lipids and nucleic acid (Simberg et al., 2003). This association facilitates LNP-DNA/RNA structural reorganization, aggregation, and dissociation of the complexes. FBS contains several blood proteins, including endonucleases, albumin, lipoproteins, fibrinogen, and heparin. One of the recent observations made by researchers suggested that lipids of lipid particles interact and fuse with serum protein, destabilizing the lipoplex or polyplex complex (Vitiello et al., 1998). Thus, a release of some nucleic acid molecules might happen with a consequent loss in transfection efficiency. Furthermore, serum proteins, by binding to lipid membranes, can induce an increase in particles size and a consequent reduction in the zeta potential (Marchini et al., 2009). This effect contributes to make the interaction between lipoplexes and cell membrane weaker. These observations were in agreement with what has been shown in the results reported here. For all the formulations tested, the presence of FBS in the growing media interfered with transfection and reduced the ability of formulations to efficiently transport SAM inside cells for a complete antigen transcription. However, an opposite effect was seen when LNPs were

159

used for SAM delivery. In this case FBS seemed to be required for a good transfection. The cause of this phenomenon might be attributed to the presence of apolipoprotein E (ApoE) in serum. High potency of DLin-KC2-DMA LNP (an analogue of lipid X employed here) for gene silencing in hepatocytes has been attributed to association with ApoE, which led to uptake through the scavenging receptors (Wolfrum et al., 2007, Sahay et al., 2010). Another possibility is that serum may likely induce switch from clathrin-dependent to caveolae-mediated internalization (Farhood et al., 1995).

Moreover, the greater ability of either DOTAP or DDA liposomes to induce antigen expression might be helped by the presence of the fusogenic helper lipid DOPE in the liposomes formulation utilised. DOPE has a relatively small head-group, phosphoethanolamine, and two bulky and unsaturated oleyl chains, creating a cone-like shape. This lipid geometry can stabilize the non-bilayer hexagonal (H_{II}) phase, which is found in transitional structures during membrane fusion and/or bilayer disruption (Hattori et al., 2005). Hence, previous studies on transfection efficiency have shown that DOPE aided transfection in mixtures of DOTAP, (Hui et al., 1996) suggesting that inverted hexagonal lipoplexes transfect more efficiently than lamellar lipoplexes. In addition, cationic lipids cause the swelling and rupture of the lysosomes by sequestering protons and their counterions (the "proton sponge effect") and create an osmotic imbalance similar to that created by lysosomotropic compounds (Boussif et al., 1995).

Moreover, the potency of polymeric NPs to transfect fibroblasts might also be attributed to the presence of the biodegradable polymer PLGA in the formulation. This block co-polymer was widely employed in gene therapy, especially for DNA or siRNA delivery. The potential advantage of biodegradable carriers compared with their non-degradable counterparts is their reduced toxicity and the prevention of the polymer accumulation in the cells after repeated administration (Luten et al., 2008). Furthermore, the degradation of the polymer can be used as a tool to release the nucleic acids into the cytosol (Luten et al., 2008). For example, it has been seen that the siRNA delivery and resultant silencing efficiency of PLGA NPs were better than those of commercialized gene transfection agent (Heo and Lim, 2014). Furthermore, recent studies have shown that antigen-loaded PLGA particle enhances and prolongs antigen cross-presentation in DCs that induce cytotoxic T cell responses (Johansen et al., 2000, Lee et al., 2011b). The mechanism of the enhanced therapeutic effect given by PLGA has been recently elucidated. Panyam and co-workers (Panyam et al., 2002) found that surface cationization of PLGA based NPs could be related to NP behaviour (Mukherjee et al., 1997) in the endocytic vesicles. The early endocytic vesicles have a physiological pH (Mukherjee et al., 1997), at which PLGA would be negatively charged and hence would be repelled by the negatively charged endosomal membrane. However, the secondary endosomes and lysosomes

are predominantly acidic (pH between 4 and 5) (Mukherjee et al., 1997), therefore, NPs would be cationic hence interacting with the negatively charged membrane, leading to their escape into the cytoplasmic compartment. The mechanism of escape proposed within the cited paper was not related to the opening of the endo-lysosomal vesicles, but it was attributed to localized destabilization of the endo-lysosomal membrane at the point of contact with PLGA NP, followed by extrusion of the NP through the membrane. Furthermore, at acidic pH the hydrolysis of PLGA is accelerated therefore leading to a fast release of the encapsulated bioactive molecule and a consequent higher accumulation in the cytosol. A sustained release mechanism is crucial for non-replicative drugs i.e. DNA or RNA based compounds in order to enhance antigen production. However, a slow release of SAM might not be necessary due to its intrinsic self-replicating properties. Moreover, to enhance endosomal escape, the addition of cationic materials such as chitosan or cationic lipid to PLGA NPs formulation might be beneficial (Stigliano et al., 2013). This mechanism of action is an important advantage in the use of PLGA NPs as cytoplasmic delivery vehicles. Besides, phagocytosis and pinocytosis (including clathrin-mediated endocytosis, caveolae-mediated endocytosis and macropinocytosis) are the two main endocytic pathways used for NP uptake (Khalil et al., 2006). These different pathways differ in the composition of the coat, the size of the vesicles and the fate of the internalized molecule (Khalil et al., 2006). Generally, caveolae-vesicles induce the intracellular migration of materials with a size of 50–80 nm. NPs with a similar size as viral pathogens are efficiently recognised and taken up by APCs for the induction of the immune response (Xiang et al., 2006). NPs with a size between 20 and 200 nm are preferentially taken up by DCs, through the pinocytosis mechanism, while macrophages uptake larger NPs, from 0.5 to 5 μm, through macropinocytosis and phagocytosis (Xiang et al., 2006). However, despite differences in the endocytic pathway, all particles could deliver both SAM-GFP and SAM-Rabies to BHK cells and induced antigen transfection. However, according to data reported here, SAM-Rabies encapsulating DOTAP NPs, SAM-Rabies encapsulating DOTAP and DDA liposomes resulted in greater antigen expression. Thus, these formulations will be the candidates to test for *in vivo* immune response.

4.5 Conclusions

Within this chapter, four different cationic delivery systems were evaluated according to their ability to efficiently trigger antigen expression *in vitro* in different cell lines. The results suggested that particles can be simply and effectively sterilised using γ-irradiation. Moreover, it was shown that toxicity in both MBDM, MBDDCs and BHK was cationic lipid dose dependent. In terms of uptake in BMDM, while SAM-DOTAP formulations were taken up by cells in a comparable manner, DDA particles showed a greater difference among them, with SAM encapsulating liposomes and SAM adsorbing emulsions having much higher uptake. In BHK cells, even though no significant difference in particles uptake has been shown by

expressing data as percentage of DilC+ cells, discrepancies among formulations in uptake efficiency were indeed evident by analysing mean fluorescence intensity values (MFI), with DOTAP SLNs and NPs having significantly higher MFI values compared to the other formulations; however, despite this, absolute values were inferior compared to 5% FCS condition. In FCS-free media, NPs resulted in the highest MFI, which directly translated in more polymeric particles uptake by BHK. Moreover, it was shown that moving from DOTAP to DDA reduced the overall MFI of formulations. However, despite the promising results on cellular internalisation, antigen expression in BMDM was not achieved. On the other hand, *in vitro* potency (IVP) assays in BHK cell line with both SAM-GFP and SAM-Rabies based formulations showed that DOTAP polymeric nanoparticles and both DDA and DOTAP liposomes had the greater ability to induce antigen expression in BHK cells, despite the choice of the antigen and the presence of serum. Thus, these formulations were selected to progress *in vivo* to better understand their immunogenicity in a mouse model.

CHAPTER 5

Pharmacokinetics and Immunogenicity studies in a mouse model
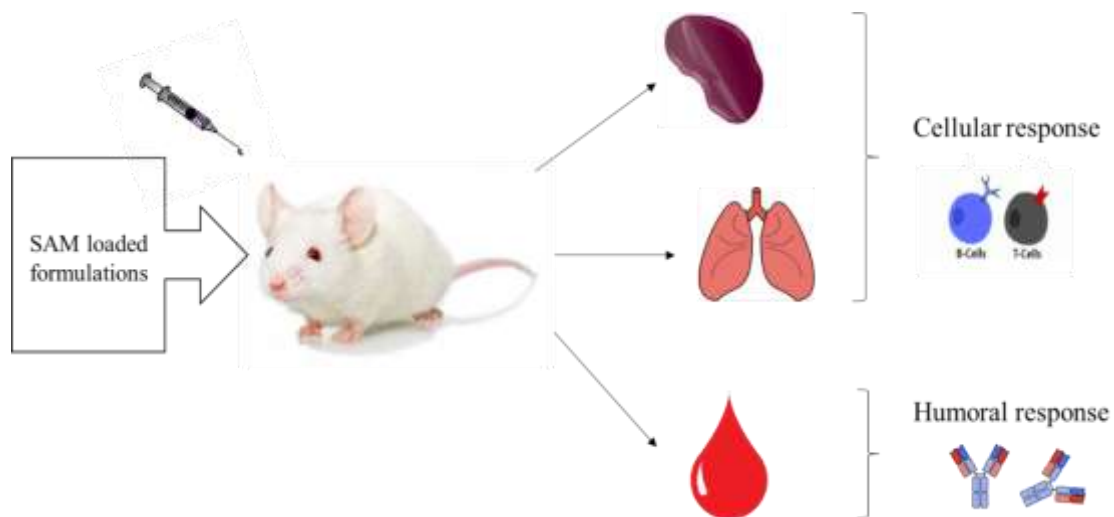
5.1 Introduction

The rabies virus is an enveloped, single stranded, negative-sense RNA virus of the Lyssavirus genus, with an estimated annual global human mortality of about 24,000 to 90,000 (Knobel et al., 2005). Despite extensive effort in preventing the spread of the virus, rabies is still one of the major causes of death from infectious diseases in humans, especially in developing countries (Evans et al., 2012), with infection being acquired from transcutaneous or mucosal exposure to saliva of a rabid animal. The rabies virus genome encodes for five structural proteins: nucleoprotein (N), phosphoprotein (P), matrix protein (M), glycoprotein (G) and the viral RNA polymerase (L). However, G protein is the only target for neutralizing antibodies, which provide full protection against virus challenge (Ertl, 2009).

Efficacious rabies vaccines for humans are already on the market (Warrell, 2012) and these include three killed virus tissue culture vaccines licensed for use in the developed world: human diploid cell vaccine (Imovax Rabies, licensed in the UK), purified chick embryo cell vaccine (Rabipur/RavAvert licensed in the USA) and a purified vero cell vaccine (Verorab, licensed in Europe). Despite their indisputable efficacy, the production process is very expensive. Besides, rabies vaccines for pre-exposure prophylaxis must be given three times to achieve protective immunity, which can last 3–4 years, while for post-exposure prophylaxis the number of administrations rises until 4–5. Therefore, more cost-effective alternatives which require less frequency of administrations might be really advantageous. Several approaches are in preclinical development. One of the most recent is nucleic acid based vaccines. RNA or DNA encoding the antigen(s) of interest are one of the most advanced platforms for vaccination; in particular, self-amplifying RNA (SAM), where the gene sequences encoding structural proteins in the RNA viruses are replaced by mRNA encoding antigens of interest as well as by RNA polymerase for replication and transcription, has been successfully assayed with many different antigens as vaccines candidates. Moreover, they have been shown to be effective in several animal species, including mice, nonhuman primates, and humans (Geall et al., 2012b). However, due to SAM biological instability and impossibility of directly crossing cell membrane, a safe and effective delivery system is needed. Ideally, the delivery system should interact with target cells and being taken up upon receptor-mediated endocytosis; further it should be able to escape from the endosomal compartment into the cell cytoplasm, where the RNA machinery is located, while avoiding degradation by lysosomal enzymes. Furthermore, delivery systems for systemic administration should be nontoxic and highly immunostimulatory upon administration (Geall et al., 2013).

The use of cationic formulations as experimental adjuvants for subunit peptide or nucleic acid vaccines is well documented. Studies from the past decades on adjuvant mechanisms showed

that the adjuvanticity of such formulations may be due to a combination of various pathways including formation of depot, induction of cytokines and chemokines, recruitment of immune cells, enhancement of antigen uptake and presentation, and promoting antigen transport to draining lymph nodes (Freimark et al., 1998, Henriksen-Lacey et al., 2011b). Over the years, it has become clear that adjuvants activate innate immune responses to create a local immuno-competent environment at the injection site. Depending on the type of innate responses activated, adjuvants can alter the quality and quantity of adaptive immune responses. Understanding the mechanisms of action of adjuvants will provide critical information on how innate immunity influences the development of adaptive immunity, help in rational design of vaccines against various diseases, and can inform on adjuvant safety. Despite a substantial body of literature regarding the suitability of cationic particulates as vaccine immunomodulators or delivery systems, contradictory statements are reported with respect to the adjuvanticity of these formulations and a consensus on their precise mechanism of action and their effect on the immune system is still lacking (Carmonaribeiro, 2000, Freimark et al., 1998). The logic for cationic particulates as vaccines carriers is based on the assumption that these systems are able to deliver the antigen to antigen-presenting cells (APCs) and thus enhance antigen-specific immune responses (Cox and Coulter, 1997, Banchereau and Steinman, 1998). Herein this context, dendritic cells (DCs) are important for their ability to efficiently induce primary immune responses and to elicit immunological memory. Moreover, many papers support the hypothesis that the increased permanency of carriers at the injection site - depot effect – may help to prolong the antigen retention at the inoculation site thereby increasing the time of vaccine exposure to the immune cells (Henriksen-Lacey et al., 2010a). The depot effect has been attributed to electrostatic forces between the net negatively charged serum proteins and local cells and the positively charged formulation thereby leading to carrier aggregation and precipitation at the injection site with consequent antigen retention (Henriksen-Lacey et al., 2010a). However, the need for a depot effect to increase immunogenicity remains controversial, as it has been seen that it is not always correlated with increased adjuvanticity (Hutchison et al., 2012). Within the present chapter, the pharmacokinetics *in vivo* of either DOTAP or DDA based polymeric nanoparticles (NPs), solid lipid nanoparticles (SLNs) and cationic nanoemulsions (CNE) encapsulating SAM vaccine were compared. In this study, self-amplifying RNA vaccine encoding for a green fluorescent protein (GFP) – SAM-GFP – was used as model antigen. The aim was to understand the biodistribution of different cationic delivery systems in an animal model and evaluate any retention in the injection site as well as any accumulation and toxicity in the other organs. To follow the movement of formulations *in vivo*, a radiolabeling technique was used.

Moreover, biodistibution studies were correlated with immunogenicity. Although there has been an important development of non-viral delivery systems for RNAi (Kanasty et al., 2013),

the experience with mRNA or self-amplifying RNA is very poor. Self-amplifying RNA vaccines have been delivered mainly as naked RNA or with specific non-viral vectors (lipid nanoparticles (Geall et al., 2012b) or cationic nanoemulsions (Ott et al., 2002)), following intramuscular injection. The practical utility of viral vectors, however, is limited by manufacturing considerations, cost-effectiveness, and potential adverse health effects. Moreover, very limited data have been published on non-viral delivery of RNA replicons, although it is a highly attractive approach. Furthermore, it has been shown that induction of antigen-specific immunity can be achieved by administering RNA vaccines through several routes, i.e. intravenous, intradermal, subcutaneous, intranodal, and intrasplenic (Ulmer et al., 2012). Additionally, mRNA has also been used via intradermal application to induce its uptake by Langerhans cells and dermal dendritic cells for further transport to the lymph node. However, any data about the immunogenicity of these SAM based delivery systems after intranasal administration has not yet been reported.

5.1.2 Aim and objectives
Within this chapter it has been attempted to:

- Understand the pharmacokinetic profile of different cationic formulations; the biodistribution in a mouse model was performed and different particles attributes – presence of SAM and cationic lipid composition- were evaluated and compared.

- Find the correct antigen dose to induce high antibodies and cellular responses *in vivo* and to compare the adjuvant properties of selected cationic candidates after i.m. injection. For this purpose, DOTAP NPs, DOTAP liposomes and DDA liposomes were selected as potential candidates. Either 1.5 µg or 0.15 µg/dose SAM encoding for rabies glycoprotein (SAM-Rabies) was encapsulated within the three delivery systems and used as vaccine of interest. The commercial vaccine Rabipur, which is an inactivated virus rabies vaccine, was used as comparison, while GSK CNE and gold standard LNPs were used as positive controls.

- Evaluate if changing the route of administration might affect carriers' potency; SAM encapsulating candidates were administered intradermally and intranasally, and formulations immunogenicity was evaluated according to IgG titres and cellular response. To do so, DOTAP NPs and DOTAP SLNs were selected.

- Evaluate if any correlation between biodistribution and immunogenicity might exist

5.2 Materials and Methods
5.2.1 Materials
Poly (D, L-lactide-co-glycolide) lactide: glycolide (50:50), mol wt 30,000-60,000, Dimethyl Sulfoxide, Tristearin (Grade II-S, ≥90%) Cholesterol and squalene were obtained from Sigma-Aldrich Company ltd. Dipalmitoylphosphatidylcholine (DSPC), 1,2-dimyristoyl-rac-glycero-

3-methoxypolyethylene glycol-2000 (DMG-PEG2000), Dimethyldioctadecylammonium (DDA) and 1,2-dioleoyl-3-trimethylammonium-propane (DOTAP) were obtained from Avanti Polar Lipids. alamarBlue was obtained from Bio-Rad Laboratories, Inc. Ethanol, methanol, 1,1'-Dioctadecyl-3,3,3',3'-Tetramethylindocarbocyanine Perchlorate (DilC), LIVE/DEAD™ Fixable Aqua Dead Cell Stain, Lipofectamin2000), Gibco phosphate buffer saline (PBS), RPMI 1640 Medium, Tween 20 and Span 80 were obtained from Fisher Scientific UK. Dulbecco's Modified Eagle Medium (DMEM) and foetal bovine serum (FBS) were obtained from Gibco. APC-labelled anti-CD11c, FITC-labeled anti-F4/80 antibodies and anti-Fc antibody (Fc block) were obtained by BD Biosciences UK. Penicillin-streptomycin, L-glutamine, cholesterol (Chol) and pontamine blue were purchased from Sigma. TRIS Ultra-Pure was obtained from ICN Biomedicals. Cytofix-cytoperm solution was obtained from BD Biosciences. Tertiary cationic lipid X was provided by Discovery, Drug Product Development department Rockville, USA

5.2.2 *In vivo* biodistribution of adjuvants and their associated antigen

5.2.2.1 Preliminary studies: preparation of cationic formulations in presence of cholesterol

Cholesterol-DOTAP based SLNs, NPs and liposomes were produced with Nanoassemblr (TFR 10 mL/min and FFR 1:1), while CNE was produced using microfluidisation method (refer to chapter 3 for formulations details). Each lipid stock contained final [DOTAP] of 1 mg/mL and 500 ng/mL of cholesterol. Samples were dialysed against TRIS buffer 10 mM pH 7.4 in order to remove organic solvent.

5.2.2.2 Preliminary studies: release study of ^{3}H-Cholesterol from formulations

In order to prove that ^{3}H-Cholesterol (^{3}H-Chol) was retained in formulations lipid layer during time, a release study with ^{3}H-Chol labelled formulations was performed. DOTAP based SLNs, NPs and liposomes were produced with Nanoassemblr (TFR 10 mL/min and FFR 1:1), while CNE was produced using microfluidisation method (see chapter 3 for formulations details). Each lipid stock contained [DOTAP] of 2 mg/mL and 500 ng/mL of ^{3}H-Chol. Samples were dialysed against TRIS buffer 10 mM pH 7.4 at 37°C, and 1 mL aliquots were taken from the outer buffer after 30 min, 1, 2, 4, 6, 24, 48, 72, 96,1 20, 144 and 168 hours. The outer volume in the beaker was maintained constant replacing the withdrawn aliquot with an equal volume of buffer. The amount of released tritium over time has been quantified using liquid scintillation counter (PerkinElmer Tri-Carb 2810TR).

5.2.2.3 Preliminary studies: effect of Foetal Bovine Serum (FBS) on particles size

A stability study which mimics a biological environment in vitro has been carry out in order to understand if cationic formulations were stable once injected in mice. To achieve that, SLNs, NPs, CNE and liposomes were mixed with a solution of Foetal Bovine Serum (FBS): Phosphate-buffered saline (PBS) 50:50 vol/vol, then placed in a 15 mL falcon tube at 37°C.

A 200 µL aliquot was taken from each sample after 0, 1, 2, 4, 24 and 48 hours and the volume was replaced with the same amount of FBS:PBS solution. Formulations were characterised in terms of size, PDI and Z-potential after each time-point using Zetasizer Nano ZS.

5.2.2.4 *In vivo* study: tracking the movement of radiolabelled formulations in a mouse model

The *in vivo* biodistribution study procedures strictly adhered to the 1986 Scientific Procedures Act (UK – project licence number PPL3003289/ personal licence number IC2992F8F). All protocols have been subject to ethical review and were carried out in a designated establishment. Groups of four female 6–8-week-old BALB/c mice (20-25g) were housed appropriately and given a standard mouse diet ad-libitum. In order to track their movement, adjuvants were formulated with ^{3}H-Chol. In brief, ^{3}H-Chol was incorporated to either DOTAP or DDA based SLNs, NPs or CNE lipid mixture and co-formulated with the appropriate buffer described in chapter 3; when specified, formulations were prepared in the presence of 1.5 µg/dose of SAM encoding for a green fluorescence protein (GFP) added to the aqueous phase. Particles were formulated by either microfluidics or microfluidizer and dialyzed against 10 mM TRIS pH 7.4 (refer to chapter 3 for details). Finally, trehalose was added to a final concentration of 10% w/v to maintain isotonicity upon injection. Each dose (50 µL) contained 25 µg of cationic lipid (either DOTAP or DDA) and 25 ng of ^{3}H-Chol (200 KBq/dose). The concentration of cholesterol was low enough not to change the size of the formulations. 3 – 4 days before injection, mice were injected with 200 µL of Chicago Blue (0.5 % w/v) subcutaneously (s.c.) into the neck scruff as a marker for lymph nodes. Formulations were injected intramuscularly (i.m.) in the right quadriceps muscle. Mice were terminated at relevant time points (6, 24 and 48 hours or 6, 24, 48, 72 and 96 hours) post injection (p.i) and tissue from the site of injection (SOI) and draining lymph nodes (popliteal lymph node – PLN, inguinal lymph node – ILN) on the side of the SOI were collected for analysis. Briefly, samples were solubilized completely in 10 M NaOH (2 mL) at 60 °C overnight and subsequently bleached with 30% w/v hydrogen peroxide (200 µL) for 2 h at 60 °C. Then, 10 mL of Ultima Gold Scintillation cocktail were added. Radiation was quantified in a Liquid Scintillation Analyser Tri-Carb 2810 TR (Perkin Elmer). The percentage of injected dose (%ID) was calculated with respect to the original dose as follows:

$$\text{Eq (5.1)} \qquad \% \text{ ID} = \frac{\text{counts (cpm) in organ}}{\text{counts (cpm) in original dose}} \text{ x } 100$$

5.2.3 Evaluation of immune responses *in vivo* of different selected adjuvants and their associated antigen

5.2.3.1 Determination of Rabies-specific serum antibody titres by ELISA

Mouse model was chosen since it is the most widely used model to mimic human immune system. Project licence "AWB 2015 01", CPR/2015/01. All animal studies were ethically reviewed and carried out in accordance with European directive 2010/63/EEC and the GSK policy on the Care welfare and treatment of animals. Animals were placed in cages with an individually ventilated caging system and given a standard mouse diet ad-libitum. Groups of 10 female BALB/c mice aged 6–8 weeks and weighing about 20–25 g were immunized with SAM-Rabies antigen encapsulating DOTAP liposomes, DDA liposomes and DOTAP NPs at days 0 and 28 and the responses were compared to the commercial, inactivated virus rabies vaccine, Rabipur. SAM-Rabies adsorbing CNE and SAM-Rabies encapsulating gold standard LNPs were used as positive controls. The mice received 1.5 and 0.15 µg of SAM-Rabies in 50 µl of the formulation in the left quadriceps. Similarly, 1/20 of Rabipur clinical dose was administered via intramuscular (i.m.) injection to control groups. Serum samples were collected on days 0, 14, 27, and 43 after the first vaccination. Rabies G-specific IgG titres were determined by ELISA using a commercially available kit (PLATELIA™ RABIES II). The assay was performed following manufacturer's instructions. Reagents were stored at 2–8 ∘C and placed at room temperature for at least 30 min before use. Briefly, each sample was pre-diluted 1:100 in sample buffer and 100 µL is incubated in a microplate well sensitised with the rabies virus glycoprotein for 60±5 min at 37±1 ∘C. A negative (R3) and two positive controls (R4a and b) were tested in each run. The positive controls are calibrated against the WHO international standard for rabies immunoglobulin. R4b (4 equivalent units (EU)/mL) is used to establish a reference curve after successive two-fold serial dilutions (S5 = 2 EU/mL, S4 = 1 EU/mL, S3 = 0.5 EU/mL, S2 = 0.25 EU/mL, S1 = 0.125 EU/mL). After three washing cycles with 1× washing solution by the use of a microplate washer (type PW41 or PW40, Bio-Rad), horseradish peroxidase-conjugated protein A (10× concentrated, to be diluted in 1× washing solution prior to use) was incubated 1 h±5 min at 37±2 ∘C in a microplate incubator (type IPS, Bio-Rad). Following five washes, the linked peroxidase conjugate was visualized with 3,3',5,5'-tetramethylbenzidine incubated for 30±5 min at room temperature. The enzyme reaction is stopped by addition of 1N sulphuric acid solution. Absorbance was measured at 450–620 nm with the use of a microplate reader (type PR3100, Bio-Rad) with specific rabies program. The dose–OD response curve allows the determination of the titre of each serum. Sera titres were expressed in equivalent unit per ml (EU/mL).

5.2.3.2 Intracellular cytokine staining (ICS) in speenocytes

Spleens from immunized mice were removed at day 43 after the first vaccination. To assess T-cell responses, single-cell suspensions were prepared from spleens and 15×10^6 cells/mL were plated with anti-CD28 mAb at a final concentration of 2 µg/mL and anti-CD107a FITC

(5 µg/mL). As positive control, cells were also pre-incubated for 2 hours at 37°C with anti-CD3 mAb (1 µg/mL). Moreover, as *ex vivo* restimulation, cells were stimulated for 4 hours with Rabies G1-G2-G3 peptide pool at 10 µg/mL. Brefeldin A (5 µg/mL) was added to each condition for the last 4 hours. For flow cytometry analyses, cells were then stained with Live/Dead Near InfraRed, fixed and permeabilized with Cytofix/Cytoperm, and then incubated with anti-CD16/CD32 Fc block. T cells were further stained with anti-CD3-APC, anti–CD4 BV510, anti–IFN-γ Brilliant Violet 785, anti–IL-2 PE-Cy5.5, anti–TNF Brilliant Violet 605, and anti–CD44 V450, anti-IL17 PE and anti-CD8 PE. Samples were acquired on a LRSII special order and analysed using FlowJo software version 9.7.4. Frequencies of antigen-specific T cells were calculated after subtracting the background measured in the corresponding negative control for each cytokine.

5.2.4 *In vivo* comparison of different routes of administrations for SAM formulations

5.2.4.1 Determination of Rabies-specific serum antibody titres by ELISA

Mouse model was chosen since it is the most widely used model to mimic human immune system. Project licence "AWB 2015 01", CPR/2015/01. All animal studies were ethically reviewed and carried out in accordance with European directive 2010/63/EEC and the GSK policy on the Care welfare and treatment of animals. Animals were placed in cages with an individually ventilated caging system and given a standard mouse diet ad-libitum.

Groups of 10 female BALB/c mice aged 6–8weeks and weighing about 20–25 g were immunized with SAM-Rabies antigen encapsulating DOTAP SLNs and DOTAP NPs at days 0 and 28. The commercial, inactivated virus rabies vaccine, Rabipur was used as comparator, while SAM-Rabies encapsulating gold standard LNPs was used as positive control. Mice received 0.15 µg of SAM-Rabies in 50 µL of the formulation via i.m. injection or 0.15 µg of SAM-Rabies in 20 µL via intradermal (i.d.) or 1.5µg of SAM-Rabies in 50 µL of the formulation intranasally (i.n). Similarly, 1/20 of Rabipur clinical dose (CD) was administered intramuscularly and intranasally, while 1/50 CD was administered intradermally. Serum samples were collected on days 0, 14, 27, 43 and 99 after the first vaccination. Rabies G-specific IgG titres were determined by ELISA using a commercially available kit (PLATELIA RABIES II). The assay was performed following manufacturer's instructions (refer to section 5.2.3.1).
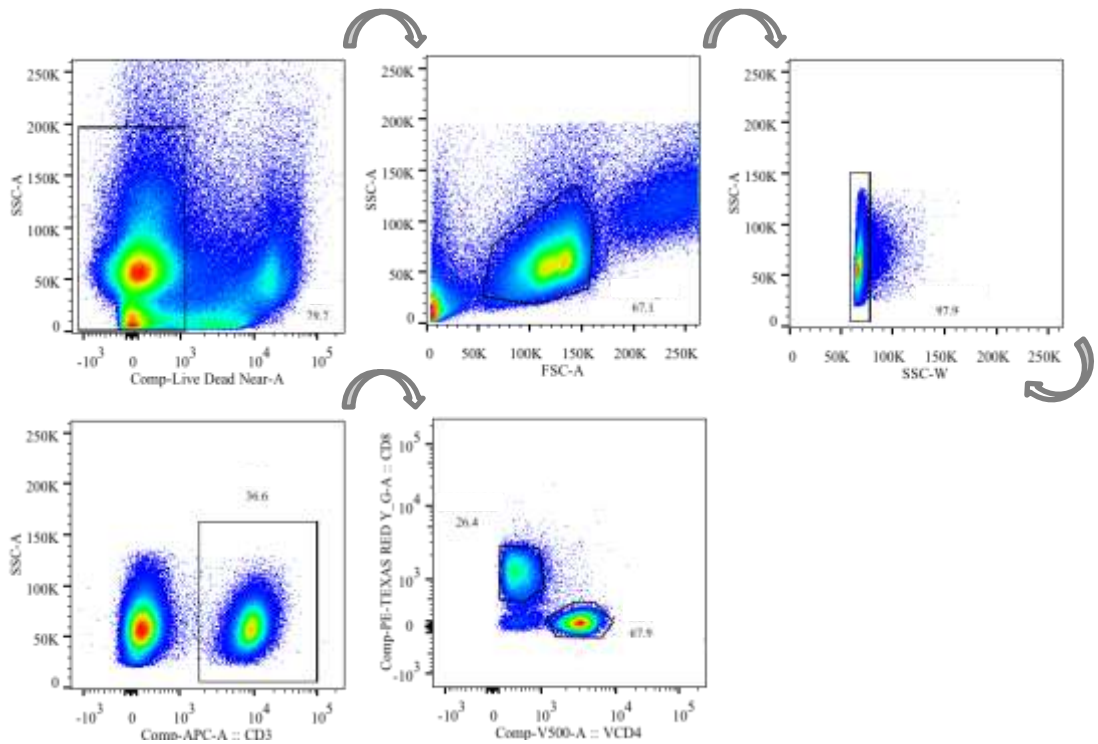
On CD4+
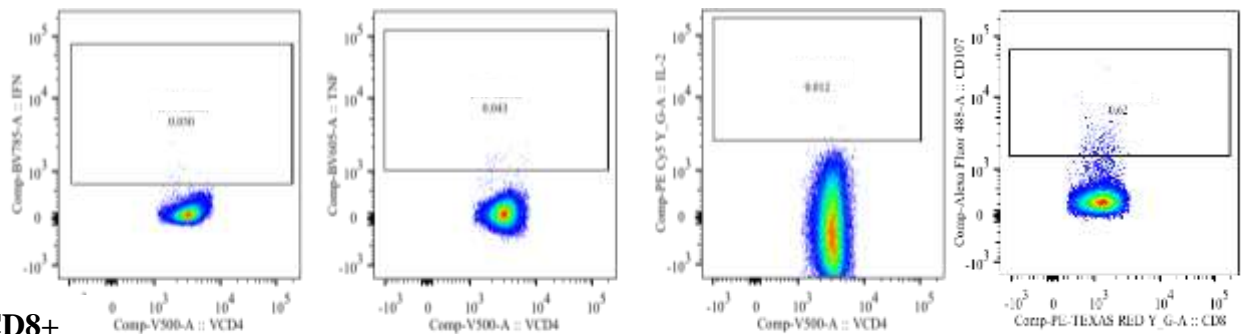
On CD8+
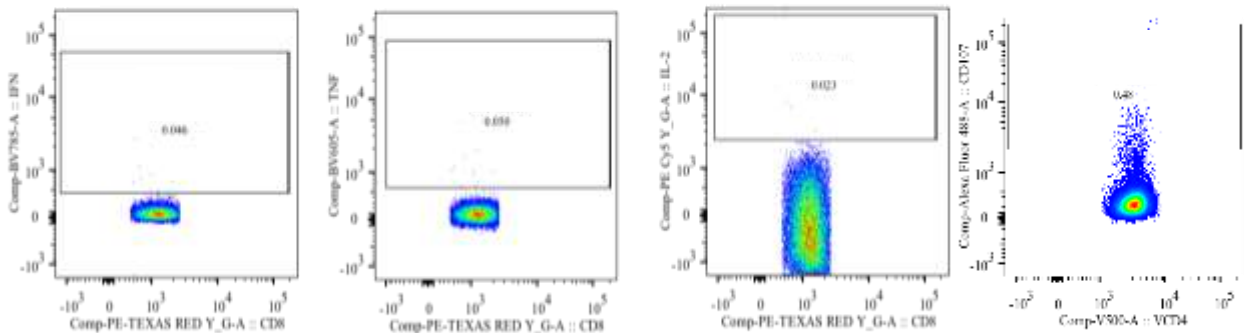
Figure 5. 1 Gating strategy and representative dot plots to evaluate the immune response elicited by different selected adjuvants and their associated antigen after i.m. injection *in vivo*. Splenocytes were negatively selected based on dye exclusion, and lymphocytes were further identified based on morphology. CD3+ T cells were selected after discrimination of singlets and CD4+ and CD8+ T cells were identified based on CD4 and CD8 expression, respectively. Figure shows representative dot plots of cytokine+ (IFN-γ, IL-2, TNFα and CD107a) cells identified among the CD4+ or CD8+ subset.

On CD4+

On CD8+
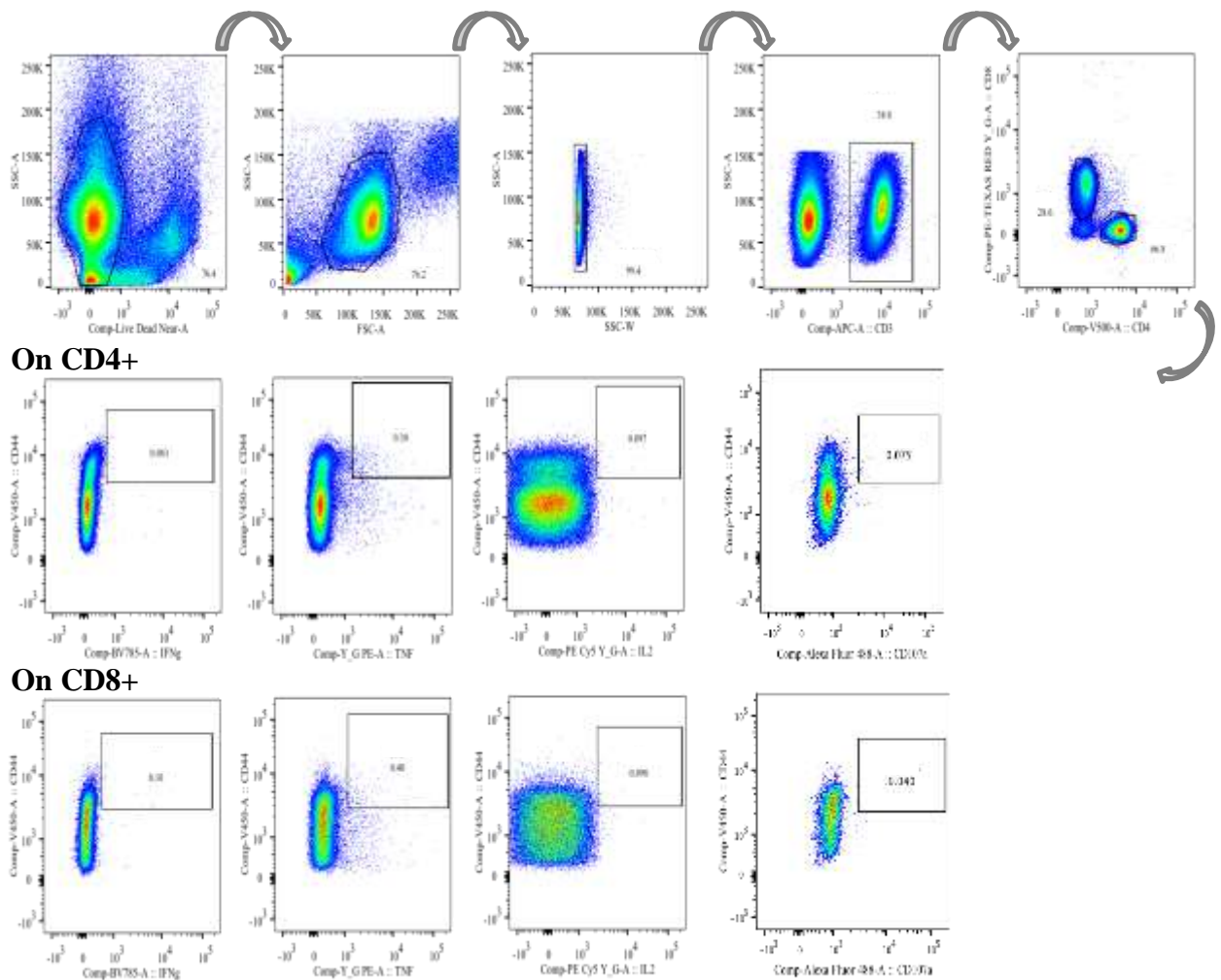
Figure 5. 2 Gating strategy and representative dot plots to evaluate the immune response elicited by different selected adjuvants and their associated antigen after either i.m., i.d. or i.n. injection *in vivo*. Live cells were negatively selected based on dye exclusion, and lymphocytes were further identified based on morphology. CD3+ T cells were selected after discrimination of singlets and CD4+ and CD8+ T cells were identified based on CD4 and CD8 expression, respectively. Figure shows representative dot plots of cytokine+ (IFN-γ, IL-2, TNFα and CD107a) cells identified among the CD4+ or CD8+ CD44high T cell subsets.

5.2.4.2 Intracellular cytokine staining (ICS) in spenocytes

Spleens from immunized mice were removed at day 43 after the first vaccination. Analysis of the antigen-specific T-cell response was performed following the protocol described in section 5.2.3.2.

5.2.4.3 Lung processing and characterization of T cells

Lungs were collected from intranasally immunized mice at day 43 after the first vaccination. Lung tissue was completely dissociated with Gentlemax Dissociator (Milteny Biotec). Briefly, lung tissue was digested in Hank's Balanced Salt Solution containing calcium and magnesium in presence of collagenase D (2 mg/ml) and DNAse I (80 units/ml) for 30 min at 37°C, and then homogenized until obtaining a single-cell suspension. Then, $2x10^6$ cells were seeded into

96-well U-bottom plates stained with Live/Dead Near InfraRed, fixed and permeabilized, plated with anti-CD28 mAb (2 μg/mL) and anti-CD107a FITC (5 μg/mL). As positive control, cells were added to wells coated with anti-CD3 mAb (1 μg/mL). Moreover, as ex vivo restimulation, cells were stimulated for 4 hours Rabies G1-G2-G3 peptide pool at 10 μg/mL. Brefeldin A (5 μg/mL) was added to each condition for the last 4 hours. For flow cytometry analysis, cells were incubated with anti-CD16/CD32 Fc block. T cells were further stained with anti-CD62L-APC, anti-CD103-BV711 as markers for cell surface staining. Moreover, anti-CD3-APC, anti-CD4-BV510, anti-CD8 PE, anti–IFN-γ Brilliant Violet 785, anti–IL-2 PE-Cy5.5, anti–TNF PE, and anti–CD44 V421, anti-IL-17 PE were used as intracellular markers. Samples acquisition and analysis were performed as previously described.

5.3 Results

5.3.1 Preliminary tests prior to biodistribution study

5.3.1.1 Physicochemical characterization of cationic formulations containing cholesterol

Since ^{3}H-Chol was selected as antigen tracker in an *in vivo* model, a preliminary study on possible particles physico-chemical property alterations after cholesterol addition was undertaken. For this purpose, the same amount of non-radiolabelled cholesterol/dose was added to each cationic formulation, and particles were characterised in terms of size, PDI and Z-potential. As it shown in Figure 5.3A and B size, PDI and Z-potential of cholesterol-containing formulations were similar to their cholesterol-free counterparts. More precisely, the hydrodynamic size of DOTAP based liposomes, SLNs, NPs and CNE was around 41, 103, 53 and 90 nm respectively, while when cholesterol was added diameters were around 32, 136, 67 and 116 nm respectively. All formulations showed unimodal size distributions with PDI below 0.3. The zeta potential remained highly positive as evidenced by the high Z-potential values (> 20 mV) (Figure 5.3B).

5.3.1.2 Release study of formulations containing ^{3}H-Cholesterol

The ability of ^{3}H-Chol to remain within the formulations, either anchored to the lipid bilayer of the liposomes or to SLN, NPs or CNE lipid matrix, was investigated. To do so, ^{3}H-Chol DOTAP based liposomes, SLNs, NPs and emulsions were dialyzed for 96 h, in such a way that release of ^{3}H-Chol was quantified in the dialysis buffer at different time points. As seen in Figure 5.4, the percentage of ^{3}H-Chol released from the formulations was negligible compared to the total amount (below 2%) hence demonstrating that the majority of ^{3}H-Chol remained within formulations lipid layer.
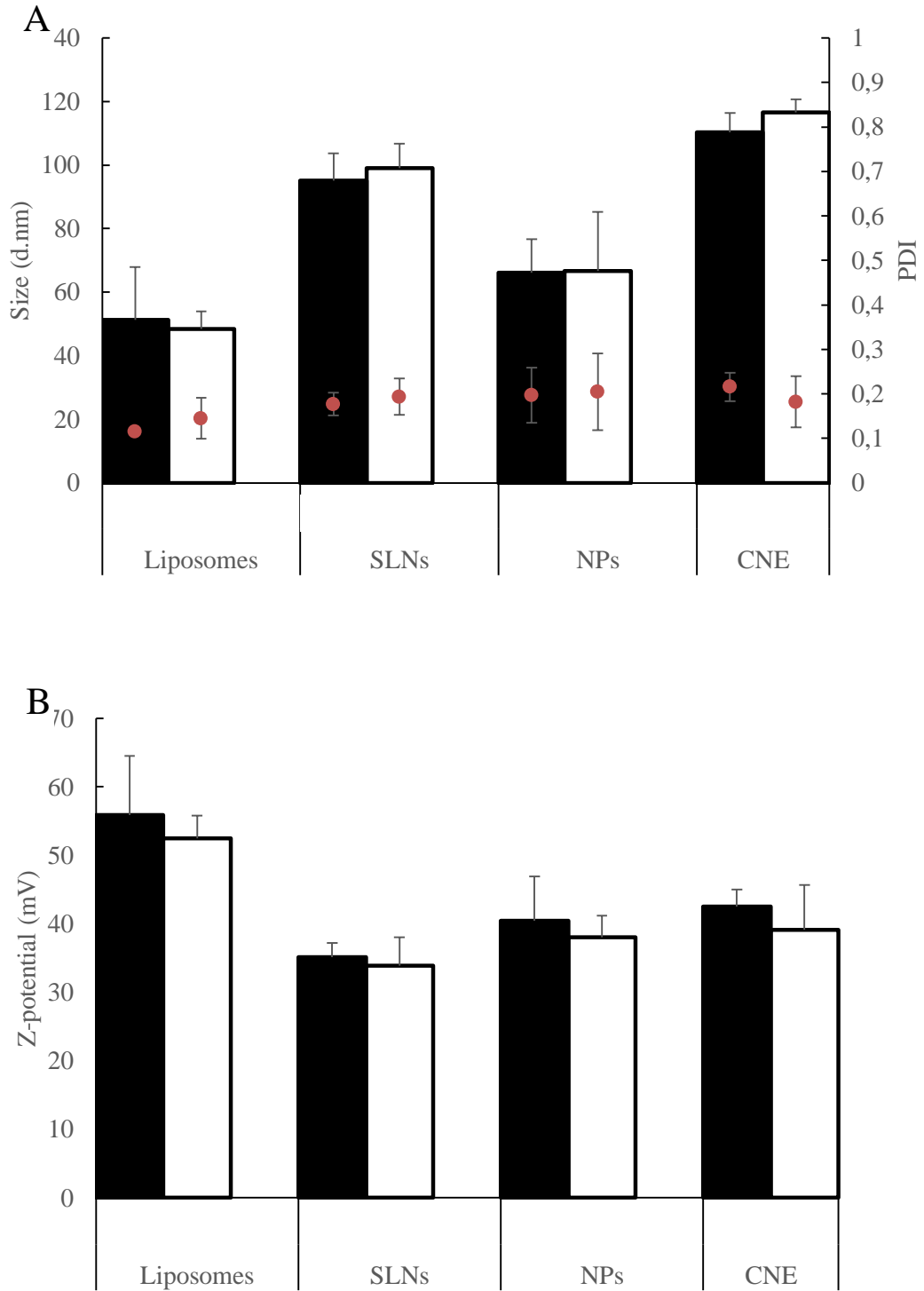
Figure 5. 3 Formulations attributes after cholesterol addition. A) Size (columns), PDI (lines) and B) Zeta potential of DOTAP based Liposomes, SLNs, NP and CNE in the absence (black) or in the presence (white) of cholesterol. Formulations with TFR 10 mL/min and FRR 1:1 had been tested. Results are expressed as the means of three independent experiments ± S.D.
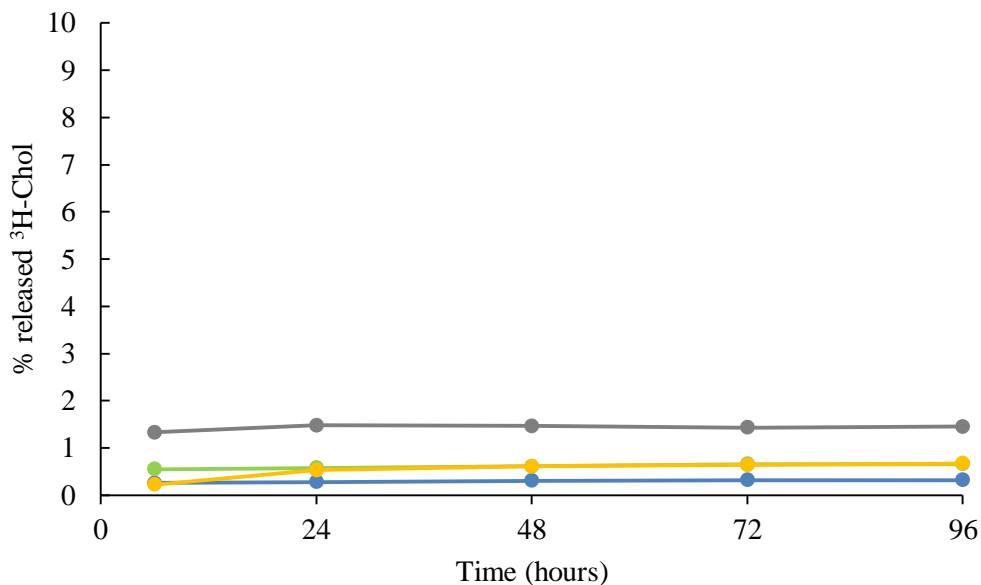
Figure 5. 4 Release study of formulations containing ^{3}H-Chol Release study of ^{3}H-Chol labelling DOTAP based solid lipid nanoparticles (SLNs - blue), polymeric nanoparticles (NPs - green), liposomes (yellow) and cationic nanoemulsions (CNE - grey). N=1.

5.3.1.3 Investigating formulations stability *in vitro* simulating a physiological environment

The stability of DOTAP based liposomes, NPs, SLNs and CNE was studied in 50% FBS, thus simulating an *in vivo* environment (Figure 5.5). Parameters like size, polydispersity index and zeta potential were evaluated at different time points. As shown in Figure 5.5A the hydrodynamic size of DOPE:DOTAP liposomes gradually increased over time from below 40 nm in the absence of FBS to 80 – 100 nm after 6 hours in the presence of FBS. After 3 – 4 days, both size and PDI highly increased. A similar trend was observed when NPs were tested. An immediate visible aggregation of particles occurred upon exposure to 50% FBS. As shown in Figure 5.5 B particles diameter increased over time until reaching the maximum value of above 450nm after 96 hours incubation.

In line with what has been observed so far, the presence of FBS in the outer media altered SLNs diameter in a significant manner along the timeframe tested (Figure 5.5D). More specifically, despite an initial increase in diameter noted after 24 hours incubation (size >460 nm), particles breakage seemed to occur at further time points and a plateau was reached after 2 days (size around 220nm). On the other hand, CNE size and PDI were constant despite the incubation time and the presence of serum in the outer media, thus CNE characteristics seemed to be highly stable during time, with no significant changes in droplet attributes (size approximately around 150 nm, PDI <0.2 - Figure 5.5C). Moreover, the cationic nature of the particles was reduced until neutrality in presence of 50% FBS, despite differences in formulations composition (Figure 5.5).
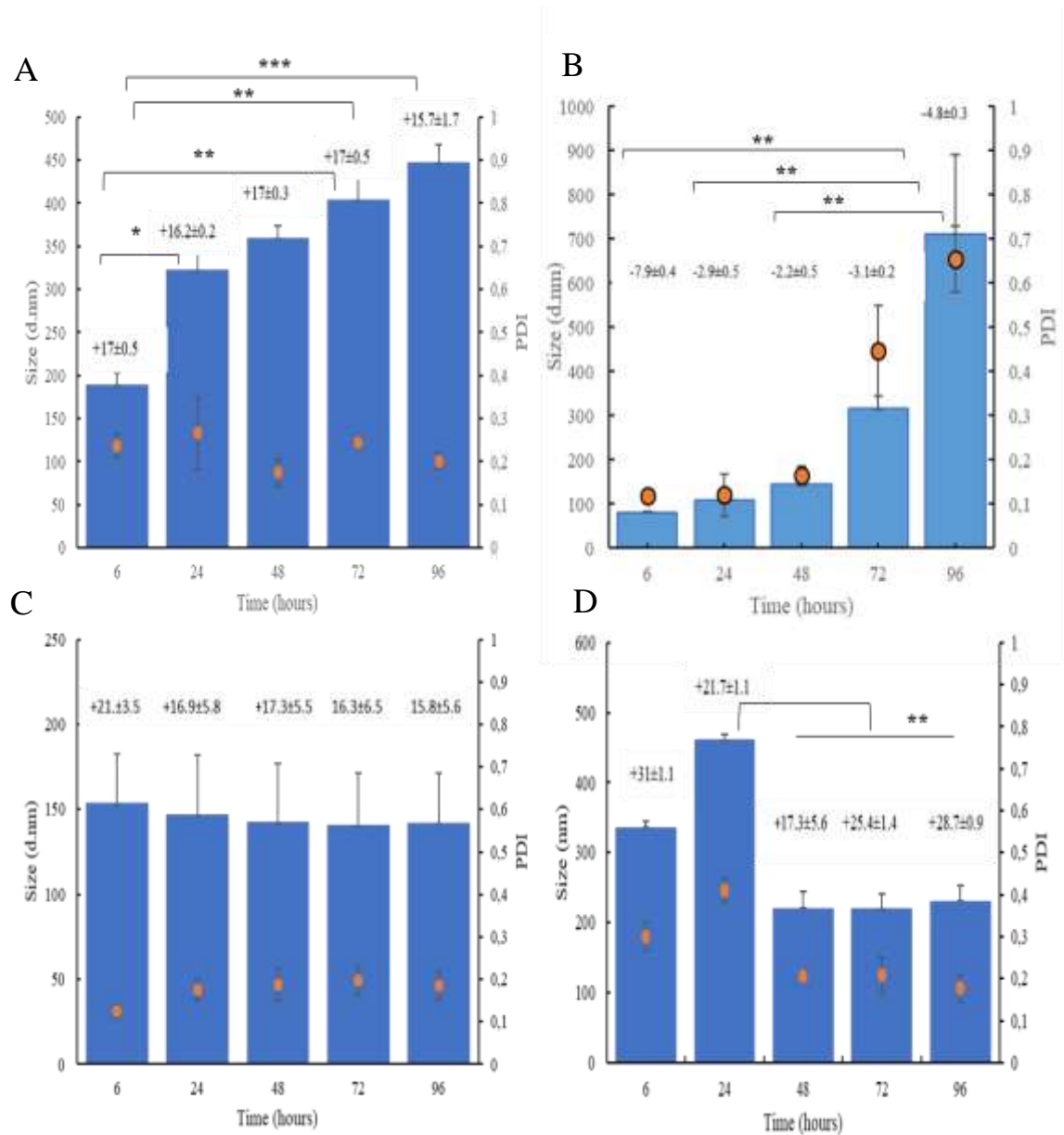
Figure 5. 5 Stability study of cationic formulations in FBS:PBS. Size (bars), PDI (dots) and Z-potential (values) of DOTAP based A) liposomes B) SLNs, C) CNE and D) NPs in presence of 50% FBS. Results are represented as mean ± SD of 3 measurements. Statistical analysis was performed using one-way ANOVA test.

5.3.2 Biodistribution study

5.3.2.1 *In vivo* tracking of empty DOTAP NPs, SLNs and CNE at the site of injection, lymph nodes and organs

The movement of DOTAP based NPs, SLNs and CNE in animal body was investigated using a radiolabelling technique to measure particles at chosen time-points and in specific organs (Figure 5.6 and 5.7). The results in Figure 5.6 show that the concentration of the three cationic candidates remained high at the site of injection (SOI) up to 2 days with a gradual clearance upon injection. However, the percentage of dose at SOI and draining lymph nodes was both size- and formulation composition-dependent. More precisely, with respect to polymeric particles, the injection of cationic NPs led to a deposition of the particles at the injection site (Figure 5.6A) with more than 95% of the original dose remaining 6 hours post injection and approximately 50% remaining at day 2. In contrast, SLNs were removed faster than NPs from the injection site (Figure 5.7A) with only 34% of the initial dose remaining by day 2. Despite that, 96 hours p.i. both NPs and SLNs seemed to be drained in a similar manner with just 18% and 23% of the initial NPs and SLNs dose at the SOI respectively (Figure 5.6A and 5.7A).
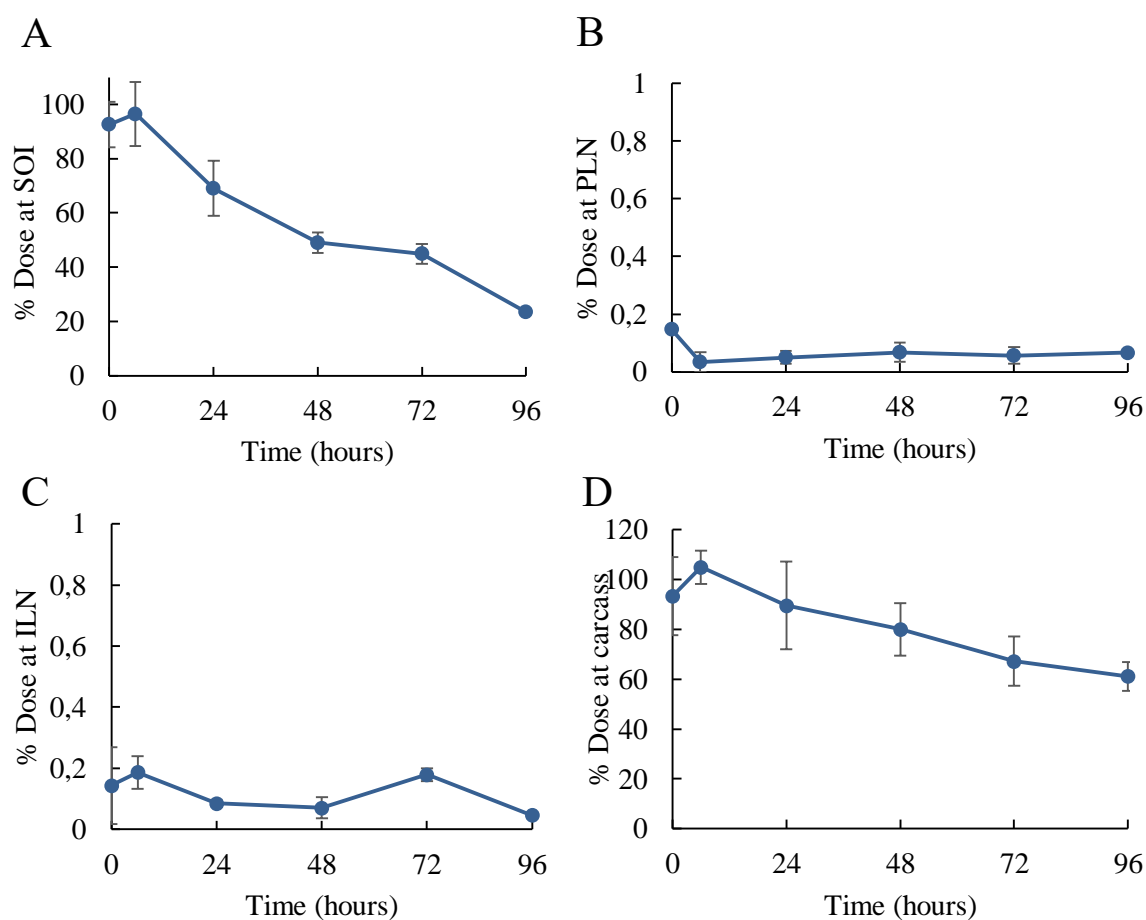
Figure 5. 6 Biodistribution of DOTAP based polymeric nanoparticles (NPs). Percentage of dose determined at A) site of injection (SOI), B) popliteal lymph node (PLN), C) inguinal lymph node (ILN) and D) whole carcass. Results are expressed as the mean ± SD of four animals.
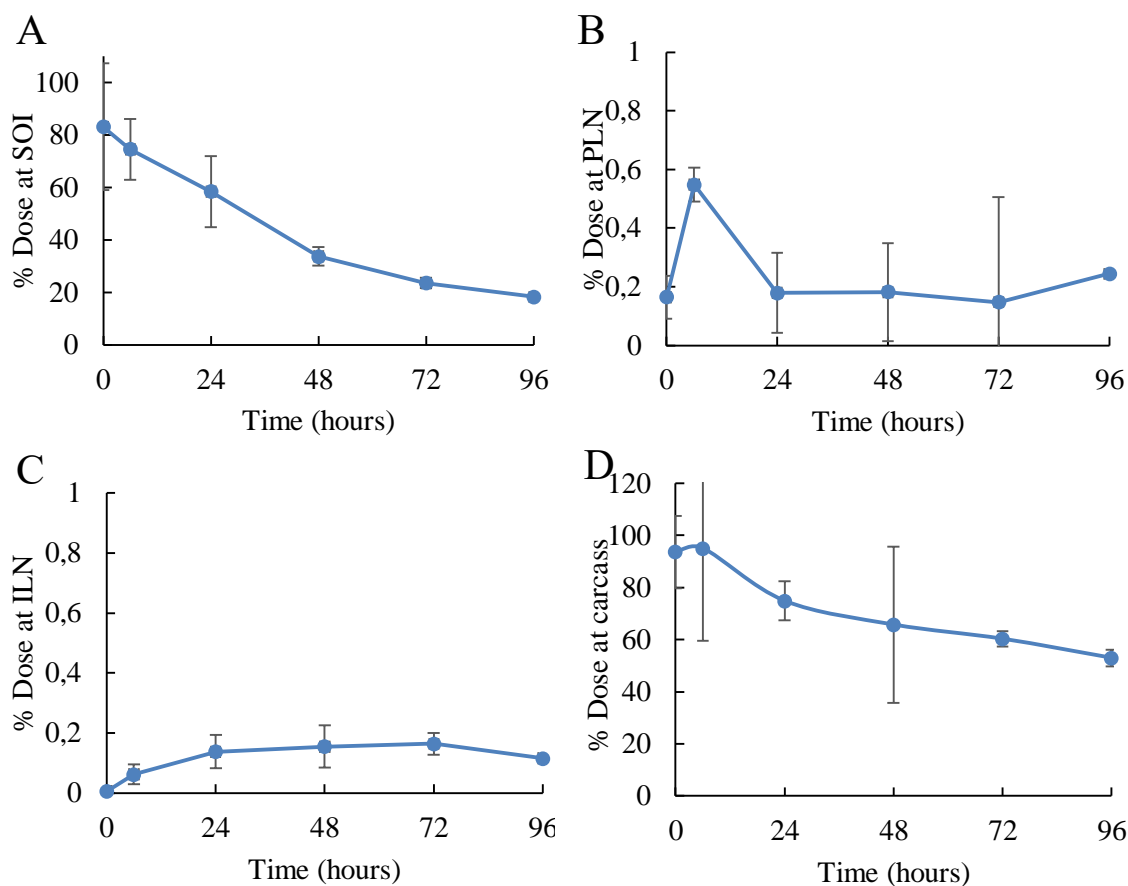
Figure 5. 7 Biodistribution of DOTAP based solid lipid nanoparticles (SLNs).
Percentage of dose determined at A) site of injection (SOI), B) popliteal lymph node (PLN),
C) inguinal lymph node (ILN) and D) whole carcass. Results are expressed as the mean ±
SD of four animals.

The distribution of polymeric and solid lipid and particles to the draining popliteal lymph node
(PLN) is represented in Figures 5.6B and 5.7B respectively. As shown, above 0.5% of the
total injected SLNs dose was measured 6 hours post injection (Figure 5.7B), while a reduction
to around 0.2% at further time points was measured. These values were higher compared to
the ones of polymeric nanoparticles, which were between 0.03 and 0.15% (Figure 5.6B).
However, accumulation of NPs and SLNs in the inguinal lymph node seemed to be
comparable, with values between 0.18% and 0.15% during the timeframe tested (Figure 5.6C
and 5.75C respectively).

Regarding CNE, the draining profile from the injection site was shown in Figure 5.8A;
compared to lipid and polymeric particles, the CNE droplets seemed to be retained longer in
the leg muscle, with more than 65% of the initial injected dose 2 days p.i. Furthermore, the
percentage of dose detected in the popliteal lymph node was comparable with what has been
obtained for SLNs and NPs (Figure 5.8B). Moreover, the presence of CNE at ILN resulted to

be inferior (<0.08%) compared to SLNs and NPs counterparts, especially at latest time points. Besides, the pontamine blue dye was used as a marker for infiltrating monocytes to the injection site (Kaur et al., 2014). Images in Figure 5.9 showed that all formulations induced monocyte infiltration; however, the kinetics and intensity varied. More precisely, SLNs and NPs induced the lowest monocyte influx to the leg muscle with weak blue staining being evident at day 4 p.i. Indeed, CNE induced a brighter blue colour in the injection site even after 6 hours p.i. For all samples tested, mass balance data were between 80% and 100% at early time points confirming the suitability of the method for tracking formulations *in vivo* with high particles recovery even after few days p.i. (Fig 5.6D, 5.7D and 5.8D).
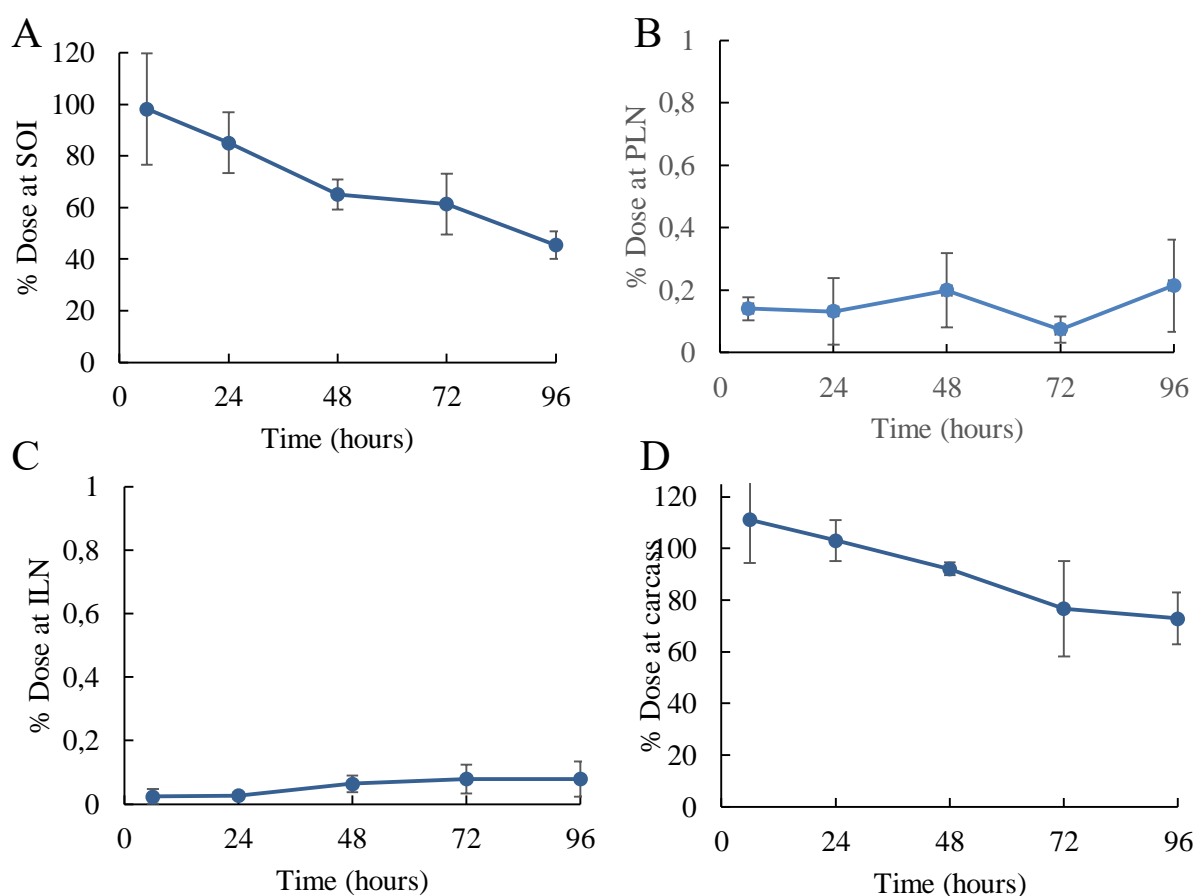
Figure 5. 8 Biodistribution of DOTAP based cationic nanoemulsions (CNE). Percentage of dose determined at A) site of injection (SOI), B) popliteal lymph node (PLN), C) inguinal lymph node (ILN) and D) whole carcass. Results are expressed as the mean ± SD of four animals.
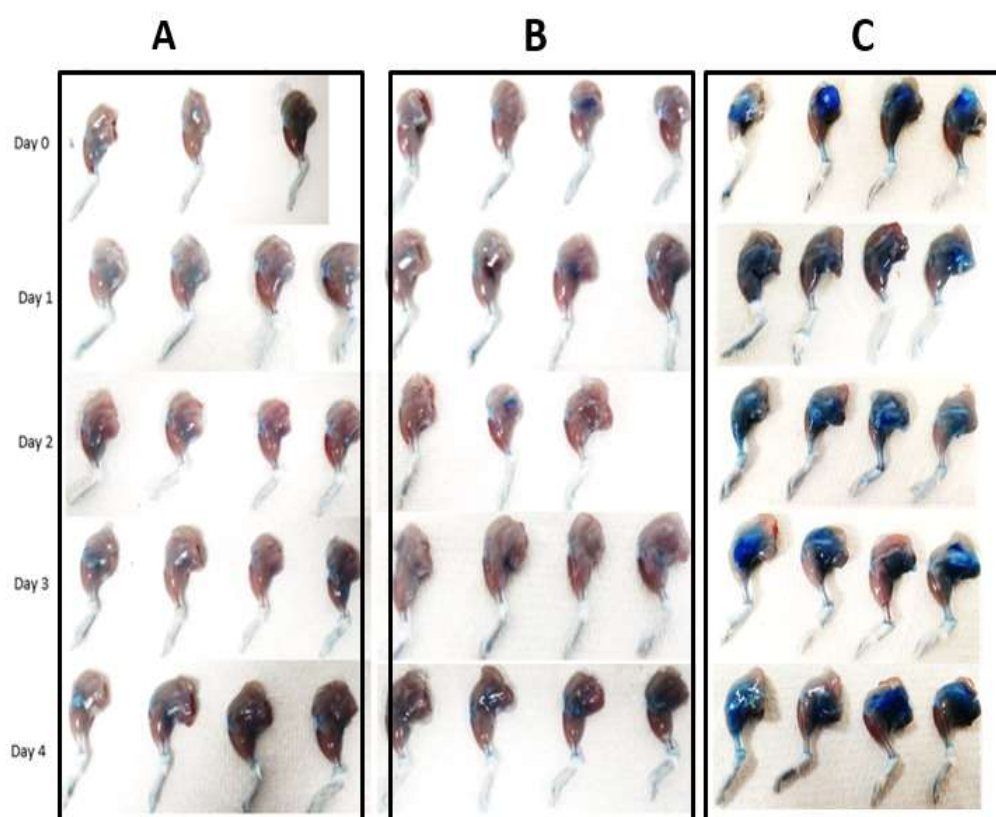
Figure 5. 9 Representative images of the site of injection after I.M. administration of different cationic formulations. Blue staining (pontamine blue) indicates monocyte extravasation at the site of injection due to danger and inflammation signals. Figure showing pontamine blue staining at the injection site (quadriceps) after injection (i.m.) of SLNs (A), NPs (B) and CNE (C).

5.3.2.2 Biodistribution of adjuvants and their associated antigen: *in vivo* tracking of SAM-GFP loaded DOTAP NPs, SLNs and CNE

The distribution *in vivo* of both empty DOTAP based SLNs, NPs and CNE was compared to their SAM-loaded counterparts. Herein, self-amplifying RNA encoding for a green fluorescence protein (SAM-GFP) was used as model antigen. Regarding CNE, as shown in figure 5.10A, empty cationic nanoemulsions remained longer in the injection site (SOI). More in detail, almost 100% of the injected CNE dose was recovered at SOI after 6 hours, while SAM-CNE was faster drained (78% of the initial dose). Despite this difference, according to the statistical analysis the distribution profile was not significantly different. At latest time points this trend seemed to be attenuated: for instance, above 65% of both empty and SAM adsorbing CNE was detected 48 hours post injection (p.i.). The popliteal lymph node (PLN) is the local lymphoid tissue to which antigen detected in the quadriceps (SOI) drains. Therefore, the presence of formulations in the PLN was investigated. It was found that, the concentration of both empty and loaded CNE was similar in the popliteal lymph node with no

significant difference 2 days p.i. (Figure 5.10B). Similar observations were reported for droplets in the ILN, where the accumulation of SAM-loaded and SAM-free CNE was comparable (Figure 5.10C).

With respect to solid lipid nanoparticles (SLNs), the biodistribution profile from the injection site to the organs is shown in Figure 5.10D-5.10F. In contrast with what has been shown for emulsions, the presence of nucleic acid inside particles seemed to reduce the speed at which the carrier was drained from the leg muscle (Figure 5.10D); more precisely, 6 hours p.i. SLNs concentration at the SOI was quite comparable (around 90% of the initial dose) despite the presence of SAM. However, at further time points, empty SLNs concentration was significantly lower compared to the SAM loaded counterparts; for example, at 24 hours p.i. almost 60% of the empty SLNs dose was measured at the quadriceps, while around 80% of SAM loaded particles were still present ($p<0.05$). This trend became more evident at the last time point, where empty and SAM loaded SLN concentrations were 48% and 77% respectively ($p<0.01$). On the other hand, empty particles tended to accumulate faster in the lymphatics. As it was shown in figure 5.8E, which represents the particles content in the popliteal lymph node (PLN), empty SLNs were 10-folds more abundant than the loaded counterparts 6 hours p.i.; while SAM loaded SLNs concentration seemed to be reduced at PLN, a consequent accumulation of those particles at the inguinal lymph node (ILN) occurred. These differences became significant at further time points. Moreover, after 48 hours the loaded particles were twice more abundant compared to the empty ones ($p<0.05$).

Regarding polymeric nanoparticles (NPs), the biodistribution profile is shown in Figure 5.10G-5.10I. Figure 5.10G represents the percentage of initial particles dose at the injection site: at the earliest time point empty and SAM loaded NPs concentrations were not significantly different compared to their SAM free counterparts. However, after 48 hours p.i., the percentage of loaded and empty particles were 65 and 48% respectively ($p<0.01$). Thus, a tendency of smaller empty particles to accumulate at popliteal lymph node was observed (Figure 5.10E). More precisely, empty NPs were 10-times more abundant than loaded ones 6 hours p.i. ($p<0.05$) at PLN, while the difference in distribution profile seemed to be negligible at the other isolated lymph node.

All antigen loaded formulations induced monocyte infiltration; however, the kinetics and intensity were found to be formulation-dependent. As shown by images in figure 5.11, the presence of nucleic acid in particles core did not affect the blue colour intensity given by pontamine blue labelled monocytes. Images of isolated legs demonstrated a weak localized blue staining for SLNs and NPs at the injection site caused by pontamine blue and any noticeable changes in the intensity of blue staining at the site of injection was observed during time for both formulations (Fig. 5.11 B and C); on the contrary, SAM-CNE shown in figure

5.11A seemed to induce more recruitment of monocytes in the SOI, with significantly brighter blue colour in the leg muscle, even after 6 hours p.i.
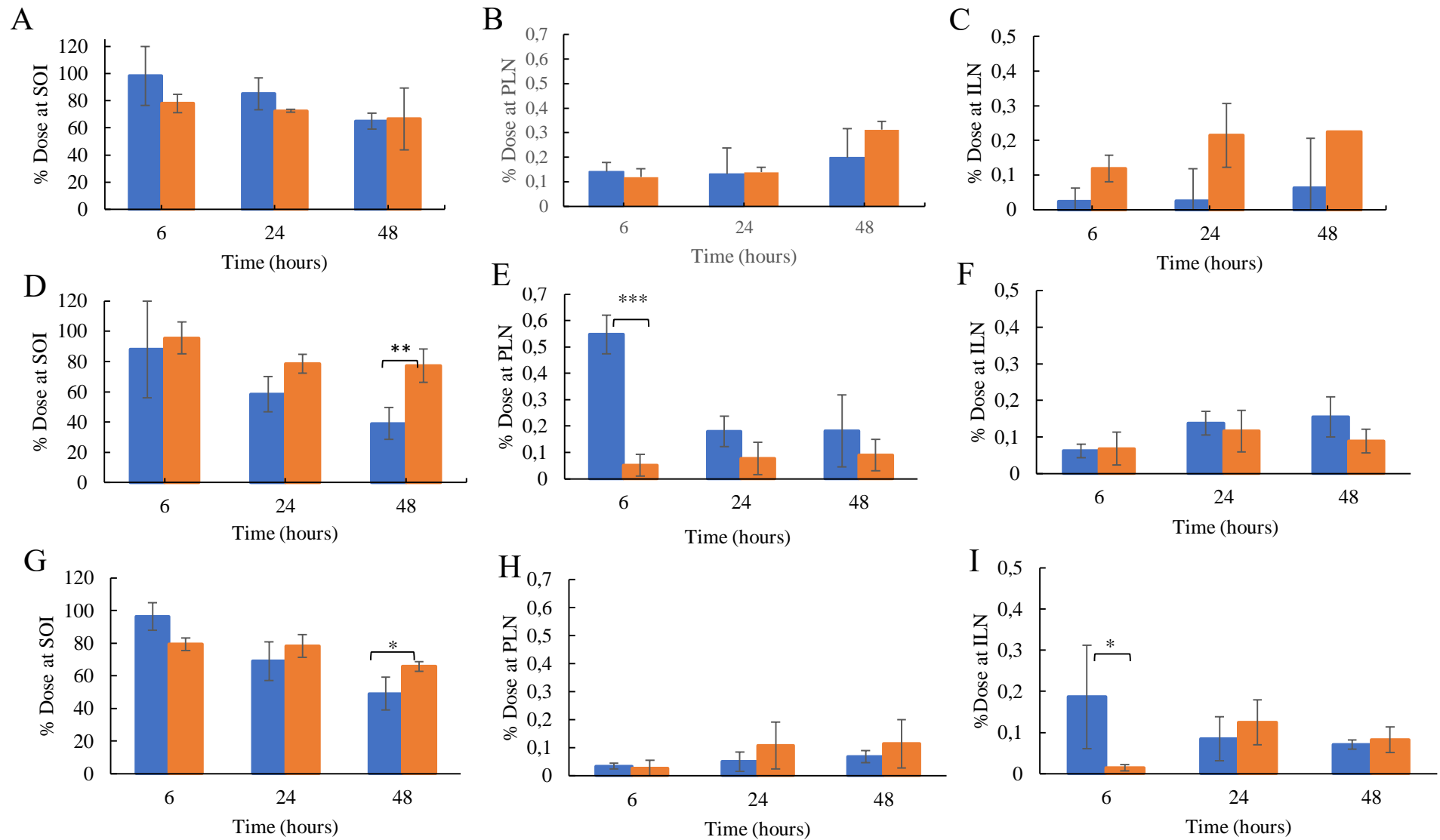
Figure 5. 10 *In vivo* **biodistribution of SAM-loaded cationic DOTAP based CNE, SLNs, NPs in CD1 mice upon intramuscular injection**. SAM-loaded formulations (orange) were compared to empty ones (blue). The percentage of dose was analyzed at the site of injection (CNE – **A**, SLNs – **D**, NPs – **G**), popliteal lymph node (CNE – **B**, SLNs – **E**, NPs – **H**) and inguinal lymph node (CNE – **C**, SLNs – **F**, NPs – **I**). Statistical analysis was performed using the Mann−Whitney test.
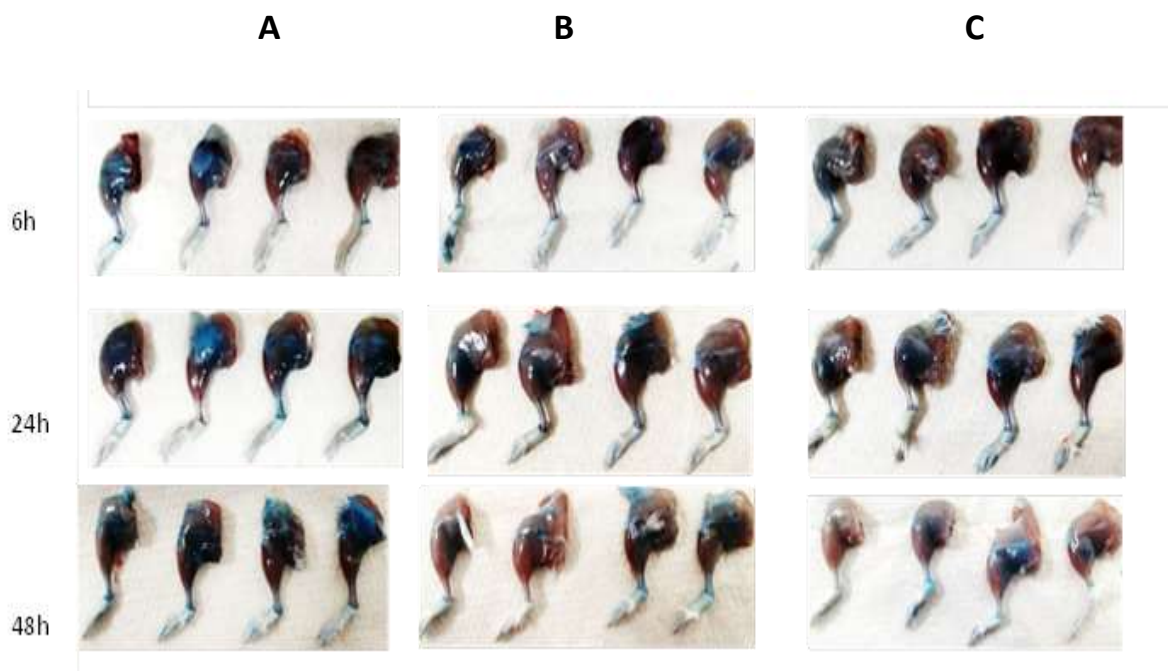
Figure 5. 11 Representative images of the site of injection after I.M. administration of SAM loaded DOTAP based formulations. A) CNE, B) SLNs and C) NPs. Blue staining (pontamine blue) indicates monocyte extravasation at the site of injection due to danger and inflammation signal.

5.3.2.3 Bio-distribution of adjuvants and their associated antigen: evaluation of changing from DOTAP to DDA on SLNs, NP and CNE drainage profile *in vivo*

Despite an extensive body of literature reporting the immunostimulatory capacities of cationic compounds and their capability to form an antigen depot (Zabner, 1997), less is known regarding the role that the type of cationic lipid plays in inducing an efficient immune response. Hence, within this work, two of the most widely used cationic lipids – DOTAP and DDA - have been selected to formulate potential adjuvants for a SAM based vaccine, and their distribution in the mouse body was compared. DOTAP or DDA based SLNs, NPs and CNE formulations were evaluated according to their ability to form an antigen depot at the site of injection (SOI), popliteal (PLN) and inguinal (ILN) lymph nodes. Since no significant difference has been shown in the particles' drainage kinetics, only SAM-loaded formulations were considered.

Figure 5.13 showed the distribution of SAM-loaded CNE, SLNs and NPs at the SOI and in the lymphatics. As it is represented in Figure 5.13 A, D and G the change from DOTAP to DDA did not alter particles distribution from the injection site to the rest of the mice body; all DDA based formulations induced a depot effect at the leg muscle with no significant difference among formulations. For example, after 48 hours all carrier concentrations were between 66 and 78%.

Furthermore, by looking at Figure 5.13 B, E and H, which represent the percentage of dose detected at the PLN, differences between DDA based and DOTAP based particles were evident. For example, DDA:CNE tended to accumulate faster at PLN, with a peak which it 5 times higher compared to its DOTAP counterpart (Figure 5.13 B) 24 hours p.i. However, at further time points this trend seemed to be attenuated, with both DDA:CNE and DOTAP:CNE doses being non statistically different. On the contrary, DOTAP:NPs seemed to have a higher accumulation at the popliteal lymph node 6 hours p.i. (Figure 5.13 H), while difference was negligible at further time points. On the other hand, the percentage of all formulations at the inguinal lymph node resulted to be <0.3%, (Figure 5.13 I). Furthermore, the images of the leg muscles in Figure 5.12 highlighted a brighter blue stain at the SOI given by DDA based carriers. CNE and SLNs showed a higher presence of blue stain compared to NPs which might be correlated to the higher monocyte infiltration.
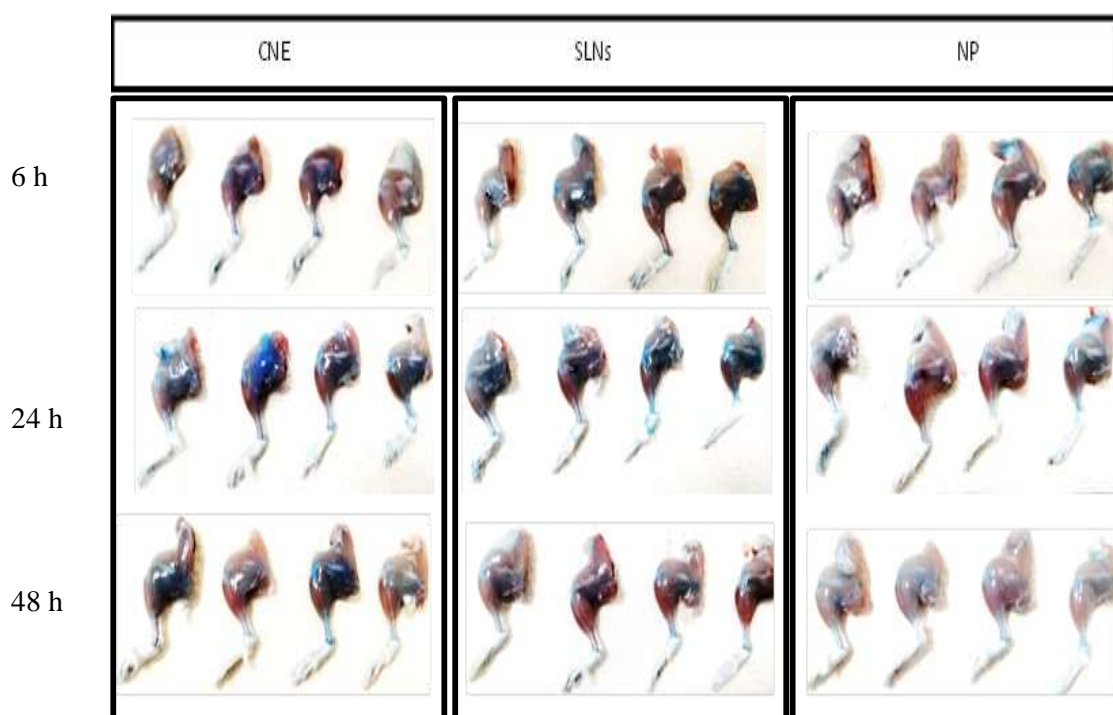
Figure 5. 12 Representative images of the site of injection after I.M. administration of DDA based formulations. CNE (left), SLNs (centre) and NPs (right). Blue staining (pontamine blue) indicates monocyte extravasation at the site of injection due to danger and inflammation signal.
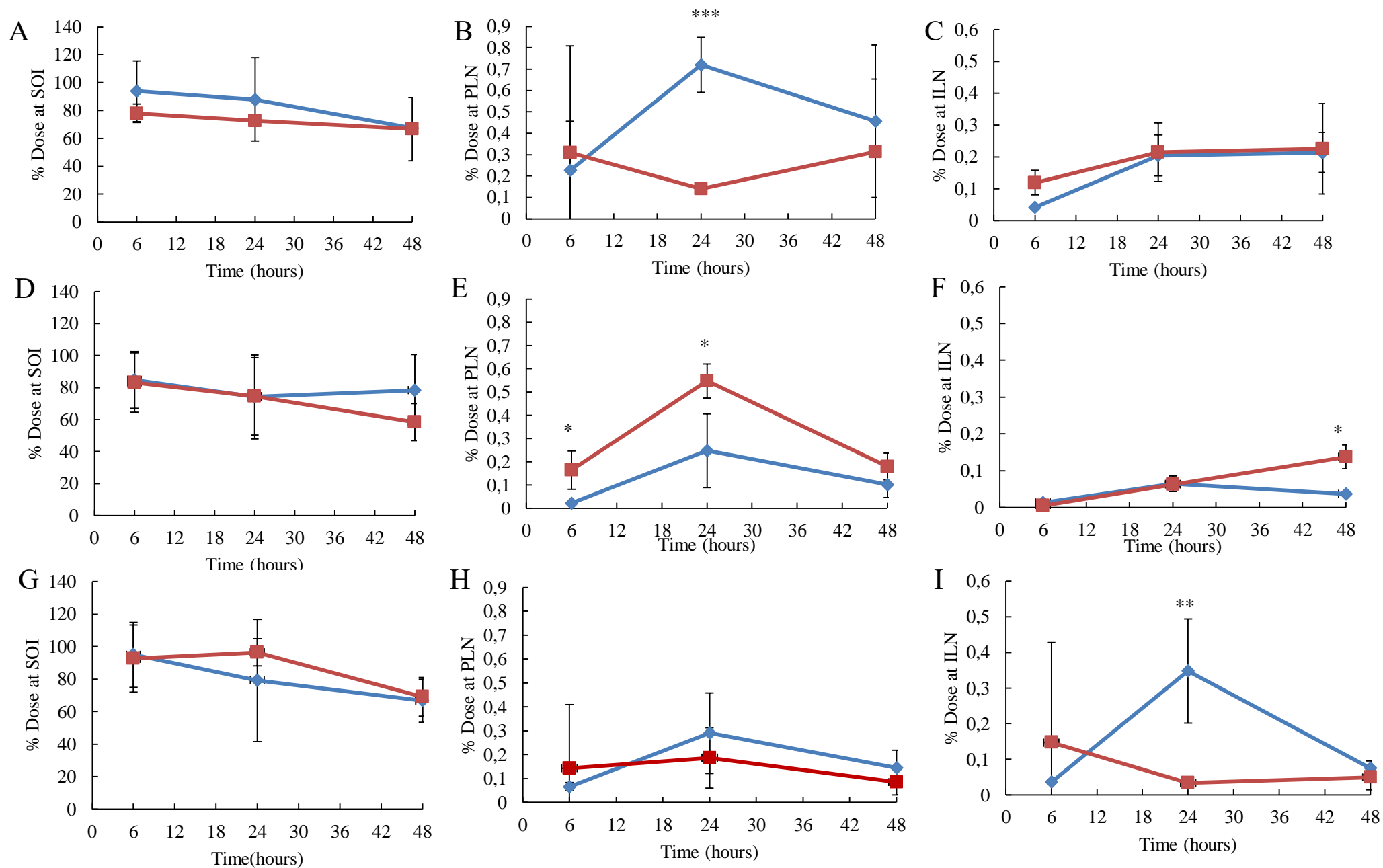
Figure 5. 13 *In vivo* biodistribution of SAM-loaded CNE, SLNs, NPs upon intramuscular injection. DOTAP based formulations (red lines) were compared to DDA ones (blue lines). The percentage of dose was analyzed at the site of injection (CNE – **A**, SLNs – **D**, NPs – **G**), popliteal lymph node (CNE – **B**, SLNs – **E**, NPs – **H**) and inguinal lymph node (CNE – **C**, SLNs – **F**, NPs – **I**). Statistical analysis was performed using the Mann−Whitney test.

5.3.2.4 Bio-distribution of adjuvants and their associated antigen: the effect of surface charge on pharmacokinetics of emulsions in mice

In order to evaluate how the surface charge might affect the clearance rates of nanoemulsions, the distribution *in vivo* of cationic DDA or DOTAP based CNE was compared to an anionic MF59-like formulation. Since no significant difference in the *in vivo* drainage from the SOI has been seen between unloaded CNE and its SAM adsorbing counterparts, the anionic MF59-like distribution profile has been compared only with antigen-free DDA or DOTAP based CNE.

As shown in Figure 5.14A, cationic CNE remained longer in the injection site (SOI). More in detail, between 80 and 90% the injected cationic CNE dose was recovered at SOI after 6 hours, while MF59 formulation drained faster (around 69% of the initial dose). This trend was maintained at further time points: for instance, while above 70 and 80% of both DOTAP and DDA CNE respectively was detected 24 hours post injection, just 58% of MF59-like initial dose remained in the leg muscle after 1 day. At the last time point this difference became significant, especially compared with DDA emulsion ($p < 0.001$). On the other hand, the anionic emulsion seemed to go faster to the popliteal lymph node (PLN- Figure 5.14B). More precisely, after 48 hours, the percentage of anionic droplets was above 1.2%, while both DDA CNE and DOTAP CNE ones were 0.4 and 0.3 respectively. The accumulation profile in the inguinal lymph node is shown in Figure 5.14C; anionic droplets tended to accumulate at ILN to a greater extent compared to their cationic counterparts, especially at earlier time points. Specifically, 6 hours p.i. MF59-like concentration was almost 0.2%, while DDA and DOTAP CNE ones were significantly lower ($p < 0.05$). However, this behaviour seemed to be attenuated at further time points, where the gap between formulations was not significant.
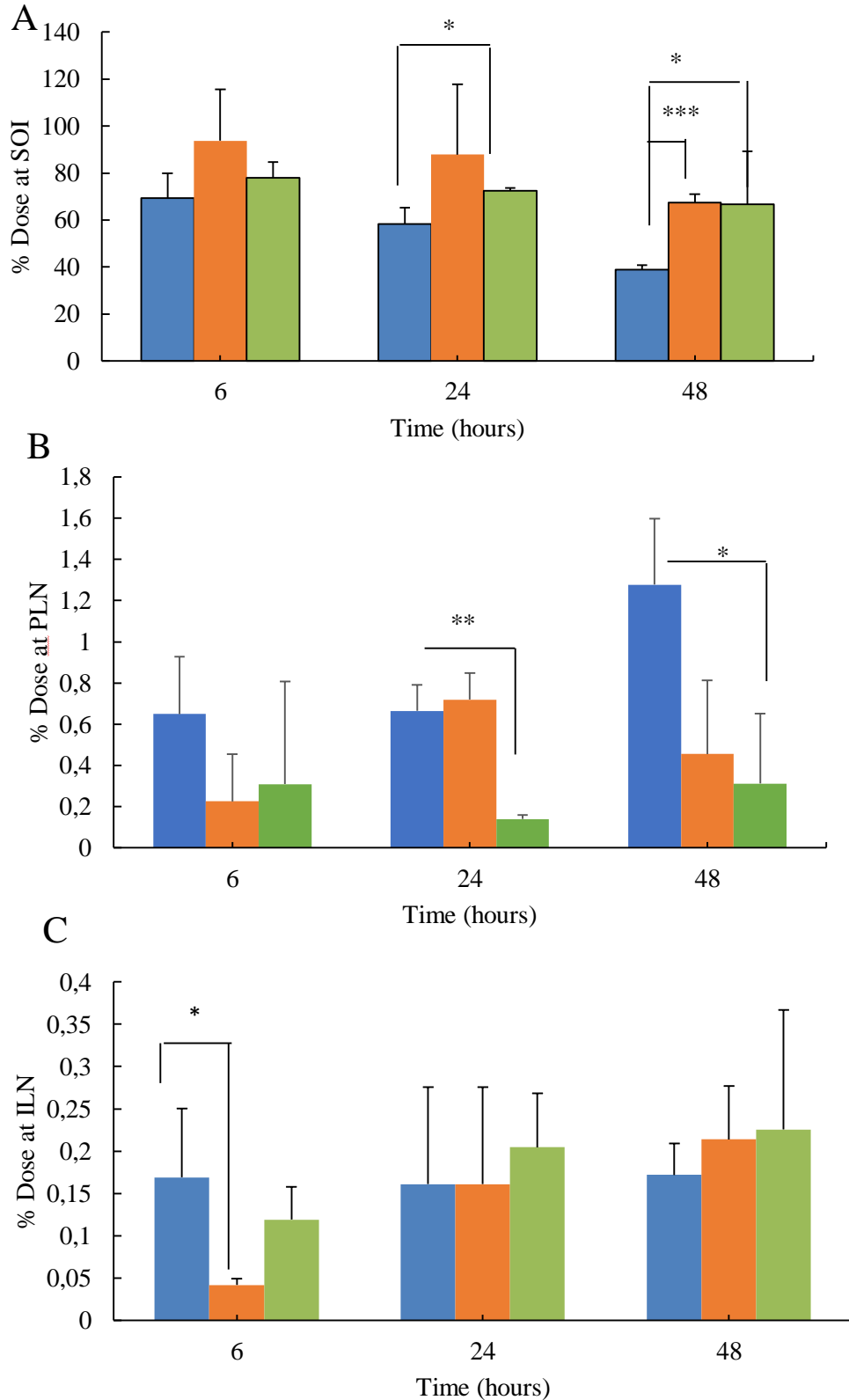
Figure 5. 14 Cationic nanoemulsions remained longer at the site of injection compared to anionic counterparts. Anionic MF59-like formulation (blue columns) were compared to SAM-free DDA based CNE (orange columns) and SAM-free DOTAP based CNE (green columns). The percentage of dose was analyzed at the site of injection (A), popliteal lymph node (B) and inguinal lymph node (C). Statistical analysis was performed using the Kruscal Wallis method.

5.3.3 Immunogenicity study

5.3.2.4 Immunogenicity of different vaccine candidates encoding rabies glycoprotein G after intramuscular injection

Immunogenicity of SAM-Rabies vaccines was performed in BALB/c mice. Candidates were selected according to *in vitro* potency (IVP) results shown in chapter 6. *In vitro* antigen expression highlighted that SAM-Rabies encapsulating DOTAP liposomes, DDA liposomes and DOTAP NPs resulted in the most efficient transfection (chapter 4.3.6). Therefore, IVP was used as rational approach to screen among formulations, to select the most promising candidates to test *in vivo*. Herein DOTAP liposomes, DDA liposomes and DOTAP NPs encapsulating a self-amplifying RNA rabies vaccine that encoded the rabies glycoprotein G antigen, were compared to the commercial, inactivated virus rabies vaccine, Rabipur. LNPs and GSK formulated CNE were used as controls. Figure 5.15 showed the immunogenicity of SAM-Rabies vaccine delivered by the mentioned delivery systems at different time points. After 2 weeks post one immunisation, all candidates triggered IgG titres level below the limit of detection (0.125 EU/mL – Figure 5.15A), while controls were immunogenic at both doses tested (1.5 and 0.15 µg). More precisely, LNPs encapsulating 1.5 µg /dose of SAM elicited a geometric mean titer (GMT) of around 30 EU/mL, while lowering SAM dose of 10 folds reduced GMT to around 13 EU/mL. However, comparing LNPs and CNE responses, lipid nanoparticles elicit 10-fold and 20-fold higher titres compared to cationic emulsions at 1.5 and 0.15 µg SAM respectively ($p < 0.01$). Moreover, IgG elicited by Rabipur were comparable with CNE low dose (Figure 5.15A). After 4 weeks post first injection (Figure 5.15B), NPs at both SAM doses resulted in high response with IgG responses comparable to those induced by both the commercial vaccine and CNE 0.15 µg. More interestingly, NPs GMT was above 0.5 EU/mL, which is considered an indication of protection. Despite an improvement in IgG level, GMT induced by both liposomes remained below the protective threshold (Figure 5.15B). However, LNPs at the highest SAM dose were the most effective adjuvants (GMT >20 EU/mL). At day 43 – 2 weeks after the second immunisation – titres generally busted (Figure 5.15C). The trend highlighted previously was maintained after the boost, with LNPs eliciting 100-fold higher response compared to NPs and liposomes at the highest SAM dose. Regarding CNE, GMT at 1.5 µg SAM was equivalent to Rabipur (around 70 EU/mL), while CNE at the lowest dose was significantly inferior ($p < 0.05$). Moreover, while a correlation between IgG titres level and antigen dose occurred when SAM was delivered with both LNPs and CNE, a dose response was negligible for SAM delivered with NPs or liposomes (Figure 5.15C). Further, 4 weeks after the second immunisation, the potency of three candidates seemed to slightly improve, especially for DOTAP liposomes at highest SAM dose, the GMT of which was equivalent to NPs counterpart (around 9) at the same antigen dose (Figure 5.15D). Despite that, at 1.5 µg SAM
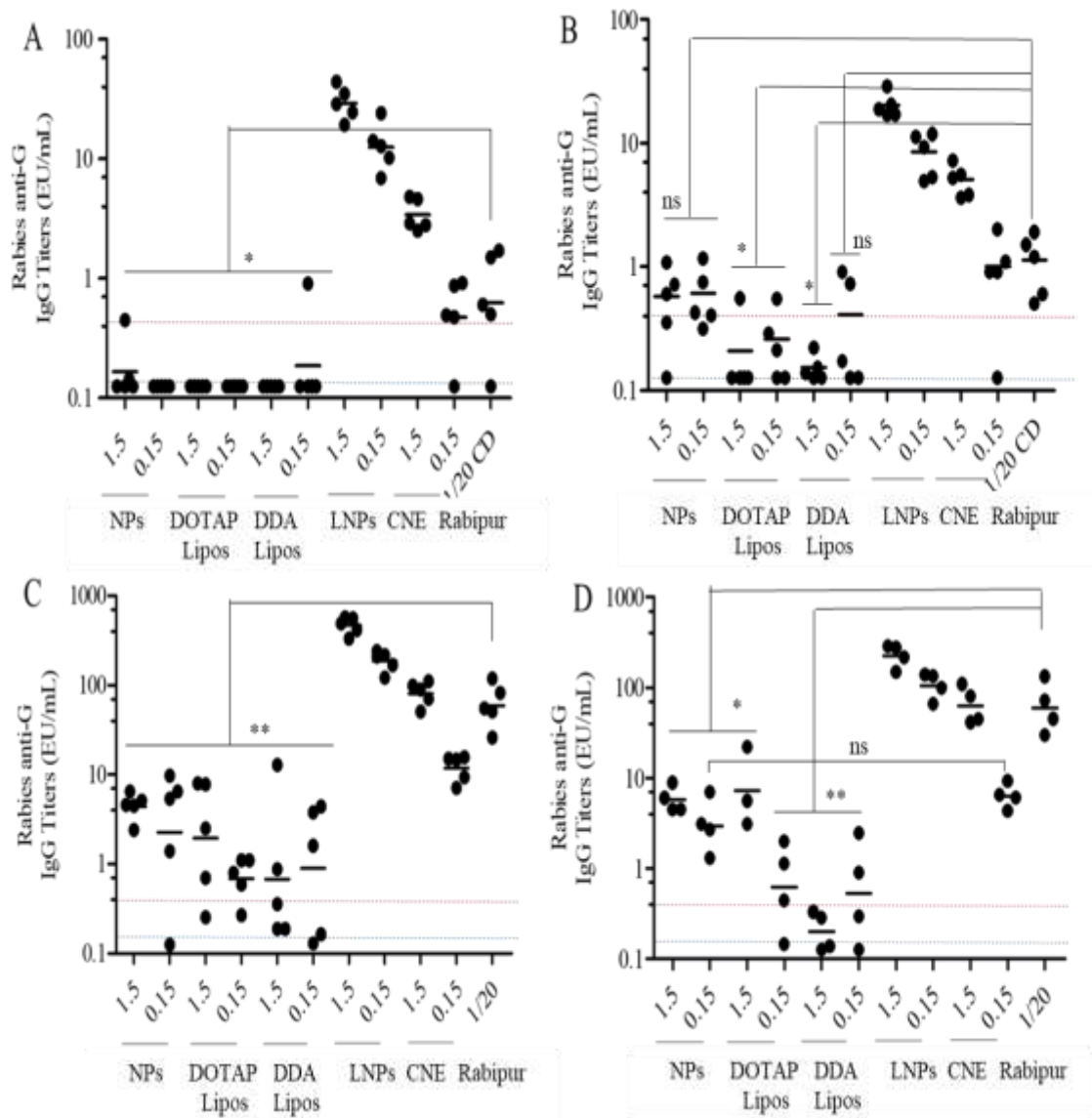
Figure 5. 15 Immunogenicity of SAM-Rabies vaccine delivered by different cationic carriers. Groups of ten BALB/c mice were immunized i.m. on days 0 and 28 with either 1.5 or 0.15 μg of self-amplifying RNA encoding for rabies G protein encapsulating DOTAP polymeric nanoparticles (NPs), DOTAP Liposomes (DOTAP Lipos) or DDA Liposomes (DDA Lipos) and compared with the commercial vaccine Rabipur (1/20 of human dose). CNE and gold standard LNPs were used as positive controls. Specific IgG titres were measured by enzyme-linked immunosorbent assay (ELISA). Data are from pools of two mice of the same group (depicted as dots), and the geometric mean titres (GMTs) are solid lines. Sera were collected and analysed A) 2 weeks B) 4 weeks C) 6 weeks and D) 8 week after the first immunisation. Titres < 0.125 EU/mL (dotted blue line) were considered below the limit of detection, while titres >0.5 EU/mL (dotted red line) were considered protective. Intergroup comparison was analysed using the one-way ANOVA test (Dunnett's multiple comparison test).
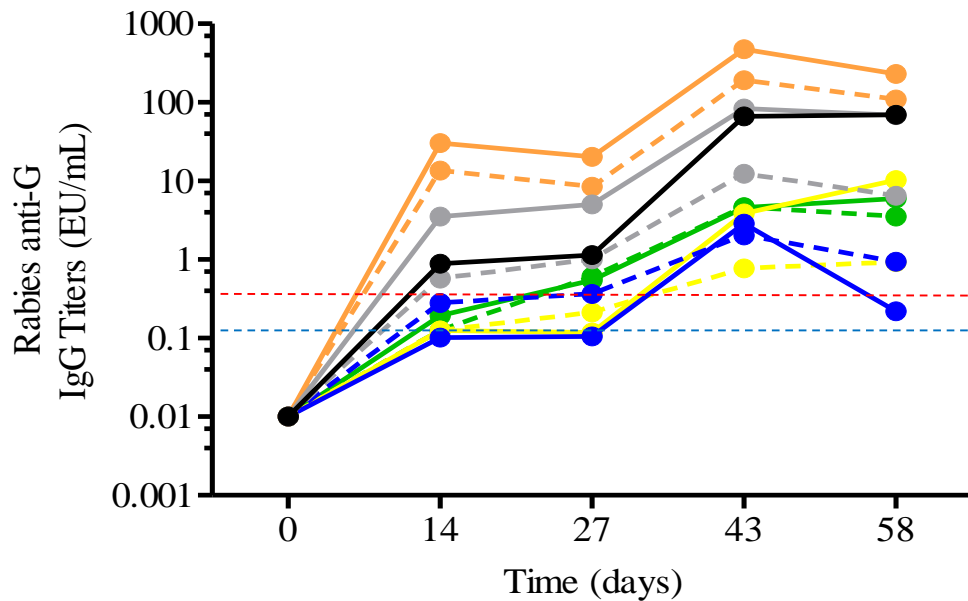
Figure 5. 16 Time course of rabies anti-G ELISA titres. Groups of ten BALB/c mice were immunized i.m. on days 0 and 28 with DOTAP polymeric nanoparticles (NPs – green line)), DOTAP Liposomes (DOTAP Lipos – yellow line) or DDA Liposomes (DDA Lipos – blue line) encapsulating either 1.5 (solid lines) or 0.15 µg (dash lines) of self-amplifying RNA encoding for rabies G protein. Candidates were compared with the commercial vaccine Rabipur (1/20 of human dose – black line). CNE (grey line) and gold standard LNPs (orange line) were used as positive controls. Geometric mean titres (GMTs) of specific IgG titres were reported for day 0 (pre-immune) 14, 27, 43 and 58 after the first immunisation. Titres < 0.125 EU/mL (dotted blue line) were considered below the limit of detection, while titres >0.5 EU/mL (dotted red line) were considered protective.

none of the three candidates tested could induce IgG titres level comparable to any of the controls or to the commercial vaccine, which had a GMT above 80 EU/mL (Figure 5.15D). Interestingly, at 0.15 µg SAM NPs were as potent as CNE to elicit antibody titres, with the GMT non-significantly different.

Figure 5.16 shows the time course of rabies anti-G ELISA titres elicited by SAM-Rabies delivered by different formulations. In accordance with what has been reported above, LNP and CNE-delivered self-amplifying RNA rabies vaccines produced measurable rabies virus antibody titres at all-time points tested, with the 1.5 µg/dose of SAM/LNP and SAM/CNE eliciting higher titres at day 43, at least comparable with the commercial vaccine. Regarding candidates, they were less potent to induce strong antibody response. However, the immunogenicity of NPs and CNE at 0.15 µg/dose of SAM seemed to be comparable at all time points, with the titres and kinetics measured after the second vaccination being well above the protective threshold of 0.5 EU/mL.

5.3.2.5 T-cell responses of different vaccine candidates encoding rabies glycoprotein G after intramuscular injection

Generally, the net frequencies of Rabies-specific CD8+ T-cells (Figure 5.17B) were significantly higher compared to CD4+ T-cells counterparts (Figure 5.17A): frequencies of rabies-specific CD4+ T cells ranged from 0.1-0.2% to 1.2%, while CD8+ T cells percentage went up to 5%. For example, with NPs at 1.5 µg SAM the percentage of CD4+ and CD8+ T cells were around 0.4 and 1.8% respectively ($p<0.05$) (Figure 5.17 A and B); further, CD4+ T cells of mice treated with 1.5 µg of SAM encapsulated in LNP were around 1.2% while CD8+ counterparts were almost 5% ($p<0.001$) (Figure 5.17 A and B). The majority of rabies-specific CD4+ T cells were TNF-γ+ and IFN-γ+, while most of CD8+ T cells were IFN-γ+ and IFN-γ+/TNF-α+, characteristic of an effector phenotype. With respect to T cell total frequency, none of the candidates induced significantly higher CD4+ or CD8 + T cell compared to Rabipur.

Total percentage of antigen splenic T cell responses of different vaccine candidates encapsulating SAM encoding rabies glycoprotein G after intramuscular injection demonstrated a slight dose response when assessed at 2 weeks post second immunisation (Figure 5.17). For instance, looking at SAM delivered with LNPs, the frequency of CD4+ cells at 1.5 µg SAM were significantly higher ($p<0.5$) compared to the one at low SAM dose. Moreover, CD8+ cells were 3-fold more abundant with NPs encapsulating 1.5 µg SAM compared to the lower dose. However, the dose response was not significantly evident for the other two candidates (DOTAP and DDA liposomes), which induced equivalent CD4+ and CD8+ percentage regardless the antigen dose tested (Figure 5.17).

To provide an indication of the potential cytotoxic potential of the cells, the surface expression of CD107a was assessed, as a measure of the degranulation process (Zaritskaya et al., 2010) upon *in vitro* antigen stimulation of splenocytes from immunized animals. Results are shown in Figure 5.18. After two immunizations with SAM at two different doses in combination with NPs or liposomes, the majority of NP-specific CD4+ T cells were CD107a- (Figure 5.18A. An equivalent result was obtained for positive controls (LNPs and CNE) and the comparator (Rabipur). This suggested that SAM formulations did not induce cytotoxic CD4+ T cells. However, considering specific CD8+ T cells, only the immunization with SAM encapsulating LNPs and CNE induced high frequency of CD107a+ cells comparable to the commercial vaccine, while candidates were less potent than Rabipur in inducing cytotoxic T cell. With respect to the cell phenotype, a combination of Th0 (IL-2+/TNF-α+, TNF-α+, and IL-2+) and multifunctional Th1 (IFN-γ+/IL-2+/TNF-α+ and combinations) phenotype was observed in CD4+ T cells 2 weeks after the second immunization (Figure 5.19A).
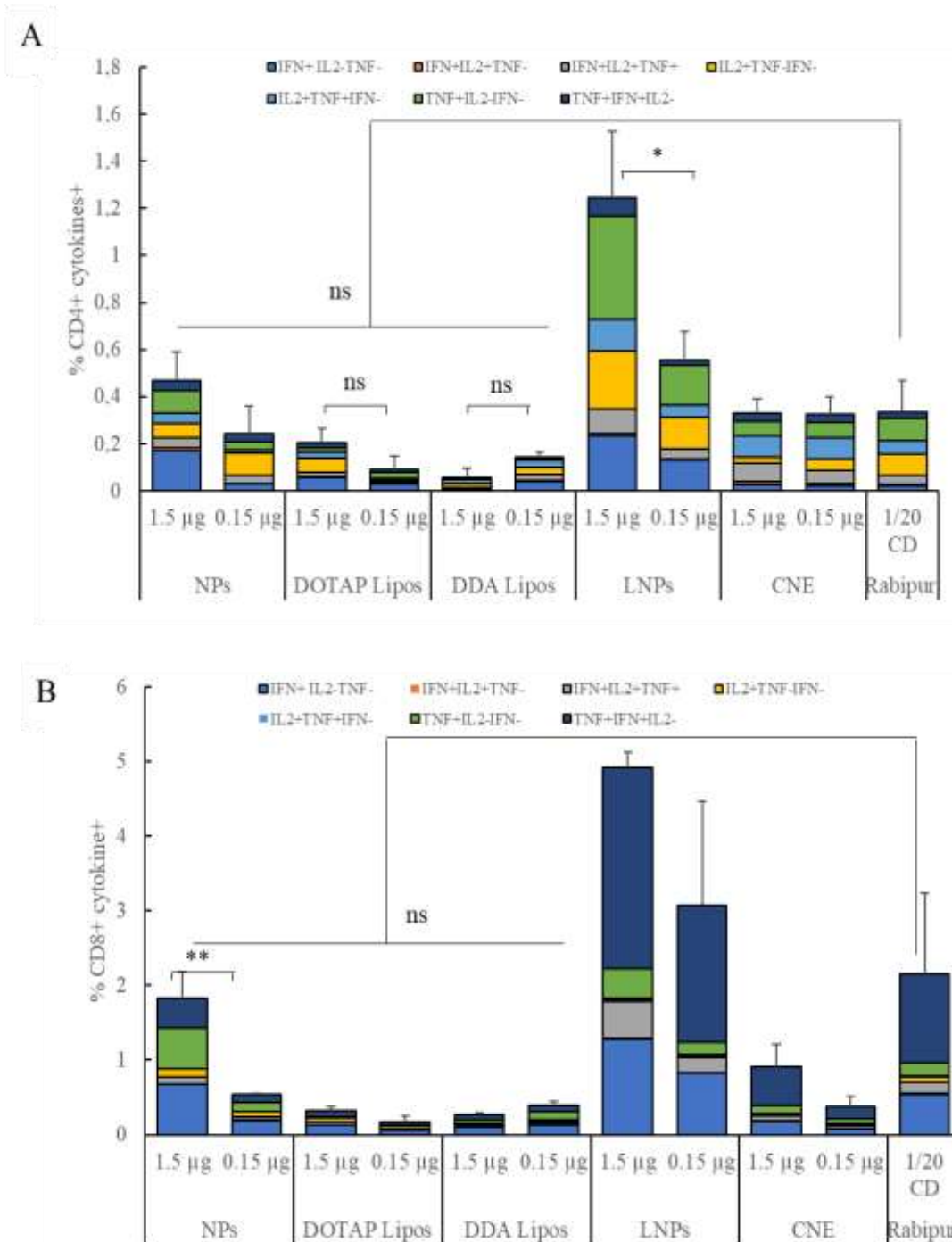
Figure 5. 17 Candidates induced levels of antigen-specific CD4+ or CD8+ T cells comparable to Rabipur. Splenic A) CD4+ T cells, and B) CD8+ T cells 2 weeks after two intramuscular immunizations spaced 4 weeks apart in BALB/c mice (N=3). Mice were immunized with either 1.5 or 0.15µg/dose of self-amplifying RNA expressing rabies G glycoprotein adjuvanted with either polymeric nanoparticles (NPs), DOTAP Liposomes (DOTAP Lipos) or DDA Liposomes (DDA Lipos). Candidates were compared with the commercial vaccine Rabipur (1/20 of human dose). CNE and gold standard LNPs were used as positive controls. Splenocytes were stimulated with rabies G1-G2-G3 peptide, stained for intra-cellular cytokines, and subjected to flow cytometry. Color code indicates the different combinations of cytokines produced by the respective cells. Unstimulated cells were used as control. Intergroup comparison was analysed using the one-way ANOVA test (Dunnett's multiple comparison test).

193
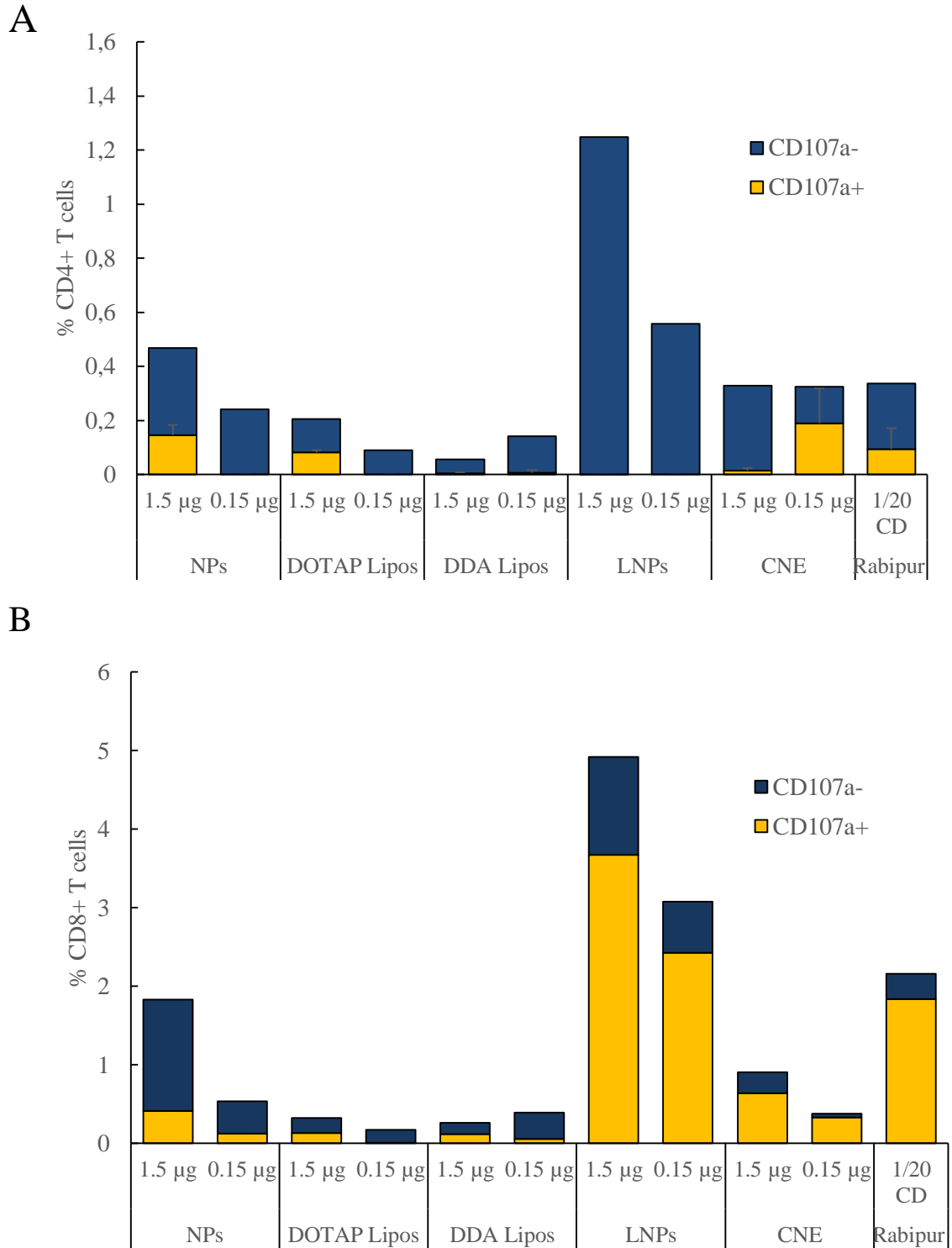
Figure 5. 18 Percentages of cytotoxic CD4+ or CD8+ T cells. The induction of rabies-specific CD4+ or CD8+ T cells by either 1.5 µg or 0.15 µg/dose of SAM encapsulating nanoparticles (NPs) DOTAP liposomes (DOTAP Lipos) and DDA liposomes (DDA Lipos) was characterised 2 weeks after the second immunization. Candidates were compared with the commercial vaccine Rabipur (1/20 of human dose). CNE and gold standard LNPs were used as positive controls. Surface expression of CD107a on splenocytes stimulated *in vitro* with rabies G1-G2-G3 peptide was assessed by flow cytometry. Data show the frequency of cytokine-secreting A) CD4+ or B) CD8+ T cells that express (yellow bars) or not (blue bars) CD107a. Unstimulated cells were used as control.

A
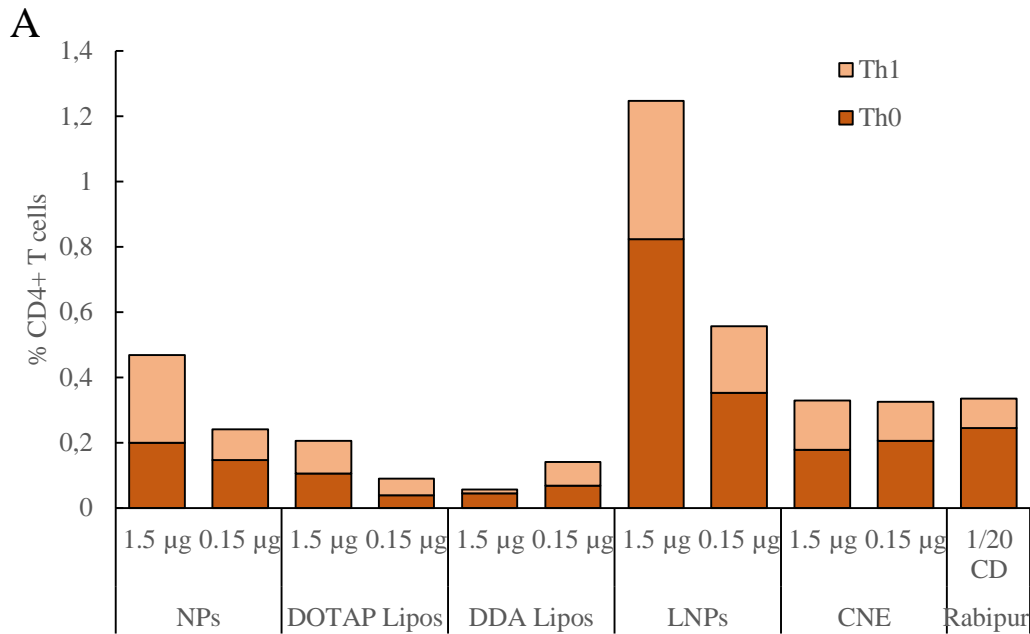
Figure 5. 19 Characterization of phenotype of CD4+ T cells. Rabies specific CD4+ cells induced by either 1.5 µg or 0.15 µg/dose of SAM encapsulating nanoparticles (NPs) DOTAP liposomes (DOTAP Lipos) and DDA liposomes (DDA Lipos) were measured 2 weeks after the second immunization. Candidates were compared with the commercial vaccine Rabipur (1/20 of human dose). CNE and gold standard LNPs were used as positive controls. Activated CD4+ T cells phenotype was characterised as either Th0 (TNF-α+, IL-2+, IL-2+/ TNF-α+ - dark red) or Th1 (IFN-γ+/TNF-α+/IL-2+, IFN-γ +, IFN-γ+/TNF-α+ and IFN-γ+/IL-2+ - light red).

5.3.2.6 Evaluating the immunogenicity of two vaccine candidates encoding rabies glycoprotein G by three different routes of administration

To better understand the differences between the immunogenicity profiles of newly formulated antigen-expressing nucleic acids particles, formulations were administered in BALB/c mice by the intramuscular (i.m.), intradermal (i.d.) or intranasal (i.n.) routes. Previously collected *in vivo* data showed that polymeric nanoparticles at 0.15 µg/dose SAM were as potent as the positive control CNE to induce high levels of antibody titres (Figure 5.15 and 5.16). Accordingly, DOTAP NPs at this antigen concentration was selected as candidate. Moreover, since in *vitro* potency (IVP) was demonstrated not to be the only criteria to take in consideration when screening among candidates to test *in vivo* due to poor correlation between protein expression and immunogenicity (Hassett et al., 2019), solid lipid nanoparticles were also considered. Therefore, DOTAP NPs and DOTAP SLNs encapsulating 0.15 µg/dose of a self-amplifying RNA rabies vaccine encoding for rabies glycoprotein G antigen were compared to the commercial, inactivated virus rabies vaccine, Rabipur. SAM encapsulating gold standard LNPs was used as control. Moreover, CNE was not included in the study as it

was not expected to be active in the acidic and proteolytic environment of the mucosae, which affect the stability and functionality of adsorbed SAM. The immunogenicity of i.m.-injected SAM-Rabies NPs, SLNs and LNPs was compared with i.m.-injected inactivated virus rabies vaccine Rabipur, and data were reported in Figure 5.20A. It was noted that, 2 weeks after the first immunisation, LNPs were the most effective while SLNs were as effective as the commercial vaccine, as measured by the G-specific IgG geometric mean titres (GMT of 5 EU/mL vs. 0.6 EU/mL; Figure 5.20A). Interestingly, SLNs GMT was ≥ 0.5 EU/mL, the WHO recommended protective level. However, when SAM was formulated within NPs, IgG titres (GMT<0.125 EU/mL) were substantially lower than those elicited by SLNs, LNP or Rabipur (Figure 5.20A). 4 weeks after the first immunization, the trend seemed to be slightly different. Overall, LNPs elicited the highest IgG titres (GMT around 8 EU/mL); however, IgG titres induced by NPs and SLNs were significantly higher compared to the commercial vaccine ($p<0.001$ – Figure 5.20A). Despite this increase, after the second immunization, LNPs and Rabipur were significantly more immunogenic compared to the newly formulated candidates, with GMT of LNPs> Rabipur>>SLNs>NPs.

Figure 5.20B showed the immunogenicity of formulations administered intradermally. As described for formulations injected i.m., before the boost, SLNs were significantly more effective compared to Rabipur but less potent compared to the positive control LNPs ($p<0.05$); regarding NPs, the potency of inducing G-specific IgG titres was comparable to the vaccine on the market (GMT around 0.7 EU/mL). However, 2 weeks after the second immunization, SLNs were as potent as Rabipur to induce IgG titre in mice, while NPs were
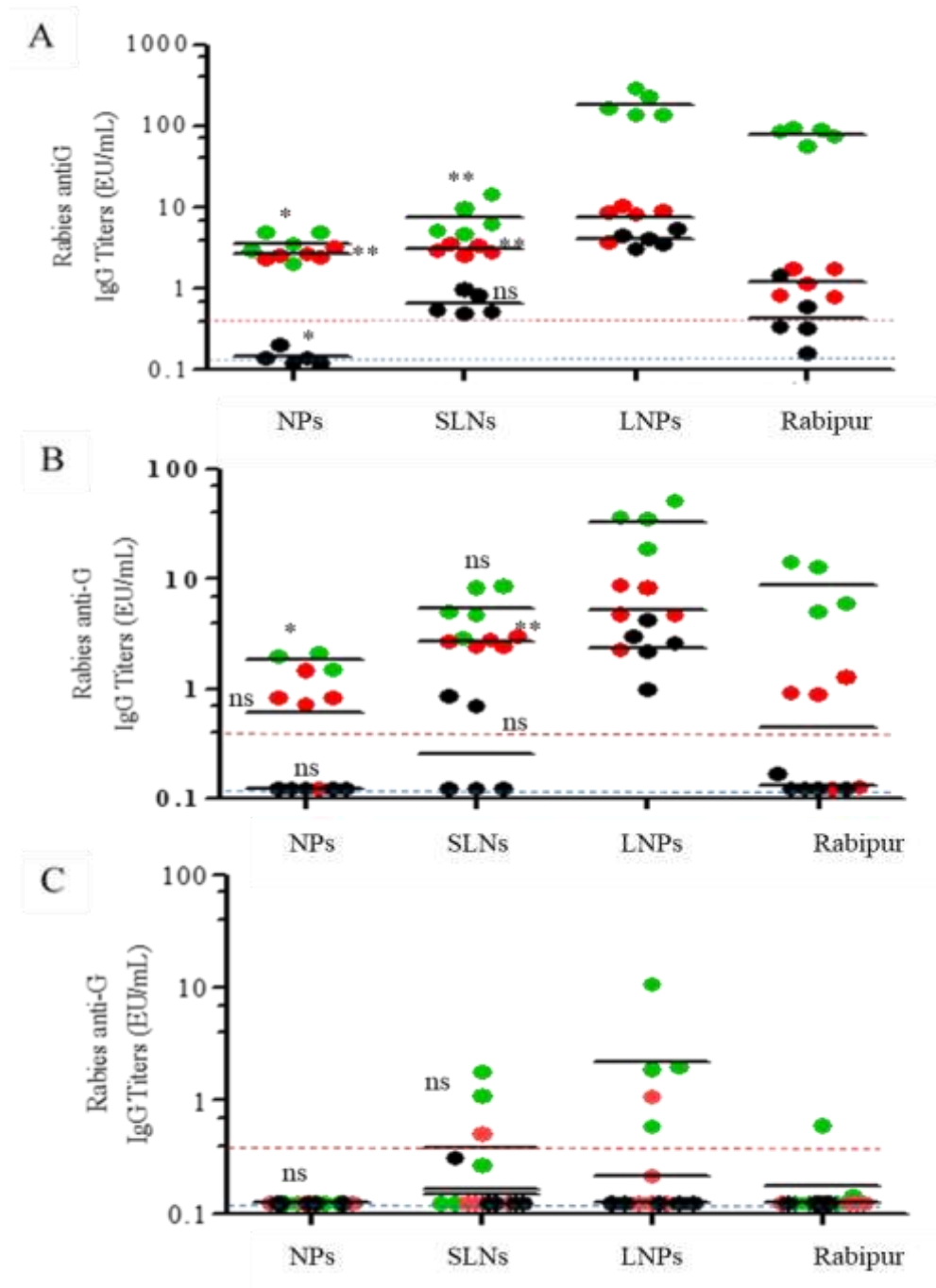
Figure 5. 20 Immunogenicity of cationic candidates loading SAM-Rabies vaccine administered by three different routes. Groups of ten BALB/c mice were immunized A) intramuscularly (i.m.) B) intradermally (i.d) or C) intranasally (i.n.) on days 0 and 28 with DOTAP polymeric nanoparticles (NPs) and DOTAP solid lipid nanoparticles (SLNs) encapsulating 0.15 μg/dose or 1.5 μg/dose of self-amplifying RNA encoding for rabies G protein. Candidates were compared with the commercial vaccine Rabipur (1/20 i.m. and i.n. or 1/50 i.d. of human dose). LNPs were used as positive controls. Data are from pools of two mice (depicted as dots), and the geometric mean titres (GMTs) are solid lines. Sera were collected and analysed 2 weeks (black dots), 4 weeks (red dots) and 6 weeks (green dots) after the first immunisation. Titres < 0.125 (dotted blue line) were considered below the limit of detection, while titres >0.5 (dotted red line) were considered protective. Intergroup comparison was analysed using the one-way ANOVA test (Dunnett's multiple comparison test).
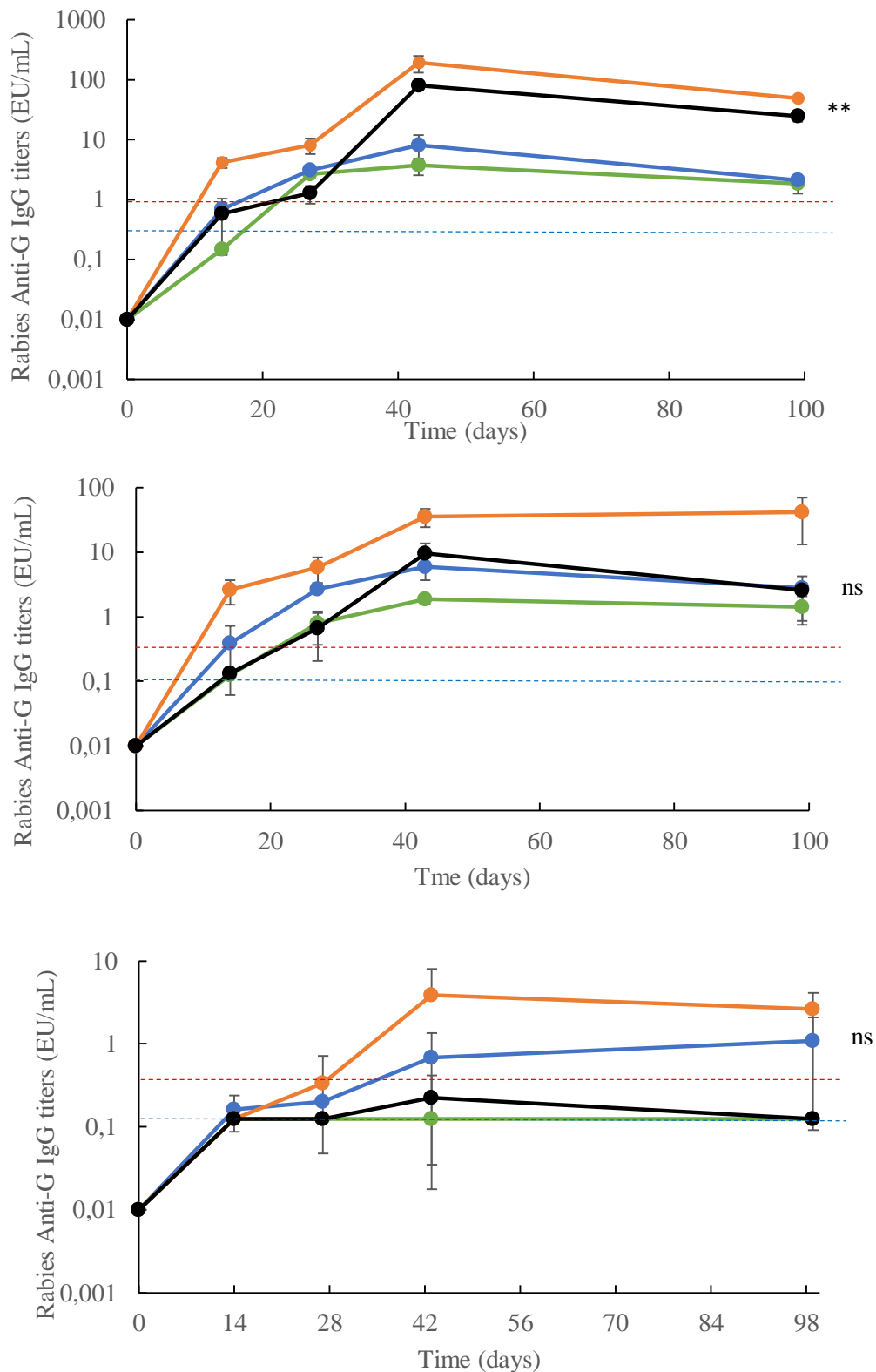
Figure 5. 21 Formulations elicited long-lasting immune response up to 99 days post first immunization. Groups of ten BALB/c mice were immunized A) i.m. B) i.d. and C) i.n. on days 0 and 28 with DOTAP polymeric nanoparticles (green line) or DOTAP SLNs (blue line) encapsulating either 0.15 µg of self-amplifying RNA encoding for rabies G protein. Candidates were compared with the commercial vaccine Rabipur (black line). LNPs (orange line) were used as positive controls. Titres < 0.125 EU/mL (dotted blue line) were considered below the limit of detection, while titres >0.5 EU/mL (dotted red line) were considered protective. One-way ANOVA test (Dunnett's multiple comparison test) was used for statistical analysis.

Figure 5. 22 Percentages of antigen-specific CD4+ or CD8+ T cells after antigen administration by different routes. Splenic CD4+ T cells (A,C,E) and CD8+ T cells (B,D,F) 2 weeks after two immunization via either intramuscular (A and B), intradermal (C and D) or intranasal (E and F) administration spaced 4 weeks apart in BALB/c mice (N=3). Mice were immunized with 0.15μg/dose of self-amplifying RNA expressing rabies G glycoprotein formulated with either polymeric nanoparticles (NPs) or solid lipid nanoparticles (SLNs). Candidates were compared with the commercial vaccine Rabipur (1/20 i.m. and i.n. or 1/50 i.d. of human dose). LNPs was used as positive control. Splenocytes were stimulated with rabies G1-G2-G3 peptide, stained for intra-cellular cytokines, and subjected to flow cytometry. Colors code indicates the different combinations of cytokine produced by the respective cells. Unstimulated cells were used as control. Intergroup comparison was analysed using the one-way ANOVA test (Dunnett's multiple comparison test).

199

significantly less potent (p<0.05). LNPs remained the most immunogenic, as measured by GMT>35 EU/mL (Figure 5.20B). With respect to formulations injected intranasally, the immunogenicity profile was shown in Figure 5.20C. As represented by IgG titres levels, before the boost, only mice which received SAM loaded SLNs and LNPs were responders; however, GMT was below the protective threshold for both formulations. Moreover, weeks after the second immunization, although non- statistically different, SLNs induced a better response compared to both Rabipur and NPs. More precisely, while no responders were observed among mice receiving SAM NPs, only the serum of one mouse high IgG titres level was measured when Rabipur was administered i.n. On the other hand, SAM encapsulating SLNs and LNPs were protective (GMT >0.6 and >7 EU/mL respectively), with a larger number of responders (60% and 80% respectively vs 0% (NPs) and 20% (Rabipur) – Figure 5.20C). Overall, IgG titres measured in mice sera immunized i.n. were notably lower compared to both i.d. and i.m. counterparts. Time course of rabies anti-G ELISA titres elicited by SAM-Rabies delivered by different formulations and routes of administration is shown in Figure 5.21. In accordance with what has been reported above, both candidates injected i.m. were able to elicit high IgG titres 99 days post first immunization, therefore inducing long-lasting humoral immunity (Figure 5.21A). However, the potency was significantly lower (p<0.001) compared to the commercial vaccine (Figure 5.21A), as already seen 2 weeks after the boost. Interestingly, after i.d. administration, both NPs and SLNs were as efficient as Rabipur to produce protective IgG titres at day 99 post prime (Figure 5.21B). Further, when injected intranasally, NPs were unable to induce any rabies specific antibody titres after 99 days post prime (Figure 5.21C), as was the case with the commercial vaccines, with 0% of responders. On the contrary, SLNs elicited protective IgG titres 99 days after the first immunization and 50% of were responders, although the GMT was not significantly different from the one of the comparator (Figure 5.21C).

To confirm this finding, a T-cell assay was performed on splenocytes from 3 animals per group after the second immunization with SAM NPs or SLNs, using the rabies vaccine on the market as a comparator and LNPs as a control (Figure 5.22). SAM vaccines in general showed better or at least equivalent T-cell responses in comparison to Rabipur. Data reported here revealed that i.d. and i.m. administrations of SAM vaccines induced an increase in the antigen-specific CD8+ T-cell population compared to the CD4+ counterparts (Figure 5.22 A-B and C-D). the majority of CD8+ T cells were IFN-γ+, TNF+ and IL-2+ cells. However, when SAM formulations were administered intranasally, CD4+ and CD8+ T cell levels were comparable (Figure 5.22 E and F). Nevertheless, the overall amount of activated T cells was higher for i.m. and i.d routes compared to i.n. route (Figure 5.22), in agreement with the observed IgG titres.

Moreover, antigen-specific CD4+ T cells phenotype was a combination of Th0 and Th1 and it was not influenced by route of administration and the SAM delivery system composition (Figure 5.23 A,C,E). However, phenotype analysis on CD8+ T cell showed that SAM formulations tended to induce predominantly IFN-γ+/TNF+/IL-2+ and IFN-γ+/ TNF+ cytokines, suggesting a polarization toward Th1 phenotype (Figure 5.23 B,D.F).

Further, cytotoxic activity induced by SAM formulations was evaluated analysing expression of CD107a on activated T cells surface (Figure 5.24). As shown previously, few CD4+ CD107a+ cells were detected 2 weeks after the second immunization among the three routes tested (Figure 5.24 A,C,E). On the other hand, higher frequencies of cytotoxic CD8+ T were measured and, by changing administration route, differences among candidates were observed (Figure 5.24 B,D.F). Specifically, candidates injected i.m. induced very low percentage of CD8+ T CD107+ cells compared to the positive control, while no significant difference was observed in comparison with Rabipur (Figure 5.24 B). However, when administered i.d. CD8+ T CD107+ cells induced by SLNs were comparable with the LNPs and superior with respect to the commercial vaccine (Figure 5.24 D). This trend was maintained even after i.n. administration, with both candidates inducing CD8+ cytotoxic T lymphocytes in a similar manner to the control and in a greater extent compared to the licensed vaccine (Figure 5.24 F).

T cell assay on lungs of intranasally immunized mice (Figure 5.25) showed that SAM encapsulating SLNs CD4+ were IFN-γ+, TNF-α+ and IL2+, and the frequency was comparable to the positive control LNPs and higher that Rabipur (Figure 5.25A). Besides, both SLNs and NPs were equally able to elicit activation of CD8+ cytokines with no significant difference among candidates and positive controls (Figure 5.25B). However, phenotype analysis revealed that CD4+ T cells were more Th0 polarized (Figure 5.25C), while the majority of CD8+ T cells were mainly IFN-γ+ and TNF-α+ (Figure 5.25D). Cell-mediated cytotoxicity evaluation highlighted that while low percentage of CD107a+ cells was induced by both candidates and controls (Figure 5.25E), delivery of SAM within SLNs enhanced CD8+ CD107a+ production compared to the positive control LNPs (Figure 5.25F). However, CD8+ cytotoxic T lymphocyte response was comparable to the one induced by Rabipur i.m. (Figure 5.25F).
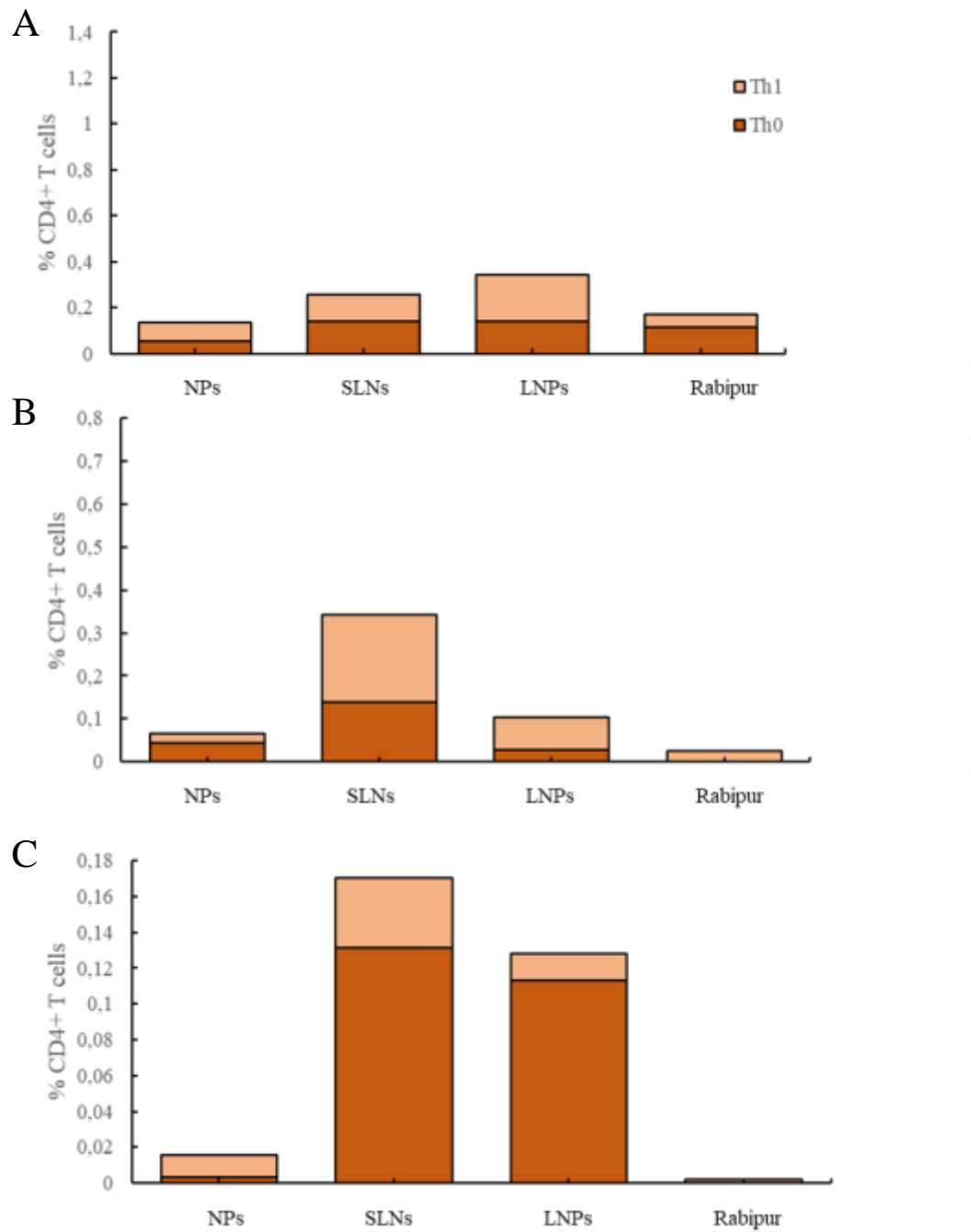
Figure 5. 23 CD4+ T cells phenotype is administration route dependent. Rabies specific CD4+ T cells induced by SAM encapsulating nanoparticles (NPs) or solid lipid nanoparticles (SLN) injected either intramuscularly (0.15 µg/dose - A), intradermally (0.15 µg/dose B) or intranasally (1.5 µg/dose C) were measured 2 weeks after the second immunization. Candidates were compared with the commercial vaccine Rabipur (1/20 of human dose i.m. and i.n, 1/50 of human dose i.d.). LNPs was used as positive control. Phenotype of activated CD4+ T cells after A) i.m. B) i.d. and C) i.n. administration was characterised as either Th0 (TNF-α+, IL-2+, IL-2+/ TNF-α+ - dark red) or Th1 (IFN-γ+/TNF-α+/IL-2+, IFN-γ +, IFN-γ+/TNF-α+ and IFN-γ+/IL-2+ - light red).
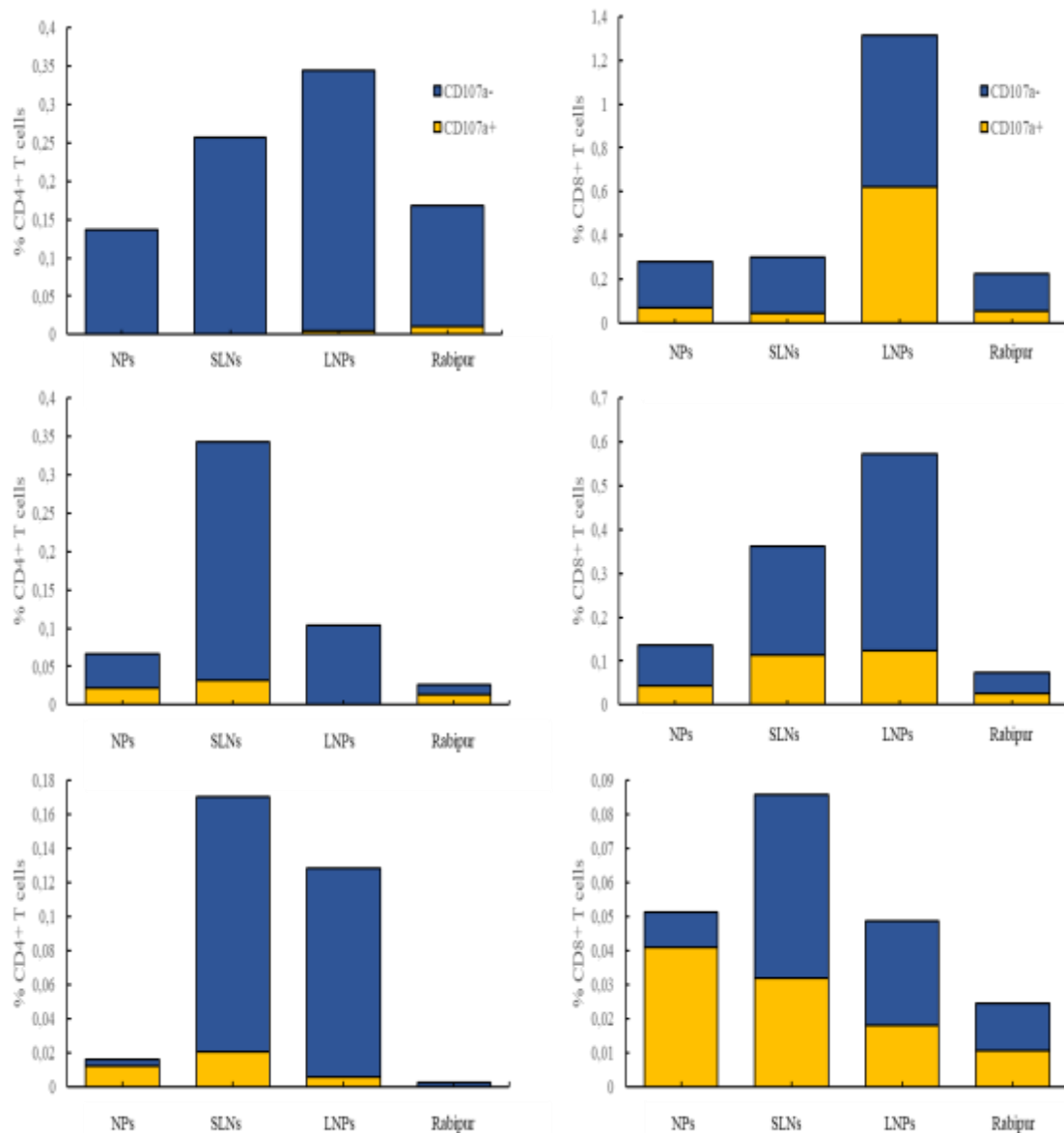
Figure 5. 24 SAM encapsulating formulations induced cytotoxic CD8+ T cells production. The induction of rabies-specific CD4+ or CD8+ T cells by 0.15 µg/dose of SAM encapsulating nanoparticles (NPs) or solid lipid nanoparticles (SLNs) injected by intramuscular (A and B), intradermal (C and D) or intranasal (E and F) route was characterised 2 weeks after the second immunization. Candidates were compared with the commercial vaccine Rabipur (1/20 of human dose i.m. and i.n. or 1/50 of human dose i.d.). LNPs were used as positive control. Surface expression of CD107a on splenocytes stimulated *in vitro* with rabies G1-G2-G3 peptide was assessed by flow cytometry. Data show the frequency of cytokine-secreting CD4+ (A,C,E) or CD8+ T (B,D,F) cells that express (yellow bars) or not (blue bars) CD107a. Unstimulated cells were used as control.
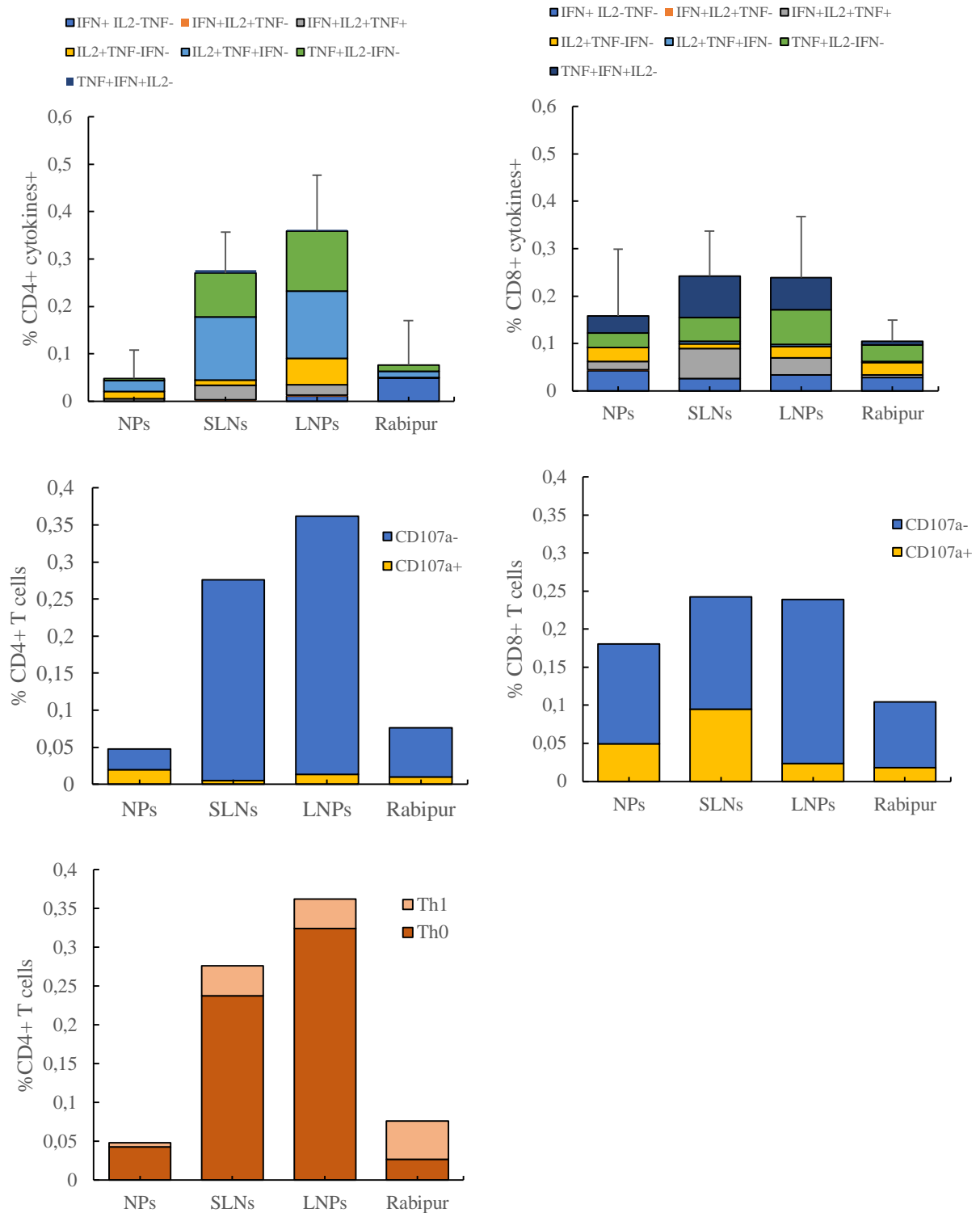
Figure 5. 25 T cell assay in lungs after intranasal injection of SAM formulation. Lungs of BALB/c mice (n = 3) immunized intranasally twice, 4 weeks apart, with 1.5 μg of SAM NPs or SAM SLNs were used to quantify cellular immunity. Candidates were compared with the commercial vaccine Rabipur (1/20 of human dose). LNPs were used as positive control. A) CD4+ T cells and B) CD8+ T cells expressed as combinations of TNF-α, IFN-γ and IL2 cytokine produced by the respective cells. C) CD4+ T cells and D) CD8+ T cells plotted as percentage of either CD107a+ (yellow) or CD107- (blue) cells. E) CD4+ T cells represented as either Th0 (light red) or Th1 (dark red) phenotype Intergroup comparison was analysed using the one-way ANOVA test (Dunnett's multiple comparison test).

5.4 Discussion

Despite the efficacy of current commercial vaccines against rabies, there is still extensive work to develop more cost-effective alternatives and improved vaccines to reduce the toll of rabies disease in developing countries. Ideally, these vaccines need to be inexpensive, safe, and able to provide sustained protection, preferably after a single administration. Within this chapter an innovative approach was employed, by using a self-amplifying RNA (SAM) vaccine which encodes for rabies glycoprotein G. "Naked" delivery of a self-amplifying RNA vaccine has shown to be suitable as a prophylactic rabies vaccine (Saxena et al., 2009). However, Saxena and co-workers highlighted that commercial vaccine Rabipur was more immunogenic than unformulated SAM (Saxena et al., 2009). Besides, many papers reported enhanced immunogenicity when SAM was delivered through a particulate delivery system. For example, it has been seen that unformulated self-amplifying RNA could protect mice from influenza (HA) challenge; however, two 10 µg doses were required and the HA-specific antibody titres were highly variable between mice (Fleeton et al., 2001). On the contrary, when SAM was encapsulated within 1,2-dilinoleyloxy-3-dimethylaminopropane (DLinDMA) based LNPs, 10 and 100 times less antigen dose (0.1 µg or 1.0 µg) was sufficient to elicit influenza virus neutralizing antibody titres as high as those elicited by the licensed influenza vaccine (Hekele et al., 2013). Moreover, a cationic nanoemulsion (CNE) delivery system based on MF59 formulation was widely described as an efficient delivery system for SAM vaccines. More precisely, it was found that 0.015 µg of SAM encoding for respiratory syncytial virus glycoprotein F (RSV-F) elicited a geometric mean titre (GMT) comparable to a 1,000-fold higher dose (15 µg) of unformulated SAM RNA or pDNA in mice (Brito et al., 2014b). This benefit might be due to greater SAM protection from biological degradation and cell internalisation given by the carrier, with consequent higher antigen expression *in vivo*. These finding suggested that implementation of delivery systems for RNA delivery might be highly advantageous.

5.4.1 Biodistribution of cationic formulations in and a mouse model: particles induced a depot effect at the injection site

Herein, taking advantage of these data, the pharmacokinetics and immunogenicity of different cationic particles were evaluated. Results from particles biodistribution showed that, using a radiolabelling method, it was possible to efficiently track formulations in a mouse model (Figure 5.6-5.8). Preliminary studies reported here demonstrated that ^{3}H-cholesterol label was not released from the formulations and remained either anchored in the lipid bilayer of the liposomes or inside the particle (Figure 5.4). Moreover, the addition of radiolabelled probe did not alter formulations physicochemical parameters (Figure 5.3). The use of radiolabelled probes is a well stablished technique for carriers or organic molecules detection in animal

body (Henriksen-Lacey et al., 2011b). Radiolabelled particles provided many advantages for clinical monitoring of the distribution of therapeutics in real time to predict therapeutic efficacy. This technique is based on the detection of radiations emitted by the nuclide in the organ of interest, thereby allowing to quantify particles placing in the body and to determine the specific dose needed to achieve the required distribution at the target site.

Results reported here showed that DOTAP based formulations (SLNs, NPs and CNE) were well retained at the injection site after intramuscular inoculation with >60% of initial dose at least for 48 hours p.i. (Figure 5.6-5.8). However, the retention efficiency varied among formulations, with NPs and SLNs tending to accumulate faster in the lymphatics, especially at earliest time points, compared to CNE (Figure 5.6-5.8). The use of cationic formulations for antigen delivery in vaccines is a well-documented method to increase the immune recognition against otherwise inert or poorly immunogenic subunit proteins (Christensen et al., 2011). Within this study, one of the most commonly used cationic phospholipid (DOTAP) was combined with either a polymer (PLGA), a non-polar lipid (Tristearin) or with the cholesterol precursor squalene. DOTAP is commonly cited as transfection agents (Fletcher et al., 2006) and vaccine delivery systems for both DNA-encoded (Perrie et al., 2001) and protein (Walker et al., 1992) antigens. Structurally the presence of an ammonium ion headgroup confers to the lipid a net cationic charge at physiological pH. Previous studies have shown that cationic formulations induced a greater immune response compared to neutral or anionic ones (Yan et al., 2007).

This superiority of cationic carriers could be due to non-specific cell damage at the SOI (Shi and Rock, 2002). Furthermore, it has been proved that the addition of antigen by electrostatic interactions to the positively charged formulation increased the antigen presentation to APCs by forming an antigen depot at SOI. The depot effect might occur because of the *in vivo* aggregation, due to the cationic surface charge that attracts negatively charged serum protein. This fact limits the passive draining of the formulations from the injection site to the rest of the body, enhancing the permanency of particles at the SOI, with a consequent continuous presentation of the antigen to the immune cells (Henriksen-Lacey et al., 2010a). In the case reported in the chapter, all formulations tested were found to be able to induce a depot effect in the leg muscle, but the retention efficiency varied upon formulations. This suggested that a positive surface charge is not the only physicochemical property that determines the immunological properties of particles. Other properties such as membrane fluidity, head group structure might also influence the deposition of formulations and antigen at the injection site and the ensuing immune response (Henriksen-Lacey et al., 2011a).

5.4.2 The effect of particle size on formulations pharmacokinetics

Many papers reported that particles size might have an impact on the *in vitro* uptake and *in vivo* distribution of formulations. Studies conducted with the vaccine adjuvant CAF01, composed of DDA and trehalose 6,6'-dibehenate (TDB), and its associated antigen (Ag85B-ESAT-6) revealed that cationic liposomes from 200 to >2000 nm exhibited similar clearance rates from the injection site upon intramuscular injection (Henriksen-Lacey et al., 2011b, Kaur et al., 2012a). Indeed, in recent studies looking at the distribution of cationic chitosan nanocapsules after sub-cutaneous administration, 100 nm particles drained more rapidly to the lymph nodes compared to those of 200 nm and this size reduction also improved interaction with both migratory and resident antigen presenting cells in the lymph nodes, suggesting a combination of free- and cell-mediated transport to the lymph nodes (Cordeiro et al., 2019). This could explain why similar pharmacokinetic profiles were observed for CAF01 formulated at different sizes, since none of the formulations were below 100 nm. Moreover, depletion of dendritic cells *in vivo* completely abolished trafficking of 500 nm polystyrene particles to the lymphatics but did not affected drainage of 20 nm particles (Manolova et al., 2008). Besides, different pharmacokinetic profiles were recently observed *in vivo* for small (40 nm) and large (>500 nm) DOTAP or DDA based liposomes upon intramuscular injection, with large liposomes showing longer retention at the injection site but limited drainage to the local lymph nodes compared to small liposomes (Lou et al., 2019), in line with findings reported here. Furthermore, it has been seen that size might be involved in particles trafficking to local lymph nodes and uptake by local antigen presenting cells (APCs). For example, it was reported that large (560 nm) vesicles were able to improve antigen processing compared to smaller (around 100 nm) vesicles (Brewer et al., 2004). Moreover, it was observed that DC tended to take up more particles with a diameter between 0.5 nm and 0.2 µm, while smaller particle (20-100nm) were taken up less and they reached the lymphatics faster (Manolova et al., 2008). These observations confirm data reported herein the chapter, where SLNs and NPs with a diameter around 50 nm accumulated faster in the lymphatics compared to CNE larger droplets (around 200 nm). This particle-size-dependent kinetics in the PLN suggested a role for cellular uptake and trafficking of CNE from the SOI to the closest lymph node, as opposed to a passive draining for SLNs and NPs which induced an enhanced concentration of smaller particles in the PLN or ILN.

5.4.3 The effect of Pegylation on formulations biodistribution

It is well documented that the presence of PEG may affect the distribution and uptake profile of formulations. Literature widely reported that, in the case of cationic liposomes with surface charge density similar to that of the cell, the strength of electronic interactions between cell membrane and particles layer is reduced when PEG layer thickness increased (Dan, 2002). Hence, the presence of rigid barriers (e.g., grafted polymer brush surfaces) or the modification

of physicochemical attributes of particle surface (e.g., hydrophilicity/hydrophobicity) might have an impact on protein adsorption efficiency with a consequent reduction of phagocytic recognition of nanomaterials. For instance, PEG is often being used to formulate stealth drug carrier; due to the aqueous shield PEGylated particles have a longer blood circulation times and reduced phagocytosis (Walkey and Chan, 2011) .Herein, it has been proved that the presence of 2% mol/mol PEG in lipid nanoparticles induced a faster drainage of SLNs in the PLN, compared to non-PEGylated NPs and CNE (Figure 5.6-5.8) .

5.4.4 The effect of antigen addition on formulations pharmacokinetics

This size-dependent *in vivo* clearance was also maintained after the addition of the antigen, with larger (>200nm) loaded SLNs and NPs better retained at the injection site compared to empty counterparts (around 50 nm) (Figure 5.10). No significant differences were observed between antigen-free or antigen-adsorbing CNE, probably due to similarity of droplets size values (185 nm vs 210 respectively). Again, cationic charge is not the only parameter which drives the distribution of carriers *in vivo*, but other factors, such as particle size, might play a relevant role. Looking at percentage of particles in lymph nodes, the smaller the size the faster was the drainage to ILN and PLN (Figure 5.10). The nanoparticles size-dependent kinetics in the lymph nodes suggested a role for cellular uptake and trafficking of formulations from the SOI to the PLN and ILN, especially for larger particles. On the other hand, the drainage of smaller particles seemed to be passive. Moreover, the presence of PEG on particles surface might influence carrier distribution in mice, inducing a faster accumulation in the lymphatics. The increased permanency of SAM loaded particles at the injection site might be of interest as it was reported that internalization of mRNA vaccines occurs primarily by nonimmune cells at the injection site and the antigen is expressed mainly by muscle cells, fibroblast, and keratinocytes (Iavarone et al., 2017). However, dose-limiting toxic side effects need to be considered when developing charged delivery systems (Lv et al., 2006b).

5.4.5 The effect of cationic lipid choice on formulations pharmacokinetics

The change from DOTAP to DDA did not significantly alter formulations clearance profile *in vivo* (Figure 5.13). A comparative study between DDA and DOTAP based liposomes in mice was also conducted elsewhere to show that the choice of cationic lipid did not have a dramatic impact on the biodistribution (Lou et al., 2019). This observation was in contradiction to what has been seen by Henriksen-Lacey and co-workers who found that the draining of DOTAP:TDB liposomes from the SOI was significantly faster compared to DDA counterpart (Henriksen-Lacey et al., 2011a). However, it might be worth to underline that, in this study, it was also found that the proportion of antigen retained at the SOI when delivered with DOTAP:TDB liposomes was higher than the liposome itself; this may suggest instabilities in the bilayer of DOTAP:TDB liposomes and/or dissociation of the antigen from DOTAP:TDB liposomes.

5.4.6 The effect of surface charge on formulations pharmacokinetics

Head-to-head study among cationic DDA or DOTAP CNE and anionic MF59-like droplets confirmed that cationic charge is a crucial factor to increase the particles deposition at the injection site, thereby enhancing associated antigen presentation to the immune cells (Figure 5.14). Herein it was proven that negatively charged emulsions tended to be quickly drained from the SOI to the lymph nodes compared to their cationic counterparts (Figure 5.14). In line with these findings, a comparative study between highly cationic DDA:TDB liposomes and neutral DSPC:TDB liposomes showed that injection of cationic liposomes led to a deposition of vesicles at the SOI with more than 80% of the original dose remaining at day four and approximately half of the dose still present in the leg 14 days p.i (Henriksen-Lacey et al., 2010b). On the other hand, DSPC:TDB liposomes were faster cleared from the leg muscle and just 6% of the initial dose was found after 14 days (Henriksen-Lacey et al., 2010b). This fact might be due to the aggregation phenomena which happen *in vivo*: the high content of negatively charged protein in organic serum tends to opsonize positively charged particles more that neutral counterparts. This limits the passive drainage of antigen and liposomes from the tissue. Accordingly, it was noticed that the concentration of neutral DSPC:TDB liposomes was significantly higher in the PLN as compared to DDA:TDB liposomes, especially at earlier time points (Henriksen-Lacey et al., 2010a). The results presented here strongly support the antigen depot effect attributed to cationic formulations compared to negative ones, whereas a better accumulation of negatively charged MF59-like formulation at the PLN and ILN occurred (Figure 5.14).

5.4.7 Evaluating the ability of cationic particles to induce monocytes infiltration at the injection site

Interestingly, differences among formulations were detected in the ability to induce monocytes infiltration in the leg muscle. Although all antigen loaded formulations induced monocyte infiltration (Figures 5.9, 5.11, 5.12) the kinetics and intensity was found to be formulation-dependent, with cationic nanoemulsions inducing the highest recruitment of monocytes in the SOI, with brighter blue colour in the leg muscle, even after 6 hours p.i. (Figure5.9, 5.11, 5.12). These observations were in line with what has been found in the literature. It is well documented that MF-59 like formulations induce rapid recruitment of neutrophils and monocytes that participate in antigen transport to draining lymph nodes (Ott et al., 1995). It is also reported that the mechanism of action of these kinds of emulsions is mainly local, creating an 'immunocompetent environment' at the injection site which activate cells to take up the co-injected antigen (Calabro et al., 2013). Moreover, in agreement with findings reported in this chapter, it was postulated that a major target cell type for MF59-like formulations could be monocytes recruited from the site of adjuvant action, which take up the

antigen and undergo an adjuvant induced enhanced differentiation towards a dendritic cell phenotype (Seubert et al., 2008).

5.4.8 Comparison among selected cationic particles on their potency to elicit immune response *in vivo*

IgG titres from the first immunogenicity study showed that, 4 weeks after the first immunization, NPs were protective and as immunogenic as the commercial vaccine Rabipur and the positive control GSK formulated CNE at 0.15 µg/dose of SAM (Figure 5.15B). However, despite the augmented potency of Rabipur after the boost, NPs at lower dose remained as potent as CNE to elicit antibody titres *in vivo* (Figure 5.15D). PLGA is one of the most widely studied polymers in the vaccine field (Lü et al., 2009) due to its low toxicity, biodegradability, and sustained release capability (Panyam and Labhasetwar, 2003). After being taken up by cells, PLGA nanoparticles were shown to release their gene contents to the cytoplasmic space over extended periods of time (Panyam et al., 2002) although accelerated hydrolysis in acidic endosomal compartments. Therefore, PLGA nanoparticles for delivering siRNA oligo have attracted great interests as an alternative delivery system to the commonly used polycationic carriers that are unavoidably toxic and/or non-biodegradable. In addition, it was proved that PLGA NPs escape the endo-lysosomal compartment and slowly release the encapsulated nucleic acid in the cytosol, resulting in sustained gene expression especially for non-replicative RNA/DNA (Panyam et al., 2002). This might explain why IgG titres level elicited by NPs were significantly inferior 2 weeks post boost (Figure 5.15C) compared to the positive control CNE, while they became comparable 4 weeks after the second immunization (Figure 5.15D); it might be worth noticing that SAM adsorption onto CNE surface facilitates the immediate release of nucleic acid at target site (Patil and Panyam, 2009). Thus, for future works, it might be interesting to reconsider vaccination schedule applied here and measure humoral response induced by SAM NPs at later time points. In order to increase nucleic acid association, PLGA nano/microparticles are usually formulated with cationic materials such as DOTAP, cetyltrimethylammonium bromide (CTAB) or polyethylenimine (PEI) (Nguyen et al., 2009a). PLGA/CTAB microparticles were recently developed into stage I clinical trials by Novartis for HIV-1 DNA vaccination. Moreover, it has been seen that the encapsulation of DNA encoding hepatitis B surface antigen (HBsAg) into PLGA nanoparticles could enhance immunity in mice (Nandedkar, 2009).

Despite promising results on antigen transfection *in vitro* (refer to chapter 4 of this present thesis), DOTAP and DDA liposomes did not elicit a strong humoral response in mice and the variability among mice was very high (Figure 5.15). For example, after the boost, DOTAP liposomes encapsulating 1.5 µg/dose of SAM were as immunogenic as NPs at the same antigen dose; however, by reducing SAM dose of 10-fold the potency of DOTAP liposomes was significantly inferior compared to NPs (Figure 5.15). The poor correlation between

protein expression and immunogenicity was reported by Blakney's work where different LNPs (based either on DDA, DOTAP or C12-200) showed different *in vitro* and *in vivo* antigen expression, but comparable antibody titres level *in vivo (*Blakney et al., 2019*)*. This fact was also seen elsewhere (Hassett et al., 2019). Here authors reported that that the R^2 of mRNAs encoding firefly luciferase expression and H10N8 influenza hemagglutinin (HA) antigen immunogenicity was = 0.54, despite the delivery system employed (either MC3-LNPs or DOTAP LNPs) (Hassett et al., 2019). Moreover, poor correlation between protein expression and immunogenicity *in vivo* were detected for DOTAP-containing LNPs at low SAM dose (0.001 mg/kg) (Hassett et al., 2019).

Interestingly, after the boost, while both liposomes elicited low comparable IgG level at 0,15µg/dose of SAM, at higher antigen dose DOTAP liposomes were more potent compared to DDA counterparts (Figure 5.15). Reasons might be several. For example, a relationship between both immunogenicity and expression *in vivo* and particles size was observed, with the best performing formulations being 75–95 nm (Hassett et al., 2019). As discussed in chapter 3 of this thesis, DOTAP liposomes were around 75 nm in size, while DDA particles diameter was around 200nm. This finding might partially explain differences in IgG titres between DOTAP and DDA liposomes (Figure 5.15). In contrast, studies using DDA and DOTAP liposomes have shown the opposite effect. DDA is commonly employed due to adjuvating properties which have previously been shown to enhance immunogenicity of protein vaccines (Nordly et al., 2011). However, it might be worth to notice that generally DDA liposomes induce an insufficient immune response, especially against weak antigens (Brandt et al., 2000a). Accordingly, it has been shown in numerous studies that the level and quality of the immune response induced by DDA-based liposomes can be extensively enhanced by the incorporation of immunostimulators such as monophosphoryl lipid A (MPL), trehalose dibehenate (TDB), monomycoloyl glycerol (MMG) and/or Poly I:C. Monophosphoryl lipid A (Casella and Mitchell, 2008, Christensen et al., 2008). Moreover, it was observed that fully saturated lipids might not be suitable for mRNA and siRNA delivery, while lipids containing 2 to 3 unsaturation in the hydrocarbon chain tend to assume non bilayer H_{II} structures more rapidly. These structures are known to destabilise endosomal membrane and facilitate RNA release in the cytosol (Hafez et al., 2001a).

The T-cell assay on spleen cells from mice that received the boost showed an increase in the antigen specific CD8+ T-cell response compared to CD4+ one and the total frequencies of cytokines production was in correlation with the observed IgG levels (Figure 5.17). Overall, NPs were more effective in promoting cellular rather than humoral immunity. More specifically, NPs showed a greater CD8+ cell response compared to CD4+ one, especially at the highest SAM dose tested, which was superior to those of both DOTAP and DDA

liposomes and comparable to those of CNE and Rabipur (Figure 5.17). Moreover, CD4+ Th1 polarization was due to high secretion of IFN-γ and TNF-α (Figure 5.19), generally associated with an effector phenotype. It is well documented in literature that self-amplifying RNA vaccines induce a higher specific CD8+:CD4+ T cells ratio in immunized mice and a CD4+ Th1/ CD8+ cytotoxic T cell phenotype (Vogel et al., 2018, Brazzoli et al., 2015, Brito et al., 2014b). Furthermore, antigen-specific CD4 T cells are known to be directly involved in helping the effector function of CD8 T cells (Kalams and Walker, 1998, Sun et al., 2004). In addition to intracellular cytokine expression, NPs at high SAM dose induced cell surface expression of CD107a, a specific marker for degranulation associated with cytotoxic activity (Figure 5.18), although the total level of cytotoxic CD8+ T cells was inferior with respect to both positive controls (LNPs and CNE) and the comparator (Figure 5.18). CD8+ T cells play a crucial role in virus clearance; depletion of CD8+ T cells in SAM-influenza (HA) immunized mice reduced survival rate upon lethal viral challenge, confirming the functional contribution of antigen-specific CD8 T cells in mediating viral clearance and conferring protection against virus infection (Hemann et al., 2013). Because the shortest period of incubation of the rabies virus may be less than 2 weeks, effective rabies vaccines should elicit strong humoral and cellular immune responses in a short time to clear virus infection (Charlton et al., 1987). It has been reported that CD8+ T cells were significantly activated in mice immunized with a rabies virus vaccine vector expressing IFN-β as an adjuvant (Faul et al., 2008). Results reported here showed differences in CD8+ T activation induced by the SAM candidates tested, with NPs eliciting higher CD8+ T proliferation compared to both liposomes, which is consistent with differences in immunogenicity. It has been seen that PLGA might play a role in directing the immune response. For instance, the loading of Hepatitis B core antigen into PLGA NPs (300 nm) induced a stronger cellular immune response as compared with Hepatitis B core antigen alone in a mouse model. Moreover, a correlation between particle size and immunogenicity was evaluated previously, with NPs ranging 200–600 nm associated with higher levels of IFN-γ production related to a Th1 response, whereas increasing particles size up to 2000 nm promoted IL-4 secretion related to a Th2 response (Gregory et al., 2013).

5.4.9 Investigation of immunogenicity induced by polymeric and solid lipid nanoparticles administered by three different routes

As discussed above, prior to the boost, antibody titres level induced by either NPs or SLNs injected i.m. were comparable with or superior to those elicited by the commercial vaccine (Figure 5.20 A). However, 2 weeks after the boost, SLNs were significantly more potent to elicit IgG titres compared to NPs, although GMT was still inferior with respect to Rabipur. These differences in potency between SLNs and NPs might be attributed to several aspects. For example, the different solvent/aqueous ratio (FRR) at which formulations were produced in the Nanoassemblr could affect antigen structural stability. It has been seen that solvent

content above 25% during the mixing process might induce RNA transient denaturation, with consequently less bioactivity *in vivo* (Leung et al., 2015). Therefore, in order to minimize this effect, many papers reported that the ideal FRR to formulate ionizable lipid based LNPs is 3:1 aqueous/organic phase (Zhang et al., 2006). In the case reported within this thesis chapter NPs were produced at FRR of 1:1 due to aggregation phenomena occurring at higher rates (refer to chapter 3 of this thesis), whereas it was possible to formulate SLNs at FRR 3:1, at which particles were stable and homogeneously distributed. Moreover, the presence of PEG on the SLN surface might be responsible for the higher potency compared to NPs. The PEG lipid employed here has short (C14) acyl chains which, as seen elsewhere, generated PEG-lipid that can dissociate from the LNP after injection *in vivo*, resulting in potent LNP for siRNA systems (Ambegia et al., 2005). C14 PEG was chosen to reduce *in vivo* anti-PEG immunity, which was seen to be correlated with reduced circulation lifetime and faster clearance (Tam et al., 2013). *In vivo* there are many bioactive materials that the PEG-lipid can associate with including lipoproteins, cells in the circulation and endothelial cells. On the contrary, the major molecules *in vitro* would be serum lipoproteins and albumin, and potentially the plasma membranes of cells (Simoes et al., 2005). It was found that PEGylation *in vitro* might inhibit uptake, while the presence of 2% mol/mol into particles formulation was beneficial for effective immunogenicity (Kulkarni et al., 2017). This contradictory behaviour might also explain the discrepancy between poor *in vitro* expression and increase immune response *in vivo* observed herein this thesis with SLNs (refer to chapter 4). PEG has been used extensively to improve the pharmacokinetic properties of different therapeutic agents and drug nanocarriers. For instance, in a previous study, PEGylated SLNs administered intravenously showed improved *in vivo* transfection capacity and lower toxicity compared to non-PEGylated SLNs (Montana et al., 2007). This might be attributed to the reduced aggregation of positively charged nanoparticles with negatively charged serum proteins and consequently less accumulation in the lungs, liver, and spleen (Simoes et al., 2005). Besides, the lower potency of NPs might be also attributed to particles structure. In a study conducted by Colombo and co-workers, DOTAP:PLGA encapsulating siRNA particles were observed by atomic force microscopy (AFM) and cryo-transmission electron microscopy (cryo-TEM) combined with small angle X-ray scattering (SAXS) and confocal laser scanning microscopy (CLSM)(Colombo et al., 2015). Studies suggested that the siRNA-loaded particles are characterized by a core–shell structure consisting of a PLGA matrix core coated with lamellar DOTAP structures with siRNA localized both in the core and in the shell. Researchers suggested that, as a consequence of this structural organization, siRNA release dynamics mechanisms can be described as i) release of siRNA–DOTAP complexes from the lamellar DOTAP structures on the surface of the particles, eventually combined with ii) diffusion-mediated sustained release and iii) matrix erosion-mediated release (Colombo et al., 2015).

The combination of these multiple mechanisms resulted in a burst release of siRNA, followed by diffusion- and erosion-mediated release, which suggested a co-existence of noncomplexed siRNA, which is released as a burst, and siRNA–DOTAP complexes. The released, noncomplexed siRNA has a poor transfection efficiency, which might explain the reduced potency of NPs compared to SLNs at the same SAM dose (Colombo et al., 2015).

Interestingly, a different trend in IgG titres profile was seen when SAM formulations were administered intradermally. In this case, before the boost, all mice immunized with either SLNs or NPs were responders and elicited antibodies level which was superior to Rabipur, while 2 weeks after the boost, the immunogenicity of SAM loaded SLNs was as high as the vaccine on the market (Figure 5.20 B); moreover, solid lipid nanoparticles were able to induce long-lasting adaptive immunity in a similar manner to the commercial vaccine (Figure 5.21 B). This finding highlighted that a single dose of SAM loaded SLNs was sufficient to elicit greater humoral immunity then the commercial vaccine; besides, the adaptive immunity induced by SAM-SLNs was long-lasting and comparable to the commercial vaccine. According to Rabipur prophylaxis, in previously unvaccinated individuals three doses should be administered to ensure that treatment is successful. These repeated injections inevitably reduce patients' compliance which can lead to vaccine failure if the therapy is not properly followed. Furthermore, the cost of a full course of vaccination, particularly in parts of Asia and Africa, would remain prohibitive (Hicks et al., 2012). Therefore, a vaccine that could achieve protection against rabies, but with fewer injections, would be of great benefit. Thus, solid lipid nanoparticles might represent a more cost-effective alternative for the treatment of rabies. SLNs have been used extensively to incorporate various drugs, as well as imaging agents with the benefits of using physiological and nontoxic lipids (Mehnert and Mäder, 2001). Despite many advantages, this type of nanoparticle remains largely unexplored for sustained oligonucleotide delivery. In addition, a substantial body of literature still focused on intramuscular as preferred injection route for vaccines, although intradermal vaccination was proved to be advantageous for the delivery of plasmid DNA or RNA vaccine to the dermal region, a skin layer abundant in professional APCs in the form of dendritic dermal cells (DDCs) and Langerhans cells (LCs) (Combadiere and Liard, 2011). Moreover, intradermal route was proven to be suitable for DNA-based vaccines delivery through "needle free injection" technology (Ravi et al., 2015), which was seen to improve immunogenicity because of broader dispersion of the injectate than conventional injection (Levine, 2003). This might be of great benefit to improve immunogenicity and develop pain free and cost-effective vaccination. Accordingly, the application of SLNs in dermal delivery were successful due to several reasons. For example, SLNs offer an occlusive effect due to film formation on the skin surface, which reduces trans epidermal water loss. Occlusion also favours drug penetration into the skin. The high specific area of nanometer-sized SLNs enhances contact of

encapsulated drug with the stratum corneum (Jenning et al., 2000). Intradermal application of SLNs was also shown elsewhere to deliver several compounds like Podophyllotoxin, all-trans retinoic acid or ketoprofen (Kakadia and Conway, 2014). The success of SLNs as dermal carriers was attributed to the ability of particles to avoid systemic uptake, with preferential epidermal localization. Moreover, SLNs increased the accumulation of bioactive molecules in the stratum corneum due to small diameters (Chen et al., 2006). Further, the presence of PEG on particles surface might act as skin penetration enhancer. Previous studies showed that PEG had a significant effect on drug penetration when skin structures were hygroscopically manipulated (Sarpotdar et al., 1986). Moreover, the long-lasting response induced by SLNs could be associated to the sustained release of antigen. It may be safely assumed that prolonged immunity results in enhanced protection against a pathogen (Pulendran and Ahmed, 2006). Accordingly, due to the ability to trap drugs within the solid rigid lipid matrix, SLNs have been widely employed to prolong antigen release, therefore enhancing the permanency of the antigen in the injection site and favouring its presentation to APC (Kakadia and Conway, 2014). It was supposed that the sustained release might be dependent on the higher *in vitro* intracellular stability compared to, for example, liposomes, because of which intracellular delivery may be relatively delayed, thereby giving rise to sustained release of its contents (Xue and Wong, 2011). Similar observations of an enhanced stability of SLNs have also been reported for *in vivo* experiments. Recently, DOTAP/Tristearin/PEG SLNs were used to induce *in vivo* sustained release of siRNA after intradermal injection (Lobovkina et al., 2011). Such sustained release of siRNA is indicative of the presence of siRNA within the SLN matrix.

IgG titres elicited by SAM formulations injected intranasally showed that generally very weak response was elicited by candidates, positive control LNPs and the comparator after one antigen dose, whereas the administration of a second dose enhanced the humoral immunity induced by SLNs and LNPs, both higher compared to those induced by Rabipur (Figure 5.20C). The overall poor antibody response induction might be attributed to the lack of a mucosal adjuvant within the formulations i.e. cholera toxin (CT), which are known to enhance immune responses to vaccines when administered via mucosal route(Fukuyama et al., 2015, Rhee et al., 2012). The superiority of SLNs compared to polymeric nanoparticles might be related to the presence of PEG on particles surface which could contribute to overcome the mucosal barrier. As reported elsewhere, PEG enhanced the mobility of particles through the mucus layer, due to its hydrophilicity and neutral surface properties. A study conducted by Vila et al., using intranasal PLA nanoparticles encapsulating tetanus toxoid, showed that non-PEGylated PLA nanoparticles suffered an immediate aggregation upon injection, whereas the PEG-coated nanoparticles remained totally stable (Vila et al., 2004). Authors speculated that PLA nanoparticles were unable to reach the epithelium membrane because they aggregated in

the overlying mucus, consequently affecting the potency of immune response (Vila et al., 2004). In literature, many works indicated that PEG coating caused mucoadhesion or mucopenetration, presumably by interpenetrating polymer network effects between the PEG and the mucus mesh (Ensign et al., 2012) and/or hydrogen bonding (Marks and Lowman, 2011). Generally, polymer concentration in the range of 2-5 mol% may exhibit sufficient mucopenetrating property for biomedical applications. By eliminating the hydrophobic interactions between mucin fibers and hydrophobic nanoparticles core, PEGylation may allow delivery of rapidly moving particles to the mucosa at higher concentrations than otherwise possible with uncoated particles. This might also potentially increase the concentration of therapeutics that can be delivered to the mucosal surfaces of the body (Dawson et al., 2004). On the contrary, the absence of PEG on NPs surface might induce aggregation in the nostril and a consequent mucociliary clearance, which could reduce the residence time of the SAM in the nasal cavity. Moreover, SLNs were seen to be efficient in escaping the RES, thereby prolonging the residence time in the nose (Brioschi et al., 2009).

With respect to the T cell response in spleens different routes of administration elicited different cell activation pathways. SAM loaded SLNs and NPs injected i.m. and i.d. induced comparable CD4+ and CD8+ cell levels, which were non- significantly different compared to those of Rabipur (Figure 5.22). Interestingly, intranasal administration of SLNs increased production of activated CD4+ T cells compared to Rabipur. Moreover, those activated T cells showed a predominant Th0 phenotype. In the lungs, a similar trend was observed with higher production of Th0 CD4+ T cells induced by SLNs compared to the vaccine on the market (Figure 5.25). The aforementioned better CD4 response was attributed to a great production of IL-2 cytokine and related combinations induced by SAM adjuvanted with SLNs. Accordingly, literature reported that intranasal administration of vaccine protein subunits increased IL-2 proliferation *in vivo* (Tomoda et al., 1995, Kang et al., 2012). It was observed that continued presence of IL-2, throughout the period of the immune response might have a role in enhancing vaccine potency (Heath, 1995). Besides, it has been documented that interleukin 2 could act as an adjuvant to increase the potency of inactivated rabies virus vaccine (Nunberg et al., 1989). Together with this finding, authors also reported that IL-2 induced minimal increase of rabies neutralizing antibody titres, despite enhanced vaccinal protection. Therefore, it was concluded that cellular immunity plays an important role in protection against rabies virus infection (Mifune et al., 1981). In fact, protection against peripheral rabies virus challenge could be obtained in the absence of detectable virus-neutralizing antibodies by using a vaccine consisting of the rabies virus ribonucleoprotein (Dietzschold et al., 1987). Other studies have also noted a lack of correlation between virus-neutralizing antibody titre and protection in rabies vaccination (Dietzschold et al., 1987). Regarding cytotoxic T cells activation in spleens, data showed that, despite the administration

route, few CD107a+ CD4+ T cells were elicited by all candidates tested, while CD8+ cytotoxic T cells were activated in a greater extent. Moreover, no differences were seen in CD8+ CD107a+ cells between candidates and Rabipur when formulations were injected i.m., whereas after i.d. and i.n. injection SLNs were more potent than the vaccine on the market in activating CD8 cytotoxic T cells (Figure 5.24). A similar trend was observed in lungs (Figure 5.24), which was found to be consistent and in correlation with the observed IgG titres levels and with data reported in literature (Magini et al., 2016, Rittig et al., 2011, Phua et al., 2014). Notably, cytotoxic T lymphocytes (CTLs) play a crucial role in the local clearance or containment of mucosal viral infections.

5.5 Conclusions

In the present chapter, the pharmacokinetic profiles *in vivo* of either SAM loaded or antigen-free cationic polymeric nanoparticles (NPs), solid lipid nanoparticles (SLNs) and cationic nanoemulsions (CNE) showed that positive surface charge is not the only parameter which drives the distribution of carriers *in vivo*, but other factors, such as particle size, might play a relevant role, with smaller and PEGylated particles accumulating faster to the lymph nodes. Moreover, the change of cationic lipid did not significantly alter formulations clearance profile *in vivo*. Despite promising results on antigen transfection *in vitro* SAM loaded liposomes did not elicit a strong humoral response in mice at all time points tested, confirming the poor correlation between *in vitro* antigen expression and immune response. On the contrary, prior to the boost, SAM NPs at the lowest antigen dose were as potent as the commercial vaccine to elicit humoral response after i.m. injection. This proved that the association between self-amplifying RNA vaccine and polymeric nanoparticles resulted in more cost-effective Rabies vaccine alternatives which possessed potency comparable to the licenced vaccine. Further, all SAM vaccine candidates could induce cellular response – especially Rabies-specific CD8+ T-cells – although the frequency of activated T cells was inferior compared to Rabipur. Interestingly, SLNs injected i.m. showed increased immunogenicity compared to both NPs and the licenced vaccine after a single dose, confirming the suitability of SAM platform in combination with a particulate delivery system to induce efficient immunity *in vivo*. Moreover, the potency of SLNs was also seen after intradermal administration, where SLNs were as potent as Rabipur to elicit IgG titre in mice after two antigen doses, inducing both innate and adaptive immunity in a similar extent to the vaccine on the market. This finding is directly associated with development of a considerably more economical rabies vaccine approach, which require reduced frequency of administration and long-lasting immunity, along with the possibility of painless (i.e. needle free) administration. Overall, these improvements would be of great benefit for patients' compliance. Herein it was also reported

that two doses of SAM SLNs injected i.n. induced a humoral immunity which was higher than the one elicited by Rabipur. Interestingly, intranasal administration of SLNs increased production of activated CD4+ IL-2+ T cells compared to the licenced vaccine in both spleens and lungs. However, despite significant difference observed among formulations in the ability to elicit both humoral and cellular immune response, immunogenicity did not correlate with biodistribution; carriers' pharmacokinetics were indeed similar probably due to the short timeframe tested. All together, these findings are encouraging and demonstrate that coformulation of SAM vaccine and solid lipid nanoparticles might be a valid and more advantageous alternative to commercially available rabies vaccines, with augmented patients' safety and compliance.

CHAPTER 6

Conclusions

6.1 Final conclusions

The starting aim of the present thesis project was to develop more novel and cost-effective alternatives to already established vaccines against Rabies using a self-amplifying RNA platform (SAM). In order to maintain antigen biological integrity and enhance the *in vitro* and *in vivo* expression, SAM was combined with four cationic delivery systems – liposomes, solid lipid nanoparticles (SLNs), polymeric nanoparticles (NPs) and cationic nanoemulsions (CNE). Microfluidics and Microfluidisation were tested first as new manufacturing technologies. Herein, as a validation step, anionic SLNs encapsulating protein model antigen (OVA) were first produced. Data reported herein this project highlighted that it is possible to effectively formulate, manufacture, purify and monitor the particle size of SLNs produced by two different methods. Within this study, SLNs at approx. 200 nm or below containing low and high PEGylation and incorporating OVA were formulated with both techniques. The modification of the PEGylation allowed to explore these delivery systems as potential adjuvants (low PEGylation) and for therapeutic drug delivery (high PEGylation). However, despite promising results obtained with microfluidisation - rapid manufacture (2 cycles) and at a low pressure (20,000 psi) and removal of non-entrapped protein achieved after 12 diafiltration cycles - the need for large volumes for sample production might limit its applicability for development of new formulations at early stage or for samples containing expensive excipients. Therefore, Microfluidisation was used only for the size reduction of CNE due to incompatibility between CNE components and microfluidics chip. Moreover, microfluidics was demonstrated to be a valid alternative method for high-throughput manufacturing of both empty and protein loaded solid lipid nanoparticles preparation which require low operating volumes (between 1 and 5 mL). Both the total flow rate and the flow rate ratio were identified as critical process parameters and particles physicochemical attributes were confirmed to be suitable for pre-clinical and clinical applications. Furthermore, using microfluidics method it was possible to combine particles manufacturing and drug encapsulation in a single process step, with evident benefits for time of production.

The adoption of these methods for further development of cationic adjuvants for a self-amplifying RNA vaccine was found to be successful. Results suggested that, by applying either Microfluidics or Microfluidisation, narrow size and monodisperse particles with highly positive electronic dense core were obtained. Moreover, the addition of nucleic acid either inside or outside particles notably increased formulations average diameter, without however detrimentally compromise formulations stability. Indeed, particles physicochemical attributes were confirmed to be suitable for pre-clinical and clinical applications. Moreover, cationic carriers were equally able to protect SAM from biological degradation and either encapsulate or adsorb the whole antigen amount added at the beginning.

Further, it was proved that particles can be simply and effectively sterilised using γ-irradiation prior to incubation with cells. *In vitro*, the four different cationic delivery systems were evaluated according to their ability to efficiently trigger antigen expression in different cell lines. It emerged that toxicity in both MBDM, DCs and BHK was cationic lipid dose dependent. In terms of uptake in BMDM, while SAM loading DOTAP based formulations uptake was comparable 24 hours post incubation, DDA based particles showed a greater difference among them, with SAM encapsulating liposomes and SAM adsorbing emulsions having much higher uptake. In BHK cells, even though no significant difference in particles uptake has been shown by expressing data as percentage of DilC+ cells, discrepancies among formulations in uptake efficiency were indeed evident by analysing mean fluorescence intensity values (MFI), with DOTAP SLNs and NPs having significantly higher MFI values compared to the other formulations; however, despite this, absolute values were inferior compared to 5% FCS condition. In FCS-free media, NPs resulted in the highest MFI, which directly translated in more polymeric particles uptake by BHK. Moreover, it was shown that moving from DOTAP to DDA reduced the overall MFI of formulations. However, despite the promising results on cellular internalisation, antigen expression in BMDM was not achieved. On the other hand, *in vitro* potency (IVP) assays in BHK cell line with both SAM-GFP and SAM-Rabies based formulations showed that DOTAP polymeric nanoparticles and both DDA and DOTAP liposomes had the greater ability to induce antigen expression in BHK cells, despite the choice of the antigen and the presence of serum. Thus, these formulations were selected to progress *in vivo* to better understand their immunogenicity in a mouse model.

The pharmacokinetic profiles *in vivo* of either SAM loaded or antigen-free cationic NPs, SLNs and CNE showed that positive surface charge is not the only parameter which drives the distribution of carriers, but other factors, such as particle size, might play a relevant role, with smaller and PEGylated particles accumulating faster to the lymph nodes. Moreover, the change of cationic lipid did not significantly alter formulations clearance profile *in vivo*. Despite promising results on antigen transfection *in vitro* SAM loaded liposomes did not elicit a strong humoral response in mice at all time point tested, confirming the poor correlation between *in vitro* antigen expression and immune response. On the contrary, prior to the boost, SAM NPs at the lowest antigen dose were as potent as the commercial vaccine to elicit humoral response after i.m. injection. This proved that the association between self-amplifying RNA vaccine and polymeric nanoparticles resulted in a valid Rabies vaccine alternative which possessed potency comparable to the licensed vaccine after a single dose. Further, all SAM vaccine candidates injected i.m. could induce a cellular response – especially Rabies-specific CD8+ T-cells – although the frequency of activated T cells was inferior compared to Rabipur. Interestingly, SLNs injected i.m. showed increased immunogenicity compared to both NPs and the licensed vaccine after a single dose, confirming the suitability of SAM platform in

combination with a particulate delivery system to induce efficient immunity *in vivo*. Moreover, the potency of SLNs was also seen after intradermal administration, where SLNs were as potent as Rabipur to elicit IgG titer in mice after two antigen doses, inducing both adaptive immunity in a similar extent to the vaccine on the market. This finding is directly associated with development of a considerably more economical rabies vaccine approach, which require reduced frequency of administration and long-lasting immunity, along with the possibility of painless (i.e. needle free) administration. Overall, these improvements would be of great benefit for patients' compliance. Herein it was also reported that two doses of SAM SLNs injected i.n. induced a humoral immunity which was higher than the one elicited by Rabipur. Interestingly, intranasal administration of SLNs increased production of activated CD4+ IL-2+ T cells compared to the licensed vaccine in both spleens and lungs. However, despite significant difference observed among formulations in the ability to elicit both humoral and cellular immune response, immunogenicity did not correlate with biodistribution; carriers' pharmacokinetics were indeed similar probably due to the short timeframe tested.

All together, these findings are encouraging and demonstrate that coformulation of SAM vaccine and solid lipid nanoparticles might be a valid and more advantageous alternative to commercially available rabies vaccines, with augmented patients' safety and compliance

CHAPTER 7

References

7.1 References

1998. Analytical Methods for the Characterization of Cationic Lipid–Nucleic Acid Complexes. 9**,** 341-351.

A L AUDOUY, S., LEIJ, L., HOEKSTRA, D. & MOLEMA, G. 2002. In Vivo Characteristics of Cationic Liposomes as Delivery Vectors for Gene Therapy. *Pharmaceutical research,* 19**,** 1599-605.

ABDELAZIZ, H. M., FREAG, M. S. & ELZOGHBY, A. O. 2019. Chapter 5 - Solid Lipid Nanoparticle-Based Drug Delivery for Lung Cancer. *In:* KESHARWANI, P. (ed.) *Nanotechnology-Based Targeted Drug Delivery Systems for Lung Cancer.* Academic Press.

ABOU-SALEH, R., SWAIN, M., EVANS, S. & THOMSON, N. 2014. Poly(ethylene glycol) Lipid-Shelled Microbubbles: Abundance, Stability, and Mechanical Properties. *Langmuir : the ACS journal of surfaces and colloids,* 30.

ADRIAN, J. E., MORSELT, H. W. M., SÜSS, R., BARNERT, S., KOK, J. W., ÁSGEIRSDÓTTIR, S. A., RUITERS, M. H. J., MOLEMA, G. & KAMPS, J. A. A. M. 2010. Targeted SAINT-O-Somes for improved intracellular delivery of siRNA and cytotoxic drugs into endothelial cells. *Journal of Controlled Release,* 144**,** 341-349.

AFONSO, C. L., AMARASINGHE, G. K., BANYAI, K., BAO, Y., BASLER, C. F., BAVARI, S., BEJERMAN, N., BLASDELL, K. R., BRIAND, F. X., BRIESE, T., BUKREYEV, A., CALISHER, C. H., CHANDRAN, K., CHENG, J., CLAWSON, A. N., COLLINS, P. L., DIETZGEN, R. G., DOLNIK, O., DOMIER, L. L., DURRWALD, R., DYE, J. M., EASTON, A. J., EBIHARA, H., FARKAS, S. L., FREITAS-ASTUA, J., FORMENTY, P., FOUCHIER, R. A., FU, Y., GHEDIN, E., GOODIN, M. M., HEWSON, R., HORIE, M., HYNDMAN, T. H., JIANG, D., KITAJIMA, E. W., KOBINGER, G. P., KONDO, H., KURATH, G., LAMB, R. A., LENARDON, S., LEROY, E. M., LI, C. X., LIN, X. D., LIU, L., LONGDON, B., MARTON, S., MAISNER, A., MUHLBERGER, E., NETESOV, S. V., NOWOTNY, N., PATTERSON, J. L., PAYNE, S. L., PAWESKA, J. T., RANDALL, R. E., RIMA, B. K., ROTA, P., RUBBENSTROTH, D., SCHWEMMLE, M., SHI, M., SMITHER, S. J., STENGLEIN, M. D., STONE, D. M., TAKADA, A., TERREGINO, C., TESH, R. B., TIAN, J. H., TOMONAGA, K., TORDO, N., TOWNER, J. S., VASILAKIS, N., VERBEEK, M., VOLCHKOV, V. E., WAHL-JENSEN, V., WALSH, J. A., WALKER, P. J., WANG, D., WANG, L. F., WETZEL, T., WHITFIELD, A. E., XIE, J. T., YUEN, K. Y., ZHANG, Y. Z. & KUHN, J. H. 2016. Taxonomy of the order Mononegavirales: update 2016. *Arch Virol,* 161**,** 2351-60.

AKINC, A., QUERBES, W., DE, S., QIN, J., FRANK-KAMENETSKY, M., JAYAPRAKASH, K. N., JAYARAMAN, M., RAJEEV, K. G., CANTLEY, W. L., DORKIN, J. R., BUTLER, J. S., QIN, L., RACIE, T., SPRAGUE, A., FAVA, E., ZEIGERER, A., HOPE, M. J., ZERIAL, M., SAH, D. W. Y., FITZGERALD, K., TRACY, M. A., MANOHARAN, M., KOTELIANSKY, V., FOUGEROLLES, A. D. & MAIER, M. A. 2010. Targeted delivery of RNAi therapeutics with endogenous and exogenous ligand-based mechanisms. *Molecular therapy : the journal of the American Society of Gene Therapy,* 18**,** 1357-1364.

ALDAYEL, A. M., O'MARY, H. L., VALDES, S. A., LI, X., THAKKAR, S. G., MUSTAFA, B. E. & CUI, Z. 2018. Lipid nanoparticles with minimum burst release of TNF-α siRNA show strong activity against rheumatoid arthritis unresponsive to methotrexate. *Journal of Controlled Release,* 283**,** 280-289.

ALEGRE, M. L., LEEMANS, J., LE MOINE, A., FLORQUIN, S., DE WILDE, V., CHONG, A. & GOLDMAN, M. 2008. The multiple facets of toll-like receptors in transplantation biology. *Transplantation,* 86**,** 1-9.

ALI, M. H., KIRBY, D. J., MOHAMMED, A. R. & PERRIE, Y. 2010. Solubilisation of drugs within liposomal bilayers: alternatives to cholesterol as a membrane stabilising agent. 62**,** 1646-1655.

ALLÉMANN, E., GURNY, R. & DOELKER, E. 1992. Preparation of aqueous polymeric nanodispersions by a reversible salting-out process: influence of process parameters on particle size. *International Journal of Pharmaceutics,* 87**,** 247-253.

ALMEIDA, A. J., RUNGE, S. & MÜLLER, R. H. 1997. Peptide-loaded solid lipid nanoparticles (SLN): Influence of production parameters. *International Journal of Pharmaceutics,* 149**,** 255-265.

ALMEIDA, A. J. & SOUTO, E. 2007. Solid lipid nanoparticles as a drug delivery system for peptides and proteins. *Advanced Drug Delivery Reviews,* 59**,** 478-490.

ALMOFTI, R., HARASHIMA, H., SHINOHARA, Y., ALMOFTI, A., LI, W. & KIWADA, H. 2003. Lipoplex size determines lipofection efficiency with or without serum. *Molecular membrane biology,* 20**,** 35-43.

AMBEGIA, E., ANSELL, S., CULLIS, P., HEYES, J., PALMER, L. & MACLACHLAN, I. 2005. Stabilized plasmid–lipid particles containing PEG-diacylglycerols exhibit extended circulation lifetimes and tumor selective gene expression. *Biochimica et Biophysica Acta (BBA) - Biomembranes,* 1669**,** 155-163.

ANDERLUZZI, G., LOU, G., SU, Y. & PERRIE, Y. 2019. Scalable manufacturing of solid lipid nanoparticles. *Pharmaceutical Nanotechnology,* 07.

ANDERLUZZI, G. & PERRIE, Y. 2019. Microfluidic Manufacture of Solid Lipid Nanoparticles: A Case Study on Tristearin-Based Systems. *Drug Delivery Letters,* 9**,** 1-12.

ANDERSON, A. & SHWIFF, S. A. 2015. The Cost of Canine Rabies on Four Continents. *Transbound Emerg Dis,* 62**,** 446-52.

ANSAR AHMED, S., GOGAL, R. M. & WALSH, J. E. 1994. A new rapid and simple non-radioactive assay to monitor and determine the proliferation of lymphocytes: an alternative to [3H]thymidine incorporation assay. *Journal of Immunological Methods,* 170**,** 211-224.

ANSELMO, A., ZHANG, M., KUMAR, S., VOGUS, D., MENEGATTI, S., ., M. H. & ET AL. 2015. Elasticity of Nanoparticles Influences Their Blood Circulation, Phagocytosis, Endocytosis and Targeting. *ACS Nano,* 9**,** 3169-3177.

ANTON, N., BENOIT, J.-P. & SAULNIER, P. 2008. Design and production of nanoparticles formulated from nano-emulsion templates—A review. *Journal of controlled release : official journal of the Controlled Release Society,* 128**,** 185-99.

ASUMADU-MENSAH, A., SMITH, K. W. & RIBEIRO, H. S. 2013. Solid Lipid Dispersions: Potential Delivery System for Functional Ingredients in Foods. 78**,** E1000-E1008.

ATKINS, G. J., FLEETON, M. N. & SHEAHAN, B. J. 2008. Therapeutic and prophylactic applications of alphavirus vectors. *Expert Rev Mol Med,* 10**,** e33.

B JEFFS, L., R PALMER, L., G AMBEGIA, E., GIESBRECHT, C., EWANICK, S. & MACLACHLAN, I. 2005. A Scalable, Extrusion-Free Method for Efficient Liposomal Encapsulation of Plasmid DNA. *Pharmaceutical research,* 22**,** 362-72.

BACHMANN, M. F., KOPF, M. & MARSLAND, B. J. 2006. Chemokines: more than just road signs. *Nature Reviews Immunology,* 6**,** 159.

BACON, A., CAPARROS-WANDERLEY, W., ZADI, B. & GREGORIADIS, G. 2002. Induction of a cytotoxic T lymphocyte (CTL) response to plasmid DNA delivered by Lipodine™. *Journal of liposome research,* 12**,** 173-83.

BAHL, K., SENN, J. J., YUZHAKOV, O., BULYCHEV, A., BRITO, L. A., HASSETT, K. J., LASKA, M. E., SMITH, M., ALMARSSON, Ö., THOMPSON, J., RIBEIRO, A., WATSON, M., ZAKS, T. & CIARAMELLA, G. 2017. Preclinical and Clinical Demonstration of Immunogenicity by mRNA Vaccines against H10N8 and H7N9 Influenza Viruses. *Molecular Therapy,* 25**,** 1316-1327.

BAILEY, S. R., NELSON, M. H., HIMES, R. A., LI, Z., MEHROTRA, S. & PAULOS, C. M. 2014. Th17 cells in cancer: the ultimate identity crisis. *Front Immunol,* 5**,** 276.

BALBINO, T. A., AZZONI, A. R. & DE LA TORRE, L. G. 2013. Microfluidic devices for continuous production of pDNA/cationic liposome complexes for gene delivery and vaccine therapy. *Colloids and Surfaces B: Biointerfaces,* 111**,** 203-210.

BALLY, F., GARG, D. K., SERRA, C. A., HOARAU, Y., ANTON, N., BROCHON, C., PARIDA, D., VANDAMME, T. & HADZIIOANNOU, G. J. P. V. 2012. Improved size-tunable preparation of polymeric nanoparticles by microfluidic nanoprecipitation. 5045-5051.

BANCHEREAU, J. & STEINMAN, R. M. 1998. Dendritic cells and the control of immunity. *Nature,* 392**,** 245-52.

BANDHOLTZ, L., KREUGER, M. R., SVANHOLM, C., WIGZELL, H. & ROTTENBERG, M. E. 2002. Adjuvant modulation of the immune responses and the outcome of infection with Chlamydia pneumoniae. *Clinical and experimental immunology,* 130**,** 393-403.

BANGHAM, A. D., STANDISH, M. M. & WATKINS, J. C. 1965. Diffusion of univalent ions across the lamellae of swollen phospholipids. *Journal of Molecular Biology,* 13**,** 238-IN27.

BARNIER-QUER, C., ELSHARKAWY, A., ROMEIJN, S., KROS, A. & JISKOOT, W. 2013. Adjuvant effect of cationic liposomes for subunit influenza vaccine: influence of antigen loading method, cholesterol and immune modulators. *Pharmaceutics,* 5**,** 392-410.

BATTAGLIA, L., GALLARATE, M., PANCIANI, P. P., UGAZIO, E., SAPINO, S., PEIRA, E. & CHIRIO, D. 2015. Techniques for the Preparation of Solid Lipid Nano and Microparticles.

BAYLOR, N. W., EGAN, W. & RICHMAN, P. 2002. Aluminum salts in vaccines--US perspective. *Vaccine,* 20 Suppl 3**,** S18-23.

BECKER PERES, L., BECKER PERES, L., DE ARAÚJO, P. H. H. & SAYER, C. 2016. Solid lipid nanoparticles for encapsulation of hydrophilic drugs by an organic solvent free double emulsion technique. *Colloids and Surfaces B: Biointerfaces,* 140**,** 317-323.

BEHR, J. P., DEMENEIX, B., LOEFFLER, J. P. & PEREZ-MUTUL, J. 1989. Efficient gene transfer into mammalian primary endocrine cells with lipopolyamine-coated DNA. *Proceedings of the National Academy of Sciences of the United States of America,* 86**,** 6982-6986.

BELLIVEAU, N. M., HUFT, J., LIN, P. J. C., CHEN, S., LEUNG, A. K. K., LEAVER, T. J., WILD, A. W., LEE, J. B., TAYLOR, R. J., TAM, Y. K., HANSEN, C. L. & CULLIS, P. R. 2012. Microfluidic Synthesis of Highly Potent Limit-size Lipid Nanoparticles for In Vivo Delivery of siRNA. *Molecular Therapy - Nucleic Acids,* 1**,** e37.

BHAMBERE, D., A. GAIDHANI, K., HARWALKAR, M. & S. NIRGUDE, P. 2015. LYOPHILIZATION / FREEZE DRYING – A REVIEW. *World Journal of Pharmaceutical Research,* 4**,** 516-543.

BILATI, U., ALLEMANN, E. & DOELKER, E. 2005. Poly(D,L-lactide-co-glycolide) protein-loaded nanoparticles prepared by the double emulsion method--processing and formulation issues for enhanced entrapment efficiency. *J Microencapsul,* 22**,** 205-14.

BJORK, S. M. & JOENSSON, H. N. 2019. Microfluidics for cell factory and bioprocess development. *Current Opinion in Biotechnology,* 55**,** 95-102.

BJORKMAN, P. J., SAPER, M. A., SAMRAOUI, B., BENNETT, W. S., STROMINGER, J. L. & WILEY, D. C. 1987. Structure of the human class I histocompatibility antigen, HLA-A2. *Nature,* 329**,** 506-12.

BLAKNEY, A. K., MCKAY, P. F., YUS, B. I., ALDON, Y. & SHATTOCK, R. J. 2019. Inside out: optimization of lipid nanoparticle formulations for exterior complexation and in vivo delivery of saRNA. *Gene Therapy,* 26**,** 363-372.

BODMEIER, R. & HUAGANG, C. 1990. Indomethacin polymeric nanosuspensions prepared by microfujidization. *Journal of Controlled Release,* 12**,** 223-233.

BOGERS, W. M., OOSTERMEIJER, H., MOOIJ, P., KOOPMAN, G., VERSCHOOR, E. J., DAVIS, D., ULMER, J. B., BRITO, L. A., CU, Y., BANERJEE, K., OTTEN, G. R., BURKE, B., DEY, A., HEENEY, J. L., SHEN, X., TOMARAS, G. D., LABRANCHE, C., MONTEFIORI, D. C., LIAO, H.-X., HAYNES, B., GEALL, A. J. & BARNETT, S. W. 2015. Potent immune responses in

rhesus macaques induced by nonviral delivery of a self-amplifying RNA vaccine expressing HIV type 1 envelope with a cationic nanoemulsion. *The Journal of infectious diseases,* 211**,** 947-955.

BORCHARD, G. 2001. Borchard, G. Chitosans for gene delivery. Adv Drug Deliv Rev 52: 145-150. *Advanced drug delivery reviews,* 52**,** 145-50.

BOTTEGA, R. & EPAND, R. M. 1992. Inhibition of protein kinase C by cationic amphiphiles. *Biochemistry,* 31**,** 9025-9030.

BOUCHEMAL, K., BRIANCON, S., COUENNE, F., FESSI, H. & TAYAKOUT, M. 2006. Stability studies on colloidal suspensions of polyurethane nanocapsules. *J Nanosci Nanotechnol,* 6**,** 3187-92.

BOUSSIF, O., LEZOUALC'H, F., ZANTA, M. A., MERGNY, M. D., SCHERMAN, D., DEMENEIX, B. & BEHR, J. P. 1995. A versatile vector for gene and oligonucleotide transfer into cells in culture and in vivo: polyethylenimine. *Proceedings of the National Academy of Sciences of the United States of America,* 92**,** 7297-7301.

BOWIE, A. G. & UNTERHOLZNER, L. 2008. Viral evasion and subversion of pattern-recognition receptor signalling. *Nat Rev Immunol,* 8**,** 911-22.

BRAASCH, D., JENSEN, S., LIU, Y., KAUR, K., ARAR, K., A WHITE, M. & COREY, D. 2003. RNA Interference in Mammalian Cells by Chemically-Modified RNA †. *Biochemistry,* 42**,** 7967-75.

BRACK, C., HIRAMA, M., LENHARD-SCHULLER, R. & TONEGAWA, S. 1978. A complete immunoglobulin gene is created by somatic recombination. *Cell,* 15**,** 1-14.

BRANDT, L., ELHAY, M., ROSENKRANDS, I., LINDBLAD, E. B. & ANDERSEN, P. 2000a. ESAT-6 subunit vaccination against Mycobacterium tuberculosis. *Infection and immunity,* 68**,** 791-795.

BRANDT, L., ELHAY, M., ROSENKRANDS, I., LINDBLAD, E. B. & ANDERSEN, P. 2000b. ESAT-6 Subunit Vaccination againstMycobacterium tuberculosis. 68**,** 791-795.

BRAZZOLI, M., MAGINI, D., BONCI, A., BUCCATO, S., GIOVANI, C., KRATZER, R., ZURLI, V., MANGIAVACCHI, S., CASINI, D., BRITO, L. M., DE GREGORIO, E., MASON, P. W., ULMER, J. B., GEALL, A. J. & BERTHOLET, S. 2015. Induction of Broad-Based Immunity and Protective Efficacy by Self-amplifying mRNA Vaccines Encoding Influenza Virus Hemagglutinin. *Journal of virology,* 90**,** 332-344.

BREITFELD, D., OHL, L., KREMMER, E., ELLWART, J., SALLUSTO, F., LIPP, M. & FORSTER, R. 2000. Follicular B helper T cells express CXC chemokine receptor 5, localize to B cell follicles, and support immunoglobulin production. *J Exp Med,* 192**,** 1545-52.

BREWER, J., POLLOCK, K., TETLEY, L. & RUSSELL, D. 2004. Vesicle Size Influences the Trafficking, Processing, and Presentation of Antigens in Lipid Vesicles. *Journal of immunology (Baltimore, Md. : 1950),* 173**,** 6143-50.

BRGLES, M., HABJANEC, L., HALASSY, B. & TOMASIĆ, J. 2009. Liposome fusogenicity and entrapment efficiency of antigen determine the Th1/Th2 bias of antigen-specific immune response. *Vaccine,* 27**,** 5435-42.

BRIGELIUS-FLOHE, R. & TRABER, M. G. 1999. Vitamin E: function and metabolism. *Faseb j,* 13**,** 1145-55.

BRILLO, J., INES POMMRICH, A. & MEYER, A. 2011. Relation between Self-Diffusion and Viscosity in Dense Liquids: New Experimental Results from Electrostatic Levitation. *Physical review letters,* 107**,** 165902.

BRIOSCHI, A. M., CALDERONI, S., ZARA, G. P., PRIANO, L., GASCO, M. R. & MAURO, A. 2009. Chapter 11 - Solid lipid nanoparticles for brain tumors therapy: State of the art and novel challenges. *In:* SHARMA, H. S. (ed.) *Progress in Brain Research.* Elsevier.

BRITO, L. A., CHAN, M., SHAW, C. A., HEKELE, A., CARSILLO, T., SCHAEFER, M., ARCHER, J., SEUBERT, A., OTTEN, G. R., BEARD, C. W., DEY, A. K., LILJA, A., VALIANTE, N. M., MASON, P. W., MANDL, C. W., BARNETT, S. W., DORMITZER, P. R., ULMER, J. B.,

SINGH, M., O'HAGAN, D. T. & GEALL, A. J. 2014a. A cationic nanoemulsion for the delivery of next-generation RNA vaccines. *Mol Ther,* 22**,** 2118-29.

BRITO, L. A., CHAN, M., SHAW, C. A., HEKELE, A., CARSILLO, T., SCHAEFER, M., ARCHER, J., SEUBERT, A., OTTEN, G. R., BEARD, C. W., DEY, A. K., LILJA, A., VALIANTE, N. M., MASON, P. W., MANDL, C. W., BARNETT, S. W., DORMITZER, P. R., ULMER, J. B., SINGH, M., O'HAGAN, D. T. & GEALL, A. J. 2014b. A Cationic Nanoemulsion for the Delivery of Next-generation RNA Vaccines. *Molecular Therapy,* 22**,** 2118-2129.

BURKE, B., SUMNER, S., MAITLAND, N. & LEWIS, C. E. 2002. Macrophages in gene therapy: cellular delivery vehicles and in vivo targets. 72**,** 417-428.

BURNET, F. M. 1976. A modification of Jerne's theory of antibody production using the concept of clonal selection. *CA Cancer J Clin,* 26**,** 119-21.

BUSATTO, S., VILANILAM, G., TICER, T., LIN, W. L., DICKSON, D. W., SHAPIRO, S., BERGESE, P. & WOLFRAM, J. 2018. Tangential Flow Filtration for Highly Efficient Concentration of Extracellular Vesicles from Large Volumes of Fluid. *Cells,* 7.

CALABRO, S., TRITTO, E., PEZZOTTI, A., TACCONE, M., MUZZI, A., BERTHOLET, S., DE GREGORIO, E., O'HAGAN, D. T., BAUDNER, B. & SEUBERT, A. 2013. The adjuvant effect of MF59 is due to the oil-in-water emulsion formulation, none of the individual components induce a comparable adjuvant effect. *Vaccine,* 31**,** 3363-9.

CAMPBELL, P. I. 1983. Toxicity of some charged lipids used in liposome preparations. *Cytobios,* 37**,** 21-6.

CAMPBELL, R. B., BALASUBRAMANIAN, S. V. & STRAUBINGER, R. M. 2001. Phospholipid-cationic lipid interactions: influences on membrane and vesicle properties. *Biochimica et Biophysica Acta (BBA) - Biomembranes,* 1512**,** 27-39.

CAPRIOTTI, A. L., CARACCIOLO, G., CARUSO, G., FOGLIA, P., POZZI, D., SAMPERI, R. & LAGANÀ, A. 2011. Differential analysis of "protein corona" profile adsorbed onto different nonviral gene delivery systems. *Analytical Biochemistry,* 419**,** 180-189.

CARACCIOLO, G., CALLIPO, L., DE SANCTIS, S. C., CAVALIERE, C., POZZI, D. & LAGANA, A. 2010. Surface adsorption of protein corona controls the cell internalization mechanism of DC-Chol-DOPE/DNA lipoplexes in serum. *Biochim Biophys Acta,* 1798**,** 536-43.

CARACCIOLO, G., POZZI, D., CAMINITI, R., MARCHINI, C., MONTANI, M., AMICI, A. & AMENITSCH, H. 2007. Transfection efficiency boost by designer multicomponent lipoplexes. *Biochimica et Biophysica Acta (BBA) - Biomembranes,* 1768**,** 2280-2292.

CARACCIOLO, G., POZZI, D., CAPRIOTTI, A. L., CAVALIERE, C., FOGLIA, P., AMENITSCH, H. & LAGANA, A. 2011. Evolution of the protein corona of lipid gene vectors as a function of plasma concentration. *Langmuir,* 27**,** 15048-53.

CARMONA-RIBEIRO, A. M., ORTIS, F., SCHUMACHER, R. I. & ARMELIN, M. C. S. 1997. Interactions between Cationic Vesicles and Cultured Mammalian Cells. *Langmuir,* 13**,** 2215-2218.

CARMONARIBEIRO, A. 2000. Interactions between cationic liposomes and drugs or biomolecules. Anais da Academia Brasileira de Ciências 72: 39-43. *Anais da Academia Brasileira de Ciências,* 72**,** 39.

CARTER, D. & REED, S. G. 2010. Role of adjuvants in modeling the immune response. *Curr Opin HIV AIDS,* 5**,** 409-13.

CASELLA, C. R. & MITCHELL, T. C. 2008. Putting endotoxin to work for us: monophosphoryl lipid A as a safe and effective vaccine adjuvant. *Cellular and molecular life sciences : CMLS,* 65**,** 3231-3240.

CERQUEIRA, M., PINHEIRO, A., SILVA, H., RAMOS, P., AZEVEDO, M. A., FLORES-LÓPEZ, M., RIVERA, M., BOURBON, A., RAMOS, O. & VICENTE, A. 2014. Design of Bio-nanosystems for Oral Delivery of Functional Compounds. *Food Engineering Reviews,* 6.

CHAMPION, J. A. & MITRAGOTRI, S. 2006. Role of target geometry in phagocytosis. 103**,** 4930-4934.

CHARLTON, K. M., CASEY, G. A. & CAMPBELL, J. B. 1987. Experimental rabies in skunks: Immune response and salivary gland infection. *Comparative Immunology, Microbiology and Infectious Diseases,* 10**,** 227-235.

CHATTERJEE, S. & PAL, J. K. 2009. Role of 5'- and 3'-untranslated regions of mRNAs in human diseases. *Biol Cell,* 101**,** 251-62.

CHAUDHURY, M. K. & WHITESIDES, G. M. 1991. Direct measurement of interfacial interactions between semispherical lenses and flat sheets of poly(dimethylsiloxane) and their chemical derivatives. *Langmuir,* 7**,** 1013-1025.

CHEN, D.-B., YANG, T.-Z., LU, W.-L. & ZHANG, Q. 2001. In Vitro and in Vivo Study of Two Types of Long-Circulating Solid Lipid Nanoparticles Containing Paclitaxel. *Chemical and Pharmaceutical Bulletin,* 49**,** 1444-1447.

CHEN, H., CHANG, X., DU, D., LIU, W., LIU, J., WENG, T., YANG, Y., XU, H. & YANG, X. 2006. Podophyllotoxin-loaded solid lipid nanoparticles for epidermal targeting. *Journal of Controlled Release,* 110**,** 296-306.

CHOI, W.-J., KIM, J.-K., CHOI, S.-H., PARK, J.-S., AHN, W. S. & KIM, C.-K. 2004. Low toxicity of cationic lipid-based emulsion for gene transfer. *Biomaterials,* 25**,** 5893-5903.

CHOI, Y. & CHANG, J. 2013. Viral vectors for vaccine applications. *Clinical and experimental vaccine research,* 2**,** 97-105.

CHONO, S., TANINO, T., SEKI, T. & MORIMOTO, K. 2006. Influence of particle size on drug delivery to rat alveolar macrophages following pulmonary administration of ciprofloxacin incorporated into liposomes. *Journal of Drug Targeting,* 14**,** 557-566.

CHRISTENSEN, D., KIRBY, D., FOGED, C., AGGER, E. M., ANDERSEN, P., PERRIE, Y. & NIELSEN, H. M. 2008. α,α'-trehalose 6,6'-dibehenate in non-phospholipid-based liposomes enables direct interaction with trehalose, offering stability during freeze-drying. *Biochimica et Biophysica Acta (BBA) - Biomembranes,* 1778**,** 1365-1373.

CHRISTENSEN, D., KORSHOLM, K. S., ANDERSEN, P. & AGGER, E. M. 2011. Cationic liposomes as vaccine adjuvants. *Expert Rev Vaccines,* 10**,** 513-21.

CHUNG, S. K., SHIN, G. H., JUNG, M. K., HWANG, I. C. & PARK, H. J. 2014. Factors influencing the physicochemical characteristics of cationic polymer-coated liposomes prepared by high-pressure homogenization. *Colloids and Surfaces A: Physicochemical and Engineering Aspects,* 454**,** 8-15.

CIANI, L. 2004. DOTAP/DOPE and DC-Chol/DOPE lipoplexes for gene delivery: zeta potential measurements and electron spin resonance spectra. *Biochimica et Biophysica Acta (BBA) - Biomembranes*.

COLLETIER, J.-P., CHAIZE, B., WINTERHALTER, M. & FOURNIER, D. 2002. Protein encapsulation in liposomes: efficiency depends on interactions between protein and phospholipid bilayer. *BMC Biotechnology,* 2**,** 9.

COLOMBO, S., CUN, D., REMAUT, K., BUNKER, M., ZHANG, J., MARTIN-BERTELSEN, B., YAGHMUR, A., BRAECKMANS, K., NIELSEN, H. M. & FOGED, C. 2015. Mechanistic profiling of the siRNA delivery dynamics of lipid–polymer hybrid nanoparticles. *Journal of Controlled Release,* 201**,** 22-31.

COMBADIERE, B. & LIARD, C. 2011. Transcutaneous and intradermal vaccination. *Human Vaccines,* 7**,** 811-827.

CONRAD, M. L., YILDIRIM, A. Ö., SONAR, S. S., KıLıÇ, A., SUDOWE, S., LUNOW, M., TEICH, R., RENZ, H. & GARN, H. 2009. Comparison of adjuvant and adjuvant-free murine experimental asthma models. 39**,** 1246-1254.

CONZELMANN, K. K. 1998. Nonsegmented negative-strand RNA viruses: genetics and manipulation of viral genomes. *Annu Rev Genet,* 32**,** 123-62.

CORDEIRO, A. S., CRECENTE-CAMPO, J., BOUZO, B. L., GONZÁLEZ, S. F., DE LA FUENTE, M. & ALONSO, M. J. 2019. Engineering polymeric nanocapsules for an efficient drainage and biodistribution in the lymphatic system. *Journal of Drug Targeting,* 27**,** 646-658.

COX, J. C. & COULTER, A. R. 1997. Adjuvants—a classification and review of their modes of action. *Vaccine,* 15**,** 248-256.

CU, Y., BRODERICK, K. E., BANERJEE, K., HICKMAN, J., OTTEN, G., BARNETT, S., KICHAEV, G., SARDESAI, N. Y., ULMER, J. B. & GEALL, A. 2013a. Enhanced Delivery and Potency of Self-Amplifying mRNA Vaccines by Electroporation in Situ. *Vaccines,* 1**,** 367-383.

CU, Y., BRODERICK, K. E., BANERJEE, K., HICKMAN, J., OTTEN, G., BARNETT, S., KICHAEV, G., SARDESAI, N. Y., ULMER, J. B. & VACCINES, A. G. J. 2013b. Enhanced Delivery and Potency of Self-Amplifying mRNA Vaccines by Electroporation in Situ.

CUI, J., LI, C., GUO, W., LI, Y., WANG, C., ZHANG, L., ZHANG, L., HAO, Y. & WANG, Y. 2007. Direct comparison of two pegylated liposomal doxorubicin formulations: Is AUC predictive for toxicity and efficacy? *Journal of Controlled Release,* 118**,** 204-215.

CULLIS, P. R. & DE KRUIJFF, B. 1979. Lipid polymorphism and the functional roles of lipids in biological membranes. *Biochim Biophys Acta,* 559**,** 399-420.

DACHEUX, L., DELMAS, O. & BOURHY, H. 2011. Human rabies encephalitis prevention and treatment: progress since Pasteur's discovery. *Infect Disord Drug Targets,* 11**,** 251-99.

DALWADI, G., BENSON, H. A. E. & CHEN, Y. J. P. R. 2005. Comparison of Diafiltration and Tangential Flow Filtration for Purification of Nanoparticle Suspensions. 22**,** 2152-2162.

DALWADI, G. & SUNDERLAND, V. 2007. *Purification of PEGylated Nanoparticles Using Tangential Flow Filtration (TFF).*

DAN, N. 2002. Effect of liposome charge and PEG polymer layer thickness on cell-liposome electrostatic interactions. *Biochimica et biophysica acta,* 1564**,** 343-8.

DASS, C. R. & CHOONG, P. F. M. 2006. Selective gene delivery for cancer therapy using cationic liposomes: In vivo proof of applicability. *Journal of Controlled Release,* 113**,** 155-163.

DAVID J. BEEBE, GLENNYS A. MENSING, A. & WALKER, G. M. 2002. Physics and Applications of Microfluidics in Biology. 4**,** 261-286.

DAVIDSEN, J., ROSENKRANDS, I., CHRISTENSEN, D., VANGALA, A., KIRBY, D., PERRIE, Y., AGGER, E. M. & ANDERSEN, P. 2005. Characterization of cationic liposomes based on dimethyldioctadecylammonium and synthetic cord factor from M. tuberculosis (trehalose 6,6'-dibehenate)—A novel adjuvant inducing both strong CMI and antibody responses. *Biochimica et Biophysica Acta (BBA) - Biomembranes,* 1718**,** 22-31.

DAVIS, D. & GREGORIADIS, G. 1987. Liposomes as adjuvants with immunopurified tetanus toxoid: influence of liposomal characteristics. *Immunology,* 61**,** 229-234.

DAWSON, M., WIRTZ, D. & HANES, J. 2004. Enhanced Viscoelasticity of Human Cystic Fibrotic Sputum Correlates with Increasing Microheterogeneity in Particle Transport. *The Journal of biological chemistry,* 278**,** 50393-401.

DE BEUCKELAER, A., POLLARD, C., VAN LINT, S., ROOSE, K., VAN HOECKE, L., NAESSENS, T., UDHAYAKUMAR, V. K., SMET, M., SANDERS, N., LIENENKLAUS, S., SAELENS, X., WEISS, S., VANHAM, G., GROOTEN, J. & DE KOKER, S. 2016. Type I Interferons Interfere with the Capacity of mRNA Lipoplex Vaccines to Elicit Cytolytic T Cell Responses. *Molecular Therapy,* 24**,** 2012-2020.

DE GREGORIO, E., TRITTO, E. & RAPPUOLI, R. 2008. Alum adjuvanticity: unraveling a century old mystery. *Eur J Immunol,* 38**,** 2068-71.

DE LIMA, G. F., DE SOUZA, A. G. & ROSA, D. S. 2018. Effect of adsorption of polyethylene glycol (PEG), in aqueous media, to improve cellulose nanostructures stability. *Journal of Molecular Liquids,* 268**,** 415-424.

DE NARDO, P., GENTILOTTI, E., VAIRO, F., NGUHUNI, B., CHAULA, Z., NICASTRI, E., ISMAIL, A. & IPPOLITO, G. 2018. A retrospective evaluation of bites at risk of rabies transmission

across 7 years: The need to improve surveillance and reporting systems for rabies elimination. *PLoS One,* 13**,** e0197996.

DE SERRANO, L. O. & BURKHART, D. J. 2017. Liposomal vaccine formulations as prophylactic agents: design considerations for modern vaccines. *Journal of Nanobiotechnology,* 15**,** 83.

DEERING, R. P., KOMMAREDDY, S., ULMER, J. B., BRITO, L. A. & GEALL, A. J. 2014. Nucleic acid vaccines: prospects for non-viral delivery of mRNA vaccines. *Expert Opin Drug Deliv,* 11**,** 885-99.

DIETZSCHOLD, B., WANG, H. H., RUPPRECHT, C. E., CELIS, E., TOLLIS, M., ERTL, H., HEBER-KATZ, E. & KOPROWSKI, H. 1987. Induction of protective immunity against rabies by immunization with rabies virus ribonucleoprotein. *Proceedings of the National Academy of Sciences of the United States of America,* 84**,** 9165-9169.

DIMOV, N., KASTNER, E., HUSSAIN, M., PERRIE, Y. & SZITA, N. 2017. Formation and purification of tailored liposomes for drug delivery using a module-based micro continuous-flow system. *Scientific Reports,* 7**,** 12045.

DRAKE, J. R. 2019. Signaling Cross-Talk between MHC Class II Molecular Conformers in Resting Murine B Cells. *ImmunoHorizons,* 3**,** 28-36.

DUCAT, E., EVRARD, B., PEULEN, O. & PIEL, G. 2011. Cellular uptake of liposomes monitored by confocal microscopy and flow cytometry. *Journal of Drug Delivery Science and Technology,* 21**,** 469-477.

ENSIGN, L. M., SCHNEIDER, C., SUK, J. S., CONE, R. & HANES, J. 2012. Mucus penetrating nanoparticles: biophysical tool and method of drug and gene delivery. *Advanced materials (Deerfield Beach, Fla.),* 24**,** 3887-3894.

ERTL, H. C. J. 2009. Novel Vaccines to Human Rabies. *PLOS Neglected Tropical Diseases,* 3**,** e515.

ESPUELAS, S., IRACHE, J. & GAMAZO, C. 2005. Synthetic particulate antigen delivery systems for vaccination. *Inmunologia,* 24**,** 208-223.

EVANS, J. S., HORTON, D. L., EASTON, A. J., FOOKS, A. R. & BANYARD, A. C. 2012. Rabies virus vaccines: Is there a need for a pan-lyssavirus vaccine? *Vaccine,* 30**,** 7447-7454.

FABER, M., PULMANAUSAHAKUL, R., HODAWADEKAR, S. S., SPITSIN, S., MCGETTIGAN, J. P., SCHNELL, M. J. & DIETZSCHOLD, B. 2002. Overexpression of the rabies virus glycoprotein results in enhancement of apoptosis and antiviral immune response. *Journal of virology,* 76**,** 3374-3381.

FARHOOD, H., BOTTEGA, R., EPAND, R. M. & HUANG, L. 1992. Effect of cationic cholesterol derivatives on gene transfer and protein kinase C activity. *Biochim Biophys Acta,* 1111**,** 239-46.

FARHOOD, H., SERBINA, N. & HUANG, L. 1995. The role of dioleoyl phosphatidylethanolamine in cationic liposome mediated gene transfer. *Biochimica et Biophysica Acta (BBA) - Biomembranes,* 1235**,** 289-295.

FAUL, E. J., WANJALLA, C. N., MCGETTIGAN, J. P. & SCHNELL, M. J. 2008. Interferon-beta expressed by a rabies virus-based HIV-1 vaccine vector serves as a molecular adjuvant and decreases pathogenicity. *Virology,* 382**,** 226-38.

FELGNER, P. L., GADEK, T. R., HOLM, M., ROMAN, R., CHAN, H. W., WENZ, M., NORTHROP, J. P., RINGOLD, G. M. & DANIELSEN, M. 1987a. Lipofection: a highly efficient, lipid-mediated DNA-transfection procedure. 84**,** 7413-7417.

FELGNER, P. L., GADEK, T. R., HOLM, M., ROMAN, R., CHAN, H. W., WENZ, M., NORTHROP, J. P., RINGOLD, G. M. & DANIELSEN, M. 1987b. Lipofection: a highly efficient, lipid-mediated DNA-transfection procedure. *Proceedings of the National Academy of Sciences of the United States of America,* 84**,** 7413-7417.

FERRARI, M. E., RUSALOV, D., ENAS, J. & WHEELER, C. J. 2001. Trends in lipoplex physical properties dependent on cationic lipid structure, vehicle and complexation

procedure do not correlate with biological activity. *Nucleic Acids Research,* 29**,** 1539-1548.

FERRARI, M. E., RUSALOV, D., ENAS, J. & WHEELER, C. J. 2002. Synergy between cationic lipid and co-lipid determines the macroscopic structure and transfection activity of lipoplexes. *Nucleic acids research,* 30**,** 1808-1816.

FICK, A. 1995. On liquid diffusion.pdf. *Journal of Membrane Science,* 100**,** 6.

FILION, M. C. & PHILLIPS, N. C. 1997. Toxicity and immunomodulatory activity of liposomal vectors formulated with cationic lipids toward immune effector cells. *Biochimica et Biophysica Acta (BBA) - Biomembranes,* 1329**,** 345-356.

FINKE, S., MUELLER-WALDECK, R. & CONZELMANN, K. K. 2003. Rabies virus matrix protein regulates the balance of virus transcription and replication. *J Gen Virol,* 84**,** 1613-21.

FINKELMAN, F. D., SHEA-DONOHUE, T., MORRIS, S. C., GILDEA, L., STRAIT, R., MADDEN, K. B., SCHOPF, L. & URBAN, J. F., JR. 2004. Interleukin-4- and interleukin-13-mediated host protection against intestinal nematode parasites. *Immunol Rev,* 201**,** 139-55.

FISHER, C. R., STREICKER, D. G. & SCHNELL, M. J. 2018. The spread and evolution of rabies virus: conquering new frontiers. *Nat Rev Microbiol,* 16**,** 241-255.

FLEETON, M. N., CHEN, M., BERGLUND, P., RHODES, G., PARKER, S. E., MURPHY, M., ATKINS, G. J. & LILJESTROM, P. 2001. Self-replicative RNA vaccines elicit protection against influenza A virus, respiratory syncytial virus, and a tickborne encephalitis virus. *J Infect Dis,* 183**,** 1395-8.

FLETCHER, S., AHMAD, A., PEROUZEL, E., HERON, A., MILLER, A. D. & JORGENSEN, M. R. 2006. In vivo studies of dialkynoyl analogues of DOTAP demonstrate improved gene transfer efficiency of cationic liposomes in mouse lung. *J Med Chem,* 49**,** 349-57.

FLOCH, V., LOISEL, S., GUÉNIN, E., CÉCILE HERVÉ, A., CLAUDE CLÉMENT, J., JACQUES YAOUANC, J., ABBAYES H, D. & FÉREC, C. 2000. Cation Substitution in Cationic Phosphonolipids: A New Concept To Improve Transfection Activity and Decrease Cellular Toxicity. *Journal of medicinal chemistry,* 43**,** 4617-28.

FORBES, N., HUSSAIN, M. T., BRIUGLIA, M. L., EDWARDS, D. P., HORST, J. H. T., SZITA, N. & PERRIE, Y. 2019. Rapid and scale-independent microfluidic manufacture of liposomes entrapping protein incorporating in-line purification and at-line size monitoring. *International Journal of Pharmaceutics,* 556**,** 68-81.

FOROOZANDEH, P. & AZIZ, A. A. 2018. Insight into Cellular Uptake and Intracellular Trafficking of Nanoparticles. *Nanoscale research letters,* 13**,** 339-339.

FOX, C. B., MULLIGAN, S. K., SUNG, J., DOWLING, Q. M., FUNG, H. W. M., VEDVICK, T. S. & COLER, R. N. 2014. Cryogenic transmission electron microscopy of recombinant tuberculosis vaccine antigen with anionic liposomes reveals formation of flattened liposomes. *International journal of nanomedicine,* 9**,** 1367-1377.

FREIMARK, B., BLEZINGER, P., FLORACK, V., NORDSTROM, J., LONG, S., DESHPANDE, D., NOCHUMSON, S. & PETRAK, K. 1998. Cationic lipids enhance cytokine and cell influx levels in the lung following administration of plasmid: Cationic lipid complexes. *Journal of immunology (Baltimore, Md. : 1950),* 160**,** 4580-6.

FREUND, J., CASALS, J. & HOSMER, E. P. 1937. Sensitization and Antibody Formation after Injection of Tubercle Bacilli and Paraffin Oil. *Proceedings of the Society for Experimental Biology and Medicine,* 37**,** 509-513.

FROS, J. J. & PIJLMAN, G. P. 2016. Alphavirus Infection: Host Cell Shut-Off and Inhibition of Antiviral Responses. *Viruses,* 8**,** 166.

FUKUYAMA, Y., OKADA, K., YAMAGUCHI, M., KIYONO, H., MORI, K. & YUKI, Y. 2015. Nasal Administration of Cholera Toxin as a Mucosal Adjuvant Damages the Olfactory System in Mice. *PLOS ONE,* 10**,** e0139368.

GAO, H. & HUI, K. M. 2001. Synthesis of a novel series of cationic lipids that can act as efficient gene delivery vehicles through systematic heterocyclic substitution of cholesterol derivatives. *Gene Therapy,* 8**,** 855-863.

GARCON, N., VAUGHN, D. W. & DIDIERLAURENT, A. M. 2012. Development and evaluation of AS03, an Adjuvant System containing alpha-tocopherol and squalene in an oil-in-water emulsion. *Expert Rev Vaccines,* 11**,** 349-66.

GAVI, E., KUBICKI, D., PADRON, G. A. & ÖZCAN-TAŞKıN, N. G. 2018. Breakup of nanoparticle clusters using Microfluidizer M110-P. *Chemical Engineering Research and Design,* 132**,** 902-912.

GEALL, A., VERMA, A., OTTEN, G., A SHAW, C., HEKELE, A., BANERJEE, K., CU, Y., BEARD, C., BRITO, L., KRUCKER, T., O'HAGAN, D., SINGH, M., W MASON, P., VALIANTE, N., DORMITZER, P., W BARNETT, S., RAPPUOLI, R., B ULMER, J. & MANDL, C. 2012a. *Nonviral delivery of self-amplifying RNA vaccines*.

GEALL, A. J., MANDL, C. W. & ULMER, J. B. 2013. RNA: The new revolution in nucleic acid vaccines. *Seminars in Immunology,* 25**,** 152-159.

GEALL, A. J., VERMA, A., OTTEN, G. R., SHAW, C. A., HEKELE, A., BANERJEE, K., CU, Y., BEARD, C. W., BRITO, L. A., KRUCKER, T., O'HAGAN, D. T., SINGH, M., MASON, P. W., VALIANTE, N. M., DORMITZER, P. R., BARNETT, S. W., RAPPUOLI, R., ULMER, J. B. & MANDL, C. W. 2012b. Nonviral delivery of self-amplifying RNA vaccines. 109**,** 14604-14609.

GEERAEDTS, F., GOUTAGNY, N., HORNUNG, V., SEVERA, M., DE HAAN, A., POOL, J., WILSCHUT, J., FITZGERALD, K. A. & HUCKRIEDE, A. 2008. Superior immunogenicity of inactivated whole virus H5N1 influenza vaccine is primarily controlled by Toll-like receptor signalling. *PLoS Pathog,* 4**,** e1000138.

GEIJTENBEEK, T. B. & GRINGHUIS, S. I. 2016. C-type lectin receptors in the control of T helper cell differentiation. *Nat Rev Immunol,* 16**,** 433-48.

GHIMIRE, T. R., BENSON, R. A., GARSIDE, P. & BREWER, J. M. 2012. Alum increases antigen uptake, reduces antigen degradation and sustains antigen presentation by DCs in vitro. *Immunol Lett,* 147**,** 55-62.

GIBIS, M., ZEEB, B. & WEISS, J. 2014. Formation, characterization, and stability of encapsulated hibiscus extract in multilayered liposomes. *Food Hydrocolloids,* 38**,** 28-39.

GILBERT, S. C. 2013. Clinical development of Modified Vaccinia virus Ankara vaccines. *Vaccine,* 31**,** 4241-6.

GOLDBACH, P., BROCHART, H., WEHRLÉ, P. & STAMM, A. 1995. Sterile filtration of liposomes: Retention of encapsulated carboxyfluorescein. *International Journal of Pharmaceutics,* 117**,** 225-230.

GOYAL, S., KLASSERT, T. E., SLEVOGT, H. J. M. M. & IMMUNOLOGY 2016. C-type lectin receptors in tuberculosis: what we know. 205**,** 513-535.

GRABIELLE-MADELMONT, C., LESIEUR, S. & OLLIVON, M. 2003. Characterization of loaded liposomes by size exclusion chromatography. *Journal of biochemical and biophysical methods,* 56**,** 189-217.

GREGORIADIS, G., SAFFIE, R. & DE SOUZA, J. B. 1997. Liposome-mediated DNA vaccination. 402**,** 107-110.

GREGORY, A. E., TITBALL, R. & WILLIAMSON, D. 2013. Vaccine delivery using nanoparticles. *Frontiers in cellular and infection microbiology,* 3**,** 13-13.

GULATI, P. 2009. Janeway's Immunobiology, 7th Edition by Kenneth Murphy, Paul Travers, and Mark Walport. 37**,** 134-134.

HAFEZ, I., MAURER, N. & CULLIS, P. 2001a. On the mechanism whereby cationic lipids promote intracellular delivery of polynucleic acids. *Gene therapy,* 8**,** 1188-96.

HAFEZ, I. M., ANSELL, S. & CULLIS, P. R. 2000. Tunable pH-Sensitive Liposomes Composed of Mixtures of Cationic and Anionic Lipids. *Biophysical Journal,* 79**,** 1438-1446.

HAFEZ, I. M., MAURER, N. & CULLIS, P. R. 2001b. On the mechanism whereby cationic lipids promote intracellular delivery of polynucleic acids. *Gene Therapy,* 8**,** 1188-1196.

HAMPSON, K., COUDEVILLE, L., LEMBO, T., SAMBO, M., KIEFFER, A., ATTLAN, M., BARRAT, J., BLANTON, J. D., BRIGGS, D. J., CLEAVELAND, S., COSTA, P., FREULING, C. M., HIBY, E., KNOPF, L., LEANES, F., MESLIN, F. X., METLIN, A., MIRANDA, M. E., MULLER, T., NEL, L. H., RECUENCO, S., RUPPRECHT, C. E., SCHUMACHER, C., TAYLOR, L., VIGILATO, M. A., ZINSSTAG, J. & DUSHOFF, J. 2015. Estimating the global burden of endemic canine rabies. *PLoS Negl Trop Dis,* 9**,** e0003709.

HARANDI, A. M., DAVIES, G. & OLESEN, O. F. 2009. Vaccine adjuvants: scientific challenges and strategic initiatives. *Expert Rev Vaccines,* 8**,** 293-8.

HARASHIMA, H., IIDA, S., URAKAMI, Y., TSUCHIHASHI, M. & KIWADA, H. 1999. Optimization of antitumor effect of liposomally encapsulated doxorubicin based on simulations by pharmacokinetic/pharmacodynamic modeling. *Journal of Controlled Release,* 61**,** 93-106.

HARRINGTON, L. E., HATTON, R. D., MANGAN, P. R., TURNER, H., MURPHY, T. L., MURPHY, K. M. & WEAVER, C. T. 2005. Interleukin 17-producing CD4+ effector T cells develop via a lineage distinct from the T helper type 1 and 2 lineages. *Nat Immunol,* 6**,** 1123-32.

HASSETT, K. J., BENENATO, K. E., JACQUINET, E., LEE, A., WOODS, A., YUZHAKOV, O., HIMANSU, S., DETERLING, J., GEILICH, B. M., KETOVA, T., MIHAI, C., LYNN, A., MCFADYEN, I., MOORE, M. J., SENN, J. J., STANTON, M. G., ALMARSSON, Ö., CIARAMELLA, G. & BRITO, L. A. 2019. Optimization of Lipid Nanoparticles for Intramuscular Administration of mRNA Vaccines. *Molecular Therapy - Nucleic Acids,* 15**,** 1-11.

HATTORI, Y., SUZUKI, S., KAWAKAMI, S., YAMASHITA, F. & HASHIDA, M. 2005. The role of dioleoylphosphatidylethanolamine (DOPE) in targeted gene delivery with mannosylated cationic liposomes via intravenous route. *Journal of Controlled Release,* 108**,** 484-495.

HAYWARD, R. C., UTADA, A. S., DAN, N. & WEITZ, D. A. 2006. Dewetting instability during the formation of polymersomes from block-copolymer-stabilized double emulsions. *Langmuir,* 22**,** 4457-61.

HE, Z., HU, Y., NIE, T., TANG, H., ZHU, J., CHEN, K., LIU, L., LEONG, K. W., CHEN, Y. & MAO, H.-Q. 2018. Size-controlled lipid nanoparticle production using turbulent mixing to enhance oral DNA delivery. *Acta Biomaterialia,* 81**,** 195-207.

HEATH, A. W. 1995. Cytokines as Immunological Adjuvants. *In:* POWELL, M. F. & NEWMAN, M. J. (eds.) *Vaccine Design: The Subunit and Adjuvant Approach.* Boston, MA: Springer US.

HEDLEY, M. L., CURLEY, J. & URBAN, R. 1998. Microspheres containing plasmid-encoded antigens elicit cytotoxic T-cell responses. *Nat Med,* 4**,** 365-8.

HEIDENREICH, R., JASNY, E., KOWALCZYK, A., LUTZ, J., PROBST, J., BAUMHOF, P., SCHEEL, B., VOSS, S., KALLEN, K.-J. & FOTIN-MLECZEK, M. 2015. A novel RNA-based adjuvant combines strong immunostimulatory capacities with a favorable safety profile. 137**,** 372-384.

HEINZEL, F. P., SADICK, M. D., HOLADAY, B. J., COFFMAN, R. L. & LOCKSLEY, R. M. 1989. Reciprocal expression of interferon gamma or interleukin 4 during the resolution or progression of murine leishmaniasis. Evidence for expansion of distinct helper T cell subsets. *J Exp Med,* 169**,** 59-72.

HEKELE, A., BERTHOLET, S., ARCHER, J., GIBSON, D. G., PALLADINO, G., BRITO, L. A., OTTEN, G. R., BRAZZOLI, M., BUCCATO, S., BONCI, A., CASINI, D., MAIONE, D., QI, Z.-Q., GILL, J. E., CAIAZZA, N. C., URANO, J., HUBBY, B., GAO, G. F., SHU, Y., DE GREGORIO, E., MANDL, C. W., MASON, P. W., SETTEMBRE, E. C., ULMER, J. B., CRAIG VENTER, J., DORMITZER, P. R., RAPPUOLI, R. & GEALL, A. J. 2013. Rapidly produced SAM(®) vaccine against H7N9 influenza is immunogenic in mice. *Emerging microbes & infections,* 2**,** e52-e52.

HELGASON, T., SALMINEN, H., KRISTBERGSSON, K., MCCLEMENTS, D. J. & WEISS, J. 2015. Formation of transparent solid lipid nanoparticles by microfluidization: Influence of lipid physical state on appearance. *Journal of Colloid and Interface Science,* 448**,** 114-122.

HEM, S. L. & HOGENESCH, H. 2007. Relationship between physical and chemical properties of aluminum-containing adjuvants and immunopotentiation. *Expert Rev Vaccines,* 6**,** 685-98.

HEM, S. L., JOHNSTON, C. T. & HOGENESCH, H. 2007. Imject Alum is not aluminum hydroxide adjuvant or aluminum phosphate adjuvant. *Vaccine,* 25**,** 4985-6.

HEMANN, E. A., KANG, S.-M. & LEGGE, K. L. 2013. Protective CD8 T Cell–Mediated Immunity against Influenza A Virus Infection following Influenza Virus–like Particle Vaccination. 191**,** 2486-2494.

HENRIKSEN-LACEY, M., BRAMWELL, V. W., CHRISTENSEN, D., AGGER, E. M., ANDERSEN, P. & PERRIE, Y. 2010a. Liposomes based on dimethyldioctadecylammonium promote a depot effect and enhance immunogenicity of soluble antigen. *Journal of Controlled Release,* 142**,** 180-186.

HENRIKSEN-LACEY, M., CHRISTENSEN, D., BRAMWELL, V. W., LINDENSTRØM, T., AGGER, E. M., ANDERSEN, P. & PERRIE, Y. 2010b. Liposomal cationic charge and antigen adsorption are important properties for the efficient deposition of antigen at the injection site and ability of the vaccine to induce a CMI response. *Journal of Controlled Release,* 145**,** 102-108.

HENRIKSEN-LACEY, M., CHRISTENSEN, D., BRAMWELL, V. W., LINDENSTRØM, T., AGGER, E. M., ANDERSEN, P. & PERRIE, Y. 2011a. Comparison of the Depot Effect and Immunogenicity of Liposomes Based on Dimethyldioctadecylammonium (DDA), 3β-[N-(N',N'-Dimethylaminoethane)carbomyl] Cholesterol (DC-Chol), and 1,2-Dioleoyl-3-trimethylammonium Propane (DOTAP): Prolonged Liposome Retention Mediates Stronger Th1 Responses. *Molecular Pharmaceutics,* 8**,** 153-161.

HENRIKSEN-LACEY, M., DEVITT, A. & PERRIE, Y. 2011b. The vesicle size of DDA:TDB liposomal adjuvants plays a role in the cell-mediated immune response but has no significant effect on antibody production. *J Control Release,* 154**,** 131-7.

HEO, M. B. & LIM, Y. T. 2014. Programmed nanoparticles for combined immunomodulation, antigen presentation and tracking of immunotherapeutic cells. *Biomaterials,* 35**,** 590-600.

HEYES, J., PALMER, L., BREMNER, K. & MACLACHLAN, I. 2005. Cationic lipid saturation influences intracellular delivery of encapsulated nucleic acids. *Journal of Controlled Release,* 107**,** 276-287.

HICKS, D. J., FOOKS, A. R. & JOHNSON, N. 2012. Developments in rabies vaccines. *Clinical and experimental immunology,* 169**,** 199-204.

HILGERS, L. A., SNIPPE, H., JANSZE, M. & WILLERS, J. M. 1984. Immunomodulating properties of two synthetic adjuvants: dependence upon type of antigen, dose, and time of administration. *Cell Immunol,* 86**,** 393-401.

HIPPALGAONKAR, K., MAJUMDAR, S. & KANSARA, V. 2010. Injectable Lipid Emulsions—Advancements, Opportunities and Challenges. *AAPS PharmSciTech,* 11**,** 1526-40.

HIRAYAMA, D., IIDA, T. & NAKASE, H. 2017. The Phagocytic Function of Macrophage-Enforcing Innate Immunity and Tissue Homeostasis. *International journal of molecular sciences,* 19**,** 92.

HIRSCH-LERNER, D. & BARENHOLZ, Y. 1999. Hydration of lipoplexes commonly used in gene delivery: follow-up by laurdan fluorescence changes and quantification by differential scanning calorimetry. *Biochimica et Biophysica Acta (BBA) - Biomembranes,* 1461**,** 47-57.

HIRSCH-LERNER, D., ZHANG, M., ELIYAHU, H., FERRARI, M., WHEELER, C. & BARENHOLZ, Y. 2005. Effect of "helper lipid" on lipoplex electrostatics. *Biochimica et biophysica acta,* 1714**,** 71-84.

HIRSJÄRVI, S., PELTONEN, L. & HIRVONEN, J. 2009. Effect of sugars, surfactant, and tangential flow filtration on the freeze-drying of poly(lactic acid) nanoparticles. *AAPS PharmSciTech,* 10**,** 488-494.

HOEKSTRA, S. A. D. 2001. Cationic lipid-mediated transfection in vitro and in vivo. *Molecular Membrane Biology,* 18**,** 129-143.

HOERR, I., OBST, R., RAMMENSEE, H. G. & JUNG, G. 2000. In vivo application of RNA leads to induction of specific cytotoxic T lymphocytes and antibodies. *Eur J Immunol,* 30**,** 1-7.

HOGENESCH, H., O'HAGAN, D. & FOX, C. 2018. Optimizing the utilization of aluminum adjuvants in vaccines: you might just get what you want. *npj Vaccines,* 3.

HOLTEN-ANDERSEN, L., DOHERTY, T. M., KORSHOLM, K. S. & ANDERSEN, P. 2004. Combination of the Cationic Surfactant Dimethyl Dioctadecyl Ammonium Bromide and Synthetic Mycobacterial Cord Factor as an Efficient Adjuvant for Tuberculosis Subunit Vaccines. 72**,** 1608-1617.

HONG, S.-S., KIM, S. H. & LIM, S.-J. 2015. Effects of triglycerides on the hydrophobic drug loading capacity of saturated phosphatidylcholine-based liposomes. *International Journal of Pharmaceutics,* 483**,** 142-150.

HOOPER, D. C., MORIMOTO, K., BETTE, M., WEIHE, E., KOPROWSKI, H. & DIETZSCHOLD, B. 1998. Collaboration of antibody and inflammation in clearance of rabies virus from the central nervous system. *J Virol,* 72**,** 3711-9.

HOUSELEY, J. & TOLLERVEY, D. 2009. The many pathways of RNA degradation. *Cell,* 136**,** 763-76.

HU, F. Q., HONG, Y. & YUAN, H. 2004. Preparation and characterization of solid lipid nanoparticles containing peptide. *International journal of pharmaceutics,* 273**,** 29-35.

HUANG, M.-Z., YANG, R.-J., TAI, C.-H., TSAI, C.-H. & FU, L.-M. J. B. M. 2006. Application of electrokinetic instability flow for enhanced micromixing in cross-shaped microchannel. 8**,** 309-315.

HUI, S. W., LANGNER, M., ZHAO, Y. L., ROSS, P., HURLEY, E. & CHAN, K. 1996. The role of helper lipids in cationic liposome-mediated gene transfer. *Biophysical journal,* 71**,** 590-599.

HUNTER, M., JOHNSON, N., HEDDERWICK, S., MCCAUGHEY, C., LOWRY, K., MCCONVILLE, J., HERRON, B., MCQUAID, S., MARSTON, D., GODDARD, T., HARKESS, G., GOHARRIZ, H., VOLLER, K., SOLOMON, T., WILLOUGHBY, R. E. & FOOKS, A. R. 2010. Immunovirological correlates in human rabies treated with therapeutic coma. *J Med Virol,* 82**,** 1255-65.

HUTCHISON, S., BENSON, R. A., GIBSON, V. B., POLLOCK, A. H., GARSIDE, P. & BREWER, J. M. 2012. Antigen depot is not required for alum adjuvanticity. *Faseb j,* 26**,** 1272-9.

HYVÖNEN, Z., PLOTNIECE, A., REINE, I., CHEKAVICHUS, B., DUBURS, G. & URTTI, A. 2000. Novel cationic amphiphilic 1,4-dihydropyridine derivatives for DNA delivery. *Biochimica et Biophysica Acta (BBA) - Biomembranes,* 1509**,** 451-466.

IAVARONE, C., O'HAGAN, D., YU, D., DELAHAYE, N. & ULMER, J. 2017. Mechanism of action of mRNA-based vaccines. *Expert Review of Vaccines,* 16**,** 10.

IBRAHIM, H., BINDSCHAEDLER, C., DOELKER, E., BURI, P. & GURNY, R. 1992. Aqueous nanodispersions prepared by a salting-out process. *International Journal of Pharmaceutics,* 87**,** 239-246.

ILIES, MARC A., SEITZ, WILLIAM A., CAPROIU, MIRON T., WENTZ, M., GARFIELD, ROBERT E. & BALABAN, ALEXANDRU T. 2003. Pyridinium-Based Cationic Lipids as Gene-Transfer Agents. 2003**,** 2645-2655.

INDROVA, M., BUBENIK, J., SIMOVA, J., VONKA, V., NEMECKOVA, S., MENDOZA, L. & REINIS, M. 2001. Therapy of HPV 16-associated carcinoma with dendritic cell-based vaccines: in vitro priming of the effector cell responses by DC pulsed with tumour lysates and synthetic RAHYNIVTF peptide. *Int J Mol Med,* 7**,** 97-100.

IVERSON, L. E. & ROSE, J. K. 1981. Localized attenuation and discontinuous synthesis during vesicular stomatitis virus transcription. *Cell,* 23**,** 477-84.

JAHN, A., STAVIS, S. M., HONG, J. S., VREELAND, W. N., DEVOE, D. L. & GAITAN, M. 2010. Microfluidic Mixing and the Formation of Nanoscale Lipid Vesicles. *ACS Nano,* 4**,** 2077-2087.

JAHN, A., VREELAND, W. N., DEVOE, D. L., LOCASCIO, L. E. & GAITAN, M. 2007. Microfluidic Directed Formation of Liposomes of Controlled Size. *Langmuir,* 23**,** 6289-6293.

JAHN, A., VREELAND, W. N., GAITAN, M. & LOCASCIO, L. E. 2004. Controlled Vesicle Self-Assembly in Microfluidic Channels with Hydrodynamic Focusing. *Journal of the American Chemical Society,* 126**,** 2674-2675.

JALLET, C., JACOB, Y., BAHLOUL, C., DRINGS, A., DESMEZIERES, E., TORDO, N. & PERRIN, P. 1999. Chimeric lyssavirus glycoproteins with increased immunological potential. *J Virol,* 73**,** 225-33.

JAYARAMAN, M., ANSELL, S. M., MUI, B. L., TAM, Y. K., CHEN, J., DU, X., BUTLER, D., ELTEPU, L., MATSUDA, S., NARAYANANNAIR, J. K., RAJEEV, K. G., HAFEZ, I. M., AKINC, A., MAIER, M. A., TRACY, M. A., CULLIS, P. R., MADDEN, T. D., MANOHARAN, M. & HOPE, M. J. 2012. Maximizing the Potency of siRNA Lipid Nanoparticles for Hepatic Gene Silencing In Vivo. 51**,** 8529-8533.

JENNING, V., GYSLER, A., SCHÄFER-KORTING, M. & GOHLA, S. H. 2000. Vitamin A loaded solid lipid nanoparticles for topical use: occlusive properties and drug targeting to the upper skin. *European Journal of Pharmaceutics and Biopharmaceutics,* 49**,** 211-218.

JENSEN, K. F. 2001. Microreaction engineering — is small better? *Chemical Engineering Science,* 56**,** 293-303.

JOHANSEN, P., MEN, Y., MERKLE, H. P. & GANDER, B. 2000. Revisiting PLA/PLGA microspheres: an analysis of their potential in parenteral vaccination. *European Journal of Pharmaceutics and Biopharmaceutics,* 50**,** 129-146.

JOHNSON, J. A., BAROUCH, D. H. & BADEN, L. R. 2013. Nonreplicating vectors in HIV vaccines. *Current opinion in HIV and AIDS,* 8**,** 412-420.

JOSHI, M. D. & MÜLLER, R. H. 2009. Lipid nanoparticles for parenteral delivery of actives. *European Journal of Pharmaceutics and Biopharmaceutics,* 71**,** 161-172.

JOSHI, S., HUSSAIN, M. T., ROCES, C. B., ANDERLUZZI, G., KASTNER, E., SALMASO, S., KIRBY, D. J. & PERRIE, Y. 2016. Microfluidics based manufacture of liposomes simultaneously entrapping hydrophilic and lipophilic drugs. *International Journal of Pharmaceutics,* 514**,** 160-168.

JOSHI, V. B., GEARY, S. M. & SALEM, A. K. 2013. Biodegradable particles as vaccine antigen delivery systems for stimulating cellular immune responses. *Human vaccines & immunotherapeutics,* 9**,** 2584-2590.

KAKADIA, P. G. & CONWAY, B. R. J. A. J. O. P. S. 2014. Solid Lipid Nanoparticles: A Potential Approach for Dermal Drug Delivery. 2**,** 1-7.

KAKSONEN, M. & ROUX, A. 2018. Mechanisms of clathrin-mediated endocytosis. *Nature Reviews Molecular Cell Biology,* 19**,** 313.

KALAMS, S. A. & WALKER, B. D. 1998. The Critical Need for CD4 Help in Maintaining Effective Cytotoxic T Lymphocyte Responses. 188**,** 2199-2204.

KALLEN, K.-J. & THEß, A. 2013. A development that may evolve into a revolution in medicine: mRNA as the basis for novel, nucleotide-based vaccines and drugs. *Therapeutic Advances in Vaccines,* 2**,** 10-31.

KALLEN, K. J., HEIDENREICH, R., SCHNEE, M., PETSCH, B., SCHLAKE, T., THESS, A., BAUMHOF, P., SCHEEL, B., KOCH, S. D. & FOTIN-MLECZEK, M. 2013. A novel, disruptive

vaccination technology: self-adjuvanted RNActive((R)) vaccines. *Hum Vaccin Immunother,* 9**,** 2263-76.

KANASTY, R., DORKIN, J. R., VEGAS, A. & ANDERSON, D. 2013. Delivery materials for siRNA therapeutics. *Nature Materials,* 12**,** 967.

KANG, H., WANG, H., YU, Q. & YANG, Q. 2012. Effect of intranasal immunization with inactivated avian influenza virus on local and systemic immune responses in ducks. *Poultry Science,* 91**,** 1074-1080.

KARNIK, R., GU, F., BASTO, P., CANNIZZARO, C., DEAN, L., KYEI-MANU, W., LANGER, R. & FAROKHZAD, O. C. 2008a. Microfluidic Platform for Controlled Synthesis of Polymeric Nanoparticles. *Nano Letters,* 8**,** 2906-2912.

KARNIK, R., GU, F., BASTO, P., CANNIZZARO, C., DEAN, L., KYEI-MANU, W., LANGER, R. & FAROKHZAD, O. C. 2008b. Microfluidic platform for controlled synthesis of polymeric nanoparticles. *Nano Lett,* 8**,** 2906-12.

KASHANIAN, S., BULLET, E. & ROSTAMI, E. 2014. PEG-stearate coated solid lipid nanoparticles as levothyroxine carriers for oral administration.

KASTNER, E., KAUR, R., LOWRY, D., MOGHADDAM, B., WILKINSON, A. & PERRIE, Y. 2014. High-throughput manufacturing of size-tuned liposomes by a new microfluidics method using enhanced statistical tools for characterization. *International Journal of Pharmaceutics,* 477**,** 361-368.

KASTNER, E., VERMA, V., LOWRY, D. & PERRIE, Y. 2015. Microfluidic-controlled manufacture of liposomes for the solubilisation of a poorly water soluble drug. *International Journal of Pharmaceutics,* 485**,** 122-130.

KAUR, R., BRAMWELL, V. W., KIRBY, D. J. & PERRIE, Y. 2012a. Manipulation of the surface pegylation in combination with reduced vesicle size of cationic liposomal adjuvants modifies their clearance kinetics from the injection site, and the rate and type of T cell response. *Journal of Controlled Release,* 164**,** 331-337.

KAUR, R., BRAMWELL, V. W., KIRBY, D. J. & PERRIE, Y. 2012b. Pegylation of DDA:TDB liposomal adjuvants reduces the vaccine depot effect and alters the Th1/Th2 immune responses. *J Control Release,* 158**,** 72-7.

KAUR, R., HENRIKSEN-LACEY, M., WILKHU, J., DEVITT, A., CHRISTENSEN, D. & PERRIE, Y. 2014. Effect of Incorporating Cholesterol into DDA:TDB Liposomal Adjuvants on Bilayer Properties, Biodistribution, and Immune Responses. *Molecular Pharmaceutics,* 11**,** 197-207.

KENNY, G., KAMALY, N., KALBER, T., BRODY, L., SAHURI, M., SHAMSAEI, E., MILLER, A. & BELL, J. 2010. Novel multifunctional nanoparticle mediates siRNA tumour delivery, visualisation and therapeutic tumour reduction in vivo. *Journal of controlled release : official journal of the Controlled Release Society,* 149**,** 111-6.

KHALIL, I. A., KOGURE, K., AKITA, H. & HARASHIMA, H. 2006. Uptake Pathways and Subsequent Intracellular Trafficking in Nonviral Gene Delivery. 58**,** 32-45.

KIM, B.-K., HWANG, G.-B., SEU, Y.-B., CHOI, J.-S., JIN, K. S. & DOH, K.-O. 2015. DOTAP/DOPE ratio and cell type determine transfection efficiency with DOTAP-liposomes. *Biochimica et Biophysica Acta (BBA) - Biomembranes,* 1848**,** 1996-2001.

KIM, H. R., KIM, I. K., BAE, K. H., LEE, S. H., LEE, Y. & PARK, T. G. 2008. Cationic Solid Lipid Nanoparticles Reconstituted from Low Density Lipoprotein Components for Delivery of siRNA. *Molecular Pharmaceutics,* 5**,** 622-631.

KIM, H. S., MOON, J., KIM, K. S., CHOI, M. M., LEE, J. E., HEO, Y., CHO, D. H., JANG, D. O. & PARK, Y. S. 2004. Gene-Transferring Efficiencies of Novel Diamino Cationic Lipids with Varied Hydrocarbon Chains. *Bioconjugate Chemistry,* 15**,** 1095-1101.

KISS, A. L. & BOTOS, E. 2009. Endocytosis via caveolae: alternative pathway with distinct cellular compartments to avoid lysosomal degradation? 13**,** 1228-1237.

KLINGUER-HAMOUR, C., LIBON, C., PLOTNICKY-GILQUIN, H., BUSSAT, M.-C., REVY, L., NGUYEN, T., BONNEFOY, J.-Y., CORVAïA, N. & BECK, A. 2002. DDA adjuvant induces

a mixed Th1/Th2 immune response when associated with BBG2Na, a respiratory syncytial virus potential vaccine. *Vaccine,* 20**,** 2743-2751.

KLINGUER, C., BECK, A., DE-LYS, P., BUSSAT, M. C., BLAECKE, A., DEROUET, F., BONNEFOY, J. Y., NGUYEN, T. N., CORVAïA, N. & VELIN, D. 2001. Lipophilic quaternary ammonium salt acts as a mucosal adjuvant when co-administered by the nasal route with vaccine antigens. *Vaccine,* 19**,** 4236-4244.

KLOK, R. P. & WINDHORST, A. D. 2006. Residual solvent analysis by gas chromatography in radiopharmaceutical formulations containing up to 12% ethanol. *Nuclear Medicine and Biology,* 33**,** 935-938.

KNOBEL, D. L., CLEAVELAND, S., COLEMAN, P. G., FÈVRE, E. M., MELTZER, M. I., MIRANDA, M. E. G., SHAW, A., ZINSSTAG, J. & MESLIN, F. X. 2005. Re-evaluating the burden of rabies in Africa and Asia. *Bulletin of the World Health Organization,* 83**,** 360-368.

KONDO, A. 1965. Growth characteristics of rabies virus in primary chick embryo cells. *Virology,* 27**,** 199-204.

KOOL, M., SOULLIE, T., VAN NIMWEGEN, M., WILLART, M. A., MUSKENS, F., JUNG, S., HOOGSTEDEN, H. C., HAMMAD, H. & LAMBRECHT, B. N. 2008. Alum adjuvant boosts adaptive immunity by inducing uric acid and activating inflammatory dendritic cells. *J Exp Med,* 205**,** 869-82.

KOPATZ, I., REMY, J.-S. & BEHR, J.-P. 2004. A Model for Non-Viral Gene Delivery: Through Syndecan Adhesion Molecules and Powered by Actin. *The journal of gene medicine,* 6**,** 769-76.

KOPROWSKI, H. & COX, H. R. 1948. Studies on chick embryo adapted rabies virus; culture characteristics and pathogenicity. *J Immunol,* 60**,** 533-54.

KORSHOLM, K. S., AGGER, E. M., FOGED, C., CHRISTENSEN, D., DIETRICH, J., ANDERSEN, C. S., GEISLER, C. & ANDERSEN, P. 2007. The adjuvant mechanism of cationic dimethyldioctadecylammonium liposomes. *Immunology,* 121**,** 216-226.

KOWALSKI, P. S., KUNINTY, P. R., BIJLSMA, K. T., STUART, M. C. A., LEUS, N. G. J., RUITERS, M. H. J., MOLEMA, G. & KAMPS, J. A. A. M. 2015. SAINT-liposome-polycation particles, a new carrier for improved delivery of siRNAs to inflamed endothelial cells. *European Journal of Pharmaceutics and Biopharmaceutics,* 89**,** 40-47.

KRAMPS, T. & ELBERS, K. 2017. Introduction to RNA Vaccines.

KULKARNI, J. A., MYHRE, J. L., CHEN, S., TAM, Y. Y. C., DANESCU, A., RICHMAN, J. M. & CULLIS, P. R. 2017. Design of lipid nanoparticles for in vitro and in vivo delivery of plasmid DNA. *Nanomedicine: Nanotechnology, Biology and Medicine,* 13**,** 1377-1387.

KURANE, I., INNIS, B. L., NIMMANNITYA, S., NISALAK, A., MEAGER, A. & ENNIS, F. A. 1993. High levels of interferon alpha in the sera of children with dengue virus infection. *Am J Trop Med Hyg,* 48**,** 222-9.

KUTZLER, M. A. & WEINER, D. B. 2008. DNA vaccines: ready for prime time? *Nature reviews. Genetics,* 9**,** 776-788.

LAJUNEN, T., HISAZUMI, K., KANAZAWA, T., OKADA, H., SETA, Y., YLIPERTTULA, M., URTTI, A. & TAKASHIMA, Y. 2014. Topical drug delivery to retinal pigment epithelium with microfluidizer produced small liposomes. *European Journal of Pharmaceutical Sciences,* 62**,** 23-32.

LAM, Y. C., GAN, H. Y., NGUYEN, N. T. & LIE, H. 2009. Micromixer based on viscoelastic flow instability at low Reynolds number. *Biomicrofluidics,* 3**,** 14106-14106.

LAPPALAINEN, K., JAASKELAINEN, I., SYRJANEN, K., URTTI, A. & SYRJANEN, S. 1994a. Comparison of cell proliferation and toxicity assays using two cationic liposomes. *Pharm Res,* 11**,** 1127-31.

LAPPALAINEN, K., URTTI, A., JÄÄSKELÄINEN, I., SYRJÄNEN, K. & SYRJÄNEN, S. 1994b. Cationic liposomes mediated delivery of antisense oligonucleotides targeted to HPV 16 E7 mRNA in CaSki cells. *Antiviral Research,* 23**,** 119-130.

LAYE, C., MCCLEMENTS, D. J. & WEISS, J. 2008. Formation of Biopolymer-Coated Liposomes by Electrostatic Deposition of Chitosan. 73, N7-N15.

LEE, C. Y., CHANG, C. L., WANG, Y. N. & FU, L. M. 2011a. Microfluidic mixing: a review. *Int J Mol Sci,* 12, 3263-87.

LEE, Y.-R., LEE, Y.-H., IM, S.-A., KIM, K. & LEE, C.-K. 2011b. Formulation and Characterization of Antigen-loaded PLGA Nanoparticles for Efficient Cross-priming of the Antigen. *Immune network,* 11, 163-8.

LEMAITRE, B., NICOLAS, E., MICHAUT, L., REICHHART, J. M. & HOFFMANN, J. A. 1996. The dorsoventral regulatory gene cassette spatzle/Toll/cactus controls the potent antifungal response in Drosophila adults. *Cell,* 86, 973-83.

LEMMON, J. C. M., MCFARLAND, R. J., RYBICKA, J. M., BALCE, D. R., MCKEOWN, K. R., KROHN, R. M., MATSUNAGA, T. O. & YATES, R. M. 2011. In vitro and in vivo transfection of primary phagocytes via microbubble-mediated intraphagosomal sonoporation. *Journal of Immunological Methods,* 371, 152-158.

LENG, J., EGELHAAF, S. U. & CATES, M. E. 2003. Kinetics of the micelle-to-vesicle transition: aqueous lecithin-bile salt mixtures. *Biophysical journal,* 85, 1624-1646.

LESIEUR, S., GRABIELLE-MADELMONT, C., PATERNOSTRE, M.-T. & OLLIVON, M. 1991. Size analysis and stability study of lipid vesicles by high-performance gel exclusion chromatography, turbidity, and dynamic light scattering. *Analytical Biochemistry,* 192, 334-343.

LESIEUR, S., GRABIELLE-MADELMONT, C., PATERNOSTRE, M. & OLLIVON, M. 1993. Study of size distribution and stability of liposomes by high performance gel exclusion chromatography. *Chemistry and Physics of Lipids,* 64, 57-82.

LEUNG, A. K. K., TAM, Y. Y. C., CHEN, S., HAFEZ, I. M. & CULLIS, P. R. 2015. Microfluidic Mixing: A General Method for Encapsulating Macromolecules in Lipid Nanoparticle Systems. *The Journal of Physical Chemistry B,* 119, 8698-8706.

LEVENTIS, R. & SILVIUS, J. R. 1990. Interactions of mammalian cells with lipid dispersions containing novel metabolizable cationic amphiphiles. *Biochimica et Biophysica Acta (BBA) - Biomembranes,* 1023, 124-132.

LEVINE, M. M. 2003. Can needle-free administration of vaccines become the norm in global immunization? *Nat Med,* 9, 99-103.

LI, H., WILLINGHAM, S. B., TING, J. P. & RE, F. 2008. Cutting edge: inflammasome activation by alum and alum's adjuvant effect are mediated by NLRP3. *J Immunol,* 181, 17-21.

LIANG, F., LINDGREN, G., SANDGREN, K. J., THOMPSON, E. A., FRANCICA, J. R., SEUBERT, A., DE GREGORIO, E., BARNETT, S., O'HAGAN, D. T., SULLIVAN, N. J., KOUP, R. A., SEDER, R. A. & LORE, K. 2017. Vaccine priming is restricted to draining lymph nodes and controlled by adjuvant-mediated antigen uptake. *Sci Transl Med,* 9.

LIM, J. P. & GLEESON, P. A. 2011. Macropinocytosis: an endocytic pathway for internalising large gulps. 89, 836-843.

LIMA, K. M., BONATO, V. L. D., FACCIOLI, L. H., BRANDÃO, I. R. T., DOS SANTOS, S. A., COELHO-CASTELO, A. A. M., LEÃO, S. C. & SILVA, C. L. 2001. Comparison of different delivery systems of vaccination for the induction of protection against tuberculosis in mice. *Vaccine,* 19, 3518-3525.

LIN, P. J. C., TAM, Y. Y. C., HAFEZ, I., SANDHU, A., CHEN, S., CIUFOLINI, M. A., NABI, I. R. & CULLIS, P. R. 2013. Influence of cationic lipid composition on uptake and intracellular processing of lipid nanoparticle formulations of siRNA. *Nanomedicine: Nanotechnology, Biology and Medicine,* 9, 233-246.

LINCOPAN, N., MAMIZUKA, E. M. & CARMONA-RIBEIRO, A. M. 2003. In vivo activity of a novel amphotericin B formulation with synthetic cationic bilayer fragments. *J Antimicrob Chemother,* 52, 412-8.

LINDBLAD, E. B., ELHAY, M. J., SILVA, R., APPELBERG, R. & ANDERSEN, P. 1997. Adjuvant modulation of immune responses to tuberculosis subunit vaccines. *Infection and immunity,* 65**,** 623-629.

LINDENSTRØM, T., AGGER, E., KORSHOLM, K., DARRAH, P., AAGAARD, C., SEDER, R., ROSENKRANDS, I. & ANDERSEN, P. 2009. Tuberculosis Subunit Vaccination Provides Long-Term Protective Immunity Characterized by Multifunctional CD4 Memory T Cells. *Journal of immunology (Baltimore, Md. : 1950),* 182**,** 8047-55.

LIU, J., GONG, T., WANG, C., ZHONG, Z. & ZHANG, Z. 2007. Solid lipid nanoparticles loaded with insulin by sodium cholate-phosphatidylcholine-based mixed micelles: Preparation and characterization. *International Journal of Pharmaceutics,* 340**,** 153-162.

LIU, Y., YIN, Y., WANG, L., ZHANG, W., CHEN, X., YANG, X., XU, J. & MA, G. 2013. Surface hydrophobicity of microparticles modulates adjuvanticity. *Journal of Materials Chemistry B,* 1**,** 3888-3896.

LO, C. T., JAHN, A., LOCASCIO, L. E. & VREELAND, W. N. 2010. Controlled Self-Assembly of Monodisperse Niosomes by Microfluidic Hydrodynamic Focusing. *Langmuir,* 26**,** 8559-8566.

LOBOVKINA, T., JACOBSON, G. B., GONZALEZ-GONZALEZ, E., HICKERSON, R. P., LEAKE, D., KASPAR, R. L., CONTAG, C. H. & ZARE, R. N. 2011. In vivo sustained release of siRNA from solid lipid nanoparticles. *ACS nano,* 5**,** 9977-9983.

LODMELL, D. L. & EWALT, L. C. 2001. Post-exposure DNA vaccination protects mice against rabies virus. *Vaccine,* 19**,** 2468-73.

LOU, G., ANDERLUZZI, G., WOODS, S., ROBERTS, C. W. & PERRIE, Y. 2019. A novel microfluidic-based approach to formulate size-tuneable large unilamellar cationic liposomes: Formulation, cellular uptake and biodistribution investigations. *European Journal of Pharmaceutics and Biopharmaceutics,* 143**,** 51-60.

LOUREIRO, J. & PLOEGH, H. L. 2006. Antigen presentation and the ubiquitin-proteasome system in host-pathogen interactions. *Adv Immunol,* 92**,** 225-305.

LOVE, K. T., MAHON, K. P., LEVINS, C. G., WHITEHEAD, K. A., QUERBES, W., DORKIN, J. R., QIN, J., CANTLEY, W., QIN, L. L., RACIE, T., FRANK-KAMENETSKY, M., YIP, K. N., ALVAREZ, R., SAH, D. W., DE FOUGEROLLES, A., FITZGERALD, K., KOTELIANSKY, V., AKINC, A., LANGER, R. & ANDERSON, D. G. 2010. Lipid-like materials for low-dose, in vivo gene silencing. *Proc Natl Acad Sci U S A,* 107**,** 1864-9.

LÜ, J.-M., WANG, X., MARIN-MULLER, C., WANG, H., LIN, P. H., YAO, Q. & CHEN, C. 2009. Current advances in research and clinical applications of PLGA-based nanotechnology. *Expert review of molecular diagnostics,* 9**,** 325-341.

LU, M., TAY, L. W., HE, J. & DU, G. 2016. Monitoring Phosphatidic Acid Signaling in Breast Cancer Cells Using Genetically Encoded Biosensors. *Methods Mol Biol,* 1406**,** 225-37.

LUANGTANA-ANAN, M., LIMMATVAPIRAT, S., NUNTHANID, J., CHALONGSUK, R. & YAMAMOTO, K. 2010. Polyethylene glycol on stability of chitosan microparticulate carrier for protein. *AAPS PharmSciTech,* 11**,** 1376-1382.

LUO, D. & SALTZMAN, W. M. 2000. Synthetic DNA delivery systems. *Nat Biotechnol,* 18**,** 33-7.

LUTEN, J., VAN NOSTRUM, C. F., DE SMEDT, S. C. & HENNINK, W. E. 2008. Biodegradable polymers as non-viral carriers for plasmid DNA delivery. *Journal of Controlled Release,* 126**,** 97-110.

LV, H., ZHANG, S., WANG, B., CUI, S. & YAN, J. 2006a. Lv, H, Zhang, S, Wang, B, Cui, S and Yan, J. Toxicity of cationic lipids and cationic polymers in gene delivery. J Control Release 114: 100-109. *Journal of controlled release : official journal of the Controlled Release Society,* 114**,** 100-9.

LV, H., ZHANG, S., WANG, B., CUI, S. & YAN, J. 2006b. Toxicity of cationic lipids and cationic polymers in gene delivery. *Journal of Controlled Release,* 114**,** 100-109.

M. SQUIRES, T. & R. QUAKE, S. 2005. Microfluidics: Fluid physics at the nanoliter scale. *Reviews of Modern Physics,* 77.

MAEKI, M., KIMURA, N., SATO, Y., HARASHIMA, H. & TOKESHI, M. 2018. Advances in microfluidics for lipid nanoparticles and extracellular vesicles and applications in drug delivery systems. *Advanced Drug Delivery Reviews,* 128**,** 84-100.

MAEKI, M., SAITO, T., SATO, Y., YASUI, T., KAJI, N., ISHIDA, A., TANI, H., BABA, Y., HARASHIMA, H. & TOKESHI, M. 2015. A strategy for synthesis of lipid nanoparticles using microfluidic devices with a mixer structure. *RSC Advances,* 5**,** 46181-46185.

MAGINI, D., GIOVANI, C., MANGIAVACCHI, S., MACCARI, S., CECCHI, R., ULMER, J. B., DE GREGORIO, E., GEALL, A. J., BRAZZOLI, M. & BERTHOLET, S. 2016. Self-Amplifying mRNA Vaccines Expressing Multiple Conserved Influenza Antigens Confer Protection against Homologous and Heterosubtypic Viral Challenge. *PloS one,* 11**,** e0161193-e0161193.

MAHDI JAFARI, S., HE, Y. & BHANDARI, B. 2006. Nano-Emulsion Production by Sonication and Microfluidization—A Comparison. *International Journal of Food Properties,* 9**,** 475-485.

MALLICK, S. & CHOI, J. S. 2014. Liposomes: versatile and biocompatible nanovesicles for efficient biomolecules delivery. *J Nanosci Nanotechnol,* 14**,** 755-65.

MANOLOVA, V., FLACE, A., BAUER, M., SCHWARZ, K., SAUDAN, P. & BACHMANN, M. F. 2008. Nanoparticles target distinct dendritic cell populations according to their size. *European Journal of Immunology,* 38**,** 1404-1413.

MARCHINI, C., MONTANI, M., AMICI, A., AMENITSCH, H., MARIANECCI, C., POZZI, D. & CARACCIOLO, G. 2009. Structural stability and increase in size rationalize the efficiency of lipoplexes in serum. *Langmuir,* 25**,** 3013-21.

MARCHINI, C., POZZI, D., MONTANI, M., ALFONSI, C., AMICI, A., CANDELORO DE SANCTIS, S., DIGMAN, M. A., SANCHEZ, S., GRATTON, E., AMENITSCH, H., FABBRETTI, A., GUALERZI, C. O. & CARACCIOLO, G. 2011. Role of temperature-independent lipoplex-cell membrane interactions in the efficiency boost of multicomponent lipoplexes. *Cancer gene therapy,* 18**,** 543-552.

MARGALITH, M. & VILALTA, A. 2006. Sustained protective rabies neutralizing antibody titers after administration of cationic lipid-formulated pDNA vaccine. *Genet Vaccines Ther,* 4**,** 2.

MARICHAL, T., OHATA, K., BEDORET, D., MESNIL, C., SABATEL, C., KOBIYAMA, K., LEKEUX, P., COBAN, C., AKIRA, S., ISHII, K. J., BUREAU, F. & DESMET, C. J. 2011. DNA released from dying host cells mediates aluminum adjuvant activity. *Nat Med,* 17**,** 996-1002.

MARKS, F. M. & LOWMAN, A. 2011. Enhanced mucoadhesive capacity of novel co-polymers for oral protein delivery. *Journal of biomaterials science. Polymer edition,* 22**,** 2079-2095.

MARTINO, S., DI GIROLAMO, I., TIRIBUZI, R., D'ANGELO, F., DATTI, A. & ORLACCHIO, A. 2009. Efficient siRNA delivery by the cationic liposome DOTAP in human hematopoietic stem cells differentiating into dendritic cells. *Journal of biomedicine & biotechnology,* 2009**,** 410260-410260.

MATTHEWS, K. E., DEV, S. B., TONEGUZZO, F. & KEATING, A. 1995. Electroporation for Gene Therapy. *In:* NICKOLOFF, J. A. (ed.) *Animal Cell Electroporation and Electrofusion Protocols.* Totowa, NJ: Humana Press.

MAYHEW, E., ITO, M. & LAZO, R. 1987. Toxicity of non-drug-containing liposomes for cultured human cells. *Exp Cell Res,* 171**,** 195-202.

MAYHEW, E., LAZO, R., VAIL, W. J., KING, J. & GREEN, A. M. 1984. Characterization of liposomes prepared using a microemulsifier. *Biochimica et Biophysica Acta (BBA) - Biomembranes,* 775**,** 169-174.

MCCARTHY, D. P., HUNTER, Z. N., CHACKERIAN, B., SHEA, L. D. & MILLER, S. D. 2014. Targeted immunomodulation using antigen-conjugated nanoparticles. *Wiley interdisciplinary reviews. Nanomedicine and nanobiotechnology,* 6**,** 298-315.

MCLAREN, D. G., MILLER, P. L., LASSMAN, M. E., CASTRO-PEREZ, J. M., HUBBARD, B. K. & RODDY, T. P. 2011. An ultraperformance liquid chromatography method for the normal-phase separation of lipids. *Analytical Biochemistry,* 414**,** 266-272.

MEEKEL, ARTHUR A. P., WAGENAAR, A., ŠMISTEROVÁ, J., KROEZE, JESSICA E., HAADSMA, P., BOSGRAAF, B., STUART, MARC C. A., BRISSON, A., RUITERS, MARCEL H. J., HOEKSTRA, D. & ENGBERTS, JAN B. F. N. 2000. Synthesis of Pyridinium Amphiphiles Used for Transfection and Some Characteristics of Amphiphile/DNA Complex Formation. 2000**,** 665-673.

MEHNERT, W. & MÄDER, K. 2001. Solid lipid nanoparticles: Production, characterization and applications. *Advanced Drug Delivery Reviews,* 47**,** 165-196.

MEURE, L. A., FOSTER, N. R. & DEHGHANI, F. 2008. Conventional and dense gas techniques for the production of liposomes: a review. *AAPS PharmSciTech,* 9**,** 798-809.

MIFUNE, K., TAKEUCHI, E., NAPIORKOWSKI, P. A., YAMADA, A. & SAKAMOTO, K. 1981. Essential Role of T cells in the postexposure prophylaxis of rabies in mice. *Microbiol Immunol,* 25**,** 895-904.

MINCHIN, R. F. & YANG, S. 2010. Endosomal disruptors in non-viral gene delivery. *Expert Opinion on Drug Delivery,* 7**,** 331-339.

MISLICK, K. A. & BALDESCHWIELER, J. D. 1996. Evidence for the role of proteoglycans in cation-mediated gene transfer. *Proc Natl Acad Sci U S A,* 93**,** 12349-54.

MODLIN, J. F., ARVIN, A. M., FAST, P., MYERS, M., PLOTKIN, S. & RABINOVICH, R. 2004. Vaccine Development to Prevent Cytomegalovirus Disease: Report from the National Vaccine Advisory Committee. *Clinical Infectious Diseases,* 39**,** 233-239.

MOHAMMED, A. R., BRAMWELL, V. W., COOMBES, A. G. A. & PERRIE, Y. 2006. Lyophilisation and sterilisation of liposomal vaccines to produce stable and sterile products. *Methods,* 40**,** 30-38.

MONTANA, G., BONDÌ, M. L., CARROTTA, R., PICONE, P., CRAPARO, E. F., SAN BIAGIO, P. L., GIAMMONA, G. & DI CARLO, M. 2007. Employment of Cationic Solid-Lipid Nanoparticles as RNA Carriers. *Bioconjugate Chemistry,* 18**,** 302-308.

MOON, S. L. & WILUSZ, J. 2012. In vitro transcription of modified RNAs. *Methods Mol Biol,* 941**,** 171-80.

MOORE, G. E., GERNER, R. E. & FRANKLIN, H. A. 1967. Culture of Normal Human Leukocytes. *JAMA,* 199**,** 519-524.

MORACHIS, J. M., MAHMOUD, E. A. & ALMUTAIRI, A. 2012. Physical and chemical strategies for therapeutic delivery by using polymeric nanoparticles. *Pharmacological reviews,* 64**,** 505-519.

MOREFIELD, G. L., SOKOLOVSKA, A., JIANG, D., HOGENESCH, H., ROBINSON, J. P. & HEM, S. L. 2005. Role of aluminum-containing adjuvants in antigen internalization by dendritic cells in vitro. *Vaccine,* 23**,** 1588-95.

MOREL, S., UGAZIO, E., CAVALLI, R. & GASCO, M. R. 1996. Thymopentin in solid lipid nanoparticles. *International Journal of Pharmaceutics,* 132**,** 259-261.

MORRA, M., OCCHIELLO, E., MAROLA, R., GARBASSI, F., HUMPHREY, P. & DJ, J. 1990. *On the Aging of Oxygen Plasma-Treated Polydimethylsiloxane Surfaces*.

MORRIS, J., CROWCROFT, N. S., FOOKS, A. R., BROOKES, S. M. & ANDREWS, N. 2007. Rabies antibody levels in bat handlers in the United Kingdom: immune response before and after purified chick embryo cell rabies booster vaccination. *Hum Vaccin,* 3**,** 165-70.

MORTERS, M. K., MCNABB, S., HORTON, D. L., FOOKS, A. R., SCHOEMAN, J. P., WHAY, H. R., WOOD, J. L. N. & CLEAVELAND, S. 2015. Effective vaccination against rabies in puppies in rabies endemic regions. 177**,** 150-150.

MOSER, M. & LEO, O. 2010. Key concepts in immunology. *Vaccine,* 28**,** C2-C13.

MOSMANN, T. 1983. Rapid colorimetric assay for cellular growth and survival: application to proliferation and cytotoxicity assays. *J Immunol Methods,* 65**,** 55-63.

MOSMANN, T. R., CHERWINSKI, H., BOND, M. W., GIEDLIN, M. A. & COFFMAN, R. L. 1986. Two types of murine helper T cell clone. I. Definition according to profiles of lymphokine activities and secreted proteins. *J Immunol,* 136**,** 2348-57.

MUKHERJEE, S., GHOSH, R. N. & MAXFIELD, F. R. 1997. Endocytosis. 77**,** 759-803.

MUKHERJEE, S., RAY, S. & THAKUR, R. S. 2009. Solid lipid nanoparticles: a modern formulation approach in drug delivery system. *Indian journal of pharmaceutical sciences,* 71**,** 349-358.

MULLER, R. & STEFAN, R. 1999. Solid lipid nanoparticles for controlled drug delivery. *Journal of Biomaterials Science, Polymer Edition,* 51**,** 83-83.

MÜLLER, R. H., RADTKE, M. & WISSING, S. A. 2002. Nanostructured lipid matrices for improved microencapsulation of drugs. *International Journal of Pharmaceutics,* 242**,** 121-128.

MURRE, C. 2007. Epigenetics of antigen-receptor gene assembly. *Current opinion in genetics & development,* 17**,** 415-421.

NAGPAL, K., SINGH, S. & MISHRA, D. 2010. Chitosan Nanoparticles: A Promising System in Novel Drug Delivery. *Chemical & pharmaceutical bulletin,* 58**,** 1423-30.

NANDEDKAR, T. D. J. J. O. B. 2009. Nanovaccines: recent developments in vaccination. 34**,** 995-1003.

NANDI, S. & KUMAR, M. 2010. Development in Immunoprophylaxis against Rabies for Animals and Humans. *Avicenna journal of medical biotechnology,* 2**,** 3-21.

NGUYEN, D. N., GREEN, J. J., CHAN, J. M., LANGER, R. & ANDERSON, D. G. 2009a. Polymeric Materials for Gene Delivery and DNA Vaccination. 21**,** 847-867.

NGUYEN, D. N., GREEN, J. J., CHAN, J. M., LONGER, R. & ANDERSON, D. G. 2009b. Polymeric Materials for Gene Delivery and DNA Vaccination. *Adv Mater,* 21**,** 847-867.

NORDLY, P., ROSE, F., CHRISTENSEN, D., NIELSEN, H. M., ANDERSEN, P., AGGER, E. M. & FOGED, C. 2011. Immunity by formulation design: Induction of high CD8+ T-cell responses by poly(I:C) incorporated into the CAF01 adjuvant via a double emulsion method. *Journal of Controlled Release,* 150**,** 307-317.

NUNBERG, J. H., DOYLE, M. V., YORK, S. M. & YORK, C. J. 1989. Interleukin 2 acts as an adjuvant to increase the potency of inactivated rabies virus vaccine. 86**,** 4240-4243.

O'HAGAN, D. T., OTT, G. S., DE GREGORIO, E. & SEUBERT, A. 2012. The mechanism of action of MF59 - an innately attractive adjuvant formulation. *Vaccine,* 30**,** 4341-8.

O'HAGAN, D., S OTT, G., VAN NEST, G., RAPPUOLI, R. & DEL GIUDICE, G. 2013. The history of MF59 (R) adjuvant: a phoenix that arose from the ashes. *Expert review of vaccines,* 12**,** 13-30.

OBERLE, V., BAKOWSKY, U., ZUHORN, I. S. & HOEKSTRA, D. 2000. Lipoplex Formation under Equilibrium Conditions Reveals a Three-Step Mechanism. *Biophysical Journal,* 79**,** 1447-1454.

OCTARIA, R., SALYER, S. J., BLANTON, J., PIERACCI, E. G., MUNYUA, P., MILLIEN, M., NEL, L. & WALLACE, R. M. 2018. From recognition to action: A strategic approach to foster sustainable collaborations for rabies elimination. *PLoS neglected tropical diseases,* 12**,** e0006756-e0006756.

OH, Y.-K. & PARK, T. G. 2009. siRNA delivery systems for cancer treatment. *Advanced Drug Delivery Reviews,* 61**,** 850-862.

OLBRICH, C. & MÜLLER, R. H. 1999. Enzymatic degradation of SLN—effect of surfactant and surfactant mixtures. *International Journal of Pharmaceutics,* 180**,** 31-39.

OTT, G., BARCHFELD, G. L., CHERNOFF, D., RADHAKRISHNAN, R., VAN HOOGEVEST, P. & VAN NEST, G. 1995. MF59 Design and Evaluation of a Safe and Potent Adjuvant for Human Vaccines. *In:* POWELL, M. F. & NEWMAN, M. J. (eds.) *Vaccine Design: The Subunit and Adjuvant Approach.* Boston, MA: Springer US.

OTT, G., SINGH, M., KAZZAZ, J., BRIONES, M., SOENAWAN, E., UGOZZOLI, M. & O'HAGAN, D. T. 2002. A cationic sub-micron emulsion (MF59/DOTAP) is an effective delivery system for DNA vaccines. *Journal of Controlled Release,* 79**,** 1-5.

OTT GAEL , SINGH MANMOHAN, JINA KAZZAZ, MAYLENE BRIONES, ELAWATI SOENAWAN, MILDRED UGOZZOLI & O'HAGAN, D. T. 2002. A cationic sub-micron emulsion (MF59DOTAP) is an effective delivery system of DNA vaccine.pdf. *Journal of Controlled Release,* 79**,** 5.

PAN, X., CHEN, L., LIU, S., YANG, X., GAO, J.-X. & LEE, R. J. 2009. Antitumor activity of G3139 lipid nanoparticles (LNPs). *Molecular pharmaceutics,* 6**,** 211-220.

PANYAM, J. & LABHASETWAR, V. 2003. Biodegradable nanoparticles for drug and gene delivery to cells and tissue. *Adv Drug Deliv Rev,* 55**,** 329-47.

PANYAM, J., ZHOU, W. Z., PRABHA, S., SAHOO, S. K. & LABHASETWAR, V. 2002. Rapid endo-lysosomal escape of poly(DL-lactide-co-glycolide) nanoparticles: implications for drug and gene delivery. *Faseb j,* 16**,** 1217-26.

PARK, K. 2017. The drug delivery field needs a well-diversified technology portfolio. *Journal of Controlled Release,* 245**,** 177.

PATIL, Y. & PANYAM, J. 2009. Polymeric nanoparticles for siRNA delivery and gene silencing. *International Journal of Pharmaceutics,* 367**,** 195-203.

PATRA, M., SALONEN, E., TERAMA, E., VATTULAINEN, I., FALLER, R., LEE, B. W., HOLOPAINEN, J. & KARTTUNEN, M. 2006. Under the Influence of Alcohol: The Effect of Ethanol and Methanol on Lipid Bilayers. *Biophysical Journal,* 90**,** 1121-1135.

PATTNAIK, P. 2009. Improving liposome integrity and easing bottlenecks to production. *Pharmaceutical Technology Europe,* 21**,** 24-28.

PERRI, S., GREER, C. E., THUDIUM, K., DOE, B., LEGG, H., LIU, H., ROMERO, R. E., TANG, Z., BIN, Q., DUBENSKY, T. W., JR., VAJDY, M., OTTEN, G. R. & POLO, J. M. 2003. An alphavirus replicon particle chimera derived from venezuelan equine encephalitis and sindbis viruses is a potent gene-based vaccine delivery vector. *J Virol,* 77**,** 10394-403.

PERRIE, Y., FREDERIK, P. M. & GREGORIADIS, G. 2001. Liposome-mediated DNA vaccination: the effect of vesicle composition. *Vaccine,* 19**,** 3301-3310.

PERRIE, Y., MCNEIL, S. & VANGALA, A. 2003. Liposome-mediated DNA Immunisation via the Subcutaneous Route. *Journal of drug targeting,* 11**,** 555-63.

PERRIE, Y., OBRENOVIC, M., MCCARTHY, D. & GREGORIADIS, G. 2002. LIPOSOME (LIPODINE™)-MEDIATED DNA VACCINATION BY THE ORAL ROUTE. *Journal of Liposome Research,* 12**,** 185-197.

PETSCH, B., SCHNEE, M., VOGEL, A. B., LANGE, E., HOFFMANN, B., VOSS, D., SCHLAKE, T., THESS, A., KALLEN, K. J., STITZ, L. & KRAMPS, T. 2012. Protective efficacy of in vitro synthesized, specific mRNA vaccines against influenza A virus infection. *Nat Biotechnol,* 30**,** 1210-6.

PHUA, K. K. L., STAATS, H. F., LEONG, K. W. & NAIR, S. K. 2014. Intranasal mRNA nanoparticle vaccination induces prophylactic and therapeutic anti-tumor immunity. *Scientific reports,* 4**,** 5128-5128.

PIHL, J., KARLSSON, M. & CHIU, D. T. J. D. D. T. V. 2005. Microfluidic technologies in drug discovery. 1377-1383.

POLLARD, C., DE KOKER, S., SAELENS, X., VANHAM, G. & GROOTEN, J. 2013. Challenges and advances towards the rational design of mRNA vaccines. *Trends in Molecular Medicine,* 19**,** 705-713.

PONS, M., FORADADA, M. & ESTELRICH, J. 1993. Liposomes obtained by the ethanol injection method. *International Journal of Pharmaceutics,* 95**,** 51-56.

PREHAUD, C., COULON, P., LAFAY, F., THIERS, C. & FLAMAND, A. 1988. Antigenic site II of the rabies virus glycoprotein: structure and role in viral virulence. *J Virol,* 62**,** 1-7.

PRINGLE, C. R. 1997. The order Mononegavirales--current status. *Arch Virol,* 142**,** 2321-6.

PULENDRAN, B. & AHMED, R. 2006. Translating Innate Immunity into Immunological Memory: Implications for Vaccine Development. *Cell,* 124**,** 849-863.

PULMANAUSAHAKUL, R., LI, J., SCHNELL, M. J. & DIETZSCHOLD, B. 2008. The glycoprotein and the matrix protein of rabies virus affect pathogenicity by regulating viral replication and facilitating cell-to-cell spread. *Journal of virology,* 82**,** 2330-2338.

QI, C., CHEN, Y., HUANG, J.-H., JIN, Q.-Z. & WANG, X. 2012. Preparation and characterization of catalase-loaded solid lipid nanoparticles based on soybean phosphatidylcholine. *Journal of the science of food and agriculture,* 92**,** 787-93.

QI, C., CHEN, Y., JING, Q.-Z. & WANG, X.-G. 2011. Preparation and characterization of catalase-loaded solid lipid nanoparticles protecting enzyme against proteolysis. *International journal of molecular sciences,* 12**,** 4282-4293.

QIAO, W., ZHENG, Z., QU, W. & ZHANG, S. J. J. O. T. A. O. C. S. 2012. Synthesis and Characterization of Carbamate-Linked Cationic Lipids with Hydroxyethyl Group. 89**,** 2121-2125.

QIN, L., HU, C. & YIN, L.-H. 2004. Establishment of a Knowledge Base for Prescreening Residual Solvents in Pharmaceuticals. *Chromatographia,* 59**,** 475-480.

QUINTANAR-GUERRERO, D., ALLÉMANN, E., DOELKER, E., FESSI, H. J. C. & SCIENCE, P. 1997. A mechanistic study of the formation of polymer nanoparticles by the emulsification-diffusion technique. 275**,** 640-647.

QUINTANAR-GUERRERO, D., TAMAYO-ESQUIVEL, D., GANEM-QUINTANAR, A., ALLEMANN, E. & DOELKER, E. 2005. Adaptation and optimization of the emulsification-diffusion technique to prepare lipidic nanospheres. *Eur J Pharm Sci,* 26**,** 211-8.

RAMANATHAN, V. D., BADENOCH-JONES, P. & TURK, J. L. 1979. Complement activation by aluminium and zirconium compounds. *Immunology,* 37**,** 881-888.

RANTANEN, J. & KHINAST, J. 2015. The Future of Pharmaceutical Manufacturing Sciences. 104**,** 3612-3638.

RAPPUOLI, R., MANDL, C. W., BLACK, S. & DE GREGORIO, E. 2011. Vaccines for the twenty-first century society. *Nat Rev Immunol,* 11**,** 865-72.

RAVI, A. D., SADHNA, D., NAGPAAL, D. & CHAWLA, L. 2015. Needle free injection technology: A complete insight. *International journal of pharmaceutical investigation,* 5**,** 192-199.

RAYNER, J. O., DRYGA, S. A. & KAMRUD, K. I. 2002. Alphavirus vectors and vaccination. *Rev Med Virol,* 12**,** 279-96.

REDDY, S. T., VAN DER VLIES, A. J., SIMEONI, E., ANGELI, V., RANDOLPH, G. J., O'NEIL, C. P., LEE, L. K., SWARTZ, M. A. & HUBBELL, J. A. 2007. Exploiting lymphatic transport and complement activation in nanoparticle vaccines. *Nature Biotechnology,* 25**,** 1159-1164.

REITHMEIER, H., HERRMANN, J. & GÖPFERICH, A. 2001. Lipid microparticles as a parenteral controlled release device for peptides. *Journal of controlled release : official journal of the Controlled Release Society,* 73**,** 339-50.

REJMAN, J., OBERLE, V., ZUHORN, I. S. & HOEKSTRA, D. 2004. Size-dependent internalization of particles via the pathways of clathrin- and caveolae-mediated endocytosis. *Biochem J,* 377**,** 159-69.

REN, T., ZHANG, G. & LIU, D. 2001. Synthesis of bifunctional cationic compound for gene delivery. *Tetrahedron Letters,* 42**,** 1007-1010.

REYNOLDS, J. A., NOZAKI, Y. & TANFORD, C. 1983. Gel-exclusion chromatography on S1000 Sephacryl: application to phospholipid vesicles. *Anal Biochem,* 130**,** 471-4.

RHEE, J. H., LEE, S. E. & KIM, S. Y. 2012. Mucosal vaccine adjuvants update. *Clinical and experimental vaccine research,* 1**,** 50-63.

RIBEIRO DOS SANTOS, I., RICHARD, J., PECH, B., THIES, C. & BENOIT, J. P. 2002. Microencapsulation of protein particles within lipids using a novel supercritical fluid process. *International Journal of Pharmaceutics,* 242**,** 69-78.

RITEAU, N., BARON, L., VILLERET, B., GUILLOU, N., SAVIGNY, F., RYFFEL, B., RASSENDREN, F., LE BERT, M., GOMBAULT, A. & COUILLIN, I. 2012. ATP release and purinergic signaling: a common pathway for particle-mediated inflammasome activation. *Cell Death Dis,* 3**,** e403.

RITTIG, S. M., HAENTSCHEL, M., WEIMER, K. J., HEINE, A., MULLER, M. R., BRUGGER, W., HORGER, M. S., MAKSIMOVIC, O., STENZL, A., HOERR, I., RAMMENSEE, H.-G., HOLDERRIED, T. A. W., KANZ, L., PASCOLO, S. & BROSSART, P. 2011. Intradermal Vaccinations With RNA Coding for TAA Generate CD8+ and CD4+ Immune Responses and Induce Clinical Benefit in Vaccinated Patients. *Molecular Therapy,* 19**,** 990-999.

ROBERTSON, J., MCGOVERIN, C., VANHOLSBEECK, F. & SWIFT, S. 2019. Optimisation of the Protocol for the LIVE/DEAD(®) BacLight(TM) Bacterial Viability Kit for Rapid Determination of Bacterial Load. *Frontiers in microbiology,* 10**,** 801-801.

ROCK, K. L., YORK, I. A., SARIC, T. & GOLDBERG, A. L. 2002. Protein degradation and the generation of MHC class I-presented peptides. *Adv Immunol,* 80**,** 1-70.

ROOSJEN, A., ŠMISTEROVÁ, J., DRIESSEN, C., ANDERS, JOACHIM T., WAGENAAR, A., HOEKSTRA, D., HULST, R. & ENGBERTS, JAN B. F. N. 2002. Synthesis and Characteristics of Biodegradable Pyridinium Amphiphiles Used for in vitro DNA Delivery. 2002**,** 1271-1277.

ROSENKRANDS, I., AGGER, E. M., OLSEN, A. W., KORSHOLM, K. S., ANDERSEN, C. S., JENSEN, K. T. & ANDERSEN, P. 2005. Cationic Liposomes Containing Mycobacterial Lipids: a New Powerful Th1 Adjuvant System. 73**,** 5817-5826.

RUPPRECHT, C. E., NAGARAJAN, T. & ERTL, H. 2016. Current Status and Development of Vaccines and Other Biologics for Human Rabies Prevention. *Expert Rev Vaccines,* 15**,** 731-49.

RUPPRECHT, C. E. & SALAHUDDIN, N. 2019. Current status of human rabies prevention: remaining barriers to global biologics accessibility and disease elimination. *Expert Rev Vaccines,* 18**,** 629-640.

RUYSSCHAERT, T., MARQUE, A., DUTEYRAT, J.-L., LESIEUR, S., WINTERHALTER, M. & FOURNIER, D. 2005. Liposome retention in size exclusion chromatography. *BMC Biotechnology,* 5**,** 11.

SAHAY, G., ALAKHOVA, D. Y. & KABANOV, A. V. 2010. Endocytosis of nanomedicines. *J Control Release,* 145**,** 182-95.

SAHEKI, A., SEKI, J., NAKANISHI, T. & TAMAI, I. 2012. Effect of back pressure on emulsification of lipid nanodispersions in a high-pressure homogenizer. *International Journal of Pharmaceutics,* 422**,** 489-494.

SALMASO, S., BERSANI, S., ELVASSORE, N., BERTUCCO, A. & CALICETI, P. 2009a. Biopharmaceutical characterisation of insulin and recombinant human growth hormone loaded lipid submicron particles produced by supercritical gas micro-atomisation. *International Journal of Pharmaceutics,* 379**,** 51-58.

SALMASO, S., ELVASSORE, N., BERTUCCO, A. & CALICETI, P. 2009b. Production of Solid Lipid Submicron Particles for Protein Delivery Using a Novel Supercritical Gas-Assisted Melting Atomization Process. *Journal of Pharmaceutical Sciences,* 98**,** 640-650.

SALMINEN, H., HELGASON, T., KRISTINSSON, B., KRISTBERGSSON, K. & WEISS, J. 2017. Tuning of shell thickness of solid lipid particles impacts the chemical stability of encapsulated ω-3 fish oil. *Journal of Colloid and Interface Science,* 490**,** 207-216.

SAMUEL, C. E. 2001. Antiviral actions of interferons. *Clin Microbiol Rev,* 14**,** 778-809, table of contents.

SARDESAI, N. Y. & WEINER, D. B. 2011. Electroporation delivery of DNA vaccines: prospects for success. *Current opinion in immunology,* 23**,** 421-429.

SARPOTDAR, P. P., GASKILL, J. L. & GIANNINI, R. P. 1986. Effect of Polyethlene Glycol 400 on the Penetration of Drugs Through Human Cadaver Skin In Vitro. *Journal of Pharmaceutical Sciences,* 75**,** 26-28.

SAXENA, M., VAN, T. T., BAIRD, F. J., COLOE, P. J. & SMOOKER, P. M. 2013. Pre-existing immunity against vaccine vectors--friend or foe? *Microbiology,* 159**,** 1-11.

SAXENA, S., SONWANE, A. A., DAHIYA, S. S., PATEL, C. L., SAINI, M., RAI, A. & GUPTA, P. K. 2009. Induction of immune responses and protection in mice against rabies using a self-replicating RNA vaccine encoding rabies virus glycoprotein. *Veterinary Microbiology,* 136**,** 36-44.

SCARZELLO, M., WAGENAAR, A., STUART, M. C. A., HOEKSTRA, D., ENGBERTS, J. B. F. N. & HULST, R. 2005. Sunfish Cationic Amphiphiles: Toward an Adaptative Lipoplex Morphology. *Journal of the American Chemical Society,* 127**,** 10420-10429.

SCHLAKE, T., THESS, A., FOTIN-MLECZEK, M. & KALLEN, K.-J. 2012. Developing mRNA-vaccine technologies. *RNA biology,* 9**,** 1319-1330.

SCHNARE, M., BARTON, G. M., HOLT, A. C., TAKEDA, K., AKIRA, S. & MEDZHITOV, R. 2001. Toll-like receptors control activation of adaptive immune responses. *Nat Immunol,* 2**,** 947-50.

SCHROEDER, A., LEVINS, C. G., CORTEZ, C., LANGER, R. & ANDERSON, D. G. 2010. Lipid-based nanotherapeutics for siRNA delivery. 267**,** 9-21.

SCHWARZ, C., MEHNERT, W., LUCKS, J. S. & MÜLLER, R. H. 1994. Solid lipid nanoparticles (SLN) for controlled drug delivery. I. Production, characterization and sterilization. *Journal of Controlled Release,* 30**,** 83-96.

SCHWENDENER, R. A., LAGOCKI, P. A. & RAHMAN, Y. E. 1984. The effects of charge and size on the interaction of unilamellar liposomes with macrophages. *Biochim Biophys Acta,* 772**,** 93-101.

SEIF, I., COULON, P., ROLLIN, P. E. & FLAMAND, A. 1985. Rabies virulence: effect on pathogenicity and sequence characterization of rabies virus mutations affecting antigenic site III of the glycoprotein. *Journal of virology,* 53**,** 926-934.

SEMPLE, S. C., AKINC, A., CHEN, J., SANDHU, A. P., MUI, B. L., CHO, C. K., SAH, D. W., STEBBING, D., CROSLEY, E. J., YAWORSKI, E., HAFEZ, I. M., DORKIN, J. R., QIN, J., LAM, K., RAJEEV, K. G., WONG, K. F., JEFFS, L. B., NECHEV, L., EISENHARDT, M. L., JAYARAMAN, M., KAZEM, M., MAIER, M. A., SRINIVASULU, M., WEINSTEIN, M. J., CHEN, Q., ALVAREZ, R., BARROS, S. A., DE, S., KLIMUK, S. K., BORLAND, T., KOSOVRASTI, V., CANTLEY, W. L., TAM, Y. K., MANOHARAN, M., CIUFOLINI, M. A., TRACY, M. A., DE FOUGEROLLES, A., MACLACHLAN, I., CULLIS, P. R., MADDEN, T. D. & HOPE, M. J. 2010. Rational design of cationic lipids for siRNA delivery. *Nat Biotechnol,* 28**,** 172-6.

SEMPLE, S. C., KLIMUK, S. K., HARASYM, T. O., DOS SANTOS, N., ANSELL, S. M., WONG, K. F., MAURER, N., STARK, H., CULLIS, P. R., HOPE, M. J. & SCHERRER, P. 2001. Efficient encapsulation of antisense oligonucleotides in lipid vesicles using ionizable aminolipids: formation of novel small multilamellar vesicle structures. *Biochimica et Biophysica Acta (BBA) - Biomembranes,* 1510**,** 152-166.

SEUBERT, A., MONACI, E., PIZZA, M., O'HAGAN, D. & WACK, A. 2008. The ADJUVANTS ALUMINUM HYDROXIDE and MF59 induce monocyte and granulocyte chemoattractants and enhance monocyte differentiation toward dendritic cells. *Journal of immunology (Baltimore, Md. : 1950),* 180**,** 5402-12.

SHARMA, M. L., KAUL, A., KHAJURIA, A., SINGH, S. & SINGH, G. B. 1996. Immunomodulatory Activity of Boswellic Acids (Pentacyclic Triterpene Acids) from Boswellia serrata. 10**,** 107-112.

SHESTOPALOV, I., TICE, J. & F ISMAGILOV, R. 2004. Multi-step synthesis of nanoparticles performed on millisecond time scale in a microfluidic droplet-based system. *Lab on a chip,* 4**,** 316-21.

SHI, Y. & ROCK, K. L. 2002. Cell death releases endogenous adjuvants that selectively enhance immune surveillance of particulate antigens. 32**,** 155-162.

SHIN, G., YOST, S. A., MILLER, M. T., ELROD, E. J., GRAKOUI, A. & MARCOTRIGIANO, J. 2012. Structural and functional insights into alphavirus polyprotein processing and pathogenesis. *Proc Natl Acad Sci U S A,* 109**,** 16534-9.

SILVA, A. L., MARCELINO, H. R., VERISSIMO, L. M., ARAUJO, I. B., AGNEZ-LIMA, L. F. & DO EGITO, E. S. 2016. Stearylamine-Containing Cationic Nanoemulsion as a Promising Carrier for Gene Delivery. *J Nanosci Nanotechnol,* 16**,** 1339-45.

SIMBERG, D., WEISMAN, S., TALMON, Y., FAERMAN, A., SHOSHANI, T. & BARENHOLZ, Y. 2003. The Role of Organ Vascularization and Lipoplex-Serum Initial Contact in Intravenous Murine Lipofection. *The Journal of biological chemistry,* 278**,** 39858-65.

SIMOES, S., FILIPE, A., FANECA, H., MANO, M., PENACHO, N., DUZGUNES, N. & DE LIMA, M. P. 2005. Cationic liposomes for gene delivery. *Expert Opin Drug Deliv,* 2**,** 237-54.

SIQUEIRA, G., BRAS, J. & DUFRESNE, A. 2010. New Process of Chemical Grafting of Cellulose Nanoparticles with a Long Chain Isocyanate. *Langmuir,* 26**,** 402-411.

SMERDOU, C. & LILJESTROM, P. 1999. Non-viral amplification systems for gene transfer: vectors based on alphaviruses. *Curr Opin Mol Ther,* 1**,** 244-51.

SNIPPE, H., BELDER, M. & WILLERS, J. M. 1977. Dimethyl diotadecyl ammonium bromide as adjuvant for delayed hypersensitivity in mice. *Immunology,* 33**,** 931-936.

SONG, C. X., LABHASETWAR, V., MURPHY, H., QU, X., HUMPHREY, W. R., SHEBUSKI, R. J. & LEVY, R. J. 1997. Formulation and characterization of biodegradable nanoparticles for intravascular local drug delivery. *Journal of Controlled Release,* 43**,** 197-212.

SORGI, F. L. & HUANG, L. 1996. Large scale production of DC-Chol cationic liposomes by microfluidization. *International Journal of Pharmaceutics,* 144**,** 131-139.

SOUTO, E. B., NAYAK, A. P. & MURTHY, R. S. 2011a. Lipid nanoemulsions for anti-cancer drug therapy. *Pharmazie,* 66**,** 473-8.

SOUTO, E. B., NAYAK, A. P. & MURTHY, R. S. R. 2011b. Lipid nanoemulsions for anti-cancer drug therapy. *Die Pharmazie - An International Journal of Pharmaceutical Sciences,* 66**,** 473-478.

SPUUL, P., BALISTRERI, G., HELLSTRÖM, K., GOLUBTSOV, A. V., JOKITALO, E. & AHOLA, T. 2011. Assembly of alphavirus replication complexes from RNA and protein components in a novel trans-replication system in mammalian cells. *Journal of virology,* 85**,** 4739-4751.

STAN, C. A., ELLERBEE, A. K., GUGLIELMINI, L., STONE, H. A. & WHITESIDES, G. M. 2013. The magnitude of lift forces acting on drops and bubbles in liquids flowing inside microchannels. *Lab on a Chip,* 13**,** 365-376.

STEINMAN, R. M. & COHN, Z. A. 1973. Identification of a novel cell type in peripheral lymphoid organs of mice. I. Morphology, quantitation, tissue distribution. *J Exp Med,* 137**,** 1142-62.

STIGLIANO, C., ARYAL, S., DE TULLIO, M. D., NICCHIA, G. P., PASCAZIO, G., SVELTO, M. & DECUZZI, P. 2013. siRNA-Chitosan Complexes in Poly(lactic-co-glycolic acid) Nanoparticles for the Silencing of Aquaporin-1 in Cancer Cells. *Molecular Pharmaceutics,* 10**,** 3186-3194.

STOKER, M. & MACPHERSON, I. A. N. 1964. Syrian Hamster Fibroblast Cell Line BHK21 and its Derivatives. *Nature,* 203**,** 1355-1357.

STROOCK, A. & MCGRAW, G. 2004. Investigation of the staggered herringbone mixer with a simple analytical model. *Philosophical transactions. Series A, Mathematical, physical, and engineering sciences,* 362**,** 971-86.

STROOCK, A. D., DERTINGER, S. K. W., AJDARI, A., MEZIĆ, I., STONE, H. A. & WHITESIDES, G. M. 2002. Chaotic Mixer for Microchannels. 295**,** 647-651.

SUN, J. C., WILLIAMS, M. A. & BEVAN, M. J. 2004. CD4+ T cells are required for the maintenance, not programming, of memory CD8+ T cells after acute infection. *Nature Immunology,* 5**,** 927-933.

TABATT, K., KNEUER, C., SAMETI, M., OLBRICH, C., MÜLLER, R. H., LEHR, C.-M. & BAKOWSKY, U. 2004a. Transfection with different colloidal systems: comparison of solid lipid nanoparticles and liposomes. *Journal of Controlled Release,* 97**,** 321-332.

TABATT, K., SAMETI, M., OLBRICH, C., MÜLLER, R. H. & LEHR, C.-M. 2004b. Effect of cationic lipid and matrix lipid composition on solid lipid nanoparticle-mediated gene transfer. *European Journal of Pharmaceutics and Biopharmaceutics,* 57**,** 155-162.

TAKAHASHI, M., KITAMOTO, D., ASIKIN, Y., TAKARA, K. & WADA, K. 2009. Liposomes Encapsulating Aloe vera Leaf Gel Extract Significantly Enhance Proliferation and Collagen Synthesis in Human Skin Cell Lines. *Journal of Oleo Science,* 58**,** 643-650.

TAKEUCHI, O. & AKIRA, S. 2009. Innate immunity to virus infection. *Immunol Rev,* 227**,** 75-86.

TAM, Y. Y. C., CHEN, S. & CULLIS, P. R. 2013. Advances in Lipid Nanoparticles for siRNA Delivery. *Pharmaceutics,* 5**,** 498-507.

TEIXEIRA, H., DUBERNET, C., ROSILIO, V., LAIGLE, A., DEVERRE, J. R., SCHERMAN, D., BENITA, S. & COUVREUR, P. 2001. Factors influencing the oligonucleotides release from O–W submicron cationic emulsions. *Journal of Controlled Release,* 70**,** 243-255.

THOMAS, A., GARG, S., DE SOUZA, R., OUELLET, E., THARMARAJAH, G., REICHERT, D., ORDOBADI, M., IP, S. & RAMSAY, E. 2018. Microfluidic Production and Application of Lipid. *Methods in Molecular Biology,* 1792**,** 11.

THOMPSON, A. K. & SINGH, H. 2006. Preparation of Liposomes from Milk Fat Globule Membrane Phospholipids Using a Microfluidizer. *Journal of Dairy Science,* 89**,** 410-419.

THORSEN, T., ROBERTS, R. W., ARNOLD, F. H. & QUAKE, S. R. 2001. Dynamic Pattern Formation in a Vesicle-Generating Microfluidic Device. *Physical Review Letters,* 86**,** 4163-4166.

TOKUMITSU, H., ICHIKAWA, H., FUKUMORI, Y. & BLOCK, L. H. 1999. Preparation of gadopentetic acid-loaded chitosan microparticles for gadolinium neutron-capture therapy of cancer by a novel emulsion-droplet coalescence technique. *Chem Pharm Bull (Tokyo),* 47**,** 838-42.

TOMODA, T., MORITA, H., KURASHIGE, T. & MAASSAB, H. F. 1995. Prevention of influenza by the intranasal administration of cold-recombinant, live-attenuated influenza virus vaccine: importance of interferon-γ production and local IgA response. *Vaccine,* 13**,** 185-190.

TSURUTA, L., QUINTILIO, W., COSTA, M. H. & CARMONARIBEIRO, A. 1997. Interactions between cationic liposomes and an antigenic protein: The physical chemistry of the immunoadjuvant action. *Journal of lipid research,* 38**,** 2003-11.

UEMATSU, Y., VAJDY, M., LIAN, Y., PERRI, S., GREER, C. E., LEGG, H. S., GALLI, G., SALETTI, G., OTTEN, G. R., RAPPUOLI, R., BARNETT, S. W. & POLO, J. M. 2012. Lack of interference with immunogenicity of a chimeric alphavirus replicon particle-based influenza vaccine by preexisting antivector immunity. *Clinical and vaccine immunology : CVI,* 19**,** 991-998.

UGAZIO, E., CAVALLI, R. & GASCO, M. R. 2002. Incorporation of cyclosporin A in solid lipid nanoparticles (SLN). *International Journal of Pharmaceutics,* 241**,** 341-344.

UGOLINI, G. & HEMACHUDHA, T. 2018. Rabies: changing prophylaxis and new insights in pathophysiology. *Curr Opin Infect Dis,* 31**,** 93-101.

ULMER, J. B., MASON, P. W., GEALL, A. & MANDL, C. W. 2012. RNA-based vaccines. *Vaccine,* 30**,** 4414-4418.

UNER, M. & YENER, G. 2007. Importance of solid lipid nanoparticles (SLN) in various administration routes and future perspectives. *International journal of nanomedicine,* 2**,** 289-300.

VAN DE WEERT, M., HENNINK, W. E. & JISKOOT, W. J. P. R. 2000. Protein Instability in Poly(Lactic-co-Glycolic Acid) Microparticles. 17**,** 1159-1167.

VAN DER WOUDE, I., WAGENAAR, A., MEEKEL, A. A., TER BEEST, M. B., RUITERS, M. H., ENGBERTS, J. B. & HOEKSTRA, D. 1997. Novel pyridinium surfactants for efficient, nontoxic in vitro gene delivery. *Proceedings of the National Academy of Sciences of the United States of America,* 94**,** 1160-1165.

VAN HOUTE, A. J., SNIPPE, H., SCHMITZ, M. G. & WILLERS, J. M. 1981. Characterization of immunogenic properties of haptenated liposomal model membranes in mice. V. Effect of membrane composition on humoral and cellular immunogenicity. *Immunology,* 44**,** 561-8.

VAN SWAAY, D. & DEMELLO, A. 2013. Microfluidic methods for forming liposomes. *Lab Chip,* 13**,** 752-67.

VANGASSERI, D. P., CUI, Z., CHEN, W., HOKEY, D. A., FALO, L. D. & HUANG, L. 2006. Immunostimulation of dendritic cells by cationic liposomes. *Molecular Membrane Biology,* 23**,** 385-395.

VENKATESWARLU, V. & MANJUNATH, K. 2004. Preparation, characterization and in vitro release kinetics of clozapine solid lipid nanoparticles. *Journal of Controlled Release,* 95**,** 627-638.

VERMA, R., KHANNA, P., PRINJA, S. & RAJPUT, M. 2011. Intra-dermal administration of rabies vaccines in developing countries: at an affordable cost. *Hum Vaccin,* 7**,** 792-4.

VIGHI, E., RUOZI, B., MONTANARI, M., BATTINI, R. & LEO, E. 2010. pDNA condensation capacity and in vitro gene delivery properties of cationic solid lipid nanoparticles. *International Journal of Pharmaceutics,* 389**,** 254-261.

VIGILATO, M. A. N., COSIVI, O., KNÖBL, T., CLAVIJO, A. & SILVA, H. M. T. 2013. Rabies update for Latin America and the Caribbean. *Emerging infectious diseases,* 19**,** 678-679.

VIJAYENDRAN, R. A., MOTSEGOOD, K. M., BEEBE, D. J. & LECKBAND, D. E. 2003. Evaluation of a Three-Dimensional Micromixer in a Surface-Based Biosensor. *Langmuir,* 19**,** 1824-1828.

VILA, A., SANCHEZ, A., EVORA, C., SORIANO, I., VILA JATO, J. L. & ALONSO, M. J. 2004. PEG-PLA nanoparticles as carriers for nasal vaccine delivery. *J Aerosol Med,* 17**,** 174-85.

VITALE, S. A. & KATZ, J. L. 2003. Liquid Droplet Dispersions Formed by Homogeneous Liquid–Liquid Nucleation: "The Ouzo Effect". *Langmuir,* 19**,** 4105-4110.

VITIELLO, L., BOCKHOLD, K., JOSHI, P. B. & WORTON, R. G. 1998. Transfection of cultured myoblasts in high serum concentration with DODAC:DOPE liposomes. *Gene Therapy,* 5**,** 1306-1313.

VOGEL, A. B., LAMBERT, L., KINNEAR, E., BUSSE, D., ERBAR, S., REUTER, K. C., WICKE, L., PERKOVIC, M., BEISSERT, T., HAAS, H., REECE, S. T., SAHIN, U. & TREGONING, J. S. 2018. Self-Amplifying RNA Vaccines Give Equivalent Protection against Influenza to mRNA Vaccines but at Much Lower Doses. *Molecular Therapy,* 26**,** 446-455.

VONO, M., TACCONE, M., CACCIN, P., GALLOTTA, M., DONVITO, G., FALZONI, S., PALMIERI, E., PALLAORO, M., RAPPUOLI, R., DI VIRGILIO, F., DE GREGORIO, E., MONTECUCCO, C. & SEUBERT, A. 2013. The adjuvant MF59 induces ATP release from muscle that potentiates response to vaccination. *Proceedings of the National Academy of Sciences of the United States of America,* 110**,** 21095-21100.

WAGNER, A., VORAUER-UHL, K. & KATINGER, H. 2002. Liposomes produced in a pilot scale: production, purification and efficiency aspects. *European Journal of Pharmaceutics and Biopharmaceutics,* 54**,** 213-219.

WALCZYK, D., BOMBELLI, F. B., MONOPOLI, M. P., LYNCH, I. & DAWSON, K. A. 2010. What the Cell "Sees" in Bionanoscience. *Journal of the American Chemical Society,* 132**,** 5761-5768.

WALKER, C., SELBY, M., ERICKSON, A., CATALDO, D., VALENSI, J. P. & VAN NEST, G. V. 1992. Cationic lipids direct a viral glycoprotein into the class I major histocompatibility complex antigen-presentation pathway. *Proceedings of the National Academy of Sciences of the United States of America,* 89**,** 7915-7918.

WALKEY, C. & CHAN, W. 2011. Understanding and Controlling the Interaction of Nanomaterials with Proteins in a Physiological Environment. *Chemical Society reviews,* 41**,** 2780-99.

WANG, D., CHRISTOPHER, M. E., NAGATA, L. P., ZABIELSKI, M. A., LI, H., WONG, J. P. & SAMUEL, J. 2004. Intranasal immunization with liposome-encapsulated plasmid DNA encoding influenza virus hemagglutinin elicits mucosal, cellular and humoral immune responses. *Journal of Clinical Virology,* 31**,** 99-106.

WANG, D., JING, N.-H. & LIN, Q.-S. 1996. Stearylamine Liposome as a New Efficient Reagent for DNA Transfection of Eukaryotic Cells. *Biochemical and Biophysical Research Communications,* 226**,** 450-455.

WANG, R., XIAO, R., ZENG, Z., XU, L. & WANG, J. 2012a. Application of poly(ethylene glycol)-distearoylphosphatidylethanolamine (PEG-DSPE) block copolymers and their derivatives as nanomaterials in drug delivery. *International journal of nanomedicine,* 7**,** 4185-4198.

WANG, Y., RAHMAN, D. & LEHNER, T. 2012b. A comparative study of stress-mediated immunological functions with the adjuvanticity of alum. *J Biol Chem,* 287**,** 17152-60.

WARRELL, M. J. 2012. Current rabies vaccines and prophylaxis schedules: Preventing rabies before and after exposure. *Travel Medicine and Infectious Disease,* 10**,** 1-15.

WASHINGTON, C. & DAVIS, S. S. 1988. The production of parenteral feeding emulsions by Microfluidizer. *International Journal of Pharmaceutics,* 44**,** 169-176.

WEIBEL, D. B. & WHITESIDES, G. M. 2006. Applications of microfluidics in chemical biology. *Current Opinion in Chemical Biology,* 10**,** 584-591.

WEISS, J., DECKER, E. A., MCCLEMENTS, D. J., KRISTBERGSSON, K., HELGASON, T. & AWAD, T. J. F. B. 2008. Solid Lipid Nanoparticles as Delivery Systems for Bioactive Food Components. 3**,** 146-154.

WEISSMAN, D. 2015. mRNA transcript therapy. *Expert Review of Vaccines,* 14**,** 265-281.

WHEELER, C. J., FELGNER, P. L., TSAI, Y. J., MARSHALL, J., SUKHU, L., DOH, S. G., HARTIKKA, J., NIETUPSKI, J., MANTHORPE, M., NICHOLS, M., PLEWE, M., LIANG, X., NORMAN, J., SMITH, A. & CHENG, S. H. 1996. A novel cationic lipid greatly enhances plasmid DNA delivery and expression in mouse lung. *Proceedings of the National Academy of Sciences of the United States of America,* 93**,** 11454-11459.

WHITEHEAD, K. A., LANGER, R. & ANDERSON, D. G. 2009. Knocking down barriers: advances in siRNA delivery. *Nat Rev Drug Discov,* 8**,** 129-38.

WHITESIDES, G. M. 2006. The origins and the future of microfluidics. *Nature,* 442**,** 368-373.

WIKTOR, T. J., FERNANDES, M. V. & KOPROWSKI, H. 1964. Cultivation of Rabies Virus in Human Diploid Cell Strain WI-38. 93**,** 353-366.

WILLIAMSON, D. 2013. Gregory AE, Titball RW and Williamson D. Vaccine delivery using nanoparticles. Frontiers in Cellular and Infection Microbiology , March 2013, 3, article 13, 1-13. *Frontiers in Cellular and Infection Microbiology,* 3**,** 1-13.

WISCHKE, C., ZIMMERMANN, J., WESSINGER, B., SCHENDLER, A., BORCHERT, H.-H., PETERS, J., NESSELHUT, T. & LORENZEN, D. R. 2008. Poly(I:C) coated PLGA microparticles induce dendritic cell maturation. *International journal of pharmaceutics,* 365**,** 61-8.

WISSING, S. A., KAYSER, O. & MÜLLER, R. H. 2004. Solid lipid nanoparticles for parenteral drug delivery. *Advanced Drug Delivery Reviews,* 56**,** 1257-1272.

WOLFF, J. A., MALONE, R. W., WILLIAMS, P., CHONG, W., ACSADI, G., JANI, A. & FELGNER, P. L. 1990. Direct gene transfer into mouse muscle in vivo. *Science,* 247**,** 1465-8.

WOLFRUM, C., SHI, S., JAYAPRAKASH, K. N., JAYARAMAN, M., WANG, G., PANDEY, R. K., RAJEEV, K. G., NAKAYAMA, T., CHARRISE, K., NDUNGO, E. M., ZIMMERMANN, T., KOTELIANSKY, V., MANOHARAN, M. & STOFFEL, M. 2007. Mechanisms and optimization of in vivo delivery of lipophilic siRNAs. *Nature Biotechnology,* 25**,** 1149.

WONG, J. P., ZABIELSKI, M. A., SCHMALTZ, F. L., BROWNLEE, G. G., BUSSEY, L. A., MARSHALL, K., BORRALHO, T. & NAGATA, L. P. 2001. DNA vaccination against respiratory influenza virus infection. *Vaccine,* 19**,** 2461-2467.

WRAMMERT, J., MILLER, J., AKONDY, R. & AHMED, R. 2009. Human immune memory to yellow fever and smallpox vaccination. *Journal of clinical immunology,* 29**,** 151-157.

XIANG, S. D., SCHOLZEN, A., MINIGO, G., DAVID, C., APOSTOLOPOULOS, V., MOTTRAM, P. L. & PLEBANSKI, M. 2006. Pathogen recognition and development of particulate vaccines: Does size matter? *Methods,* 40**,** 1-9.

XU, Z.-R., WANG, W.-F., LIANG, X.-F., LIU, Z.-H., LIU, Y., LIN, L. & ZHU, X. J. J. O. M. N. 2015. Protective Effects of Poly (butyl) Cyanoacrylate Nanoparticles Containing Vasoactive Intestinal Peptide Against 6-Hydroxydopamine-Induced Neurotoxicity In Vitro. 55**,** 854-864.

XUE, H. Y. & WONG, H. L. 2011. Tailoring nanostructured solid-lipid carriers for time-controlled intracellular siRNA kinetics to sustain RNAi-mediated chemosensitization. *Biomaterials,* 32**,** 2662-2672.

YAMANO, S., DAI, J. & MOURSI, A. M. J. M. B. 2010. Comparison of Transfection Efficiency of Nonviral Gene Transfer Reagents. 46**,** 287-300.

YAN, W., CHEN, W. & HUANG, L. 2007. Mechanism of adjuvant activity of cationic liposome: Phosphorylation of a MAP kinase, ERK and induction of chemokines. *Molecular Immunology,* 44**,** 3672-3681.

YANG, J. P. & HUANG, L. 1997. Overcoming the inhibitory effect of serum on lipofection by increasing the charge ratio of cationic liposome to DNA. *Gene Ther,* 4**,** 950-60.

YAROSH, O. K., WANDELER, A. I., GRAHAM, F. L., CAMPBELL, J. B. & PREVEC, L. 1996. Human adenovirus type 5 vectors expressing rabies glycoprotein. *Vaccine,* 14**,** 1257-64.

YASUDA, T., DANCEY, G. F. & KINSKY, S. C. 1977. Immunogenicity of liposomal model membranes in mice: dependence on phospholipid composition. *Proc Natl Acad Sci U S A,* 74**,** 1234-6.

YOTSUMOTO, S., SAEGUSA, K. & ARAMAKI, Y. 2008. Endosomal Translocation of CpG-Oligodeoxynucleotides Inhibits DNA-PKcs-Dependent IL-10 Production in Macrophages. *Journal of immunology (Baltimore, Md. : 1950),* 180**,** 809-16.

YU, B., LEE, R. J. & LEE, L. J. 2009. Microfluidic methods for production of liposomes. *Methods in enzymology,* 465**,** 129-141.

YUE, Z.-G., WEI, W., LV, P.-P., YUE, H., WANG, L.-Y., SU, Z.-G. & MA, G.-H. 2011. Surface Charge Affects Cellular Uptake and Intracellular Trafficking of Chitosan-Based Nanoparticles. *Biomacromolecules,* 12**,** 2440-2446.

ZABNER, J. 1997. Cationic lipids used in gene transfer. *Advanced Drug Delivery Reviews,* 27**,** 17-28.

ZARITSKAYA, L., SHURIN, M. R., SAYERS, T. J. & MALYGUINE, A. M. 2010. New flow cytometric assays for monitoring cell-mediated cytotoxicity. *Expert Review of Vaccines,* 9**,** 601-616.

ZELPHATI, O., UYECHI, L. S., BARRON, L. G., SZOKA, F. C. J. B. E. B. A.-L. & $V, L. M. 1998. Effect of serum components on the physico-chemical properties of cationic lipid/oligonucleotide complexes and on their interactions with cells. 119-133.

ZEPP, F. 2010. Principles of vaccine design-Lessons from nature. *Vaccine,* 28 Suppl 3**,** C14-24.

ZHANG, N., PING, Q., HUANG, G., XU, W., CHENG, Y. & HAN, X. 2006. Lectin-modified solid lipid nanoparticles as carriers for oral administration of insulin. *International Journal of Pharmaceutics,* 327**,** 153-159.

ZHANG, Q., YIE, G., LI, Y., YANG, Q. & NAGAI, T. 2000. Studies on the cyclosporin A loaded stearic acid nanoparticles. *International Journal of Pharmaceutics,* 200**,** 153-159.

ZHANG, X., CHEN, G., ZHANG, T., MA, Z. & WU, B. 2014. Effects of PEGylated lipid nanoparticles on the oral absorption of one BCS II drug: a mechanistic investigation. *International journal of nanomedicine,* 9**,** 5503-5514.

ZHANG, Y., LI, H., SUN, J., GAO, J., LIU, W., LI, B., GUO, Y. & CHEN, J. J. I. J. O. P. V. 2010. DC-Chol/DOPE cationic liposomes: A comparative study of the influence factors on plasmid pDNA and siRNA gene delivery. 198-207.

ZHAO, L., TORIUMI, H., WANG, H., KUANG, Y., GUO, X., MORIMOTO, K. & FU, Z. F. 2010. Expression of MIP-1alpha (CCL3) by a recombinant rabies virus enhances its immunogenicity by inducing innate immunity and recruiting dendritic cells and B cells. *J Virol,* 84**,** 9642-8.

ZHAO, Q. Q., HU, Y. L., ZHOU, Y., LI, N., HAN, M., TANG, G. P., QIU, F., TABATA, Y. & GAO, J. Q. 2012. Gene-carried hepatoma targeting complex induced high gene transfection efficiency with low toxicity and significant antitumor activity. *Int J Nanomedicine,* 7**,** 3191-202.

ZHIGALTSEV, I. V., BELLIVEAU, N., HAFEZ, I., LEUNG, A. K. K., HUFT, J., HANSEN, C. & CULLIS, P. R. 2012. Bottom-Up Design and Synthesis of Limit Size Lipid Nanoparticle Systems with Aqueous and Triglyceride Cores Using Millisecond Microfluidic Mixing. *Langmuir,* 28**,** 3633-3640.

ZIELLO, J. E., HUANG, Y. & JOVIN, I. S. 2010. Cellular endocytosis and gene delivery. *Mol Med,* 16**,** 222-9.

ZIMMERMANN, T. S., LEE, A. C., AKINC, A., BRAMLAGE, B., BUMCROT, D., FEDORUK, M. N., HARBORTH, J., HEYES, J. A., JEFFS, L. B., JOHN, M., JUDGE, A. D., LAM, K., MCCLINTOCK, K., NECHEV, L. V., PALMER, L. R., RACIE, T., ROHL, I., SEIFFERT, S., SHANMUGAM, S., SOOD, V., SOUTSCHEK, J., TOUDJARSKA, I., WHEAT, A. J., YAWORSKI, E., ZEDALIS, W., KOTELIANSKY, V., MANOHARAN, M., VORNLOCHER, H. P. & MACLACHLAN, I. 2006. RNAi-mediated gene silencing in non-human primates. *Nature,* 441**,** 111-4.

ZOOK, J. & VREELAND, W. 2010. Effects of temperature, acyl chain length, and flow-rate ratio on liposome formation and size in a microfluidic hydrodynamic focusing device. *Soft Matter,* 6**,** 1352-1360.

ZUHORN, I. S., BAKOWSKY, U., POLUSHKIN, E., VISSER, W. H., STUART, M. C. A., ENGBERTS, J. B. F. N. & HOEKSTRA, D. 2005. Nonbilayer phase of lipoplex–membrane mixture determines endosomal escape of genetic cargo and transfection efficiency. *Molecular Therapy,* 11**,** 801-810.

ZUIDAM, N. J., HIRSCH-LERNER, D., MARGULIES, S. & BARENHOLZ, Y. J. B. E. B. A. B. O. B. B. V. 1999. Lamellarity of cationic liposomes and mode of preparation of lipoplexes affect transfection efficiency. 207-220.

ZUR MÜHLEN, A., SCHWARZ, C. & MEHNERT, W. 1998. Solid lipid nanoparticles (SLN) for controlled drug delivery – Drug release and release mechanism. *European Journal of Pharmaceutics and Biopharmaceutics,* 45**,** 149-155.